Carnegie Mellon University

CARNEGIE INSTITUTE OF TECHNOLOGY

THESIS

Submitted in Partial Fulfillment of the Requirements
For the Degree of Doctor of Philosophy

TITLE

Synthesizing *in situ* Friction and Wear with *ex situ* Surface Metrology to Provide Post-mortem Tribological Analysis: Experiments and Modeling

PRESENTED BY

PATRICK S.M. DOUGHERTY

ACCEPTED BY THE DEPARTMENT OF MECHANICAL ENGINEERING

ADVISOR, MAJOR PROFESSOR	DATE
DEPARTMENT HEAD	DATE

APPROVED BY THE COLLEGE COUNCIL

DEAN	DATE

Synthesizing *in situ* Friction and Wear with *ex situ* Surface Metrology to Provide Post-mortem Tribological Analysis: Experiments and Modeling

Submitted in Partial Fulfillment of the Requirements for the Degree of

Doctor of Philosophy

in

Mechanical Engineering

Patrick S. M. Dougherty
B.S. Mechanical Engineering, Carnegie Mellon University
M.S. Mechanical Engineering, Carnegie Mellon University

Carnegie Mellon University,
Pittsburgh, PA

May, 2016

Dedicated to:

My Father, Mother, Brother and Sister,

David, Valerie, Kevin, and Colleen Dougherty,

Always remember there is nothing worth sharing, like the love that let us share our name…

Acknowledgements

My tenure at Carnegie Mellon, beginning almost 10 years ago, has not been without tenuous moments. It has been an amalgam of first steps, curiousity, and inspiration; of self-assurance, failure, and self-discovery; of second chances, true exhaustion, and incalculable joy. It is still hard to believe that it is coming to a close. Carnegie Mellon University is the one thing outside of my family and absolute closest friends, which has seen each, very different iteration of myself as I have grown to the point now where I can call myself a Dr.… from the amateur Physicist/Philosopher, the lost boy, and the professional miscreant; to the academic zealot, the lonely man, and the romantic toiler… to something now which I hope contains the right balance to carry me forward through the rest of my life as a Scientist, an Artist, a Son, a Brother, a Friend, a Husband, and a Father…

At this moment, through chance, I find myself listening to the music which kept my heart beating in the times when I would let no one else in. It is a song by Explosions in the Sky called "Your Hand in Mine, " and out of all the songs, this is the one which has always struck true no matter the moment. With these sentiments, and to this soundtrack, allow me to close the loop by thanking all who have been there for me, and perhaps forever… put the loneliness to rest.

I would like to begin by honoring those who have been crucial to my academic turnaround. The first is Dr. Richard Holman, of the Department of Physics for Carnegie Mellon University. Though he may never know it, he was the first person to let me know how insignificant talent can be, without the drive to push one's limits… without work ethic. I would like to thank Dr. Eric Grotzinger of the Mellon College of Sciences for his belief that I had much more to offer than my initial performance let on. Without the two of them I can't help but believe I may have proceeded down a very different path. I would like to thank Kurt Larsen and Bonnie Olsen of the Mechanical Engineering Department, for respectively giving me the tentative

second chance and the unwavering support I needed to excel in their department. I would like to thank Professor Phillip Leduc, the first professor with whom I had serious after class discussions, be they academic or otherwise. I am so proud to call him my mentor. He has helped me find the balance I never knew I needed between work and life.

Enough cannot be said about the help of my advisor Dr. C. Fred Higgs III. I will never forget walking up to him after the last day of Thermodynamics during my first year in engineering. I approached with the hopes of requesting a position in his lab, only to be beaten to the punch by the Professor Higgs himself. He has pushed me to be a better engineer and human being in a truly inspiring mixture of subtle behind-the-scenes touches and bare, honest conversations. His lab has always been modeled as both a business in terms of his expectations, but also as a family in terms of his empathy. As such I hope he knows that I will forever appreciate all the time and effort spent, even in the smallest detail, even when I didn't understand it, in order to make the "family," work for this son. There are innumerable ways in which he has prepped me for the life to come well beyond the technical. I feel that there will be no other engineers, save those who have called him advisor, who could be better prepared to respond to a sudden deadline, gauge the desires of the present self vs the needs of the future self, or to always remember that one must showcase one's talents without forgetting to be "humble and flexible."

There are a number of exemplary students and researchers in the PhD whom I have had the honor to know. The students I have mentored and advised were not only a constant source of inspiration, professional growth, and friendship, but were also crucial to the completion of this work. I would like to particularly thank Cecily Sunday, for her exceptional work, and for reminding me that "there's no reason it can't all be as cool as rocket science." I would like to thank Mikio David for his multiple years of dedicated research on solid lubrication. And I would also like to thank Jeffery Cole as well for his award winning work in rock drilling research. He was truly ready to help at any time, in any way shape or form, and to be a friend in addition, whenever it was needed. I would like to thank Eric Meyers and Zachary Fisher for their work on the Additive Manufacturing sections, without which I would not be moving onto the job I have chosen. Lastly, I would like to thank Ali Mcnulty and Shannon Horgan, for their help with a crucial Westinghouse project which helped pay the bills throughout my final year.

In addition to undergraduates and masters students, I want to be sure I thank all of the Doctoral members of the PFTL family. I would like to thank Dr. Emmanuel Wornyoh and Dr.

Randyka Pudjoprawoto, with whom I shared time in the Powder sub-group and who shaped much of my early tenure in the PFTL. I want to thank Dr. Jon Sierra, and Dr. Gagan Srivastava for their time spent throughout my five years, always ready to go the extra mile to polish a presentation. For their time spent in the recent years, I also want to thank Dr. Kristin Warren, Deepak Patil, and Prathamesh Desai. We were a smaller lab but we were always there to help each other improve. I want to thank Dr. Elon J. Terrel, for his mentorship and kindness, both of which will always remain with me. Lastly I want to be sure to thank the late Dr. Jeremiah Mpagazehe and Dr. Martin C. Marinack Jr. With the two of you I formed the "triumvirate" catalyzing over tribology and solidifying into friendship that will never leave me. Jeremiah, you were always there to remind me of how far I had to go before I was done working, and I include getting you to take a break amongst my greatest achievements. Marty, we always joked that the two of us managed to compliment the other's personality in a lasting way. I will forever believe that I received the lion's share of that positive influence. I thank you for that from the bottom of my heart. During our time together I believe we were part of something special, and that those nights spent in jubilant reverence at the end of every conference, competition, or string of sleepless nights… will live forever, even when we cannot. As there are innumerable others whom have called the PFTL home, and helped me along the way, I will simply say thank you to you all and to please forgive me if I have left one of you out.

There are a number of organizations and other collaborators whom I must thank as well. I would like to thank Kennametal Inc. for their in-kind contributions of expensive material samples. Tribology tends to go through surfaces rather quickly. I would like to thank the National Science Foundation under Grant no. 0946825, and for believing that my research drives were worth their generous support. I would like to thank the Timken Company, and specifically Dr. Ryan Evans, for all of their collaborative efforts on the work featuring hard tribological coatings. I want to mention Chris Dellacorte, from NASA's Glenn Research Center. He was kind enough at more than one conference to take me under his wing. He was a particularly poignant example of how if one can work ruthlessly, they can always plan for time to create a lasting experience with friends. I would also like to thank the Carnegie Mellon Shaw Fellowship, as well as all of the tremendous staff. You were always eager to help no matter how scatterbrained I might have been, and more often than not with a smile that was the difference in a long day. To Michael Scampone, Ginny Barry, Bobbi Kostiyak, Meredith Blobner, Kristi

Berneberg, Melissa Brown, thank you so much for all of the work you do. Special thanks must go out to Chris Hertz, who is just as reliable behind the desk as he always proved to be in the end-zone over the middle. Thanks Chris, for helping me with all of the details I would without fail… forget.

And now I must thank my family and friends, the ones who have stood by me these now 30 years. To Brad, my most dependable friend, you've been an example of what hard work really is at times when I most needed it. I will never forget coming in after work to your restaurant, setting up to write some paper or another, to "help" you close down around 2am. Those times were some of my happiest during my PhD, always with the knowledge that I had you working by my side and a conversation coming my way. From the lazy afternoons we spent as children, to the weeks spent riding the Atlantic waves and staring at the stars, you will always be my brother and I will forever be grateful you hit that homerun. To Bill, you are my oldest friend. You define loyalty, even when it hurts you personally. The day you asked me to play TV tag feels like the single event to which I can trace everything for which I am so grateful. Thank you my brother. To Jameson, Sean, and Ryan, I met the three of you in one of my darkest periods. You were everything I needed in three, so very different ways. Thank you for giving me back a bit of the light that was starting to dwindle. To Shane Jordan and Keegan Donovan, my younger brothers from 2 other mothers, I thank you both for keeping me young, and showing me that my family is not just those who happen to have the same name. It has been a joy to be part of your lives. To Keegan Henrikson, from the nights spent musing out into a snowy night sky, to the days of sheer aching exultation in the summer sun, you have been a man I am proud to know. It feels as though we lived a great deal these past two years, and I thank you so much for being my brother in arms and for understanding.

To my mother, there were times I did not understand the extent of your love, how it could consume you, how it could consume us. I know now. I love you and I thank you so much for everything you have done to give me life and the opportunity to experience this moment. To my Father, it feels like a lifetime since I realized just how incredible a man you really were. I feel as if I realize it again every day. "Lucky" feels a drab and sacrilegious way to describe the state of being brought up by you. It was not luck, but your blinding sense of right and dedication to your family by which I find myself here today, your son, and a PhD Graduate. To my grandmother, you already know that you have been my haven, when my brain needed to reboot. I love you and

have “since my first breath.” Thank you. To my grandfather, Joseph Murphy, I have no words potent enough to describe what you were for me. A singularly perfect mind? An impossible balance of talent, patience, and success? An embodiment of the Randian Hero? Everything I could ever aspire to be. All of it. I will try to make you proud. Thank you for it all Grandfather.

To my soon to be daughter, Angeleah, thank you for bringing much of this into perspective, and for the kiss you planted on my cheek that evening when I felt my head begin to dip beneath the waves of this ever-stormy thesis. I will never forget it. To my soon to be wife, you are the final breathtaking answer to it all. Who knew that my world could be encapsulated so elegantly in the sunlit facets of your countenance, in the delicately whispered words which form between perfect lips, in the time we’ve spent together from an account long overdrawn on any given day, in the wistful walks I take through your stunning mind… Thank you for giving me something to look forward to for the rest of my life.

Abstract

Surface wear is estimated to result in upwards of 70% of material failure in the US with costs of over 300 billion dollars per annum. Tribology is defined as the study of friction, lubrication, and wear, and while all three of these sub-disciplines stem from interactions at the asperity scale, studies involving the mechanics of industrial interfaces will often ignore their interdependence. This work makes use of a synthesis of in situ tribological data with ex situ surface characterization, in order to elucidate the mechanics of friction and wear in a number of industrial interfaces each with its own objective. *Section 1* focuses on using this technique to elucidate the mechanics of protective solid lubricants. Detailed experiments were conducted to study the formation and depletion of self-replenishing powder transfer films in both single component and composite forms. Based on the synthesis of *ex situ* and *in situ* findings, the primary wear mechanisms at each interface were described as abrasive and transfer film phenomena were described in a new way using a quasi-hydrodynamic approach. In addition to transfer films, hard tribological coatings were also studied for their ability to mitigate impact damage. Coefficient of restitution results were combined with investigations *ex situ* of the impact sites and compared to nanoindentation results of coating properties. Through synthesizing these results, it was found that more elastic coatings worked best on stiffer substrates, while harder, more brittle coatings worked best on soft substrates. In *Section 2*, the *Section 1* findings were crucial in the development of a numerical model which was presented using abrasive formulations for the wear of soft surfaces and preferential patterning. Quantitative agreement for modeling friction and surface evolution, as well as qualitative agreement for wear trends were provided for experimental values from previous studies. In *Section 3*, this technique was used to study powder rheology as it applies to flows in the additive manufacturing process. Rheological characterization was conducted for stress states akin to spreading and hopper flow on an FT4 powder rheometer, while morphological characterization was performed in collaboration with the Material Science Department at Carnegie Mellon using scanning electron microscopy. By analyzing the results in concert, it was found that morphology proved to be more important than material type or manufacturing process in governing flow properties. Spreading-like states were found to be most sensitive to factors affecting particle rolling, while hopper-like states were found to be most sensitive to factors affecting particle cohesion. In *Section 4*, the interactions of

single cutters were explored for rock substrates found during drilling for oil, gas, and geothermal heat. Experiments were conducted first for O1 tool steel buttons on Carthage Marble. Cutting with this type cutter was found to produce rough surfaces which would lead to an increase of friction force in the cut. Experiments for dry and lubricated cutting with industrial polycrystalline diamond compact cutters were performed for Carthage Marble, Nugget Sandstone, and Mancos Shale on a retrofitted UMT-3 Tribometer from Bruker. Cutting was found to produce smoother topographies and a decrease in friction. Lubricants were found to possess both a lubricating effect which would reduce COF as well as a weakening effect which would enhance rate of penetration and the load at which cutting would commence. Scraping was found to produce a scalloped topography similar to "bit-bounce." Industrial drilling fluids or "muds" were also evaluated and ranked using a figure of merit proposed within this work. By normalization with the dry scenario, muds performance in terms of friction *and* rate of penetration could be combined to provide ranking of a given mud for a given rock type. Overall it was found that implementing both *in situ* tribological data and *ex situ* surface metrology was an extremely effective way to recreate the mechanics present in industrial interfaces which are difficult to observe otherwise.

Table of Contents

List of Tables

List of Figures

Chapter 1: Background

Friction and wear have been studied extensively in a plethora of industrial scenarios, and while they are generally thought to be related at the asperity scale of contact, they are rarely coupled together. This fact stems from the complexity in their interdependence, as well as the existence of a myriad of different mechanisms for each. One of the most useful techniques for elucidating friction and wear is tribometry, in which pin-on-disc type tests are used to monitor friction and wear *in situ* between two materials, sometimes three if an interfacial medium or lubricant is also desired. In addition to *in situ* tribometry, *ex situ analysis* can often provide qualitative or sometimes quantitative insights into the dynamics of an interface. Both of these techniques are used to elucidate information about the progress of an interaction, yet often they are not used in conjunction. This work aims to utilize a synthesis of both *in situ* tribological data with *ex situ* surface metrology, in which direct inferences from both are used to construct a post-mortem analysis of the interfacial mechanics of different industrial applications.

1.1 Solid Lubrication Studies

In Tribology (the study of friction, lubrication, and wear), it is generally understood that harsher operating conditions of state-of-the art technologies will continue to render many oil-based lubricants unfit for long term tribological performance [1]. This difficulty with oils manifests itself primarily as a tendency to dissociate at temperatures above 500°C [1]. As a result, many solid powder lubricants such as graphite and Molybdenum Disulfide(MoS_2) were developed as high temperature alternatives with ultra-low coefficients of friction (μ), as low as 0.02 [1, 2]. In both cases, the solid lubricants are thought to accommodate velocity by the interfacial shearing of lamellae which comprise their molecular arrangements. There have been

extensive studies in characterizing the low friction performance of both these solid lubricants for many different applications [3-14].

After the establishment of these two powders as viable options for high-temperature lubrication, a plethora of other conditions soon followed which were well-suited for the employment of solid lubricants. These conditions include cryo-temperature environments such as those found in superconductors [5, 14], vacuum contacts found extensively in space applications [3, 14, 15], low-speed or reciprocating sliding contacts for start-up and shut-down [16], and finally, electrically conductive contacts such as those for the rail-gun or power generation industries [2, 6, 17]. In each of these situations, the nature of liquid lubricants prohibits their implementation due to issues such as freezing, outgassing, loss of load carrying capacity due to low speeds, and lack of electrical conductivity.

While many solid lubricants have been shown to be suitable replacements for oils, they are not without their own environmental constraints. For example, graphite performs well in moist environments, while MoS_2 prefers arid interfaces. This key difference stems from the chemistry of the respective lamellae, where H_2O molecules will be absorbed. While beneficial to graphite in providing hydrogen planes on which to slide, the hydrogen molecules actually prevent the smooth sliding of sulfur planes through the tribo-oxidation of dangling bonds in MoS_2 films [8, 9]. These types of differences have led to a restricted list of solid lubricant applications, while continuing to stress the need for further study to widen their robustness.

One novel method of applying these solid lubricants *in situ* (i.e., during sliding) is through film transfer [4, 10, 11, 15, 18, 19]. For transfer film lubrication, the potential to lubricate contacts *in situ* through an inherently self-replenishing process exists, as long as the transfer film is continuously deposited. In order to accomplish this, a compacted powder pellet is

often used to transfer a thin lubricant film onto a moving substrate wherever uncovered asperities exist [4, 10, 18, 19]. An intuitive schematic in which the disk asperities are exaggerated is shown for this system in fig 1.

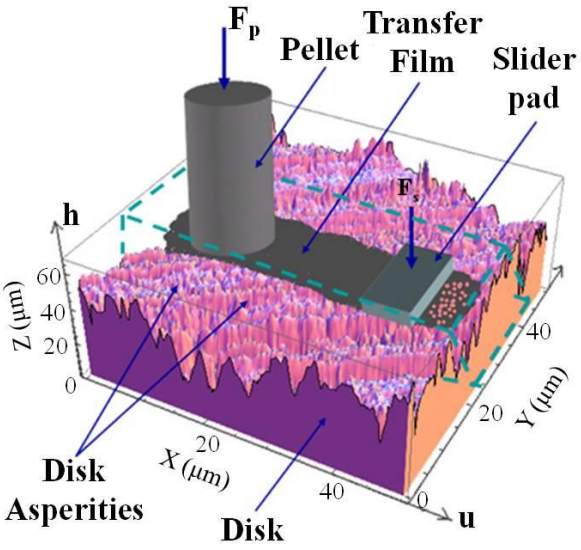

Figure 1: Schematic of the self-replenishing system

In many ways this will be similar to burnishing but without the need for smart systems or human intervention. This type of lubrication system also has a large amount of flexibility in specialty contacts because a variety of solid lubricant powders can be employed in pellet form. For instance, the potential to lubricate sliding contacts has already been explored with graphite powders, which are inherently conductive [2]. However, though graphite is known to possess moderate conductivity, its reliance on moist environments, may make it a poor choice for electrical contacts. These kinds of specific drawbacks which adversely affect the performance of homogenous transfer film lubricant in broad applications are quite common. For instance, tribo-oxidation, prohibits transfer film deposition by hardening the pellet through excessive polishing and creates higher friction during sliding [18]. In addition, powders made from multiple components in order to provide multi-functional capabilities can suffer from separation effects

and loss of frictional performance if the particle sizes aren't closely matched due to size segregation [6, 20-22].

Another popular technique for improving friction and wear performance through solid lubrication is by deposition of hard tribological coatings such as Diamond like Carbon (DLC) and Chromium Nitride (CrN). Due to their extremely hard nature, these films can often be used to mitigate other forms of damage such as that from impact, denting, micro-fracture, and spalling [1, 3, 18, 23, 24]. Generally these coatings are expected to work either by the formation of films stemming their matrix on the surface, or through the fact that they provide material properties such as extremely high hardness or enhanced elasticity [14, 23] yet are still prone to failure before the desired lifetime of the sliding interface due to wear mechanisms like abrasion, spalling, and delamination [1, 3-6, 10, 14-16, 18, 19, 23, 25-27]. Despite the success of these forms of lubrication, particularly in specifically tailored environments, their own breakdowns emphasize the need for in-depth study of their own protective mechanics. It is the goal of this section of the thesis to further explore the ability of solid lubricants in terms of both transfer films and hard tribological coatings to enhance the tribological performance of various industrial contacts.

1.2 Research Objective 1

To investigate the protective mechanics of single component transfer film, composite transfer film, and hard coating solid lubrication systems through a synthesis of *in situ* tribological data with *ex situ* surface metrology

In terms of the work involving solid lubricant mechanics, experiments were performed for different single and multi-component transfer films, as well as different hard tribological coatings. The transfer films were comprised of MoS_2, MoS_2/Cu, and MoS_2/ Sb_2O_3 and applied

using an *in situ* self-replenishing slider pad-on-disk tribometer which will be explained below. The films were studied on both tungsten carbide as well as stainless steel substrates with a focus on film deposition, depletion, oxidation, conductivity, as well as friction and wear reduction of the interface.

Tribo-Testing. Analyses of the deposition mechanics, friction, and wear of the transfer film solid lubricants were carried out on a pellet-on-disk with slider pad tribometer outfitted for self-replenishing *in situ* powder lubrication shown in fig. 2. The friction loads at both the solid lubricant compact as well as the slider-pad interface are measured using load cells, while the wear of the solid lubricant pellet is tracked using an LVDT with a resolution of 1µm.

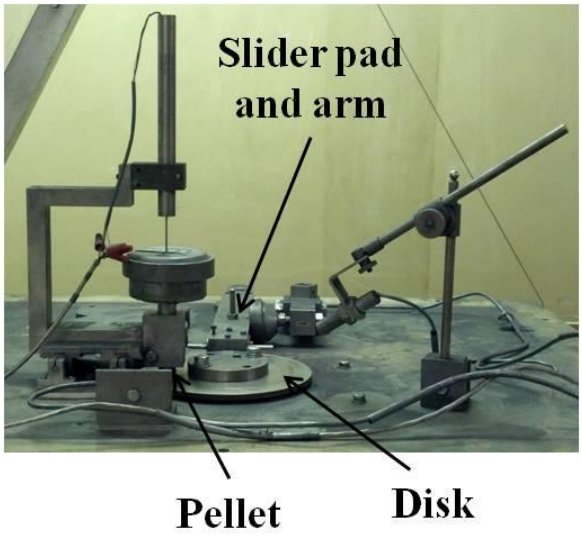

Figure 2: Pellet with slider pad-on-disk tribometer

Powder Lubricant Pellets. Solid lubricant pellets were created from loose powders, each with uniform particle sizes, in varying composition by weight. Single component lubricant pellets were made from MoS_2 with an average particle size of 1.7 µm through dry compaction at 2500 psi. Multi component lubricants were created to serve two purposes, oxidation control of the lubricant film and composite surface, and electrical conductivity. For improving oxidation

control, 1.7 µm MoS_2 and 1.5 µm Sb_2O_3 powders were combined in a 60/40 mixture by weight. For decreasing the electrical resistance of MoS_2 lubricants, 5.5 µm copper powders were combined in various percent weight compositions with 1.7 µm and 6 µm MoS_2.

Hard Tribological Coatings. The hard tribological coatings were magnetron sputtered through collaboration with the Timken Co., and comprised of tungsten doped DLC (W-DLC) as well as Chromium Nitride (CRN) at different thicknesses. The substrates used were a basic 440C stainless steel ordered from McMaster Carr, as well as 52100 alloy steel made at the Timken Co. Due to their industrial application of raceway coatings which experience primarily rolling friction and shock impacts, these coatings were investigated for their ability to reduce impact damage rather than sliding friction. Tribological data for impact testing was capture in the form of the coefficient of restitution displayed in equation (1.1).

$$COR = \sqrt{H_R / H_I} \qquad (1.1)$$

The impacts were conducted through drop testing on an in-house drop test rig (DTR) shown in Figure 3. Part A holds a spherical element through the use of a vacuum pump connected through the hose (Part B). A glass box encloses the test chamber while the lower specimen is held clamped in Part C. The impact is recorded using a high-speed video camera from Photron in order to precisely capture the rebound height for use in equation 1.1. Each material combination is tested at 9 different heights while the impact sites are marked for *ex situ* analysis.

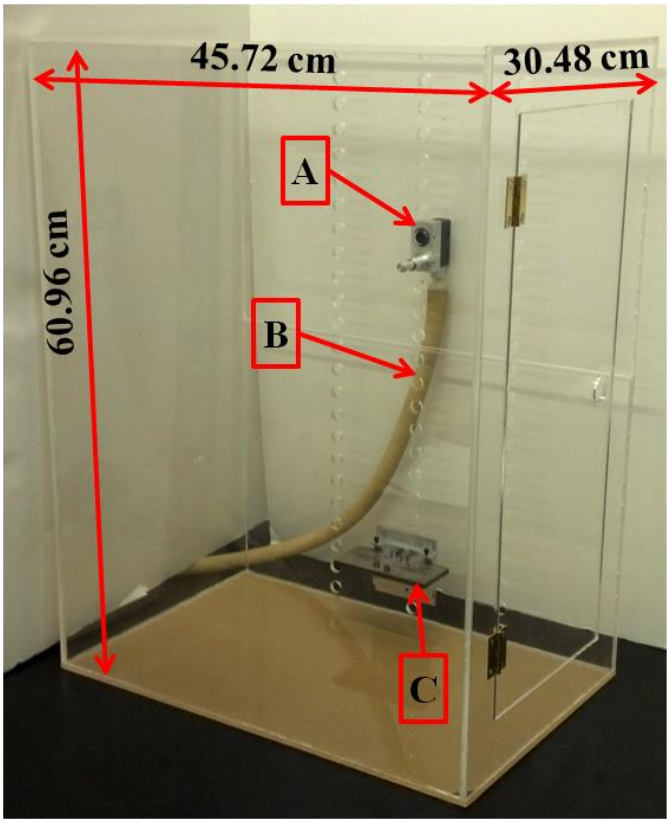

Figure 3: Drop test rig (DTR) for acquiring coefficient of restitution between rolling elements and a stationary substrate

*Ex Situ Analysis.*Powder films were examined and characterized using three different metrology instruments. A scanning white light interferometer from Zygo was used to measure the surface topography of all powder films, bare substrates, worn surfaces, impact craters. The Z resolution of the machine is rated at 0.1 nm, while a 20x objective was used to ensure a x and y resolution of 1.2 µm. This technique was chosen for its speed and accuracy, particularly when monitoring samples that may have loose debris accumulation, as well as its ability to create 3D topography data for input into numerical models. A hysitron nano-indentor, was used to characterize the hardness and elastic modulus of the bare substrates and hard tribological coatings. Lastly a scanning electron microscope (SEM) was used to in order to examine

subsurface damage as well as to ascertain information on the chemical composition of worn surfaces when applicable.

1.3 Two Body Wear Modeling

As industrial processes have continued to progress in complexity, it has been estimated that 70% of material failure in US industry is due to wear [28], resulting in a approximated cost of up to 100 Billion dollars per annum even by 1983 [29]. Although often detrimental, wear can be shown to possess beneficial aspects as well. Brake pads utilize wear to dissipate kinetic energy, while solid film lubrication often uses wear to establish lubricious transfer films [1, 18, 19, 28, 30]. While traditionally thought as a process to mitigate, this stresses an importance to understand wear on a more fundamental level.

To better explain the complexities of wear, a large breadth of work exists both in theory, experiment, and modeling. For instance, Archard [31] developed general wear laws to explain both adhesive and abrasive wear, while Challen et al. [32]and Hokkirigawa et al. [33] more specifically postulated abrasive theory behind different wear mechanisms with respect to severity of penetration. Similarly, experimental investigations have been conducted in order to validate these theoretical studies and their explanation of wear mechanisms. This includes work done by Dougherty et al. [4, 10, 18, 30, 34], Dearnaley [35], Trezona and Allsopp [26], Quintanilla and Goddard [36], and Kayaba et al. [37], in which wear mechanisms and relationships were characterized through surface examination and wear testing.

In synthesizing these theoretical and experimental works, many numerical models have also been constructed in order to predict wear behavior such that a better understanding of beneficial or detrimental wear might be gained. For instance, in chemical mechanical polishing

(CMP), simulations such as the Particle Augmented Mixed Lubrication (PAML) model [38-40] were developed to explore the beneficial wear of slurry particles in polishing copper wafers used to construct electronic circuits. In these models, a deterministic treatment was used in which surfaces were represented as a collection of cuboids called "voxels," and stresses are tracked at each asperity. Alternatively, other models have been developed in which a statistical treatment of surface contact is used in conjunction with existing, also statistical, theoretical models for wear debris generation in both lubricated and un-lubricated contacts [10, 32, 41-43].

Interestingly, many of these papers sought to treat friction and wear separately, in addition to using a static surface which does not involve over time resulting in predictions that are also static and constant. However, at the asperity level, it follows that the two phenomena would be inextricably linked due to their role as the resistance and deformation of asperity contacts. Even in terms of macroscopic behavior, this interdependence is highlighted by instances when surfaces are expected to wear while providing low friction interfaces such as self-lubricating interfaces. Often in these cases the material will undergo some type of wear process at the asperity level, such as transfer film formation, or plastic deformation, in order to improve lubricity. For instance, in Chapter 1 section 1.1, it was discussed how a sacrificial compact made of a lubricious material was used to spread a lubricating transfer film onto a hard disk. The sacrificial compact acts as one of the mating surfaces to spread its lubricious material in transfer film form through wear. In this type of configuration, shown to be inherently "self-replenishing" it is paramount to ensure a steady wear rate, or lubricant supply, into the interface while maintaining low friction during the wear process. Optimizing these types of configurations rely on ensuring a certain friction *and* wear behavior together, while *also* stressing the need to

understand surface contacts that are continually evolving. This synthesis of friction, wear, and surface evolution is highly complex and requires study both in terms of experiments and modeling, that is inherently deterministic rather than statistical. This is because statistical treatments of a surface will always include a distribution of or averaging of friction, wear, and surface evolution rather than simulating events as they would physically occur *in situ*. It is the goal of this section of the thesis to utilize a deterministic framework to simulate *in silico* two body wear which tracks both friction, wear, and surface evolution, which can be experimentally validated against results like those found in Chapter 1 Section 1.1.

1.4 Research Objective 2

Develop and Validate a computational model for 2 body friction, wear, and surface evolution; through a synthesis of *in situ* tribological data with *ex situ* surface metrology

The modeling portion of this work will utilize deterministic contact mechanics in order to model the friction and wear of two bodies in contact, and will be validated against experiments performed in objective #1. The contact and wear mechanics utilized in this work have been studied extensively and are derived from Hertzian contact mechanics coupled with abrasive wear experiments conducted by Hokkirigawa et. al [33] and Masen and Rooij [42], as well as analytical theory to apply these findings to a single asperity or a statistical collection of asperities carried out by Zhao, Maetta, and Chang [41]. These will be discussed at length in the modeling section of this thesis.

This work will differ from past attempts in that it will look to create a deterministic collection of asperities rather than use a statistical distribution. This is conducted to attempt to recreate data in which a surface is allowed to evolve naturally through the physics of wear, in order to capture true *in silico* virtual experiments and real life phenomena. The surface will be

represented as a collection of volume pixels of different heights, exactly like one would acquire from a surface profilometer. Representing surfaces in this fashion has been used in a number of numerical modeling studies to achieve highly accurate predictions of real contact area [30, 38-40, 44, 45]. However, very rarely are friction and wear coupled together with this technique such that the interactions of surfaces are not only captured at a given moment, but over time for a surface which is allowed to evolve through wear events[30, 38-40].

The work discussed herein attempts to synthesize a rigorous contact mechanics treatment, a new technique for calculating friction between asperities as they slide over one another, as well as a deterministic voxel framework using a collection of assumptions which can be summarized as follows:

1.) Surfaces will be represented as a collection of volume pixels of differing heights, identical to the data one would receive from a surface metrology tool such as an atomic force microscope or an optical interferometer. The harder surface will be assumed to be rigid in that it does not wear, and its asperity tips will be represented as Hertzian spheres of radius to be determined experimentally.

2.) Contact between interacting asperities will be tracked at each timestep with the harder spherical peaks indenting into softer asperity peaks assumed to be flat. The stresses will be calculated using Hertzian contact mechanics between the hard spherical asperity tips and the flat softer asperity tips. These mechanics expanded to transition between the elastic, elastoplastic, and plastic stress regimes, such that wear events can be determined in proportion to the amount of plastic stress present.

3.) Friction will be calculated both as the plastic flow work of indentation, as one asperity drags *through* the other, as well as the amount of overlap the asperity experiences from the previous timestep to capture the force as one asperity climbs *over* the other.

4.) The soft surface wear will be subtracted at each asperity in which the stress reached a critical limit sufficient to produce a wear particle; the surface topography will then be updated between timesteps allowing for real time surface evolution.

1.5 Additive Manufacturing Powders

Additive Manufacturing (AM) is a technique which suggests the potential to create parts faster, cheaper, expending less energy, and wasting less resources; all while drastically increasing the freedom of design complexity [46-48]. Generally the techniques of AM are categorized by the mechanism in which the metal powders are bound together, be it Direct Laser Sintering (DLS), Electron Beam Melting (EBM), or Inkjet Binding (IB). Each of these mechanisms is highly complex and in possession of its own body of work discussing constraints and challenges which also change from machine to machine. One thing which remains crucial to part creation in each powder bed process is the need to spread a uniform layer of powder at each build step [49-52]. Powder is delivered to the build area, often by a hopper, and then spread using some type of mechanical shearing implement such as a roller, rake, or wedge. The powder is then sintered or bound using one of the above mentioned mechanisms, and the process is repeated slice by slice until a final, cohesive part has been created inside the loose powder bulk. The flow behaviors of powders and granular material in general are considered to be extremely complex in the physics and engineering communities [53-58]. This is because they are discrete in nature, highly susceptible to the environmental conditions, and unable to be described by any

one value like viscosity [53, 54, 58-62]. However, understanding their own behaviors is crucial to optimizing the AM process and tackling its most serious implementation challenges[49-51].

While they stem from a myriad of factors, the most serious detractors to AM at present can all be related, at least partially, to issues at the spreading interface. Part integrity do to microstructural defects is one of the foremost issues, in which finished parts can have high porosity and/or poor surface finish [47, 49-51, 63]. It is follows that the creation of a uniform layer for sintering is an essential step to ensuring that a given layer is free of defects once the sintering process begins [49-51]. Unpredictable and non-uniform surface finish is also a common difficulty for additive manufacturing, and governed largely by the particle morphology and uniformity of the last spread layer [47, 50, 51, 61, 63, 64]. In order to achieve more reliable surface finishes which do not require expensive post-machining processes, things such as bi-modal powder distributions or nanoscale particles have been suggested, particularly for DLS or IB machines [51, 63]. While seemingly representative of a simple change, it has been shown that these alterations to the powder can cause severe impediments to uniform powder flow such as size-segregation, agglomeration, and jamming [56, 58]. These phenomena must be understood from a rheological perspective even before many of the other issues relating to the sintering step, because the creation of a uniform layer depends on smooth powder flow.

A second issue holding back AM is its currently limited material set when compared to subtractive manufacturing techniques. Due to the complex nature of powder flows, expanding the existing material set will involve a great deal of screening and optimizing flow properties to avoid issues with the powder spread and hopper delivery processes. This is directly tied to the fact that powders of different material, as well as those of the same material but of different make, have been shown to display a wide range of rheological differences [58-62, 65].

Another of the major challenges which AM faces is the need for improved build times. Currently the process is perhaps most attractive because of the complex part geometries which it can create. However, in order to take advantage of its potential for cost saving in any kind of heavy industry, it must show that it can print parts at a high rate. Currently, build times even for simple parts are quite long, and spreading represents a significant portion of time spent on a given layer. This time increases both with smaller particle sizes which demand more layers per part, as well as any spreads which must be repeated. Due to the infancy of spreading science, most machines employ rudimentary flow meters which monitor the volume of a spread. In order to maximize the utility of this elementary system, redundant spreads are used which double or triple the amount of time spreading per layer. In order to minimize build times, spreads must be done as fast as possible, as few times as possible, but without sacrificing layer uniformity. However powder flow has been shown to be highly dependent on the velocity [56, 58, 59, 66-68], and so this process currently requires a great deal of trial and error from powder to powder.

It is the belief of the author that optimizing the spreading process will be crucial to tackling this collection of challenges, and will involve understanding powder rheology with a focus on spreading as uniformly as possible but as fast as possible. Despite the potential for optimization of powder deposition through rheological characterization, there has been very little work published to study the flowability of AM powders with even less discussing how the flow can be tied to powder morphology or how it will affect the AM process. This may largely be due to the fact that most of the work leading up to 2015 has been done using basic gravimetric flow meters, in which the stress states of the powder cannot be controlled or directly correlated to those in the AM process [51, 69-71]. Without more direct matching of the stress states, the relevance of efficient flow speed to AM will remain somewhat nebulous. It is the goal of this section of the

thesis, to provide a rigorous characterization framework to describe the flow properties of AM powders such that manufacturers will be better equipped to tackle rheological issues throughout the AM process.

1.6 Research Objective 3

To relate the flow properties of metallic powders to different additive manufacturing processes, using a combination of *in situ* powder rheometry and *ex situ* microscopy

The Additive Manufacturing Portion of this research is dedicated to experimentally characterizing metal powders by relating powder morphology to flow under conditions similar to those found in an actual AM machine. The powders tested were a collection of Ti-6Al-4v powders from four different manufacturers, as well five different powder materials from the same manufacturer. More details will be given in Chapter 6.

Figure 4: FT4 Powder Rheometer

Powder Rheometry. The rheology of each powder was analyzed using a Freeman FT4 powder rheometer shown in Fig 4. The machine itself has seen extensive use for powder characterization in a wide array of industries in which powder flow is a prime concern such as powder metallurgy, pharmaceuticals, and food processing [59, 62, 68]. The machine has several advantages over simpler devices like the Hall flow meter, in that it has the ability for highly precise *in situ* data capture, and the ability to impose a variety of different stress states. This last advantage is crucial for capturing data relevant to AM, as powders will behave very differently under different stress states, and a test in which simple gravimetric flow is monitored may not be enough to describe the variety of flows in the AM process.

Despite the advantageous of the FT4 rheometer only a few papers have been published until very recently [72, 73]. In these papers, while they consider the effect of recycling on the flowability of a single powder type, very little is done to discuss how the stress state allows for comparison of the rheometry flow to flow in the AM process. In order for rheological data to be relevant to AM it is crucial that this bridge be addressed between rheometry and specific areas in an AM machine. In addition, only single powder types for a given machine are considered and so a detailed discussion of how morphology will affect powder flow between manufacturers or materials is prohibited. It is the goal of this section of the thesis to expand upon these works by elucidating how particle morphology will affect powder flow for a wide variety of AM materials and manufacturers, as well as offer insight as to how given stress states on an FT4 can be correlated to relevant flows in an AM system.

1.7 Deep Well Rock Drilling

Given the world's diminishing fossil fuel reserves, drilling expeditions are forced each year to delve deeper to uncover natural resources [74]. In fact, the creation process for wells further down than 1.5 km, often below the ocean floor, has been specified as "deep well drilling." Due to the fact that the cost of a well increases exponentially with depth [75], the drilling process can represent up to 50% of the total project costs [74]. This is a result of a number of effects. The first of which occurs during the surveying stage where smaller bore holes are carefully drilled to assess the potential for an economically viable project and the precise location of the final well. The setting up and threading of the drill string during this exploratory stage can be costly, as well as dangerous at these extreme depths, especially given the unknown conditions and formations [74-77]. The largest costs incurred from drilling the final well are not only due to the energy spent drilling, but also from the replacement of worn bits, referred to as "bit trips", when the rate-of-penetration (ROP) becomes insufficient [74-85]. After a bit failure of this kind, a project shut down must occur, and maintenance must be conducted that involves removal, disassembly, assembly, and rethreading of the drill string at the ocean floor. The bits themselves are also difficult and costly to manufacture due to their complex shapes and materials such as carbide or polycrystalline diamond compact (PDC) [76, 79, 80, 86].

With these factors in mind, it becomes apparent that understanding the drilling process in terms of reducing bit failure while maximizing ROP, is paramount to minimizing the cost and dangers associated with such deep wells. Specifically, this knowledge requires better understanding of the bit-rock interface in terms of how the bit is able to penetrate the rock *as well as* how the rock damages the bit. During the deep drilling process, there are often two types of bits used. The first is called the roller cone bit, in which three cone-shaped rollers are covered

in cutters and allowed to freely rotate and crush the rock [84, 87-89]. While still used often in rotary-percussive drilling, this bit has largely been replaced in standard rotary drilling with the PDC bit, so named for its implementation of PDC cutters [77, 78, 81, 82, 85, 87, 90, 91]. Since it features no moving parts, a large part of PDC bit design has been focused on the individual cutters, inspiring a greater drive to understand single-cutter rock interactions [82, 92]. PDC bits feature a plethora of cutter configurations in terms of orientation, rake angle, cutting face material, and cutting edge bevel, each of which can be initially evaluated using a single-cutter study. These investigations attempt to simplify the drilling interface to a single PDC cutter against the rock.

While drilling with PDC cutters, there are generally considered to be two mechanisms for material removal: scraping and cutting [78, 82, 84, 87, 89-92]. Scraping is quite similar to traditional sliding wear, and takes place on any cutter faces which are not penetrating the rock, including the undersides of the cutter and any developed wear flats. In addition to being a cause of energy dissipation, these are areas in which the contacting edge is actually flattened through excessive wear. After the loss in cutting edge, a much lower contact stress than that required for penetration and a subsequent reduction in ROP follows as a result [77, 78, 81, 82, 85, 87, 89-92]. The scraping mechanism features low ROP and a frictional response of an abrasive or adhesive nature between surfaces. During the cutting mechanism, the PDC uses its inclined face edge to penetrate the rock, develop a cutting face, and plough forward, removing large chips of the rock similar to a classical metal machining process[90, 91]. The primary difference between rock cutting and metal machining is that the rock will be brittle and far less predictable due to its porous and non-uniform bulk which introduces complex solid and fluid effects. When cutting *and* scraping occur, the ROP is high and the frictional response will be a combination of the

scraping force from the undersides and the cutting force on the cutting face [91]. This second component is often referred to as drag rather than friction in the drilling community.

Conventionally, the breadth of single cutter studies have been carried out on lathe type machines such as the vertical turret lathe (VTL) [82, 92-95]. In these machines, cutting is facilitated by the interference of a cutter against the top face of a massive cylindrical rock substrate as it rotates at high speeds. The cutter is given a constant penetration depth, usually by machining a pre-cut such that the cutter will already be overlapping with the rock surface at start up. A key feature here is that the cutter is fixed at this height and *not able to descend.* As the rock rotates, the cutter creates a chip at its fixed height until the rotation is finished.

While able to capture very high loads and speeds, this VTL has some inherent drawbacks. Firstly, the forces are purely reactionary, which prohibits the parametric study of imposed loading. This is best depicted by Fig. 5a, in which the imposed loading conditions can be seen for a lathe type machine. Secondly, since the cut is kept at one constant depth, the data is generally far more uniform and dynamically simplified than cutters experience in the field 21. This is due to the fact that the penetration into a rock surface during actual drilling will not remain constant, but will react to complex changes in the rock, normal load, or dynamics of the drill string [77, 78, 85, 92]. This in turn has led to VTL studies being carried out primarily on extremely hard rocks such as white granite, to accelerate wear and make it more akin to the severe contact found in the field even on softer rocks. It has also been proposed that ROP and cutter wear are highly dependent on the initial creation of a uniform chip at the onset of cutting [92]. During this initial creation phase, in which the contact area is primarily on the cutters edge, stresses, temperature generation, and subsequently cutter wear will be at their most severe. These events can occur throughout the drilling process, during start and stop, as well as any dynamic events in which

steady cutting is interrupted and a new cut is developed. Since the cutter in a typical VTL is not allowed to descend, it must be set at an initial depth of cut and cannot be used to study the forces and reactions present during the creation of the cut itself.

In addition, lathe-type testing makes it very difficult to study other effects which are dependent on the ability of the cutter to descend. These effects include variable penetration depths, interaction at the boundary of different types of rocks or individual grains, transitions between cutting and scraping, the hydrodynamic lift from lubrication, and dynamics such as bit-bouncing. One last difficulty with turret lathes is the technique utilized to capture extended periods of cutting. After one revolution, there will be nothing left of the rock substrate in front of the cutter. To combat this effect, most machines feature a mechanism which will allow the cutter to be moved during a test, tangentially to the cutter direction. While succeeding in being able to cut until the edge of the disk is reached, this process also results in the creation of a horizontal cutting force resisting this "feed" motion [92]. Consequently, wear profiles and forces on the cutter are further removed from the realistic drilling process.

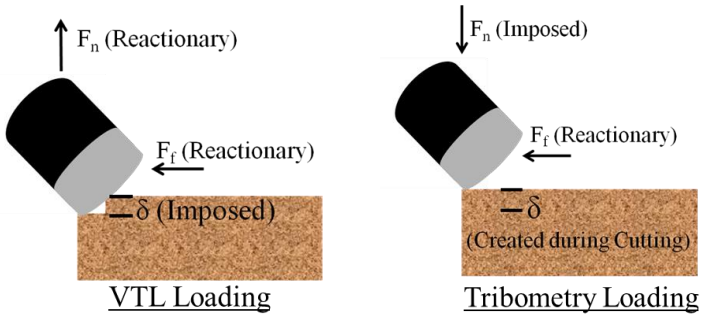

Figure 5: Loading Conditions in Typical Single Cutter PDC Studies

In the field of Tribology, the phenomena of friction, lubrication, and wear (material removal) are generally analyzed together due to their interdependence. Often this is conducted

through pin-on-disk tribometer testing (tribometry), which attempts to study the interfacial mechanics of relatively sliding surfaces *in situ*, such as friction and wear, while simplifying the complex sliding geometry [19, 28]. This is such that insights can be drawn about specific wear mechanisms in regard to their frictional response and lubrication regime. Then they can be optimized in an organized fashion [19, 28, 92, 96]. A key aspect of this process is that the pin is allowed to penetrate into the disk as the test progresses. This facilitates the unconstrained study of parameter relationships during the deformation, cutting, or wear of one material, as well as any hydrodynamic lift which occurs due to lubrication. The loading conditions are summarized in Fig. 5b. This suggests that tribometry would be a particularly useful way to study single-cutter drilling processes. For instance, using tribometry would permit the study of depth-based phenomena such as cut creation, dynamic changes in depth of cut and contact area, or even the encounter of different rock lithologies as a function of depth. In addition, it allows for the study of lubrication effects such as the creation of a hydrodynamic film and subsequent lift which reduces contact and friction in the cutter-rock interface. As a supplement to the *in situ* data, characterization of the two substrates is generally conducted *ex situ*; either with chemical, mechanical, or surface metrology tools, such that a full picture can be drawn of the interfacial interactions [18, 79]. While this type of approach seems well-suited to the validation of single-cutter designs in both ambient and deep well scenarios, with its ability to study forces outside of a purely constant DOC, very few studies exist in which tribometry was used. This is most likely due to the difficulty in applying accurate loading conditions and relevant materials on precision tribometer rigs. However there have been works such as that by Beste et al. in which carbide buttons, rather than edged PDC cutters, were characterized for friction and wear on a number of different rock substrates [79, 80]., In both of these bodies works, the loads were kept much lower

than those typically found in the field, and the cutting materials were not fully relevant to the deep-well drilling process. The importance on variable forces during dynamic events in rock cutting stresses, coupled with the potential for highly precise benchtop data acquisition through tribometry, stresses the need for dynamically varying DOC studies on the tribometer to supplement those carried out by a traditional VTL. It is the goal of this thesis to utilize the benefits of tribological analysis, while also improving the capabilities of the current body of tribometer studies to more industrially relevant materials and loading During testing, the focus will be to elucidate the tribological interactions present in the cutter/rock interface by a combination of friction and wear analysis with surface characterization of the rock substrates.

1.8 Research Objective 4

To investigate the cutting mechanics of industrially relevant deep well rock drilling materials through a synthesis of *in situ* tribological data with *ex situ* surface metrology

For the work concerned with investigating the mechanics of deep well rock drilling, rigorous single cutter experiments were carried out using two different types of cutters on a number of different substrate and lubricant combinations. In both cases the experiments were carried out on tribometers retro-fitted to provide accurate, *in situ* tribological data, but at a more manageable size for academic research. High speed, low load testing for O1 tool steel cutters under dry conditions was carried out on the same tribometer utilized previously for solid lubrication studies. High load, moderate speed studies were carried out using a Bruker UMT-3 tribometer outfitted with a lubricant chamber capable of handling industrial drilling muds and an in-house PDC cutter. This machine is featured in Fig. 6 and is capable of loading up to 1kN as well as speeds up to 3000 rpm.

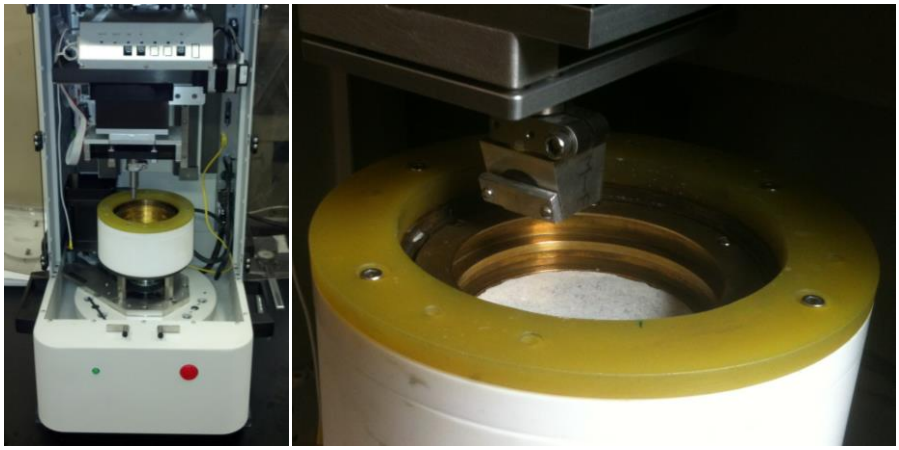

Figure 6: Bruker UMT-3 tribometer retrofitted for *in situ* tribological characterization of rock cutting mechanics

Rock substrates were chosen, based on their prevalence in industrial drilling, to be Carthage Marble, Nugget Sandstone, and Mancos Shale. Industrial lubricants using an oil, water, and synthetic base were employed from Chevron and Newpark Lubricants, as well as regular water as a base comparison. The tribometer was able to measure friction from the cutting force, as well as rate-of-penetration (ROP) as the cutter descends into the rock substrate. In addition, *ex situ* analysis was carried out using the same OI described above.

Section 1: Studies in the Protective Mechanics of Powder Transfer Films and Hard Tribological Coatings

The following section contains four chapters (Chapter 2-4) which detail experiments conducted to further the understanding of solid lubrication both in terms of transfer films and hard tribological coatings.

Chapter 2: An Investigation of the Wear Mechanism leading to Self-Replenishing Transfer Films

This chapter describes the study of in situ transfer film formation for self-replenishing solid lubrication. A similar version of this chapter has been accepted as a journal paper in the *Journal of Wear*. [Dougherty, P., Pudjoprawoto, R., Higgs III, C.F., "An investigation into the Wear Mechanism Leading to Self-Replenishing Transfer Films". *Wear*, 272(1), pp. 122-132.]

2.1 Introduction

While oil-based lubrication remains one of the most prolific areas of lubrication study, continued advancements in mechanical technologies continues to push interfacial temperatures for bearing related contacts beyond the capabilities of liquid lubrication. In fact, at temperatures above approximately 500 ºC, oil based lubricants can actually dissociate and lose their ability to carry load or provide ample lubrication [1].

Lamellar powders or solid lubricants have become a promising alternative as thick film powder flows [2, 3, 4], transfer films [1, 5] and also as multifunctional additives to existing oil based lubricants [6]. Despite extreme temperatures and pressures, these lamellar powders have shown environmentally friendly potential while also providing extremely low friction coefficients as low as 0.02 [7, 8] Furthermore, the emergence of thin transfer films applied through "pelletized" lamellar powders have proven beneficial for *in situ* solid lubrication[5] and special multifunctional applications such as sliding electrical contacts[10].However, the mechanics involved in powder lubrication, while thought to express a mixture of both hydrodynamic and morphological effects, are still largely misunderstood [3, 4, 9, 10, 12,].

This current work aims to elucidate the precise wear mechanisms which produce and remove the transfer film when a compacted powder pellet under load is slid against a hard tungsten carbide disk in the presence of a loaded slider pad. In the past, it was assumed that this was primarily governed by adhesive wear occurring at the pellet-on- disk and slider-on-disk interfaces. However, this paper conducts a detailed investigation of the tribosurfaces before and after wear testing, in which optical profilometry techniques are used to identify the most probable wear mechanisms. Furthermore this study also sheds light on the nature of the transfer film coverage. Since the friction coefficient is assumed to vary with the fraction of the asperity domain covered by solid lubricant [5, 17], there have been questions regarding whether the

transfer film coverage occurs at varying heights with uniform area, or at varying areas with uniform heights. Results from this investigation provide insight into these issues as well. The paper begins with an overview of the research problem with respect to observed lubricant deposition and depletion behaviors. It then progresses to the experiments conducted to investigate the wear mechanism leading to the pellet transfer films. Finally, the results are presented and then discussed in order to explain why abrasive wear is likely the dominant wear mode leading to the transfer films observed, and ultimately the friction coefficients measured.

2.2 Overview of the Research Problem

The annular configuration of the *in situ* self-replenishing system can be seen in Fig. 7a. During operation, a lubricious transfer film is deposited by a loaded powder pellet onto a rotating disk which carries the film into the sliding contact of a riding slider pad. Figure 7b displays a schematic of the asperity regime, which helps to highlight the self-replenishing nature of the system by exaggerating the slider pad and pellet to be on the asperity size scale. The film itself is partially removed by the slider pad and disk asperity interaction, represented in Fig. 7b by the sparsely uncovered asperities. As the disk retraces its original path, these uncovered asperities interact with the pellet and a new transfer film is deposited. Thus it is inherently "self-replenishing" [1, 5, 17]. While there have been successes in modeling thick-film powder lubrication as fifth-order rheological models in a continuum framework [9 , 3, 4 ,11, 12], the mechanics of transfer film formation *in* situ prevents this type of approach for two reasons. First, these models neglect the mechanics of the lubricant in the asperity regime, where thin transfer films reside. Second, thick-film volume remains constant during operation whereas the volume in the interface of the thin transfer film increases and decreases as wear events are continuously occurring locally and globally within the film [1, 5, 17].

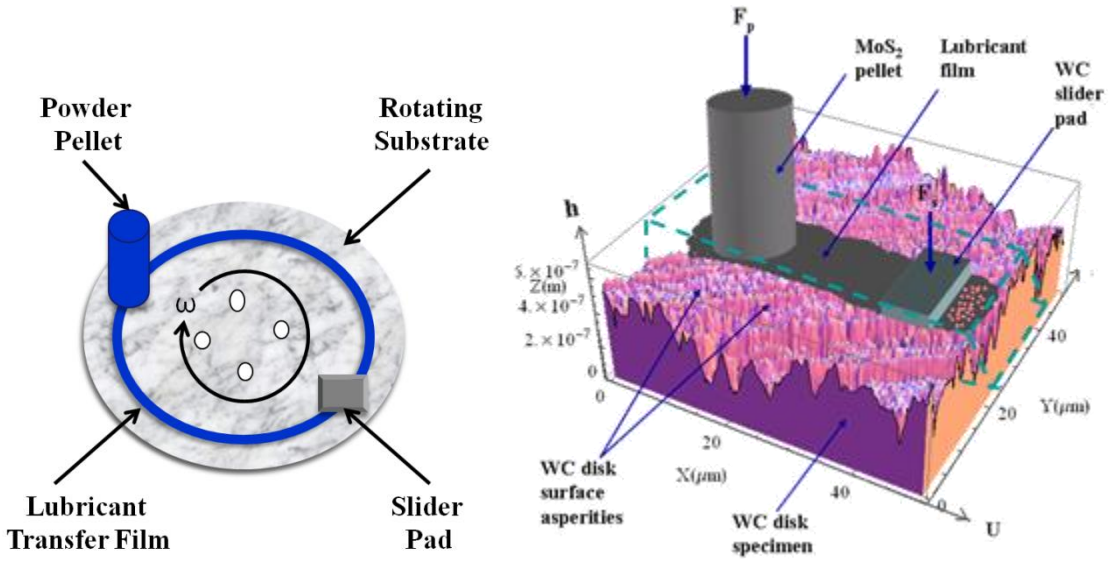

Figure 7: Visualization of the Self-Replenishing Tribosystem

Despite modeling challenges, the transfer film form of solid lubrication has great potential in the field of Tribology due to the system's potential to be self-contained and activated without external controls [13, 14, 15, 16]. In order to describe this type of tribosystem, models have been suggested which account for the transfer film mechanics through the use of competing rate equations derived from lubricant mass balances [5, 10, 13, 17]. In the Control Volume Fractional Coverage [5] model developed by Higgs and Wornyoh, a governing equation was developed to relate coefficient of friction (COF) to the deposition and depletion rates of the powder transfer film. Contrary to the rheological models which focus on distributed shear stress throughout powder films, the CVFC expresses COF as a function of the lubricant film height present within the asperity domain with uniform area coverage [5, 17]. In this type of model, a low friction coefficient is achieved by ensuring a large enough lubricant deposition rate, with respect to lubricant depletion rate, such that the lubricant coverage remains at a maximum during operation

In fractional coverage models, the deposition and depletion rates of the transfer film are formulated based on Archard's adhesive wear law as shown below [5, 17].

$$\dot{V} = \frac{K \times F \times U}{H} \quad (2.1)$$

where $\dot{V}$ is the volumetric flow rate of worn material, K is an empirical wear coefficient representing the probability of wear, F is the normal force between the bodies in sliding contact, and H is the hardness of the body being worn. K values are found typically through pin-on-disk testing in conjunction with tabulated approximations for two materials in adhesive wear [5, 17, 18].

This has three important consequences. First, these coefficients are often situation specific to the conditions present during testing. Secondly, the use of tabulated values carries a large amount of inherent error due to approximation assumptions [5, 17, 18]. And finally, these K values represent the probability of a wear event occurring, meaning they are merely a fraction between 0 and 1 meant to account for the average wear over a given time. However, due to the aforementioned transfer film models' inherent reliance on competing wear rates to determine COF, this type of averaging fails to capture the highly transient nature of the self-replenishing system.

For example, Figs. 8 and 9 display the results for two different instances where erratic wear behavior *in situ* leads to a subsequent inability to predict the transfer film dynamics of the self-replenishing system. In these figures, the pellet wear, displayed as the change in pellet height over time captured through a Linear Differential Voltage Transducer (LVDT), is graphed below friction coefficient of the slider pad. One should note that pellet "wear" actually refers to the "deposition" of lubricant film on the rotating disk as shown in Fig. 7.

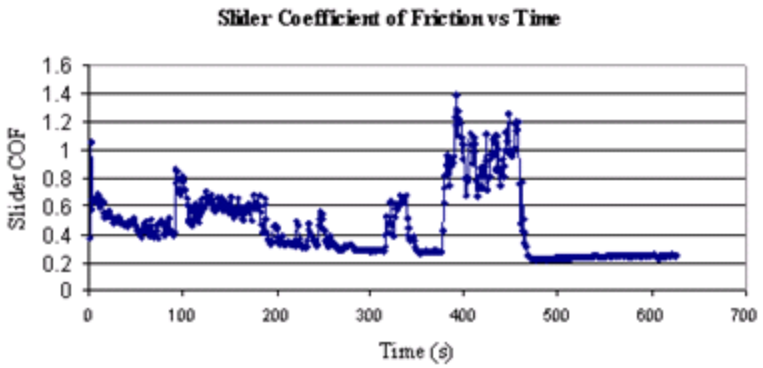

(a)

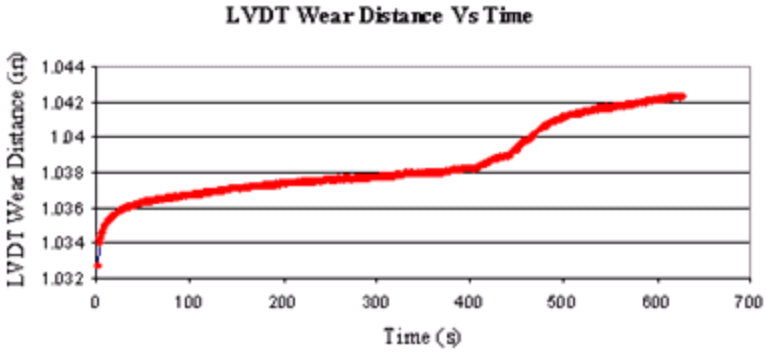

(b)

Figure 8: Lapses in Self-Replenishing. (a) Slider Friction Coefficient vs. Time. (b) Pellet Wear Length vs. Time.

The beginning of Fig. 8 displays a relatively routine run-in period, where initial wear is high and the establishment of a transfer film leads to a gradual decline in friction coefficient. However, as wear decreases, represented by a flattening of the LVDT wear slope, we see a drastic increase in friction coefficient. This is due to starvation of the slider-disk interface induced by ongoing lubricant depletion at the slider. A period of extremely high friction coefficient continues for about 100 seconds from time t = 380s to 480s, until the interface is replenished. Although wear (i.e. lubricant depletion) increases thus returning the system to equilibrium, this highly transient lapse in system lubrication is impossible to capture through the existing wear treatment and could be catastrophic in practical applications.

While decreases in pellet wear can lead to potentially hazardous starvation periods, there are also instances, as shown in Fig. 9, where increases in pellet wear are inexplicably insufficient to stabilize and lubricate the system during starvation.

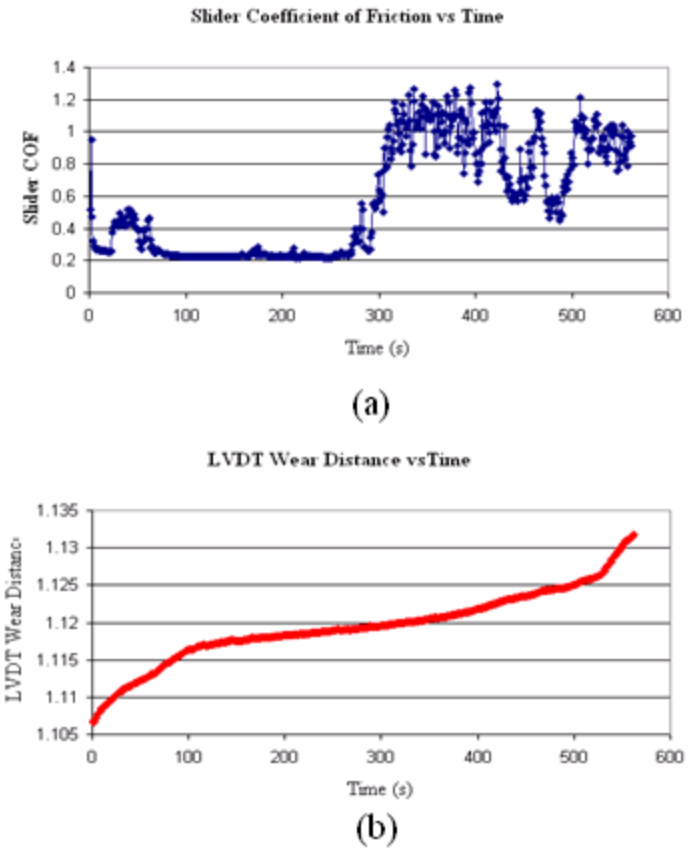

Figure 9: Indefinite Starvation through Unexplained Transfer Film Dynamic. (a) Slider Friction Coefficient vs. Time. (b) Pellet Wear Length vs. Time.

As in the case of Fig.8, low pellet wear and continued depletion by the slider leads to starvation present in Fig. 9 from time t = 100s to 300s. Contrary to predictions from our current transfer film modeling approach, the increase in pellet wear is unable to stabilize the system, thereby leading the system to "indefinite starvation." This type of system breakdown implies that something else may be happening to hinder the re-establishment of a transfer film and adequate lubrication conditions.

The combination of these two system failures in Fig. 7 and 8 helps to highlight the limitations of current modeling framework for *in situ* solid powder lubrication, both during the deposition of the transfer film as well as its operation during self-replenishment. Due to the constant nature of adhesive wear coefficients, current modeling techniques would predict a constant steady state COF at the slider/disk interface. However, transient film behavior leads to erratic and unpredictable COF in both cases. This study seeks to elucidate the precise wear

mechanisms at the pellet/disk and slider/disk interfaces in order to understand the evolution of a self-replenishing transfer film.

2.3 Experimental Set-up and Procedure

Transfer films were prepared and tested using a pellet-on-disk with slider pad tribometer [5] The pellet and slider pad COF was captured using calibrated load cells from Massload Co, while the pellet wear was captured using a linear differential voltage transducer (LVDT). The LVDT was attached to the loading mechanism above the pellet, such that a change in displacement, such as that presented in Figs 8 and 9 could be measured during pellet wear. Lubricant "pellets" were made by compacting dry molybdenum disulfide (MoS2) with an average particle diameter of 1.4 □m to a compaction pressure of 2500 psi. The slider pad and disk were constructed of sintered tungsten carbide (WC) in order to achieve negligible wear during experiment [5, 17].

Surface measurements were obtained using a Zygo NewView 7300 white light interferometer. A 20x objective was utilized in conjunction with 620x480 camera mode and minimum modulation ratio (minmod) of 8% to ensure low noise into the surface data while maintaining an XY resolution of 0.36 μm. Z resolution was rated at 0.1 nm with repeatability up to 0.01 nm RMS.

In order to investigate the specific interfaces at which the wear mechanisms may affect the transfer film process, tribometer experimentation was coupled with surface topography measurements taken with a scanning white light interferometer. First, standard tribometer runs were conducted in accordance with tribometer experiments outlined by Higgs and Wornyoh [5], to analyze the relationship between friction and wear at the pellet-disk interface. During these tests, the tribometer was allowed to run for 600 seconds with a dead load of 17.79 N (4 lbs) on the pellet. The slider pad was employed on the disk at a weight of 10 lbs, so as to facilitate depletion of the lubricant film and further wearing of the pellet. The pellet COF and wear (computed from the change in pellet length), were recorded through the load cell and LVDT.

The second branch of testing represents a combination of modified tribometer runs and optical interferometer measurements. The purpose of these runs was to aid in the visualization of transfer film behavior by examining the wear surfaces involved in the deposition and depletion of the transfer film itself. Preliminary surfaces of the pellet and disk are presented in Figs. 10

and 11 to act as control surfaces for post-test measurements. It is important to note that in Fig.10, circumferential lay lines from the polishing procedure of the WC are aligned in the direction of disk travel at the sliding interfaces.

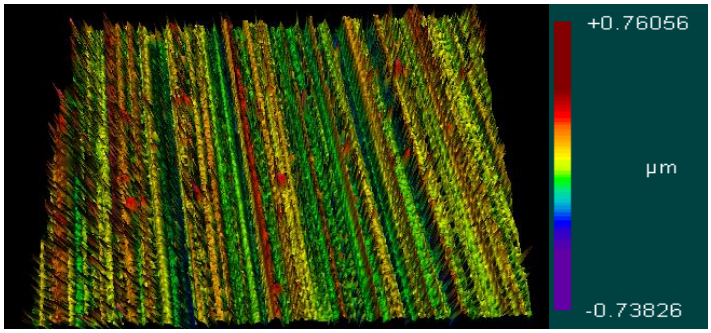

Figure 10: 3D Topography Scan of the Clean Disk (Pre-test)

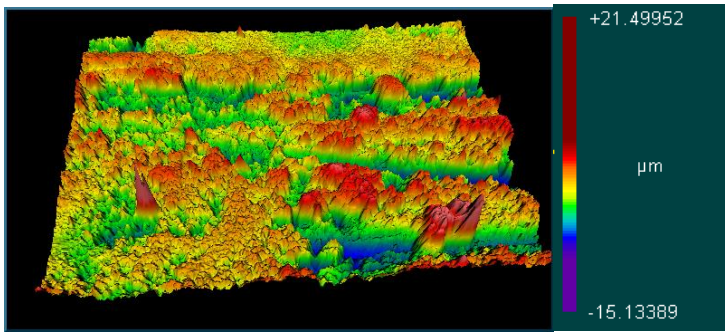

Figure 11: 3D Topography Scan of the Pre-test Pellet

Table 2.1: Roughness Parameters of the Pre-test Control Surfaces

Surface	Ra (μm)	Rms (μm)	PV (μm)	X Scan Length (mm)	Y Scan Length (mm)
Clean Disk (Fig. 4)	0.106	0.143	1.5	0.35	0.26
Pre-Test Pellet (Fig. 5)	2.410	2.995	36.633	0.71	0.53

2.3.1 Lubricant Deposition Testing

The first part of testing was conducted to facilitate lubricant deposition and prepare an adequate transfer film for study. The disk surface was run-in for 300 seconds, using the lubricant pellet at a 17.79 N (4 lb) dead weight, with no slider employed.

Both the disk and pellet were then taken to the interferometer in a sealed canister for analysis. The pellet surface was inspected at different contact points indicated by a worn, polished surface. Pellet wear topographies and roughness values were mapped and analyzed for comparison

against the control surfaces and existing examples of adhesive and abrasive wear presented in Fig. 12 [19, 20].

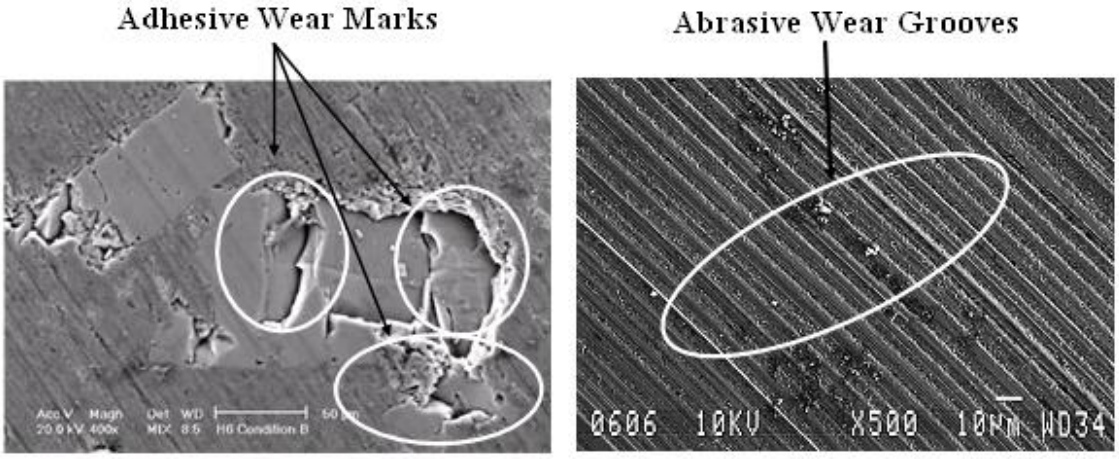

(a) (b)

Figure 12: Sample Images of (a) Adhesive Wear and (b) Abrasive Wear from Refs [19, 20].

Inspections of the established transfer films were conducted at different points along the disk surface to provide a picture of the disk after film run-in. Transfer film images and roughness values were compared against that of the clean disk presented in Fig. 4 to establish quantitative changes in surface topography due to the presence of the transfer film.

2.3.2 Lubricant Depletion Testing

Once the initial measurements were taken, the disk was returned to the tribometer for lubricant depletion testing. These tests were conducted with the slider pad only and loaded at 40.12 N (10 lbs) for 600s to ensure a noticeable change in the transfer film. At the end of each test, the disk was taken once again to the interferometer for surface measurement at different points along the wear track

2.4 Results

In this section, COF and LVDT data are analyzed to ascertain friction and wear correlations at the pellet/disk interface. Next, surface topography data is examined to qualitatively examine each interface involved in the evolution of transfer films. Lastly, roughness data provided through surface analysis is investigated to find a quantitative argument

for synthesis with the friction and wear correlations in order to propose a reprise to transfer film mechanics in later sections.

2.4.1 Investigation of Wear at the Pellet-Disk Interface

Figures 13a and 13b display the results of two pellet-on-disk with slider pad tests for pellet wear and pellet COF respectively. As explained previously, areas negligible of pellet wear correspond to flatter regions of the LVDT slope, whereas steeper regions correspond to high areas of wear. Using this relationship, it can be seen from the graphs that increases in LVDT wear correspond to actual drops in friction coefficient.

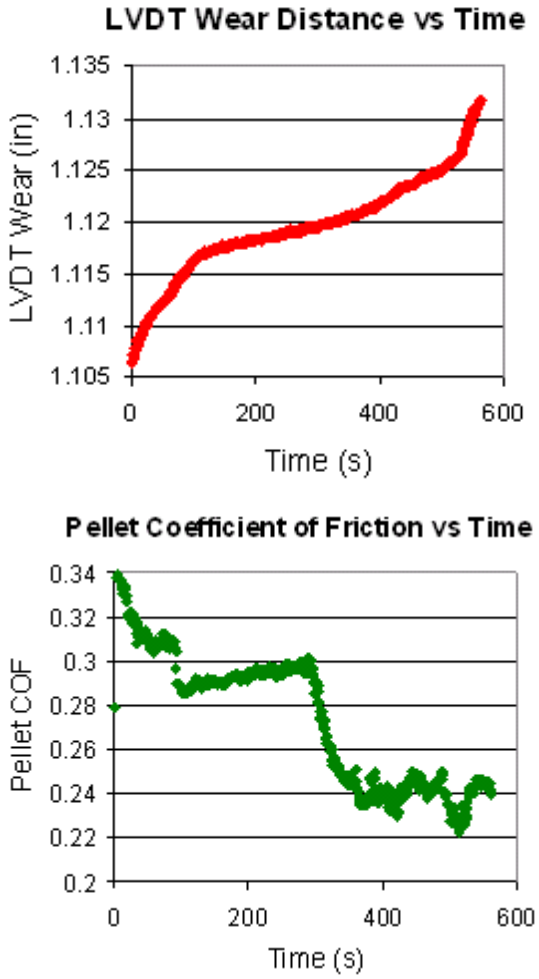

Figure 13: The Relationship between Wear and Friction in the Self-replenishing Tribosystem

While adhesive wear is known to lead to increased friction coefficient, due to the forces created between adhesive junctions on the contacting surfaces being primary components to the

friction force, abrasive wear is contrarily characterized by a decrease in friction coefficient through the carving of preferential wear tracks over time [22, 23].

While this friction and wear relationship alludes to the presence of an alternate wear mechanism, topography measurements for the worn MoS2 pellet, provide further evidence for abrasive wear. Figure 14 displays the surface topography for a worn test pellet after deposition testing. When qualitatively compared with Fig. 11 of the pre-test pellet, it can be seen that significant wear of the surface has occurred. In the case of the fresh pellet, the surface is very random, with little surface texture or orientation. However, after the establishment of the transfer film, the pellet surface in Fig. 11 acquires a set of parallel trenches similar to machined lay lines or textured surfaces similar to Fig 10.

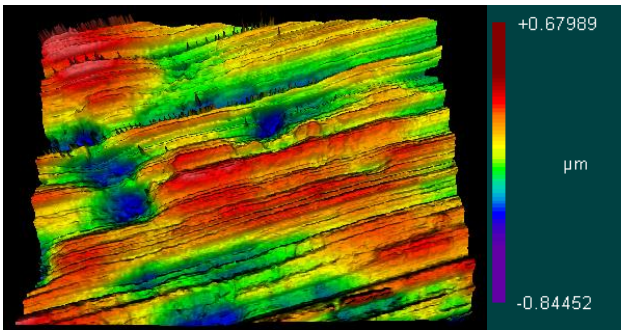

Figure 14: 3D Topography Scan of the Post-Test Pellet

Table 2.2: Roughness Comparison of the Post-test Pellet with Control Surfaces

Surface	Ra (μm)	Rms (μm)	PV (μm)	X Scan Length (mm)	Y Scan Length (mm)
Clean Disk (Fig.4)	0.106	0.143	1.5	0.35	0.26
Pre-Test Pellet (Fig.5)	2.410	2.995	36.633	0.71	0.53
Post-Test Pellet (Fig. 9)	0.155	0.193	1.524	0.35	0.26

A drastic change in pellet topography was also observed from the pre-test to post-test pellet through the roughness comparison presented in Table 2.2. In particular, average roughness values have decreased from 2.410 µm to as low as 0.155 µm. In addition, it is particularly noteworthy to compare the roughness of the post-test pellet in Fig. 14 to that of the clean disk in Fig. 10. After the conclusion of lubricant deposition testing, the pellet roughness values presented in Table 2.2 were shown to approach that of the clean disk.

2.4.2 Investigation of the Established Transfer Film

While images from the previous section present an idea of the pellet transformation during a test, the actual transfer film, as deposited on the disk surface is displayed in Fig. 15. This 3D topography scan provides insight as to the creation of the lubricant transfer film, which differs widely from the currently accepted theory of uniform area coverage.

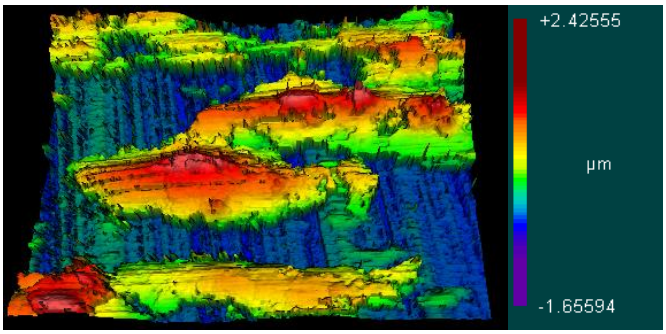

Figure 15: 3D Topography Scan of the Deposited Transfer Film

In order to differentiate the transfer film topography from disk topography, line scans shown in Fig. 16 were taken at different areas present in Fig. 15. Line scans from the relatively flat areas of Fig. 16, shown in blue, displayed nearly identical average roughness to the virgin disk (Fig. 10), whereas the other areas, highlighted in Fig. 17, displayed large deviations from this surface roughness. From this relative difference it was inferred that the disk topography is represented in blue, while the regions of differing color and roughness parameters represented deposited MoS2 film.

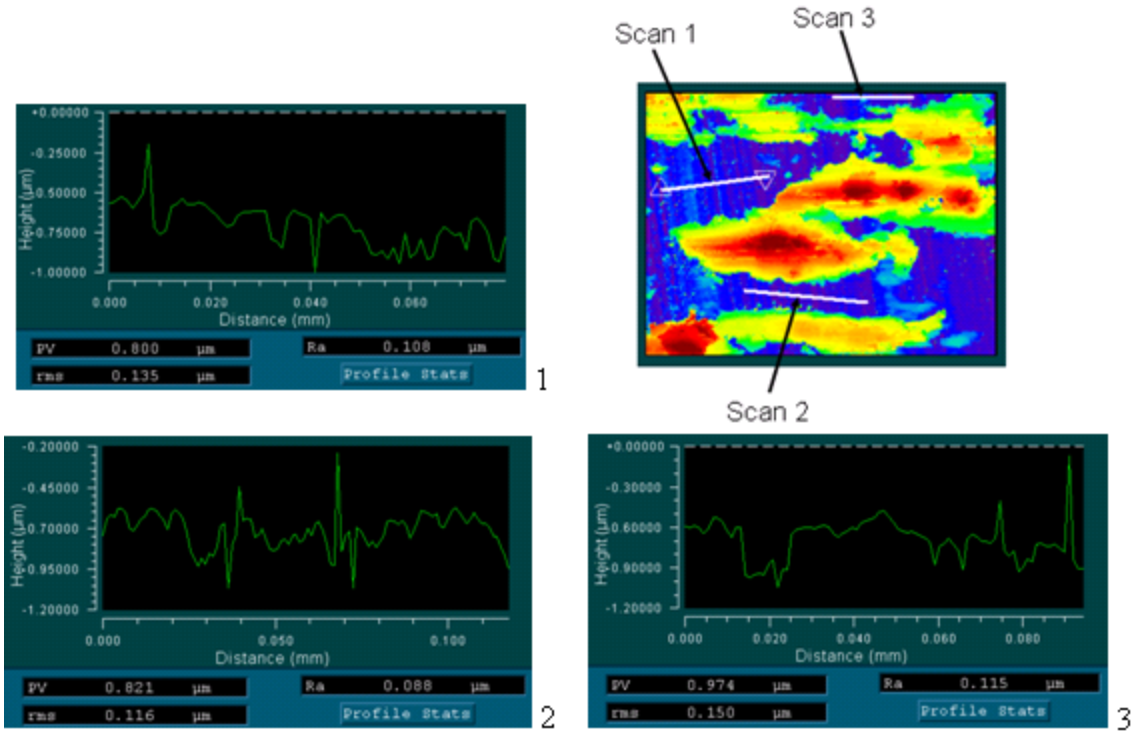

Figure 16: Line Scans Representing Disk Topography

After differentiating the topographies in Figs. 16 and 17, it can be seen at first glance that the film in Fig 15 follows a seemingly random pattern upon the surface with larger clumps spread out in the radial direction. This can be seen from the relative position of the clumps to the existing lay lines still visible on the blue disk surface.

Quantitative roughness analysis of the transfer film presented in Table 2.3 reveals that the surface topography has been fully altered from that of the clean disk. A line profile and its roughness parameters presented Fig. 17a, was taken through the larger anomalies denoted by the white line in Fig. 17b. By profiling the larger surface departures, one can see from the y-axis in Fig. 17a that these powder clumps are as high as 3 µm, while, from the x axis, sometimes as wide as 100 µm. These heights are far above that of the clean disk, indicating the presence of transfer film above the asperity regime.

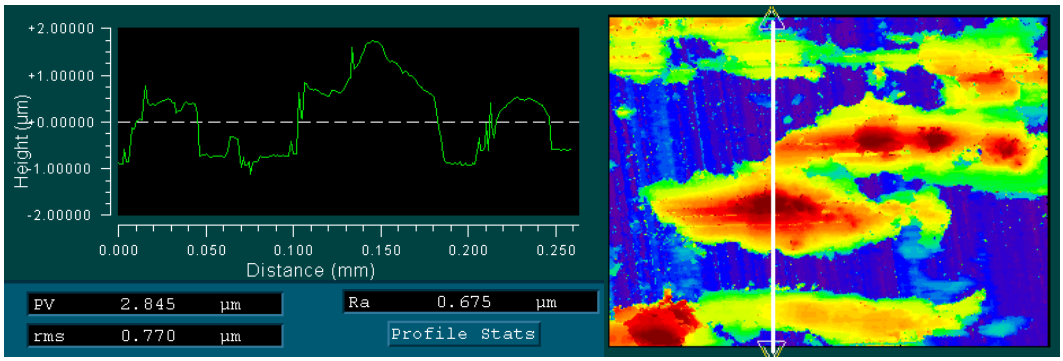

(a) (b)

Figure 17: (a) 2D Line Scan of Collected Powder on the Disk Surface, (b) 2D topographical map

Table 2.3: Roughness Comparison of the Deposited Transfer Film with Clean Disk

Surface	Ra (μm)	Rms (μm)	PV (μm)	X Scan Length (mm)	Y Scan Length (mm)
Clean Disk (Fig. 4)	0.106	0.143	1.5	0.35	0.26
Blue Scan Average (Fig. 11)	0.103	0.134	0.865	N/A	N/A
Disk and Film (3-D) (Fig. 10)	0.569	0.646	4.081	0.35	0.26
Disk and Film (2-D) (Fig. 12)	0..675	0.770	2.845	N/A	.26

2.4.3 Investigation of the Slider Pad Effect on the Established Transfer Films

While these images provide an idea of transfer film conception, the results of lubricant depletion testing will help to provide an idea of the effect of a riding slider on the fresh transfer film. It should be noted that lubricant depletion tests were conducted by imposing a state of starvation on the disk by removing the lubricant source such that a riding slider could wear away the film. While current modeling expects the removal of lubricant, and therefore a raise in COF at the slider interface, friction data taken from many depletion tests show trends to the contrary.

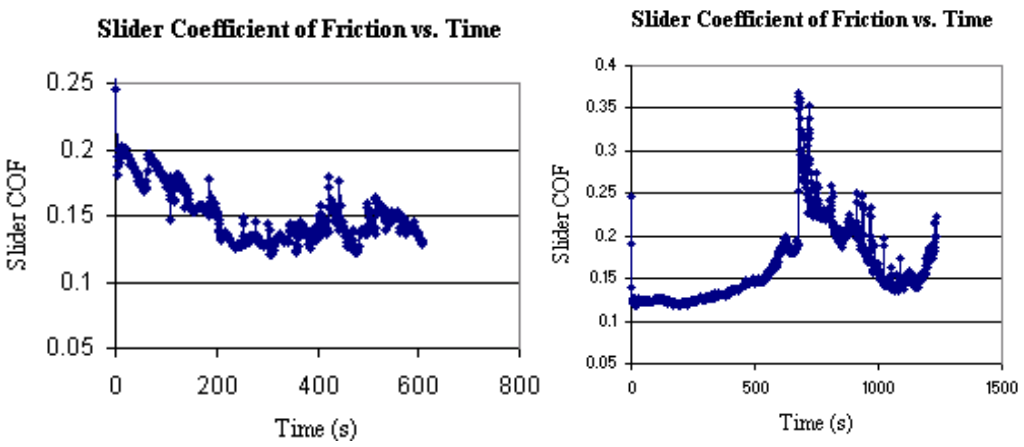

Figure 18: Slider COF during two Different Extended Depletion Tests

Figure 18 shows the COF results of two extended depletion tests where friction behavior actually decreased despite a complete removal of the lubricant source. While the second case does have an aspect of initial COF increase, both tests succeed in demonstrating that something more complex than just depletion is occurring at the slider disk interface.

By conducting surface analyses of the disk after lubricant depletion testing, a possible reasoning for this phenomenon is presented in Fig. 19. Without the continued supply of lubricant, depletion testing should result in removal of the solid lubricant from the system. From inspection of the figure however, there is a noticeable difference between the depleted disk and the original clean disk topography in the absence of solid lubricant.

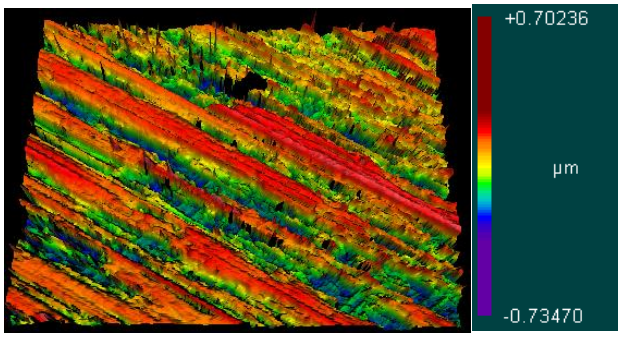

Figure 19: 3D Topography of the Depleted Transfer Film

In order to verify the presence of film above the surface, the SRz parameter and light intensity maps were calculated using the optical interferometer, as shown in Fig. 20. The SRz provides a unique understanding of two similar surfaces by taking an average of peak to valley height over an area. This is done to clearly differentiate between a surface with very uniform roughness and a surface with similar average roughness but deep valleys. For instance, if one surface has a much smaller SRz value than another surface with similar average roughness, it

implies that there may be a filling aspect occurring for the larger valleys. From Table 2.4, which shows a comparison of surface roughness between the clean disk and the disk after depletion testing, it can be seen that the SRz values for the depleted disk were about half as much as the clean disk. This implies that the valleys may have been filled with lubricant, thus lowering the SRz parameter.

Table 2.4: Roughness Comparison of the Deposited Transfer Film with Clean Disk

Surface	Ra (μm)	Rms (μm)	SRz (nm)	X Scan Length (mm)	Y Scan Length (mm)
Clean Disk (Fig. 4)	0.106	0.143	954.63	0.35	0.26
Post Depletion Disk (Fig. 13)	0.103	0.134	567.38	N/A	N/A

A light intensity map may also display key differences between similar surfaces. By showing up brightest at peaks and darkest at valleys, a distinction may be drawn between two surfaces. For instance if a build-up of film has occurred above the previous asperities, the light intensity will be higher, and will be represented by bright regions. Likewise, if valleys have begun to fill, we would imagine sharp differences in bright peaks and dark valleys to be changed to a more uniform grey.

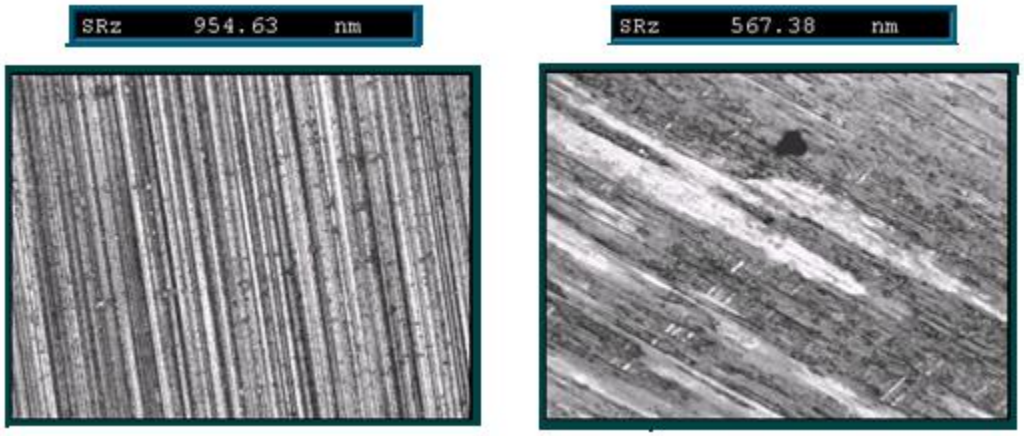

(a) (b)

Figure 20: Light Intensity Mapping of the Clean Disk (a) vs. the Depleted Transfer Film (b)

While the clean disk shows a very distinct striated pattern between peaks and valleys, the depleted disk shows a more uniform grayish finish, with wide and very high areas of bright

white. This last effect may be attributed to the build-up of film deep in the valleys and smooth film in the form of "plateaus" on top of the disk surface.

2.5 Discussion

Given the instances of unexplained wear behavior in self-replenishing powder tribosystems explained in Figs. 8, 9, 13, and 18; an investigation was undertaken to analyze interfaces involved in the transfer film evolution. This procedure yielded a series of qualitative topography observation and quantitative surface analysis, which will be combined in this section to propose alternative transfer film mechanics for an *in situ* self-replenishing tribosystem.

2.5.1 Transfer Film Inception

In order to study the creation of transfer films in a self-replenishing system, friction and wear relationships were established at the pellet interface through tribometer testing in Fig. 13. As wear increased at the pellet, a noticeable drop in friction over time was observed. Although previous works assumed that adhesive wear was the primary wear mechanism involved in the creation of MoS2 transfer films, Fig 13 displayed an inverse relationship between friction and wear characteristic of pronounced abrasive wear.

While this relationship provides initial evidence against adhesive pellet wear, surface scans taken at the pellet interface, reveal further leveraging for identifying abrasive wear as the predominant mechanism of lubricant deposition. Qualitatively this can be reasoned through the comparison of pellet topography with instances of adhesive or abrasive wear in Fig. 12. Adhesive wear would be characterized by a random pock marking at locations where adhesive junctions would have been formed and resulted in material removal during sliding [19, 22]. However, abrasive wear is identified as a pattern of parallel grooves where sliding asperities have ploughed into a surface [18, 20, 21]. This abrasive wear landscape agrees far more closely with the post-test pellet topography in Fig. 14.

This phenomenon can be explained quantitatively as well, in the close approach of pellet roughness parameters to that of the clean disk presented in Table 2.2. Despite a large difference in pre-test pellet surface roughness when compared to the clean disk, the roughness of the post-test pellet and clean disk become very similar as pellet is deformed through wear. The extremely hard WC asperities can be thought to indent and then plough easily through the soft MoS2

surface, leaving a pattern very similar to the parallel lines present on its own surface. This would result in the observed pattern of parallel grooves of similar dimension to the lay lines of the disk surface. Given the large difference in hardness between WC and MoS2, this type of abrasive ploughing [18] is supported by relationships where interactions between materials with drastically different hardness values have been shown to exhibit primarily abrasive wear [23]. It should also be noted that the post-test pellet roughness suggests that some of the particles at the surface have also been deformed, as evidenced by the roughness far lower than the characteristic diameter of the average powder particle.

2.5.2 The Pre-Slider Film

An early investigation of the film, before the employment of the riding slider, was performed through surface measurement of a transfer film after lubricant deposition testing. Recall, that these tests are conducted with only the presence of the lubricant source without any type of slider. Originally, thin powder films were theorized to adhere uniformly to the surface in the asperity regime. This effect was justified by the fact that lamellar powders, such as MoS2 and graphite, possess strong bonds within lamellar sheets, yet weak between lamellar sheets. Whole sheets of lamellar powder were thought to be removed through shearing while evenly adhering to the surface. These lamellae would coat the surface, lower friction and prevent further wear. [1, 24]

Analysis of our pre-slider film provides a different picture of the fresh transfer film, where powder collected as random, multi-particle clumps rather than mono-layer particle sheets. 2D line scan analysis of these powder clumps shows that the film to reside a full order of magnitude above the asperity domain, yet scattered around the surface, despite the previous modeling assumptions of transfer films residing at a variable height and uniform area in the asperity regime. This implies two factors: that transfer film lubrication is actually a function of area and height based coverages, and that actual transfer film lubrication likely begins as a combination of quasi-hydrodynamic or full film lubrication [9,11,12], mixed lubrication, and boundary lubricated conditions.

This random arrangement of particle clumps may also provide evidence that the pellet transfers film when sliding due to abrasive wear at the asperity scale. While adhesion would lead to more uniform coverage of lamella layers onto the surface which would prevent further wear at

a location on the disk. Abrasive wear could cause multiple clumps to fall loosely on top of each other. Disk asperities may be thought to violently plough into the pellet's surface and then continue through it, causing dislodged clumps of particles to separate randomly from the pellet. These particles could then collect together similar to a snow storm, in the multi-particle, stacked formations seen in transfer film topography presented in Fig. 15.

2.5.3 The Post-Slider Film

Analysis of transfer films after the application of a slider were also conducted in order to provide greater understanding of the mechanisms involved in lubricant depletion. Without the presence of a replenishment source, an effective starvation is simulated, and the slider should effectively "clean" the disk as the test progresses. Past modeling of this phenomenon has represented the slider acting *only* as a mechanism of lubricant removal.

In opposition to our expectations, qualitative inspection of the disk surface topography appeared to still contain large amounts of film. Despite similar roughness parameters to that of the clean disk, SRz analysis and light mapping were used to reveal the presence of a more uniform film residing both packed into the asperity valleys and collected above the asperity zone. A schematic is presented in Fig. 15 to aid in visualizing the dynamics of the riding slider pad on the transfer film.

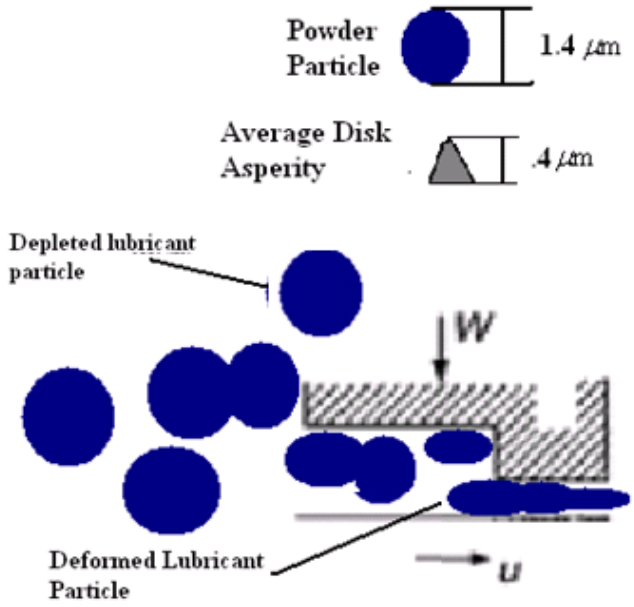

Figure 21: A Single Disk/Slider Pad Asperity Junction Visualized as a Rayleigh Step Bearing

Figure 21 models the interactions between disk asperity, transfer film, and slider pad asperity as a simple Rayleigh-step bearing configuration for visualization purposes. The contact interface between the slider and disk can be imagined as a collection of contacting asperities and the voids in between. If a disk or slider asperity is represented as the step region of the bearing, these voids between the asperities can be represented then by the entrainment region. Due to the larger size of powder particles compared to disk asperities, some of the powder is ejected from the interface as shown by the depleted lubricant particle. However, some of the very soft powder particles may be entrained into the gap leading to deformation and smoothening of the transfer film both over the surface and into the voids. Gaps that are particularly filled could actually form layers of compacted powder above the disk asperities. These compacted regions are seen as the plateaus in the light intensity mapping presented in Fig. 20b, and can act as regions of full film solid lubrication.

This type of modeling could also help to explain a phenomenon found during lubricant depletion testing, where friction values actually lower over time despite the absence of a lubricant replenishment source. The presence of a slider on the fresh film could not only act to deplete the lubricant film, but also to spread the film evenly throughout the surface, This would lead to increased lubricant coverage of the surface and therefore less friction at the slider interface even in the absence of a replenishing lubricant source.

2.6 **Summary and Conclusions**

While solid powder transfer film lubrication possesses the potential to be a viable commercial lubrication technology, much of the predictive science for its behavior is still immature. In particular, the problems of starvation and replenishment lapses impede its confident implementation into practical systems. It was the goal of this study to investigate the wear mechanisms which govern the transfer film evolution in an effort to enhance the existing knowledge a self-replenishing powder transfer film tribosystem. Based on the results from this work, Fig. 22 was developed to describe the process by which transfer films initiate and endure in a self-replenishing tribosystem. In addition, a three-step hypothesis of what is actually transpiring at each interface is also provided.

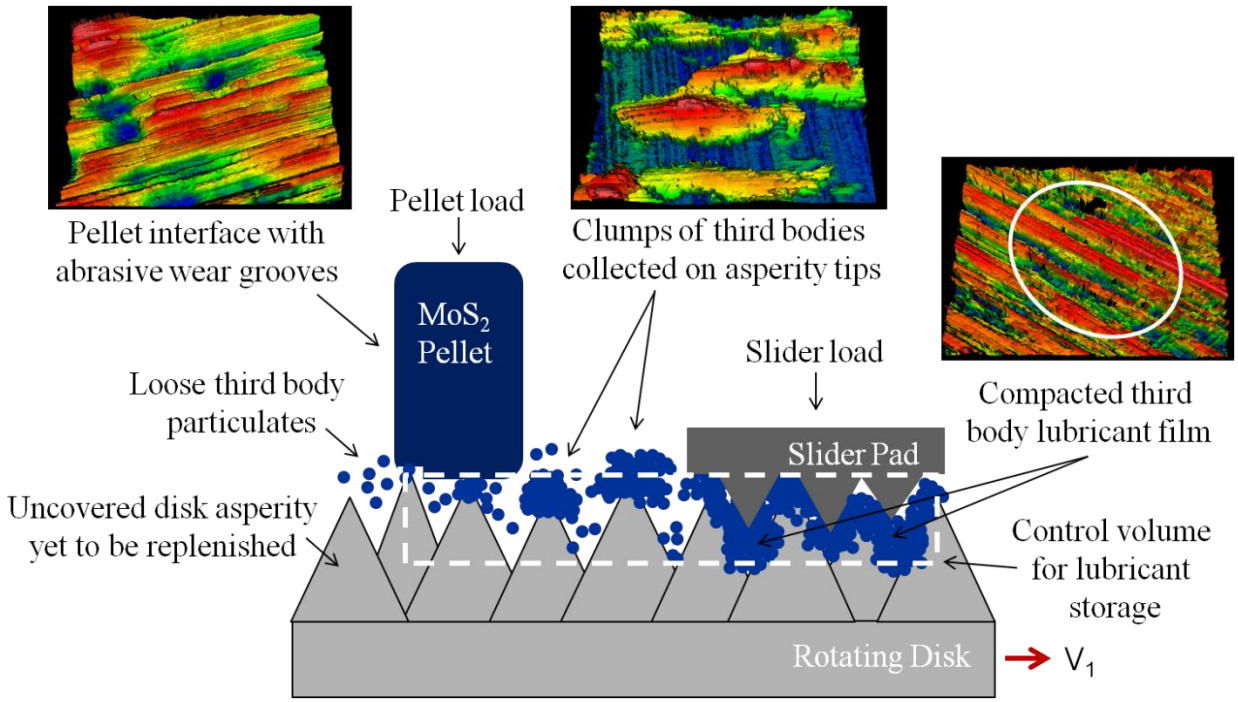

Figure 22: Schematic of Alternative Transfer Film Dynamics

1.) Pellet particles are removed primarily through abrasive wear. This is supported by both the relationship between pellet friction during periods of high wear and also by a surface topography evolution that is more characteristic of abrasive wear mechanisms.

2.) The loose third-body particulates fall and form large, multi-particle powder clumps above the asperity regime. This can be visualized intuitively as snow collecting on the top of a mountain. Evidence for this conclusion is provided through the investigation of disk surfaces after deposition testing. These measurements display a random collection of clumps which can be as large as two or three particle diameters, and as wide as 100 particle diameters.

3.) As the transfer film is carried past the riding slider, a combination of two effects occurs as displayed in Fig. 21. As soft powder particles of larger diameter interact with the slider, the result is not only a depletion or wearing away of the lubricant film, but also an entrainment effect where particles are drastically deformed in order to fill

the valleys and gaps between disk/slider asperity contacts. The slider entrainment effect can also lead to the formation of "plateaus" above disk asperities which could provide full-film quasi-hydrodynamic lubrication. This effect may be the cause for a decrease in friction coefficient despite the imposed starvation during lubricant depletion testing. Support for this conclusion is provided by both qualitative inspection of the topography change in the clean disk versus post slider disk images, changes in overall roughness parameters such as SRz, and difference in light intensity mapping between a clean disk and a post-test disk.

In closing, this work is meant to elucidate the wear mechanisms in a self-replenishing transfer film lubrication system where the sacrificial solid being worn is comprised of lubricious, lamellar powder. While previous modeling treatments may still provide acceptable results, inexplicable system behavior in highlighted cases stresses the need for a greater understanding of wear mechanisms in the transfer film process. This work aims to give evidence that asperity-scale abrasive wear is actually dictating the tribological performance of the pellet-on-disk with slider transfer film process, while also helping to uncover the state of the transfer film at different stages of the self-replenishing process. By gaining a proper understanding of the wear mechanisms leading to the deposition and depletion of the transfer film in this tribosystem, the authors hope to be able to facilitate improved modeling of self-replenishing transfer film experiments.

Chapter 3: Shear-induced Particle Size Segregation in Composite Powder Transfer Films

This chapter is concerned with the mechanics governing composite transfer film performance, and the phenomena of particle size segregation. A similar version of this chapter has been accepted as a journal paper in *Powder Technology*. [Dougherty, P., Marinack M. C., Sunday, C.M., Higgs III, C. F. "Shear-induced Particle Size Segregation in Composite Powder Transfer Films." (2014): 264, pp 133-139]

3.1 Introduction

This work aims to further the study of lubrication through solid transfer films. In particular it examines the pitfalls described in the previous chapter, in which self-replenishing solid lubrication is marred by sudden and inexplicable increases in frictional behavior. In addition, this paper explores transfer films which employ composite powders to serve a multi-functional purpose. Both the ability to provide reliable solid lubrication which is less affected by transient vacillations, and expand the utility of a given transfer film to be more robust are among the chief obstacles to the solid lubricant community.

3.1.1 Multi-functional transfer films from powder composites

In an attempt to mitigate the need for case-specific solid lubricant selection, many researchers have sought to find combinations wrought from compounds that can perform different functions. This has generated a desire to understand the complexities inherent in having a lubricating medium that is not only solid but also made of different "composite" elements. It should be noted that solid films have been studied extensively and that those which develop both naturally, through the sliding wear of the two materials [1, 97-100], *or* purposefully by design [1, 3-6, 10, 15, 18, 97, 100-104], can provide lubricating qualities. In terms of *composite* solids, Naturally occurring films were shown by Heshmat et al. to develop through the creation of wear particles which are of differing size or elemental make up [98, 100]. These films are especially important because they lead to complex interfacial behavior which may not have been expected in the original design. While these films help to emphasize the need for further study of composite interfacial phenomena, this work will be more concerned with films which were designed and applied in composite form, to serve a multifunctional purpose. For instance, by combining graphite and MoS_2 in sintered matrices, a "chameleon" effect was displayed where one type of powder would act depending on whether the contact was humid or dry [7]. In a

previous work by the authors, composite films made of either copper (Cu) and MoS_2 for electrical conductivity and lubrication, respectively, or MoS_2 and Sb_2O_3 for solid lubrication without oxidation , were shown to perform better than homogeneous films [4]. The use of Sb_20_3 and Au dopants has also been used in sputtered composite coatings to increase hardness, density, and oxidation resistance of solid lubricants [105]. Although representing an elegant possibility for alloying powders and their lubrication characteristics into a multi-functional lubricant, this approach can still lead to inherent and yet unexplained problems. For instance, many composite film studies have reported transient issues with friction performance and uniform composition [6, 21]. In those studies, the desired performance was found to deteriorate over time without a definitive explanation. In investigating this issue, it is hypothesized by the authors that particle size segregation, a well-understood phenomenon within the granular flow community, may play a role in the transient segregation or "un-mixing" of composite powder films. This "un-mixing" could then affect the capacity of the composite powder to exploit the advantages of both its constituents. This would most likely have implications not only for friction, but for other functions such as oxidation resistance or conductivity which are heavily dependent on a well-mixed uniform composition in the film [106, 107].

3.1.2 Particle segregation in granular flows

Granular flow resides under the broader dry particulate flow community, where it is similar to, but distinct from powder flow, as described by Wornyoh et al. [1]. Powder lubricants are comprised of soft particles which flatten and coalesce into a film that is also known to adhere to the surfaces during sliding. However, granular flows are comprised of hard particles which retain their shape mostly and remain distinct particles which do not stick to surfaces; as a matter of fact, they slip on surfaces excessively. Granular flow particles are known to segregate when there are small variations in particle properties. Particle segregation involves the separation of individual particle species inside of a bidisperse or polydisperse flow, which is a flow designated by having two or more species (constituents). Bi/Polydispersity in a particle flow can be due to differences in any number of particle properties or characteristics such as the restitution and friction coefficient, size, shape, material density, etc. While particle flow segregation can be induced by variations in all of these characteristics, perhaps the most prevalent is particle size segregation. For example, Ottino and Khakar [108] provide a detailed review of studies

examining both density and size segregation for a range of particle flow geometries and situations. Particle size segregation has been observed in a wide variety of natural processes and industrial applications as well. Natural processes, such as avalanches, were studied by Gray and Ancey [109] who demonstrated that in an avalanche flow, the larger particles segregate to the top, where the flow velocity is largest, and move towards the flow front. In terms of industrial applications, size segregation has been studied in hoppers [110, 111] and silos [112, 113], as well as mixers [114]. Each of these geometries is used extensively in the solids processing industries such as pharmaceuticals and food processing.

Particle size segregation is a phenomenon which is seen in granular shear flows, as the shearing force induces the separation of species comprised of different particle sizes. Size segregation in chute flow was studied computationally by Fan and Hill [115], while size segregation in an annular-type shearing geometry was experimentally studied by Khosropour et al. [53]. Shear-driven size segregation in a parallel-type shearing geometry has been studied extensively by Golick and Daniels [116] and May et al. [117, 118]. In the work of Golick and Daniels [116], a bidisperse flow using glass particles with diameters of 4 mm and 6 mm, was initially placed between two disks such that the smaller particles resided at the top, while the larger particles resided at the bottom. As the flow was sheared between parallel disks, the larger particles began to segregate to the top creating a mixed flow for a period of time. However, by the end of the experiment, the flow was fully-segregated, with the larger particles now residing at the top of the flow and the smaller particles at the bottom. This classic trend of larger particles segregating to the top occurs because the smaller particles tend to fall through the gaps between the large particles in a sieve-like fashion.

3.1.3 The potential of size segregation in composite powder transfer films

In the current work, it is proposed that the shear-induced size segregation behavior witnessed in particle flows can be used to explain the frictional performance of composite powder transfer films which are being sheared in the interface. As such, it is the objective of this paper to propose particle size segregation as the driving agent for the poor tribological performance of select composite transfer films. In two-component composite films where one of the powders is comprised of a solid lubricant component and a non-lubricant functional component, drastic increases in friction have been observed as significant sections of the film become comprised primarily of the non- lubricious constituent.

3.2 Experimental Setup and Procedure

Composite transfer films have been produced by the shearing of powder compacts often called pellets. The original motivation was to create a multi-functional solid lubricant that could be applied during sliding as an electrically conductive transfer film. The creation of these composite lubricant pellets was carried out using copper (Cu) and MoS_2 powders. Two separate MoS_2 powders (obtained from Rose Mill Co.), with particle sizes of 6 μm and 1.5 μm, were each combined with pure Cu powder to produce the composite lubricant pellets. Characterization of the Cu powder was carried out in-house using a New View 7300 Zygo Interferometer, by taking the average diameter of 20 individual particles. Their average diameter was found to be 6 μm. This resulted in two separate powder pellet configurations, one consisting of 6 μm Cu and 1.5 μm MoS_2 and another consisting of 6 μm Cu and 6 μm MoS_2. The compositions were measured by weight percent (%) and were a subset of a broader range of powders studied in previous work [4].

Testing of the composite transfer films was carried out on a pellet with slider pad-on-disk tribometer, as shown in Fig. 2. Testing consisted of two phases. In the first phase, a loaded lubricant pellet at 17.91N (4lbs) would shear a continuous thin film onto the disk for 200s. The second phase of the test would employ a slider pad at 13.33N (3lb) in order to measure coefficient of friction (μ) and to apply a continuous shear force to the established film. The nominal contact pressures at the pellet and disk interface were 62.5kPa and 20.8 kPa respectively. The linear sliding speeds for both phases were 10m/s. In order to ensure that the removal of the film was not the reason for a change in μ behavior, the pellet was kept loaded against the disk during this second phase to replenish any lost film. This process is known as "*in situ* self-replenishing powder lubrication" in the tribology community [1, 18, 102].

3.3 Results

The friction behaviors of the various transfer films are presented in Figs. 23-25. In Fig. 22, a comparison of 60% copper (Cu) and 40% MoS_2 composite films with equal and unequal particle sizes is displayed. Additionally, the μ behaviors for both a pure Cu and a pure MoS_2 transfer film are presented to contrast against the qualitative performance of the composite films. As seen in Fig. 23, it is striking that choosing an equal particle size of 6 μm for both constituents

led to a low μ similar to a pure MoS_2 film. However, choosing a composite film with a different size of 1.5 µm for the MoS_2 led to a μ which would rise slowly over time, moving towards a value similar to the pure Cu film.

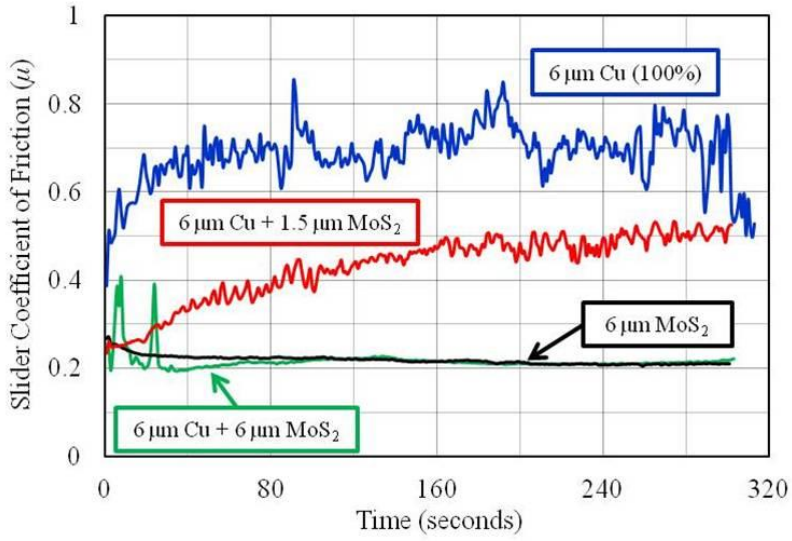

Figure 23. Slider coefficient of friction (μ) vs. time for Cu film, MoS_2 film, and composite films (60% Cu + 40% MoS_2) of equal and unequal particle sizes.

Parametric studies, which vary the composition percentage of the Cu/MoS_2 films with unequal and equal particle sizes, are shown in Figs. 24 and 25, respectively. As seen in Fig. 24 where the particle sizes differed, any composition percentage above 35% Cu led to an increase in μ over time. However, if equal particle sizes were chosen, as shown in Fig. 25, composite films containing up to 60% Cu still maintained low μ, near or below 0.2. Between 3 and 4 tests were run for each configuration, in which the qualitative trends remained reproducible, with small changes in quantitative friction values most likely due to variation in the ambient environment. As a result, the discussion of friction will focus on qualitative comparisons between configurations rather than quantitative values.

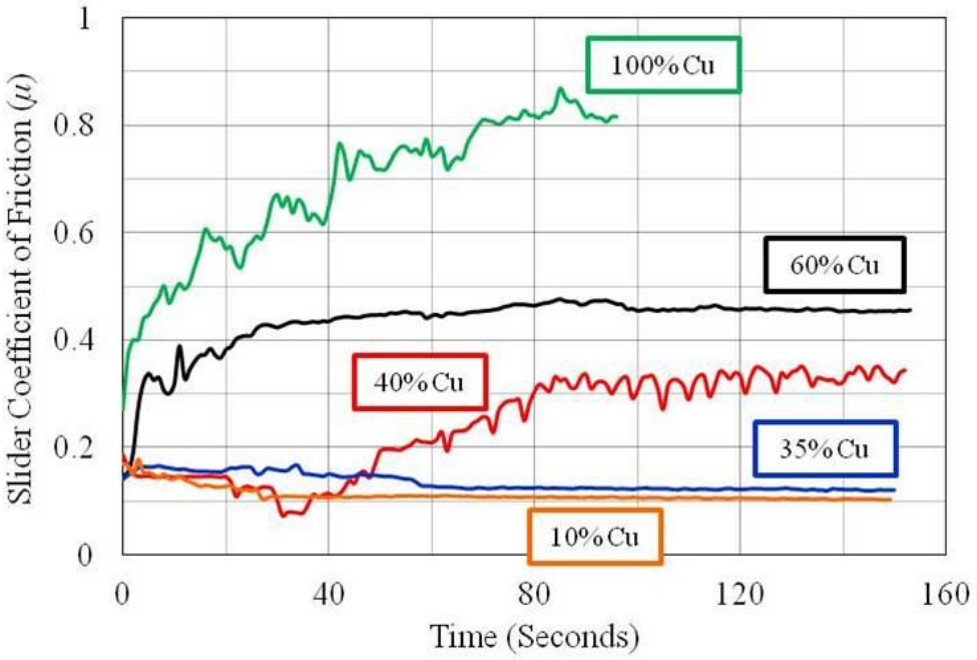

Figure 24: Slider coefficient of friction (μ) vs. time for transfer films of unequal particle sizes: 6 µm Cu + 1.5 µm MoS_2

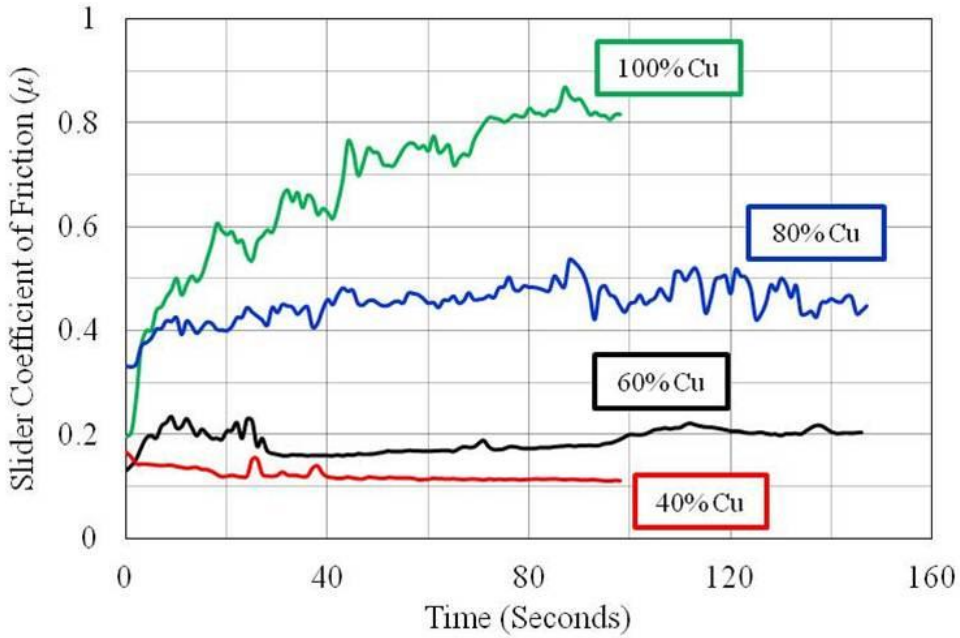

Figure 25: Slider coefficient of friction (μ) vs. time for composite transfer films of equal particle sizes: 6 µm Cu + 6 µm MoS_2.

3.4 Discussion

In reference to these results, this discussion aims to elucidate the observed frictional behaviors in Figs. 23 – 25 more rigorously, while proposing an explanation for the highly size dependent transfer film performance based on particle size segregation. In Fig. 23, this size dependence is particularly apparent. At the bottom, the pure MoS_2 provides a μ typical of low-shear solid lubricant films applied in this manner, which is at or just below 0.2 [2, 18, 102]. On the contrary, the μ of a pure Cu pellet is shown to exhibit the highest friction levels, with μ values reaching as high as ~0.8. Based on this behavior, it is quite clear that while a pure Cu film may provide exceptional conductivity, it would be unable to serve as a lubricant. Thus, multi-functional Cu/MoS_2 composites were developed in a previous study [4] to obtain a lubricant film which combined the electrical conductivity of the Cu with the lubricious behavior of the MoS_2. In this previous study, a Cu percentage of 40% proved to be a sharp threshold value for acceptable electrical conductivity. This was established qualitatively as a conductivity value surpassing the bare contact with a simple, static 2 probe sheet resistance test. As a result, it was important to increase Cu content as far beyond 40% as possible, without sacrificing lubricity.

Figure 23 includes the curves for composite Cu/MoS_2 transfer films with composition of 60/40 and particle diameter ratios of 6 μm/1.5 μm and 6 μm/6 μm. Despite the expectation of lowering μ with the addition of MoS_2, it was found that the behavior of the composite films was unsatisfactory when pairing 1.5 μm MoS_2 with 6 μm Cu. Interestingly, the μ would begin at low value, but slowly rise to a value closer to that of the pure Cu film, suggesting a transient degradation of film performance. When matching the constituents' particle sizes, a low μ (near pure MoS_2) was found to endure. In fact, equal particle sizes allowed for an increased Cu percentage of 60%, which is 20% beyond the minimum Cu content for acceptable electrical conductivity, while still maintaining low μ values.

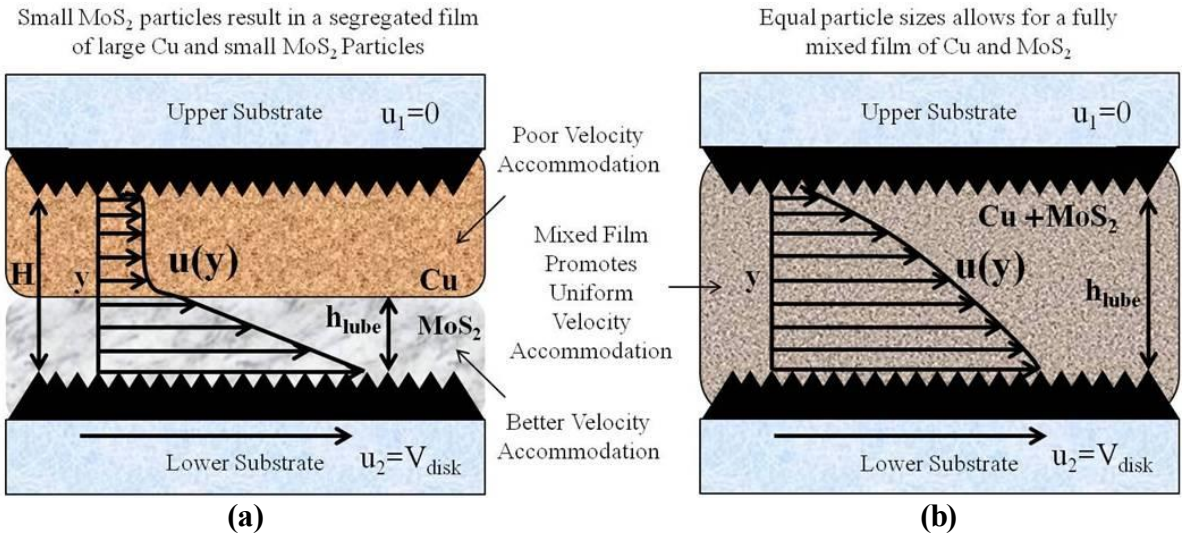

Figure 26: Conceptualization of the effect of particle size segregation on velocity accommodation and shear stress in (a) a segregated composite film and (b) a well-mixed composite film (adapted from [97]).

While otherwise mysterious, these differing μ behaviors of transfer films comprised of constituents with unequal particle sizes can be explained by the granular phenomenon of shear-induced particle size segregation. Although more difficult to imagine for powder transfer films, the process of segregation can be visualized by thinking of the composite film as a matrix of discrete particles. During the film's start-up period, it remains a well-mixed composite under shear between the disk and slider pad (see Fig. 26b). As such, the film is able to take advantage of the low μ of the lubricious additive; MoS_2 in this case. While in this state, there is sufficient MoS_2 throughout the composite film to utilize its lamellar structure and velocity accommodation between different film layers, even between the dispersed copper particles.

According to the theory of particle-size segregation, equal sized particles of MoS_2 and Cu, are likely to remain well mixed as the composite film is sheared. However, given the case of a smaller particle size MoS_2 (1.5 μm), relative to Cu (6 μm), these MoS_2 particles would eventually diffuse through the voids left between the larger Cu particles. This diffusion of the smaller particles occurs in a sieve-like fashion due to the shearing of the composite film between the slider and disk. This process will then continue until the film reaches a segregated state. At this point, the upper portion of the film would be comprised solely of larger Cu particles, while the bottom portion would be comprised solely of smaller MoS_2 particles.

It is possible to use the quasi-hydrodynamic nature of powder films, originally developed by Heshmat et al. [97, 100, 103, 104], to provide an explanation of why the friction rises as this type of segregation emerges. In a quasi-hydrodynamic powder lubricant film, such as MoS_2, shearing induces a fluid-like velocity profile across the layers, which allows the interfacial media to accommodate two sliding surfaces at different velocities. Figure 26 displays a modified version of the quasi-hydrodynamic diagram [97], in order to help visualize the effects of segregation on the velocity accommodation and frictional performance of composite films. It should be noted that this work extends the original quasi-hydrodynamic framework to include composite transfer films which are comprised of powder films with different particle size and elemental composition.

In a fully lubricious film, the interfacial media will act to decrease the overall friction by using its low resistance to shear and providing a smooth velocity gradient over the entire film thickness [97, 103, 104]. If we examine the classical relation for shear stress (τ) in a lubricant film, shown as Eq. (1), the film's low resistance to shear is similar to a low fluid viscosity (η). In powder flows this relation was expanded by Heshmat et al. to include other powder flow parameters in a fifth order rheological equation [97, 100, 103, 104]. However, for our purposes, the relation can be approximated as Eq. (3.1), which states that the shear stress in a powder film is proportional to the velocity gradient, *du/dy*.

$$\tau \propto \eta \frac{du}{dy} \tag{3.1}$$

On the other hand, if the same film was comprised of a non-lubricious material, it is believed that the film will effectively have a much higher η, resulting in a higher overall shear stress (τ). This higher shear stress will consequently result in a higher coefficient of friction (μ), as shown by Eq. (3.2), which relates μ to the shear stress (τ) integrated over the surface area (A) of the substrate.

$$\mu \propto \int_A \tau dA \tag{3.2}$$

Now with these characteristics of a quasi-hydrodynamic powder film in mind, Fig. 26a can help to explain the *quantitative* performance of a segregated powder film. In Fig. 26a, unequal particle sizes have led to full segregation in which the Cu section of the film, shaded in orange, resides on the top, while the smaller MoS_2 particles accumulate on the bottom and are

shaded lightly in gray. This segregation would have two important effects that would result in an increased μ. First, segregation causes a small portion of the velocity to be accommodated by solely Cu, which has a larger resistance to shear and therefore increases the effective viscosity of that portion of the film. As the MoS_2 segregates out of the Cu section, it cans no longer help to reduce friction between Cu layers as it would in a mixed case. Second, due to its inherently low shear strength, the majority of the velocity accommodation is still handled by MoS_2 but now across a reduced thickness, displayed as h_{lube} in Fig. 26. As a result of this reduction in h_{lube}, the velocity gradient *du/dy* in Eq. (1) must be larger to accommodate the required velocity difference between surfaces. This results in a higher overall shear stress in this section of the film according to Eq. (1). In order to calculate frictional force, one would integrate the profile of each film section as shown in Eq. (2), and combine their effects. This would explain the larger frictional force displayed in Fig. 25 by the film with different particle sizes, because segregation would cause any accommodation across the Cu section to occur with a larger η, and any accommodation across the MoS_2 section to occur at a larger *du/dy*.

Additionally, segregation can also help to explain the *qualitative* trend of the composite film with different particle sizes. As the powder film segregates, the MoS_2 would gradually diffuse to the bottom of the film. The amount of segregated Cu would grow at the top, thus forcing the MoS_2 to accommodate the majority of the change in velocity over a continuously diminishing h_{lube}. This gradual process would lead directly to a larger velocity gradient and shear stress which would increase in *proportion* to the amount of segregation present. As explained above, μ would increase over time, because it would reflect the effects of a segregating MoS_2 section. These effects would be an increase in effective viscosity in the Cu section due to a lack of MoS_2 and a smaller h_{lube}, both of which would worsen as segregation progresses. This correlates well with the experiment in Fig. 23, which displayed a slowly increasing μ value in the film for which segregation is a concern due to unequal particle sizes. By following this rationale, particle size segregation explains how the μ would not only be larger, but would also increase over time towards a value between that of the poorly lubricious and favorably lubricious constituents.

It is also possible to explore how matching the particle sizes enables the composite film to maintain low friction behaviors by considering a fully mixed film. In this case, such as in Fig. 26b, lubrication would not be a problem because low shear MoS_2 would exist at each layer of the

film. In turn this would provide velocity accommodation (i.e., a lubricious effect), even between the copper particles themselves, and allow for a more gentle velocity gradient throughout the *whole* film thickness. In other words, the lubricious particles could still act to reduce the stress between the less lubricious particles, lowering the effective viscosity throughout. If able to take advantage of the MoS_2 throughout the film, the μ according to Eq. (2), would remain low. As a result, this likely explains how preventing segregation by matching particle size, would lead to the low and stable μ witnessed in Fig. 23.

In order to further examine the effects of particle size segregation on the frictional performance of composite transfer films, parametric studies on the composition percentage of the two constituents were performed. The results of these studies were previously presented in Figs. 24 and 25, for composites with unequal and equal particle sizes, respectively. As shown in Fig. 24, lower copper percentages of 10%-35% exhibited low and smooth μ, despite the pairing of different particle sizes. In this case, it was thought that compositions above 65% MoS_2 were enough to overcome any segregation effects simply due to the large fraction of lubricant constituent in the film. However, when the Cu composition percentage goes up to 40%, segregation effects appear to present themselves, as frictional performance gradually deteriorates over time. As we increase Cu content beyond 40% (decrease MoS_2 below 60%), it is seen that these effects worsen as would be expected.

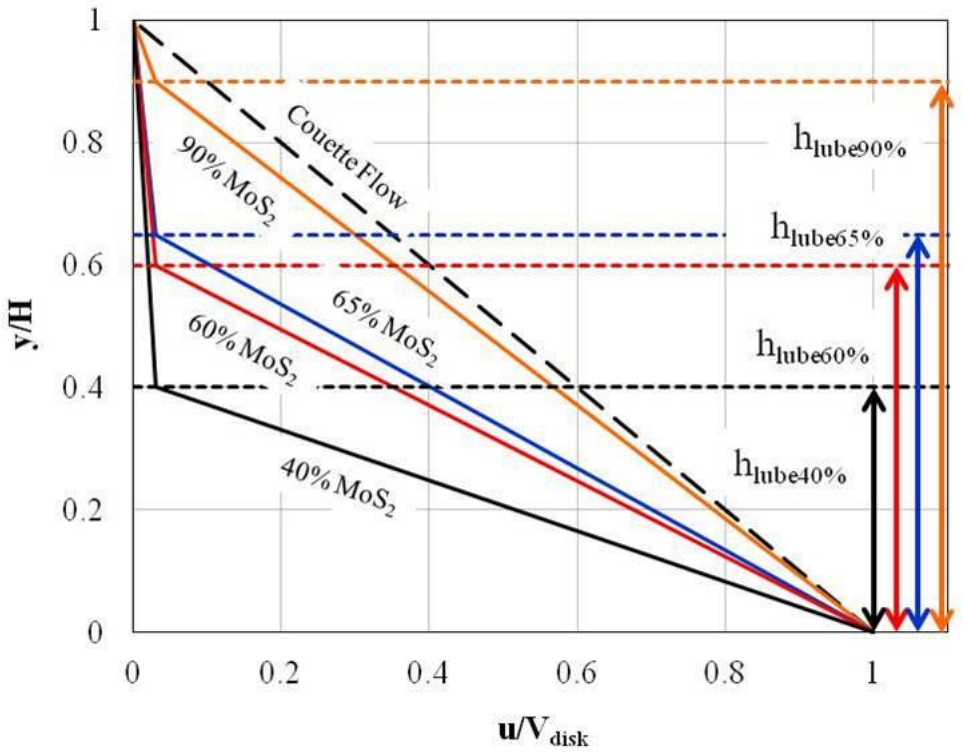

Figure 27: Conceptualization of the decreasing lubricious film thickness (h_{lube}) and its effect on velocity accommodation for composite transfer films of unequal particle sizes: 6 μm Cu + 1.5 μm MoS_2. As MoS_2 content decreases, velocity must be accommodated across a smaller lubricious film thickness (h_{lube}).

A conceptualization of the trends witnessed in Fig. 24 is displayed in Fig. 27. It is important to note that Fig. 27 does not display any physical (experimental) data. It is constructed to be illustrative of how segregation can affect velocity profiles and μ behavior for the various composition percentages studied in Fig. 24, from a powder lubrication (i.e., velocity accommodation) perspective [97, 103, 104]. With this in mind, Fig. 27 shows that higher MoS_2 (lower Cu) compositions, while still segregating, allow for a large h_{lube}. Therefore, a relatively shallow velocity gradient, although steeper than a mixed or full MoS_2 film, is maintained. This shallow velocity gradient results in a low *du/dy*, leading to reduced shear stress (τ) and low μ, as shown through Eqs. (1) and (2). However, as the Cu percentage is increased, segregation can play a larger role in the film's performance. As Cu content increases, the h_{lube} (MoS_2 portion) gets smaller due to segregation, while the Cu portion, with increased η, becomes larger. These effects are reflected in Fig. 27 which displays how segregation at different composition percentages can explain the results of Fig. 24, in which increasing Cu content in films with unequal particle sizes led to higher μ.

Given the requirement of at least 40% Cu for conductivity purposes [4], the results displayed in Fig. 24 showed that the Cu/MoS_2 composite films with *different* particle sizes are unable to provide the required benefits of both constituents. In other words, an electrically conductive lubricant, with acceptably low μ values, could not be produced at the necessary Cu percentages, presumably due to segregation in the composite film with unequal particle sizes. On the other hand, Fig. 25 shows that Cu/MoS_2 composite films with *equivalent* particle sizes can maintain low μ values (< 0.2) at the 40% Cu content necessary for acceptable electrical conductivity. Additionally, these equivalent particle size composites can continue to maintain low μ values at Cu percentages of up to 60%. However, as the Cu composition percentage increases to 80%, a higher μ value (~0.5) is witnessed in Fig. 25. This increase in μ value can be explained due to the fact that even though mixed in some areas, other areas of the film will likely be made up of mostly Cu. This is simply due to the overwhelming fraction of Cu in the film. In this instance, it becomes impossible for the MoS_2 to promote lubrication between each Cu layer in the interface.

3.4.1 A Retrospective search for segregation in transfer films

If it is true that composite powder transfer films, traditionally considered quasi-static particle systems, can actually exhibit dynamics (i.e. transient segregation behavior), then such behavior should have emerged in previous composite transfer film studies in the literature with powders of different particle sizes. This is indeed the case, as particle size segregation does emerge as a plausible explanation for otherwise unknown and inexplicable frictional behaviors elsewhere in the literature. For instance, in a past study examining the ability to create composite films for electrical conductivity, Lund et al. [6] created MoS_2/Mo and copper/graphite composite films in which each powder constituent had a *different* particle size. Both composite coatings were shown to exhibit initially low friction behavior, but after a time, the μ would begin to rise [6]. These behaviors are displayed in Fig. 28a. The trends of these curves are almost identical to the curve for 40% Cu, shown in Fig. 24, which indicated the onset of segregation behavior for Cu/MoS_2 composites with unequal particle sizes. Interestingly, the Cu particles were actually smaller than the graphite particles in this prior study [6], meaning that the Cu particles would diffuse to the bottom. However the performance in this study [6] is still the same as that witnessed in Fig. 24. This fits well in the proposed segregation framework, which focuses on

reduced velocity accommodation regardless of which constituent is on the bottom. The layout of the film in Fig. 26a would simply be flipped. More favorable μ behavior may have been obtained for both of the composites (MoS_2/Mo and Cu/graphite) in this prior study [6], if particle sizes would have been matched.

In another study by Bahadur et al. [21], copper additives were used in conjunction with nylon in order to reduce wear in polymer contacts which are shown already to exhibit anti-wear and relatively low friction transfer film behavior. In this case, the nylon powders used were less than 50 μm while the copper compound powders were on the order of 250 μm. As hypothesized within the segregation framework, there is once again a similar trend in the μ for each composite film. In Fig. 28b, the composite powders begin on the order of pure nylon, but as tests transpire, the μ again rises to much higher values. Should the particle sizes have been matched, this may be another situation in which a more stable μ may have been achieved.

Another instance where particle size segregation behaviors were found in composite films is the work of Prasad et al. [22]. In this case, micron-sized WS_2 powder, a known solid lubricant, was combined with nanometer-sized ZnO to form composite powder films with increased wear life in ambient environments under high temperature. Interestingly, Raman spectroscopy of the films taken after sliding displayed an absence of ZnO additives on the surface, despite the initial mixing of the composite powders. As an explanation, it was hypothesized that burnishing of the film resulted in an engulfing of the smaller nano-particles [22]. While the mechanism for this effect was unknown, it appears to be further evidence of segregation. The burnishing process would have acted as the shearing process, thus causing diffusion of smaller ZnO particles to the bottom of the film. This may also have been avoided if particle sizes were matched. It should be noted that low μ was able to endure, but this is most likely due to the fact that both WS_2 and ZnO are known lubricious materials [101, 119]. And so, even given segregation, both composition sections of the film would exhibit velocity accommodation and a very low resistance to shear.

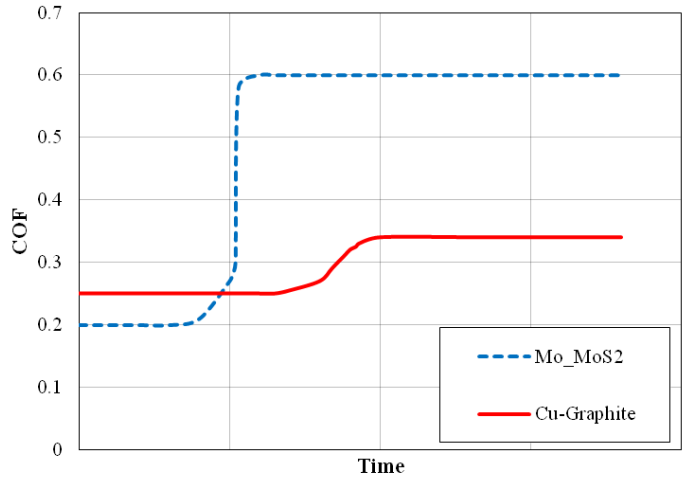

(a)

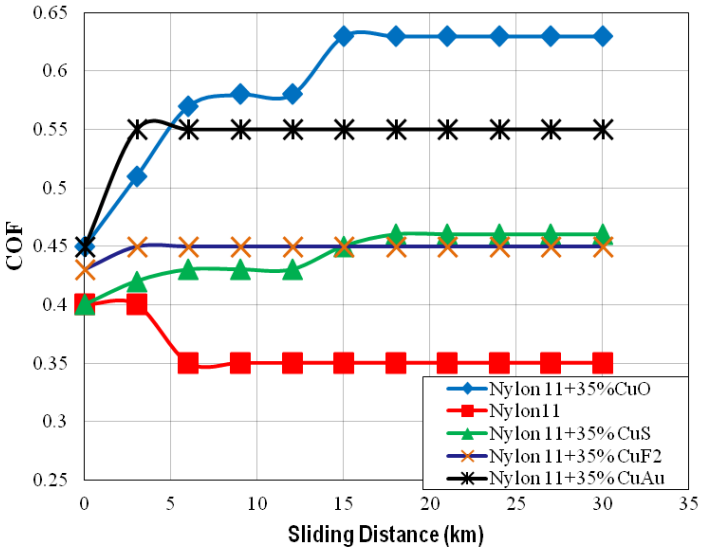

(b)

Figure 28: Prior studies examining the frictional behavior of composite transfer films. In both studies, a transient rise in coefficient of friction was witnessed. (Figures recreated from (a) Lund et al. [6] and (b) Bahadur et al. [21]).

3.5 Conclusions

While solid lubricants can perform in environments unsuitable for oils, no single material can cover the full spectrum of these demanding applications. As such, researchers have sought to take advantage of the properties and lubrication potential of numerous solid materials by combining them together into multifunctional composite solid lubricants. However, attempts to precisely engineer these composite lubricants have been thwarted by transient degradations in the

tribological performance. In particular, it was shown that in a number of studies, composite powders with unequal particle sizes displayed a gradual rise in friction despite the presence of uniformly mixed lubricant films with initially low friction values. This investigation proposed that the granular phenomenon of shear-induced particle size segregation can explain disparities in friction performance for a number of composite powder transfer films, both in this work and in the literature. As a result, several conclusions were drawn regarding the performance of composite transfer films.

Although initially displaying the benefits of each constituent, it was found that composite films with different particle sizes and only one lubricious constituent, would display an increasing μ over time. However, for the test case of a Cu/MoS_2 transfer film, utilizing equal particle sizes resulted in a low and enduring μ. This is because the smaller particles diffuse through the voids left between the larger particles as the film is agitated by shear during the lubrication process. An explanation of the interfacial velocity accommodation has been provided through the use of the quasi-hydrodynamic theory of powder lubrication, which was originally developed by Heshmat et al. In this work, the theory was extended to solid lubricant transfer films with distinct composite constituents, in order to show how segregation would lead directly to the μ trends present both in this work and in previous studies in the literature. Gradual segregation through shear would cause deterioration in frictional behavior in two ways. First, it would result in an increase in the resistance to shear (i.e., effective viscosity) in the non-lubricious section. And second, the segregation would cause a larger velocity gradient, and thus shear stress, in the lubricious portion of the film. In composite transfer film applications which require uniform composition throughout operation, considering segregation behavior may be paramount to successfully leveraging the benefits of each component.

Chapter 4: The Influence of W-DLC and CR_xN Thin Film Coatings on Impact Damage for Bearing Materials

This chapter contains a study detailing the effect of hard tribological coatings on mitigating impact damage with a focus on Rolling Element Bearings. A similar version of this chapter has been accepted as a journal paper in *Tribology Transactions.* [Dougherty, P., Marinack, M., Patil, D., Evans, R., Higgs III, C.F. "The Influence of W-DLC and Cr_xN Thin Film Coatings on Impact Damage between Bearing Materials," Accepted for Publication: *Tribology Transactions* September, 2015]

4.1 Introduction

Due to their ability to maintain low friction and high durability under demanding loading conditions, rolling element bearings (REBs) are commonly used in industrial, aerospace, energy, and automotive applications. Consequently, REB designs have been tailored over time to arrive at a number of optimal application-specific configurations with different rolling element geometries, raceway designs, and lubricants. Their inherent low friction is attributable to load transmission through small, high-pressure point or line contacts between the rolling elements and raceways. On the other hand, these concentrated point or line contact areas are susceptible to damage under impact or dynamic loading, possibly leading to a plastic deformation of the raceway surface called "true brinelling" [120].

The presence of permanent dents or other damages in the raceway from true brinelling events can drastically alter REB performance attributes such as torque, vibration, running sound, and service life. In addition, the presence of raceway surface damages can accelerate the onset of spalling damage via a mode termed "point surface origin" spalling [120]. Other complications arising from raceway damage due to impact loading or overloading may include reduced fatigue life, low dampening, and accelerated wear/debris generation. [121-123]. Often these damage modes are preceded by periods of excessive vibration as the rolling elements traverse an increasingly damaged race. In fact, there have been a myriad of studies for monitoring vibration-induced acoustic emissions as a precursor to bearing failure, given the fact that bearing vibration increases as material damages propagate [122, 124, 125].

In order to provide a quantitative measure of this process, a parameter such as the "quiet running depth" or static load capacity may be used. This is described as the ratio of rolling

element radius divided by dent depth before the material damages result in noticeable vibrations, either as acoustic emissions or as an erratic torque signature. A study to establish this threshold was described first for 440C and 52100 bearing steels with varying race and rolling element geometries by Leveille and Murphy in 1973 [126]. The experimental setup involves measuring torque signatures at low speeds (~1 rpm) before and after producing a brinell (dent), and investigating torque signatures for noticeable disturbances. This work was continued by Park, et al. for more modern REB materials [127], in which the non-dimensional threshold was agreed to be between 0.00003 and 0.00005 [121, 123, 126, 127].

While many of these studies have been done in order to evaluate bearing materials, it is important to note that material damage creation on test specimens is usually conducted through a static process, using a hard tip to slowly indent the substrate under high loads. Although this technique is standard for REB material selection, damage creation under dynamic conditions provides a much more realistic simulation of the resulting deformations expected to occur during bearing operation. For instance, under dynamic impact conditions such as those found in this investigation, even at low speeds, much smaller loads can create significantly larger damaged areas.

In order to combat the creation of raceway damages that can reduce bearing service life, efforts are often focused on improving either the lubrication regime to minimize asperity contact, or on increasing the durability of the bearing's internal contact surfaces [128]. One successful method of improving wear resistance is the implementation of solid lubricant coatings. While coatings have been frequently studied and applied in a variety of applications unsuitable for oils, the mechanisms behind their success have yet to be fully elucidated, particularly in terms of impact resistance [1, 3-6, 15, 16, 18, 102]. For instance, solid lubricant coatings are utilized specifically to protect REB surfaces by preventing or delaying abrasive wear, denting, micro-fracture, and spalling [1, 3, 8, 18]. However, while initially acting to prevent the deterioration of bearing surfaces, their own breakdown is not well understood in terms of REB lifetime prediction models [18, 102]. When compared to softer sacrificial solid lubricants such as MoS_2 and graphite, hard tribological coatings like metal doped diamond-like carbon (DLC) or chromium nitride (Cr_xN) are particularly interesting in that they are designed to remain intact for the entire service life of their substrate. However, if exceptionally severe conditions lead to damage or delamination of these hard layers, other damage modes may arise that affect REB service life.

One process in industry is to select hard tribological coatings, which feature material properties that are difficult to achieve in bearing steels, in order to achieve higher REB wear resistance. Strategies may include achieving an extremely high hardness similar to certain technical ceramics, but without sacrificing toughness. Another goal might be to design a coating layer that combines moderately high hardness and low elastic modulus properties. This second combination is represented as the Modell number, a ratio of hardness to elastic modulus, which has been utilized in the past as a figure of merit for bearings and wear- resistant materials [121, 123, 129]. A high Modell number indicates that a material is resistant to plastic deformation while also being highly elastic. This suggests that the onset of plasticity will require high stresses due to high hardness, while elastic recovery will be possible even at high levels of deformation due to the low modulus. In dynamic impacts, where the deformations can become large even at low loads, this is especially important.

The current work investigated the dynamic behavior of coated surfaces under a single impact, with focus given to the ability of hard tribological coatings to reduce damage. This ability was characterized in terms of the kinetic energy lost during impact, as well as by observations of damage reduction in coating and substrate morphology, compared to untreated steel surfaces. These factors were discussed as they pertained to material removal, deformation of the underlying substrate, and subsurface damage.

Impact sites were examined using an optical interferometer (OI) in conjunction with scanning electron microscope (SEM) images of fixed ion-beam (FIB) cross sections within the impact craters. For creating the dents and monitoring kinetic energy loss during impact, a drop-test rig (DTR) was developed. Ball-plate impact was monitored with two high-speed CCV cameras. The investigation was accomplished using techniques previously reported by the authors for impact testing and evaluation of thin film morphology [18, 130].

Table 4.1: Substrate and Coating Combinations

Sample Name	Material	Thickness
WDLC1	WC/a-C:H	2.4 µm (440C) 2.5 µm (52100)
WDLC2	WC/a-C:H	1.3 µm (440C), 1.6 µm (52100)
CRN	Cr_xN	1.5 µm
440C	Stainless Steel (unhardened)	0.635 cm (¼")
52100	AISI 52100 Steel (hardened)	0.635 cm (¼")

4.2 Experimental Setup and Procedure

The material combinations studied through these impact experiments included spherical tungsten carbide (WC) drop elements and various flat plate samples. The plates were 440C stainless steel (herein referred to as "440C") and AISI 52100 alloy steel (herein referred to as "52100"). Each plate was cut into a 15.24 cm X 15.24 cm square such that the plate could be treated as semi-infinite with respect to the impact radius which was on the order of 50-250 μm. Several plates were treated with hard tribological thin film coatings. Tungsten carbide-reinforced diamond-like carbon coatings (WC/a-C:H or W-DLC) and chromium nitride (Cr_xN) coatings were prepared on test plates by The Timken Company using closed field unbalanced magnetron sputter deposition. The coatings and their thicknesses are presented in Table 4.1.

The WDLC1 average thickness was 2.4 μm on 440C and 2.5 μm on 52100, while the WDLC2 was slightly thinner with 1.3 μm on 440C and 1.6 μm on 52100. Both of these coatings were composed of WC/a-C:H with nominally the same chemical composition, but had different microstructures imparted by processing method differences. The CRN coatings were found to have an average thickness of 1.5 μm on both substrates, and were composed of Cr_xN.

Each plate test specimen was characterized to ascertain the hardness and elastic modulus using a Hysitron nanoindenter. An average value of 10 different 10 nm indentations was collected for each material combination in order to better understand measurement error and any potential coating layer/substrate effects on the data.

Kinetic energy loss during impact was tracked by measuring the coefficient of restitution (COR) using the DTR shown in Fig. 3. This rig consists of a drop element holder (A), which provides a suction force through an air hose (B) connected to an air pump. The air pump was turned on to hold a single element in place, in this case a sphere, and then switched off to allow the element to drop from rest and collide with the substrate (C) below. The elements were held at a variety of heights between 7.62 and 48.26 cm (3 and 19 inches), to achieve results for COR and denting damage over a range of impact speeds from 1.25 to 3.12 m/s. Each trial was recorded simultaneously by two high-speed cameras. The first camera recorded the trial from above to aid in locating the impact site; a second camera recorded a front view of the trial to obtain the initial (H_I) and maximum rebound (H_R) heights necessary for calculating COR. With these heights obtained, post-processing was performed using an in-house, numerical algorithm, and COR was calculated via Eq. 1.

$$COR = \sqrt{H_R / H_I} \qquad (1)$$

Additional information on the drop test rig and the data processing procedure can be found in a previous work by the authors [130], which details extensive experimental COR studies. A drop was performed at nine heights for each material combination, including the bare substrates. These data are particularly important for two reasons. First, this methodology provides a quantitative measure of the energy dissipated due to the impact. Second, it allows for the capture of dynamic loading, which is more representative of shock events during REB operation than the static loading that is customary with materials testing. The coefficient of restitution has been used in many studies to estimate kinetic energy loss and has been investigated both heavily both in terms of experiments and modeling for a number of different materials [130-134].

Table 4.2: Modell Number for Each Substrate

Sample Name	Material	Modell Number (substrate)
WDLC1	WC/a-C:H	0.0823 (440C) 0.0962 (52100)
WDLC2	WC/a-C:H	0.0867 (440C), 0.0865 (52100)
CRN	Cr_xN	0.0770 (440c), 0.0755 (52100)
440C	Stainless Steel (unhardened)	0.0453
52100	AISI 52100 Steel (hardened)	0.0538

In addition to the coefficient of restitution measurements, each impact site was examined using an OI instrument. After each drop, the plates were marked and compared with the vertical high-speed view to ensure the capture of a given drop's impact site. The resulting dents from each impact speed were then investigated for evidence of plastic deformation and breakthrough of the coating and/or substrate.

For each site, an average was taken of three line scans to characterize the dent depth of the circular impact sites. Finally, FIB cuts were conducted at dent sites of interest to examine the microstructure of both the substrate and coating for subsurface damage. The site was prepared by initially coating it with palladium to protect the site and then cut using the FIB. It was then examined with SEM. These final results were correlated with those from the previous studies to shed light on the impact mechanics for coated substrates.

4.3 Results and Discussion

4.3.1 Nanoindentation Results Figure 29 displays nanoindentation results for each coated and uncoated substrate, with elastic modulus in Fig. 29a and hardness in Fig. 29b. The material

characterization results for the two bare steels behaved as expected in that the 52100 alloy steel was harder and had a higher modulus than the softer 440C. The nanoindentation results were very similar for both WDLC2 and WDLC1, which seems reasonable as both were made of WC/a-C:H type material using similar (although not identical) processing methods. However, the WDLC1 coating did not show nearly as much variability in elastic modulus between substrates. This is most likely due to the fact that the WDLC1 was about twice as thick and thus less sensitive to substrate effects during the measurement.

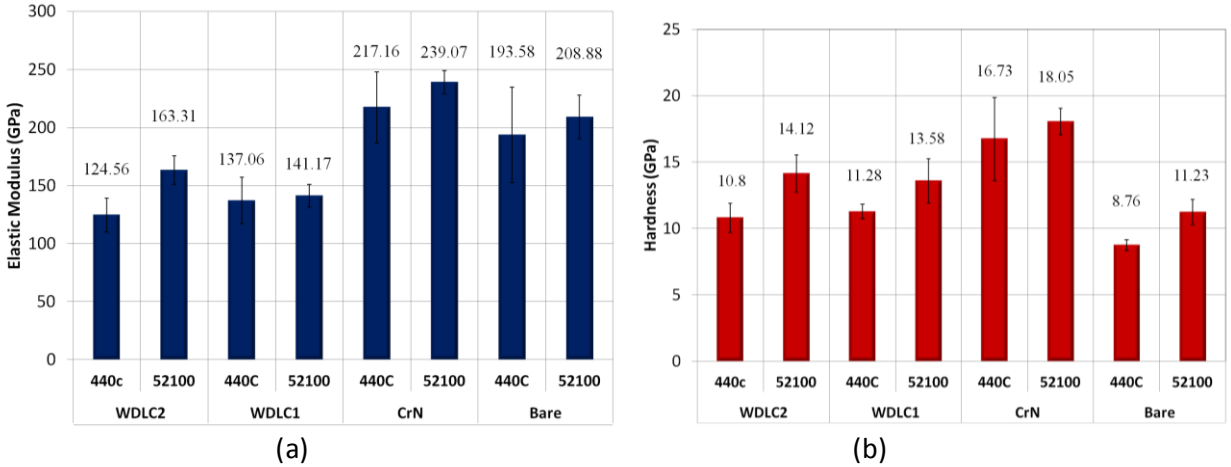

Figure 29: Nanoindentation results for (a) elastic modulus and (b) hardness of each substrate configuration

It should be noted that the selected nanoindentation depth was less than the 10% threshold, chosen thus for minimizing substrate effects described by Tsui and Pharr (10 nm indentation versus 1.5 to 2.5 µm thickness). However, even at this shallow depth it can still be difficult to completely remove substrate effects such as those in Fig. 29 [135].

For each of the WC/a-C:H coatings, WDLC1 and WDLC2, the elastic modulus was much lower than that of the two steel substrates, while the hardness was moderately higher than that of both substrates. This implies that, compared to the underlying substrate, the surface layer will be more resistant to plastic deformation as well as more elastic. It should be recalled that this combination of parameters, represented by a higher Modell, has been hypothesized as beneficial for bearings. Values for the Modell number of each test substrate are provided in Table 4.2.

The CRN coating material parameters were more representative of a stiff protective coating, featuring extremely high hardness and high elastic modulus. This implies that the coating will be much harder than the underlying substrates, but will be less elastic and potentially more prone to brittle failure.

4.3.2 Impact Testing and Surface Metrology

Fig. 30 displays the coefficient of restitution results for both of the bare substrates at nine different impact speeds. This particular parametric study, using more readily understood bare substrates, was conducted for comparison against the theory of coefficient of restitution in *Contact Mechanics* by K.L. Johnson (KLJ) [136]. This equation has been included as equation 4.1. It was observed that COR would decrease with increasing velocity and increase with hardness of the substrate. Both of these trends align well with KLJ's theory for COR (*e),* where hardness is represented as a dynamic hardness P_d and velocity as V. It should be noted that the theoretical trend was not plotted for 52100 because its yield strength lies above the values for which KLJ's equation has shown quantitative agreement. However it does follow the qualitative trends described above quite well.

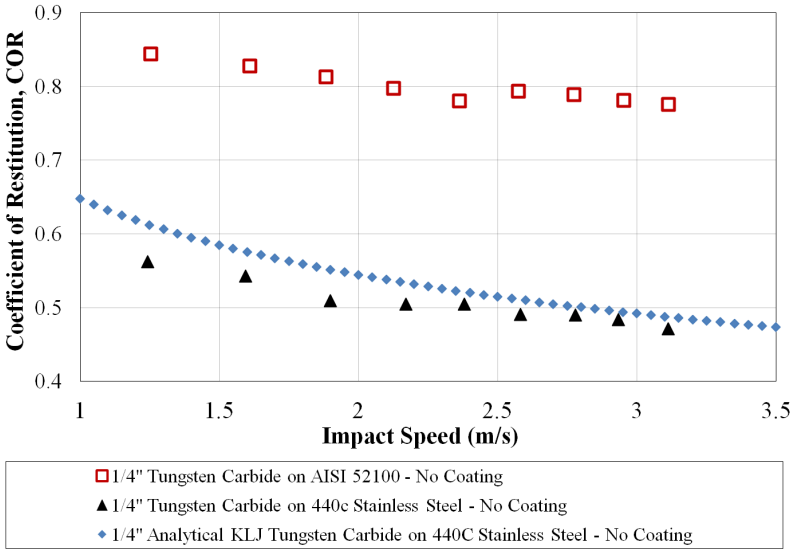

Figure 30: Coefficient of restitution of 1/4" WC spherical drop elements on 440C and 52100 steels with coinciding analytical theory from K.L. Johnson

$$COR = 3.413\left(\frac{\sigma_y^5}{E^{*4}V^2\rho_s}\right)^{1/8} \qquad (4.1)$$

5.3.2.1 Coated Surfaces on Softer 440C Substrates

While Fig. 30 presents the COR for both of the bare substrates, Fig. 31 focuses on impact testing of each coating deposited on 440C. For comparison purposes, the COR data was included for bare 440C as well. On each of the coatings, it was interesting that no definitive trend was

observed in terms of the coating's effect on kinetic energy loss (COR) relative to the bare substrate. The coated surfaces still followed the same trend of decreased COR at higher velocities, due to increased energy lost to plasticity effects, agreeing well with the theory of K.L. Johnson depicted in Equation (4.1).

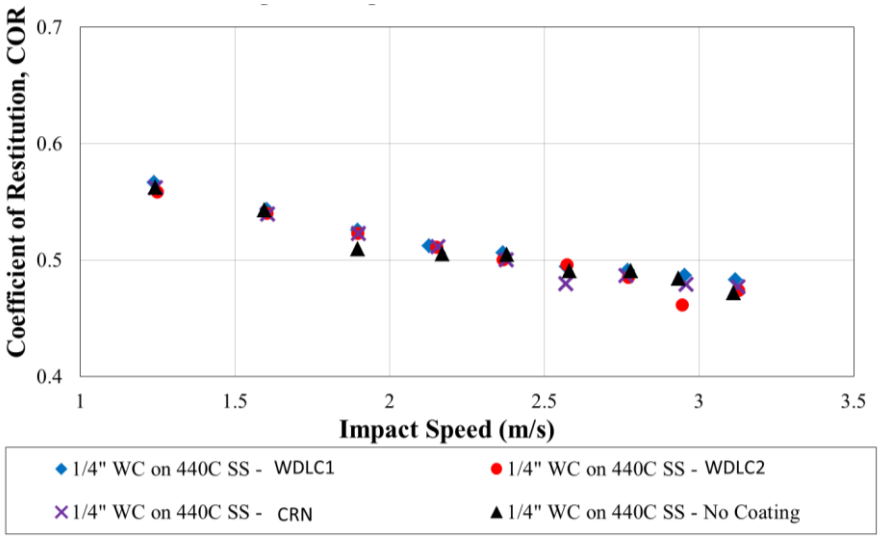

Figure 31: Coefficient of restitution of 1/4" WC spherical elements on 440C steel with and without WDLC and CRN coatings

The post-mortem surface metrology of each impact site provided more insight into the performance of each coating. Fig. 32 provides the depth of each of the coatings on 440C as a function of impact speed, as well as inset images featuring the topography scans of WDLC1 and bare 440C at impact speeds of 1.25 and 2.12 m/s. It should be noted that for the second and third impact speeds, there was a much larger reduction in dent depth for the CRN and the WDLC1 coatings respectively, than the rest of the trend suggests. This is most likely due to either a slightly oblique impact or from build-up of the coating around large peaks or valleys in the surface. At higher speeds these types of non-uniformities would most likely be negligible given the large dent depths.

It was apparent from qualitative investigation alone that plastic deformation had already taken place, even for impacts at 1.25 m/s. In fact, for the spherical elements (balls) in this study, the static load capacity threshold described in the introduction was found to be 0.6 µm. However, dent depths for the lowest test speed were above 6 µm, already beyond the threshold that would begin to produce torque disturbances during rolling according to the studies of Leveille and Park,

et al. [126, 127]. In addition, even at these moderate velocities, these dents are already about 3-4 times the coating thicknesses which can be found in Table 4.1. These findings are an important feature of dynamic impact testing, in which the imparted maximum indentation depths can be much larger than those under similar static loading. Despite an unaffected COR value, it was found that the WDLC1 and WDLC2 coatings could reduce dent depth until the 2.12 m/s drop velocity, after which no definitive depth trend could be found. In other words, for the moderate-hardness, low-modulus coatings on softer 440C, a threshold exists in which the deformation involved in the impact extends beyond the coatings' ability to reduce damage. On the other hand, the CRN coatings were actually able to reduce dent depth at all impact speeds. These effects can be explained through consideration of the material properties for both surfaces. 440C steel displayed the lowest hardness of all the tested materials at about 8 GPa. The WDLC1 and WDLC2 coatings displayed a moderate increase in hardness, about 11 GPa. Additionally, the main performance augmentation of the WDLC1 and WDLC2 coatings was a reduction in elastic modulus from about 200 to 125 GPa. While this should improve elastic recovery at smaller deformations, the dent depths on a 440C substrate – even at the lowest speeds were about twice the depth of the thickest (WDLC1) coating listed in Table 4.1. Because these strains are large compared to the coating thickness, it is reasonable to assume the contact stress would have transitioned beyond simple elastic contact into the elastoplastic regime. Therefore, the elastic effects of WDLC1 and WDLC2 should be reduced.

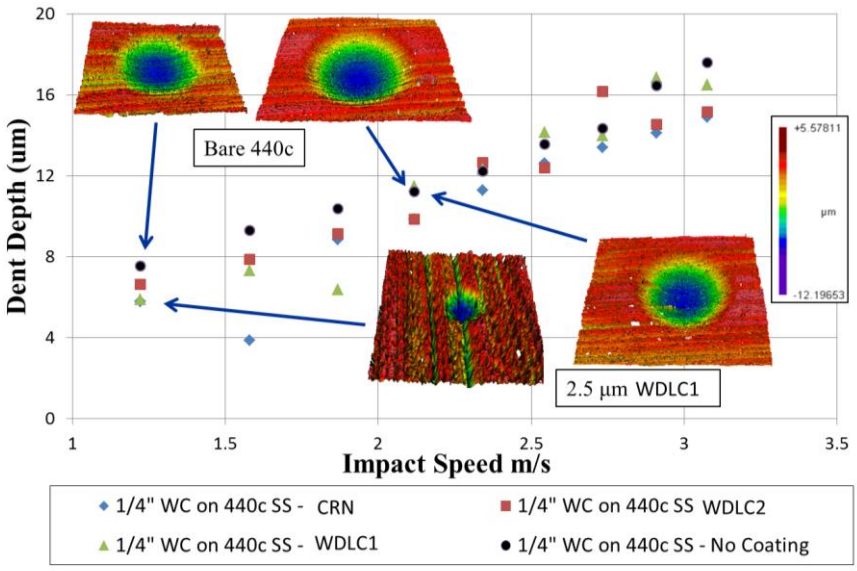

Figure 32: Dent depths of 1/4" WC spherical elements on 440C steel with and without WDLC and CRN coatings

It is most likely then, that the ability of each of these coatings to reduce dent depth at these large deformations, is proportional to their increased hardness. At the lowest speeds, the small increase in hardness of the WDLC1 and WDLC2 coatings was sufficient to reduce dent depths. On the other hand, the CRN coating was able to reduce dent depths at even higher speeds because of its higher hardness of 18-20 GPa. This analysis of the data in Fig. 32 suggest that on relatively soft substrates like 440C, the stresses and deformations may become too large to make use of highly elastic coatings like WDLC1 and WDLC2. However, a significant increase in hardness such as that of the CRN coating would be more desirable in extending the combined substrates' ability to resist plastic deformation.

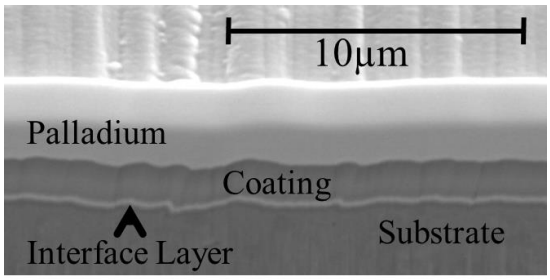

Figure 33: Annotated FIB cross section of 52100 with WDLC1 away from impact

To provide a closer look at the performance of the coatings under dynamic impacts, FIB micrographs were analyzed for subsurface damage. Each of these micrographs was taken in the center of the dent, with the cut leading to the edge. Figure 33 displays an FIB cut of 52100 with WDLC1, away from the impact, in order to orient the reader to the different layers

present in each micrograph cross section. The different layers include the coating, the substrate, and the protective palladium layer that is necessary to protect the topography and microstructure from the FIB cut itself. It should be noted that a thin bond interface layer between the coating and the substrate is visible as a narrow, brighter region due to the difference between the elemental composition of the bond layer, the functional top layer and the substrate steel.

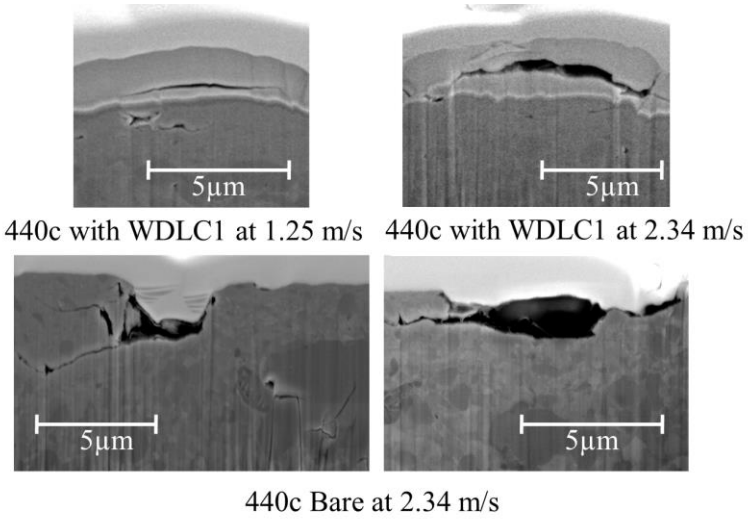

Figure 34: FIB cross sections of the impact site for 440C with WDLC1 coating at 1.25 m/s and 2.34 m/s, and 440C bare at 2.34 m/s

In Fig. 34, the FIB micrographs for 440C impacts are displayed for the 1.25 m/s drop velocity, where the coating reduced dent depth, and for 2.34 m/s, where it did not. In addition, micrographs for the bare substrate at 2.34 m/s are also included. It should be noted that while the cut was taken from the middle all the way to the edge of each dent, the damage was found to exist throughout the dent rather than being focused at either the middle or the edge. Due to the need for higher magnification in each of the micrographs, the reader is encouraged to utilize the interferometer shots in Figs. 32 and 36 in order to visualize the curvature of the dent, as they will appear quite flat in each SEM image. First, it can be seen that for both impact speeds, cracks have propagated within the bulk of the WDLC1 coating. For the 1.25 m/s impact (dent depth reduction), the cracks were hairline in appearance and singular in that they did not branch off into other crack systems. However, at the higher speed of 2.34 m/s (no effect on dent depth), the cracks were much wider and did branch off into other crack systems. In addition, small subsurface cracks can be found just below the interface layer. It should be highlighted that even though the OI results suggest that the coating had no effect on reducing dent damage at 2.34 m/s,

the observed cracks did not extend to the surface or to the interface layer. This is an important attribute particular to the coated 440C surfaces, for preventing material removal or debris generation.

While the FIB results suggest that delamination and wear debris generation were prevented in the coated 440C, this type of failure still occurred in the case of bare 440C. As shown in Fig. 34, large pits (indicative of material removal at the surface) and large subsurface cracks were created by the impact. These topographies represent potential detractors to bearing performance in two ways: First, they can add to unwanted vibrations during operation; second, any subsequent wear particles generated in their creation can lead to abrasive wear and denting damage as they are entrained through bearing roller-raceway contacts. The larger subsurface cracks represent another drop in performance, increasing the risk of fatigue and early onset failure under the cyclic stress of bearing operation. These findings help to add another layer to the analysis of coated surfaces on a soft 440C substrate previously hidden by COR testing and dent depths alone. While the ability of the WDLC coatings to reduce dent damage halted at 2.34 m/s, the WDLC1 coating was still better able to prevent material removal than the bare 440C.

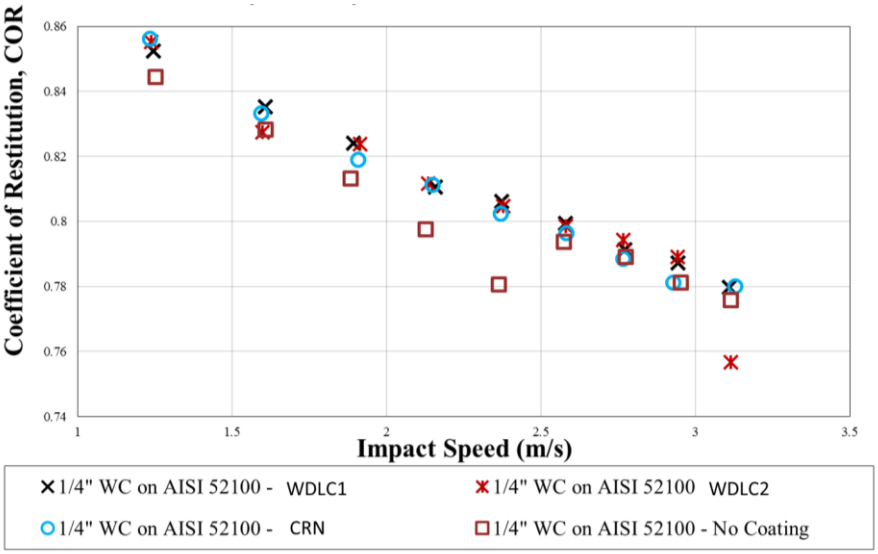

Figure 35: Coefficient of restitution of 1/4" WC spherical elements on 52100 steel with and without WDLC and CRN coatings

5.3.2.2 Coated Surfaces on Hardened AISI 52100 Substrates

The COR results for the coated surfaces on 52100, a harder alloy steel, are displayed in Fig. 35. For each speed the coating was found to have a relatively higher coefficient of restitution,

with the greatest disparity at the lower impact speeds. This suggests that the coating succeeded in reducing the amount of energy dissipation in the contact. At higher speeds, the COR values for coated surfaces were more similar to those of the bare surfaces, yet still higher on average. In both cases, this reduction in energy dissipation is most likely due to the increased hardness of each coating, and the subsequent reduction in plastic deformation, which acts to absorb impact energy. In the case of the WDLC1 and WDLC2 coatings, the lower elastic modulus would also contribute to this effect. This is because a lower modulus implies the ability to recover from larger deformations without sinking energy into irreversible plastic deformation. However, no clear trend was visible in terms of one coating being more efficient in reducing kinetic energy loss during the impact. It should be noted that when examined with a smaller y abscissa, the drops for the bare substrate between 2 and 2.5 m/s appear to drop below the trend for the other velocities. This is most likely due to roughness effects, in which the impact takes place on an asperity; thus increasing contact stress and energy lost to plastic deformation. This would also explain why the COR seems lower given a similar dent depth as much of the plastic deformation would occur as it deforms this asperity.

As was the case with 440C, a post-drop test investigation of the impact sites provided further delineation of each coating's individual performance. In Fig. 36, the dent depths of each coating at each impact speed and 3D optical interferometer scans for the bare 52100 and WDLC1 coatings are presented for analysis. The large differences between the dents found on the softer 440C substrates and those on harder 52100 are quite apparent from initial observation. For instance, in the 3D scan of the 2.34 m/s test, dent depths on 52100 ranged from 1.5–2 μm while those on 440C were closer to 12 μm. Upon closer inspection, it was found that all of the coatings on 52100 were able to reduce dent depth at every tested speed. For the CRN, this effect should stem from the added hardness. But, for the WDLC1 and WDLC2, the combination of high hardness and high elasticity (high Modell number) should act in concert to reduce damage even further. It can be seen in Table 4.2 that the Modell number for WDLC1 on 52100 was the highest at 0.0962, and that WDLC2 was 0.0865 which is still higher than CRN at 0.0755.

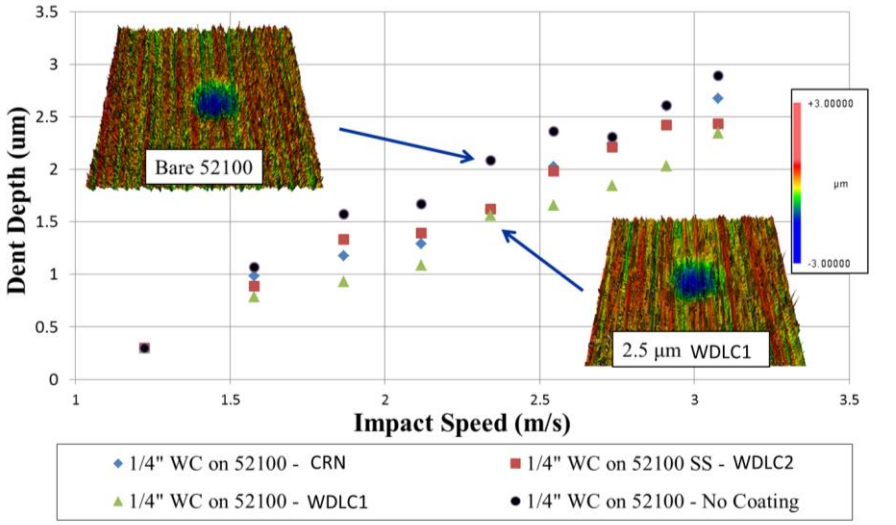

Figure 36: Dent depths of 1/4" WC spherical elements on 52100 steel with and without WDLC and CRN coatings

The ability of WDLC1 and WDLC2 to utilize both moderate hardness and low elastic modulus to reduce dent depth is showcased well in Fig. 36. Contrary to the impacts on soft 440C, the CRN coating was generally the least successful at reducing damage except at the 1.87 and 2.11 m/s velocities. For all other tests, the WDLC2, which is of similar thickness, outperformed the CRN. This is because despite its reduced hardness, WDLC2's much lower modulus provided a large increase in elasticity. The most successful coating in reducing damage was WDLC1, which combines the material properties of WDLC2 (high hardness, low modulus) with almost double the coating thickness. These rankings, in terms of damage reduction, are reflected well in the Modell numbers presented in Table 4.2. The key difference between the impacts on 440C, in which the hardest CRN coating performed the best, and the harder 52100 substrate; is that the maximum dent depths remained much smaller for 52100. These deformations were most likely small enough that the added elasticity of the WDLC1 and WDLC2 coatings were no longer surpassed, particularly for the thicker WDLC1.

The coating thickness is an interesting parameter, meriting more investigation in the future. Currently it appears that increasing the coating thickness did result in a better chance to exploit the coatings beneficial properties. Most likely this is because the thicker coating allows for a greater percentage of the impact to take place in the coating itself rather than in the substrate. In fact, the ability of an elastic coating to reduce impact damage or affect COR appears to be heavily reliant on the relative magnitude of the coating thickness compared to the potential dent

depth. For the 440C substrates, the dents were often much deeper than the coating thickness, and the ability to reduce damage was overcome at relatively low impact speeds. However, for 52100, the dent depths were generally shallower than the coating thickness, ranging from about 0.3 to 2.5 µm. Subsequently, the dent depth was always reduced for coated substrates. Dynamic testing is important for investigating this effect. Even though static indentation may indicate that a given coating has drastically enhanced material properties over the substrate, dynamic impacts can result in maximum dent depths that are too large for the properties of the coating to be exploited. Ensuring that the coating is thick enough in relation to the expected deformations appears to be a key parameter in utilizing the advantages of a coating during impact. If the maximum dent depths involved in a dynamic event are too large, substrate effects will dominate entirely.

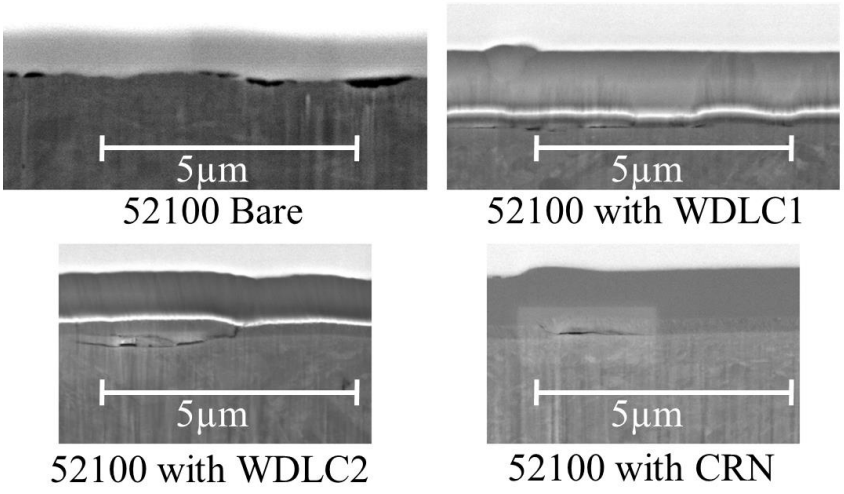

Figure 37: FIB cross sections of the impact site for each 52100 surface at 2.34m/s impact speed

The cross sections of each 52100 substrate, at 2.34 m/s, are displayed in Fig 37. For comparison, it should be noted that this was the same impact speed as the cross sections taken for 440C in Fig. 34. Through analysis of the bare substrate, one can observe damaged pits just below the palladium layer that most likely correspond to areas of material removal during the impact. Compared to the impacts on softer 440C, no subsurface damage was found and surface damage was far less drastic as should be expected given 52100's much greater hardness. For the coated surfaces on 52100, no cracks such as those found on 440C were observed in the coating's bulk.

This is most likely due to the added hardness of the substrate, which prevented the formation of dent depths large enough to induce cracking inside the coating itself.

However, small cracks were found at the interface layer between the coating and substrate. For the thinner WDLC2 coating, these cracks were relatively long and had propagated into the substrate, though they remained thin. For the WDLC1, the most successful at reducing dent damage, the cracks were smaller and had penetrated the substrate less. For the CRN, a thinner coating similar to the WDLC2 but made from much harder and stiffer material, the cracks were wider than those found in the other substrates. One of the most crucial points to remember is that while these cracks represented impact damage, they were still contained beneath the surface, as opposed to the impact on the bare 52100 substrate. In the latter case, the damage was on the surface and could be considered a potential cause of debris generation or other crack initiation. These types of surface damages might interact directly with the other contacting elements in a bearing during operation, potentially causing excess vibration and further damage.

The added substrate stiffness and resulting smaller maximum dent depths of the 52100 surfaces allowed each coating to have a greater effect. All of the coatings were found to increase COR, reduce deformation in the form of denting, and prevent damage indicative of material removal. In addition, the added stiffness of the 52100 substrate resulted in a different coating as the most successful in reducing dent damage. In this case, both the WDLC1 and WDLC2 coatings, with their low elastic moduli, outperformed the harder CRN coatings. Of these two, the most successful coating in reducing damage was the WDLC1, which was the thickest in addition to having the highest Modell number.

4.4 Summary and Conclusions

Despite their ability to handle such a large variety of operating conditions, rolling element bearings still suffer from issues such as vibration-induced damage and the creation or ingress of abrasive third body wear debris. As the bearing progresses in its life cycle, these problems are exacerbated through repeated dynamic impacts.

While one solution to improving the longevity of a bearing surface is to utilize hard tribological coatings, much of the testing for bearing surfaces is done using static indentations which cannot capture all of the dynamics potentially found in real applications. Particularly in the cases of coated surfaces, a larger breadth of investigation is needed to elucidate their

behavior during impact in order accurately describe a coating's benefit. In this work, dynamic impacts in the form of spherical element drop tests were investigated on 440C and 52100 substrates. For both coated and uncoated versions of the substrate, coefficient of restitution (COR) values were analyzed in concert with optical metrology of the dent in the form of interferometer scans, dent depths and cross-sectioned micrographs. For the softer 440C substrate, the coatings had little effect on COR. In the case of softer, more elastic WDLC coatings, they were able to reduce dent depth up to the 2.34 m/s drop velocity while the harder CrN coating was able to reduce dent depth at each drop velocity.

SEM scans revealed further that even at the lowest speeds, severe damage in the form of pits and subsurface cracks were observed in the bare untreated substrate. On the other hand, while the same impacts were able to cause cracking in the bulk of the WDLC1 coating, this damage was confined to the bulk of the coating layer without the creation of any observed wear particles. Although the dent reduction effected by the coatings was only present up to the 2.34 m/s drop velocity, this prevention of wear particle formation represents a large improvement in performance.

For the 52100 substrates, COR was found to increase at every height, most likely due to the coatings' prevention of plastic deformation and the relative increase in elasticity for the WDLC1 and WDLC2 coatings compared to untreated steel surfaces. Dent depths were also reduced, with the most successful reduction coming in the form of the thickest, most elastic of the coatings, WDLC1. SEM scans revealed minimal cracking in these coatings. However, some of these cracks (particularly in the more brittle CRN) seemed to widen and penetrate deeper beyond the interface layer. In all cases, damage was contained in the bulk of the coated surface or substrate, rather than manifesting in surface damage that could immediately affect bearing performance.

COR testing in this case may be particularly useful to the bearing community as a way to vet initial coated surfaces for resistance to impact damage without costly investigation of the impact site. An increase in COR over the bare substrate was found to indicate reduced impact damage, regardless of the coating's material properties or the tested impact speed. In the event that COR results are inconclusive, the coating may still reduce damage as seen in certain cases of the 440C tests but confirming this requires detailed investigation of the site. This suggests that if the properties of the coating such as hardness, elastic modulus and thickness could be tailored to

ensure positive COR results, the need for further detailed metrology investigations might be unnecessary.

An important difference was discovered through dynamic testing in terms of pairing coating and substrate properties. While nanoindentation results suggest that the coatings offer similar improvements over the substrate in terms of material properties, dynamic testing showed optimal performance for two different coatings on 440C and 52100. The WDLC1 coating appeared to work best on the hard 52100 substrate due to the smaller maximum dent depths relative to coating thickness and its ability to utilize its low elastic modulus. However, on the soft substrate, CRN seemed to perform the best, perhaps because the deformations involved in the impact are so large that any elasticity benefits are severely diminished.

Ensuring that the coating thickness is close to or larger than the expected dent depth appears to be a key factor in maximizing the utility of the coating. For softer substrates, large deformations may overwhelm any effects of thin coatings and result in large cracks as the coatings attempt to remain bonded to the substrate.

Section 2: Numerical Simulations of Two Body Wear

The following section contains one chapter which details the modeling of two body abrasive wear with a focus on predicting the friction and wear of solids which form lubricant transfer films.

Chapter 5: Modeling of Preferential Patterns Found During the Abrasive Wear of Random Surfaces

This chapter contains a study in which a numerical model is developed and validated for use in predicting the abrasive wear of soft surfaces, particularly those used in the formation of powder lubricant transfer films. A similar version of this chapter has been accepted as a conference paper at the Society of Tribologists and Lubrication Engineers Annual Meeting. [Dougherty, P., Stonestrom, D., Higgs III, C.F. "Modeling of Preferential Patterns Found During the Abrasive Wear of Random Surfaces" Proceedings of: STLE Annual Meeting and Exhibition. St. Louis, MO, May 2012.]

5.1 Introduction

While wear has been a rigorously studied phenomenon in Tribology, wear is still considered a highly stochastic process, where the relation between friction and wear is not always apparent. Often time, boundary and solid lubricated tribosystems display frictional behavior characterized by high wear during run-in before a lower steady-state type of friction settles in. This paper explores the possibility that this steady-state friction is actually the process of the relatively sliding surfaces reaching an equilibrium topography that is a function of the initial topographies and the local, asperity-scale, interfacial wear. This phenomenon has actually been referred to as "self- organization," where two surfaces deform or wear to accommodate the most favorable conditions for sliding.

Generally approached in a statistical framework, self-organization is considered to be a process of two surface roughnesses decreasing, coinciding with a reduction in friction and wear [131]. However, it has previously been shown that a process of preferential patterning may also occur simultaneously to this reduction [18]. This preferential patterning can be thought of as the gross projection of the harder, frontal contact geometry in the direction of sliding, and will result in an ordered "grooved" pattern. In other words, seemingly random surfaces in sliding contact will yield an ordered pattern in the softer substrate. Therefore, a micro-contact mechanics treatment of the local wear that includes the role of friction is proposed as a means of simulating the evolution of topography on the softer surface within the sliding contact. The test case in this

work involves a tribosystems consisting of a sacrificial molybdenum disulfide (MoS_2) compact sliding against a tungsten carbide (WC) disk.

5.2 A Sphere-on-Voxel Approach to Modeling Sliding Contact

The model will simulate the general case of two-body, dry wear, by employing a deterministic topography framework where voxels (i.e., cuboids representing the actual three-dimensional surface data) are used in concert with rigorous contact mechanics and an abrasive wear treatment. To simulate the evolution of the softer surface in siding contact, the following assumptions were made:

1.Contact between surfaces consists of voxels, with spheres of chosen radii embedded in the hard abrasive surface as asperity tips.

2.Contact is Hertzian and transitions between all three stress regimes— elastic, elasto-plastic, and plastic— each with its own wear and contact behavior.

3.Wear only occurs in the plastic regime and elasto-plastic regimes to the degree which the stress is fully plastic.

4. Wear and friction due to tangential resistance, may be simulated based on the degree of overlap between tangentially interacting asperities which obstruct one another's path.

5.3Contact Mechanics

In order to accurately model the wear process through varying contact conditions, the model takes into account the elastic, elasto-plastic, and plastic contact regimes, based on the work of Zhao, Maittea, and Chang [41]. A schematic of single asperity contact in the normal direction is presented in Fig. 38.

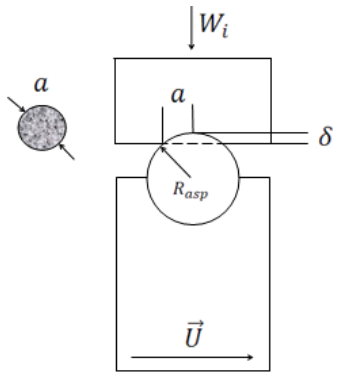

Figure 38: Schematic of sphere-on-voxel contact

$$\delta_e = \left(\frac{3\pi(0.4)H}{4E^*}\right)^2 R_{asp} \quad (1)$$

$$\delta_p = 25\delta_e \quad \text{(Theory)} \quad (2)$$

The threshold indentations are presented in Eqs. (1) and (2). Once the contact regime has been established, the resulting contact parameters are derived for each regime in terms of the indentation δ of *one* spherical asperity tip into a soft surface, in Eqs. (3)-(6).

Elastic Contact: $\delta < \delta_e$

$$W_{i,e} = \sqrt{\frac{16R_{asp}E^{*2}\delta^3}{9}} \quad (3)$$

Plastic Contact: $\delta_p \le \delta$

$$A_p = 2\pi R_{asp}\delta \quad (4)$$

$$W_{i,p} = 2\pi R_{asp}\delta * H \quad (5)$$

Elasto-plastic Contact: $\delta_e \le \delta < \delta_p$

$$W_{i,ep} = \pi R_{asp}\delta * \left[H - H(1-04)\frac{\ln\delta_p - \ln\delta}{\ln\delta_p - \ln\delta_e}\right] \quad (6)$$
$$* \left[1 - 2\left(\frac{\delta-\delta_e}{\delta_p-\delta_e}\right)^3 + 3\left(\frac{\delta-\delta_e}{\delta_p-\delta_e}\right)^2\right]$$

$$\left(\frac{\delta-\delta_e}{\delta_p-\delta_e}\right)=\mathrm{P} \tag{6a}$$

5.4 Normal Wear Modeling

For the model, a spherical indentation results in a frontal area A', which will be considered to participate in wear due to normal contact. This area is presented in Fig. 39.

$$A'=\frac{\theta}{2\pi}R_{asp}{}^2-a(R_{asp}-\delta) \tag{7}$$

$$\theta=2\sin^{-1}\left(\frac{a}{R_{asp}}\right) \tag{8}$$

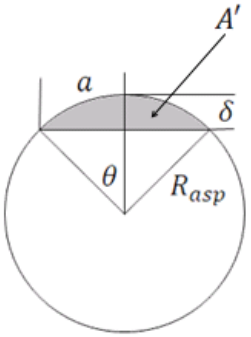

Figure 39: Schematic for A' Wear Geometry at a given indentation depth

The model assumes that wear may only occur in the case of plastic stress. As such it will also include wear from the fraction of plastic stress in the elasto-plastic regime, based on the parameter P in Eq. (6a). This parameter describes the ratio of plastic stress present during elasto-plastic contact. Lastly, the "B_{HK}" factor, based on severity of penetration, D_p, has been introduced which will incorporate the effect of different abrasive mechanisms on wear volume [33] and the presence of non-removal or plastic "side-flow" of material.

$$D_p=\frac{\delta}{a} \tag{9}$$

$$B_{Hk}=\frac{A'-A''}{A'}=0.4\tanh(12.3D_p-3)+0.4 \tag{10}$$

Given the determination of wear mechanism and frontal indentation area in terms of δ, wear volumes for the plastic and elasto-plastic contact regimes are calculated as follows:

$$V_p=A'B_{Hk}L \tag{11}$$

$$V_{i,ep}=V_{i,p}\mathrm{P}=A'B_{Hk}L\mathrm{P} \tag{12}$$

Where L is the sliding distance in one time step which will correspond to one voxel length and P is the amount of plastic flow present in the contact (6a).

5.5 Implementation of Tangential Interaction

Of crucial importance to the model is the implementation of tangential interactions which occur when obstacle asperities collide between time steps (see Fig. 40).

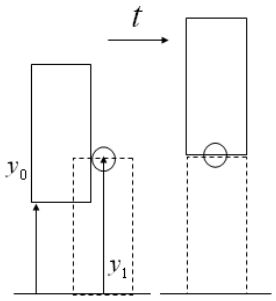

Figure 40: Schematic of Tangential Interaction

As opposed to assuming that wear happens either macroscopically as a result of gross motion *or* microscopically only as a normal indentation-then-drag action, the model attempts to capture both. This is done by examining the events when gross motion leads to these tangential impedances. At each time step, the model represents this interaction by calculating a mean path of travel based on the severity of overlap, y_0 to y_1, as shown in Fig. 40.This mean path for the spherical asperity tip, pictured in Fig. 41, will represent the motion of the asperity as it climbs over, deforms, or wears the softer obstacle asperity. This is especially relevant to capturing the wear interactions leading to preferential patterning, as well as calculating the contributions to friction by the energy believed to result from this stepping over process [28].

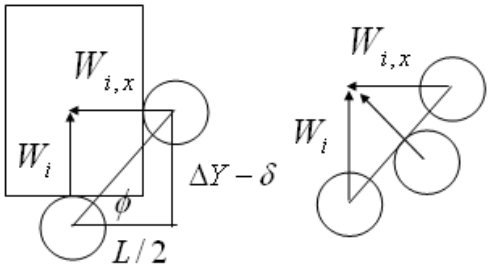

Figure 41: A linear path of asperity travel for friction modeling

Figure 41 shows the force balance on an asperity tip as it traverses this mean path. Though between steps, the resulting force in the Y direction must still act to balance the normal load on the asperity. This force will act normal to the plane of contact, resulting in a horizontal

component. The horizontal component of force may then be calculated as a function of indentation depth, normal load, and change in asperity height ΔY (between y_0 and y_1).

$$W_{i,x} = W_i \tan\phi \qquad (13)$$

$$\phi = \tan^{-1}\left(\frac{\Delta Y - \delta}{L/2}\right) \qquad (13a)$$

5.6 Results

For the tribosystems of a soft MoS_2 compact sliding against a WC disk, Figs. 42 and 43 present the cumulative wear and friction data, respectively, of the model versus tribometer experiments. Material and surface properties were input into the model to match those for the experimental system. In the early stages, the wear and friction is greater, as expected, due to the large amount of peaks which may obstruct one another. However, as these extreme asperities are worn down, the prevailing tangential obstructions decrease and more steady behaviors are observed. This trend agrees qualitatively well with the experimental results which also achieve steady sliding

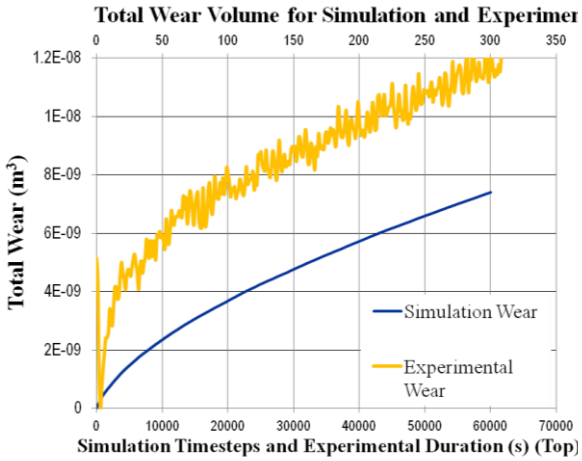

Figure 42: Wear data for modeling and experiment

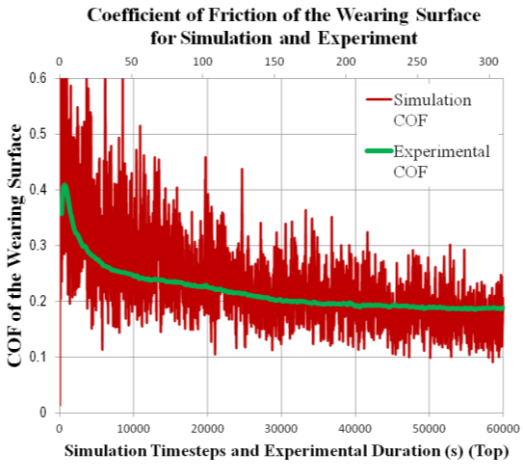

Figure 43: Friction data for modeling and experiment

The approach to steady sliding can be interpreted as a function of self-organization or a lowering in the surface roughness, but *also* of preferential patterning. As the tallest asperities travel through the soft surface, they in turn carve out their own projected "after image," thus re-organizing the surface to accommodate easy sliding on the next pass. This process is visualized best through the surface topographies presented in Fig. 44. Both the initial and final topographies for the soft surface are shown for the experiment (Fig. 44a) with the help of a Zygo optical profilometer and for the model (Fig. 44b).In both instances, though initially random, the soft

surface topography is transformed into a "grooved" pattern or texture to accommodate steady sliding conditions.

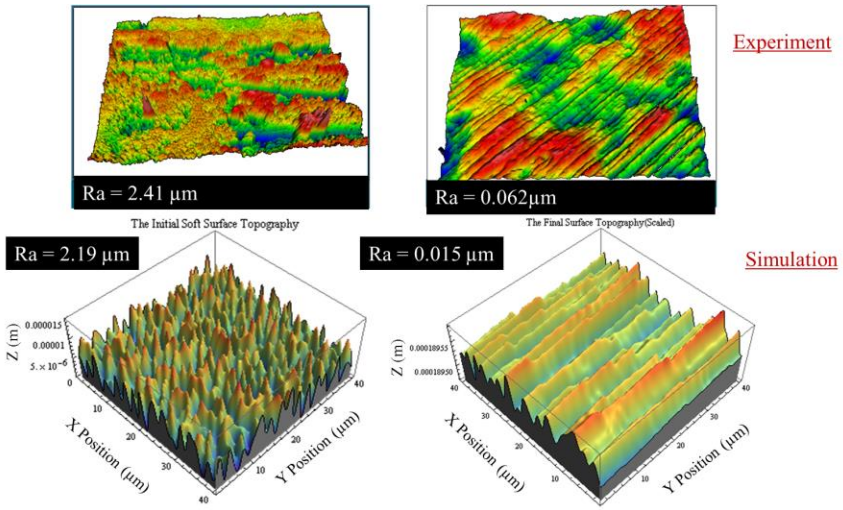

Figure 44: Initial (random) and final (preferential) topographies for (a) experiment (b) and modeling

In this case, due to the large discrepancies in hardness, no noticeable wear took place on the WC surface. Although the tribosystems in this work is soft on hard, the results provide interesting insight into the self-organization mechanism which was studied before for materials with a more similar hardness. Since one material is significantly harder, the self-organization process is isolated to one surface, consequently providing a more intuitive analysis. During contact, asperities present a topography, even in the case of nominally smooth surfaces, which is inherently detrimental to sliding. In order to accomplish translational motion, the asperities must be traversed either by climbing, deformation, or obliteration; all of which consume system energy manifested as friction. In this case, one surface experiences all of these transformations as it becomes more favorable for sliding. This results in the surface truly emulating the other, almost like an initially wavy patch of sand after a rake is pulled through. Even with random surfaces, the outlying asperities will be the ones to contact, and subsequently the ones to be preferentially patterned into the soft surface. As the pattern forms, steady-state or favorable sliding conditions are achieved.

5.7 Conclusions

Throughout this work, the interactions between hard and soft surface asperities were used to model the friction and wear present during the so-called self-organization. While generally thought of as a decrease in surface roughnesses, evidence for a relationship between surface patterning and steady sliding was leveraged using data from experiments and modeling results. The model was shown to provide qualitative agreement for friction and wear of an MoS_2 compact against WC, in addition to predicting experimentally patterned surface topographies. This suggest that our hypothesis that the low steady-state friction attained after run-in on dry and lubricated tribosystems is caused by localized wear processes producing an ordered, self-organized surface. A model incorporating a micro-contact mechanics that takes into account plasticity to predict the wear not only reproduced the friction and wear trends from experiments, they also were able to reproduce the preferential patterns resulting on the softer surface from the experiment.

Section 3 Powder Flow in Additive Manufacturing

The following section contains one chapter which details experiments in rheology and morphology characterization of additive manufacturing powders.

Chapter 6: Characterizing the Rheology and Morphology of Additive Manufacturing Powders

This chapter contains a study in which experiments were conducted to elucidate the effect of powder flow behaviors in the additive manufacturing process, as well as characterize the differences in rheology for a wide range of additive manufacturing powders.

6.1 Introduction and Motivation

As described in Chapter 1, Additive manufacturing (AM) suffers from three challenges that can be battled through greater understanding of differences in powder flow between manufacturers, materials, and different steps in the AM process. For this study, the rheology of a wide variety of AM powders was analyzed using a Freeman FT4 powder rheometer shown in Fig. 4 The machine itself has seen extensive use for powder characterization in a wide array of industries in which powder flow is a prime concern such as powder metallurgy, pharmaceuticals, and food processing [59, 62, 68]. The machine has several advantages over simpler devices like the Hall flow meter, in that it has the ability for highly precise *in situ* data capture, and the ability to impose a variety of different stress states. This last advantage is crucial for capturing data relevant to AM, as powders will behave very differently under the different stress states present in AM. A test in which simple gravimetric flow is monitored may not be enough to describe the variety of flows in the AM process.

Despite the advantages of the FT4 rheometer, only two papers to the author's knowledge have been published with an AM focus [72, 73]. In these papers, while they consider the effect of recycling on the flowability of a single powder type, very little is done to discuss how the rheometer's flow is relatable to different powder flows in AM. In order for rheological data to be relevant, it is crucial that this bridge be addressed. In addition, only single powder types for a given machine were considered in these papers, and so a discussion of how morphology changes will affect powder flow between manufacturers or materials is impossible. It is the goal of this paper to expand upon these works by elucidating how particle morphology will affect powder flow for a wide variety of AM materials and manufacturers, as well as offer insight as to how given stress states on an FT4 can be correlated to relevant flows in an AM system.

6.2 Experimental Setup and Procedure

6.2.1 Sample Additive Manufacturing Powders

The powder samples involved in this study cover a range of material systems and powder creation methods of interest to the AM community. As the resulting morphology of these creation methods were much more relevant to the thesis, than the methods themselves, specifics of the powder creation methods can be found in their respective citations. For powder bed systems, the main source of powder generally comes from the machine manufacturers (ARCAM AB and EOS) such that they can be sure to reliably print on the given machine. With that being said, they are often more expensive, and chosen from a very limited material set and so it is imperative for the cost saving potential of AM to gain the freedom to explore a wide range of vendors. The ARCAM EBM system requires coarser powder. The laser-based systems (EOS) are less sensitive to particle size, so smaller powders can be used to improve the surface finish of parts, but these powders are often highly prone to flow issues like agglomeration and jamming. Of the manufacturer-supplied powders, this study includes the standard plasma atomized [65] Ti-6Al-4V provided by ARCAM, as well as the gas atomized [61, 64] Ti-6Al-4V, Inconel 718, Al-10Si-Mg, maraging steel, and 316L stainless steel (SS) powders provided by EOS. It was confirmed that the EOS Ti-6Al-4V and Inconel 718 were atomized with argon, while the 316L used nitrogen, but information about atomization gas was not available for the Al-10Si-Mg and maraging steel.

Additionally, two non-standard Ti-6Al-4V powders in the ARCAM size range (> 45 μm) were included to compare the properties of commercially available powder to the manufacturer-supplied powders. One Ti-6Al-4V powder (Ti-6Al-4V from Ametek), was manufactured with a combination of Hydride-Dehydride (HDH) [61, 64] and plasma spheroidization [65], and was tailored to match the size range of the standard ARCAM powder (45–100 μm). Another Ti-6Al-4V powder was manufactured by Plasma Rotating Electrode Process (PREP) [61], and was by necessity was larger, with a target size range of 120–300 μm. All available information on the powders used in this study is summarized in Table 6.1.

Table 6.1: Alloy system and manufacturing method for powders

Machine	Material	Manufacturing Method
ARCAM (> 45 µm)	ARCAM Ti-6Al-4V	Plasma Atomization
	Ti-6Al-4V Ametek	Hydride-Dehydride + Plasma Spheroidization
	TI-6Al-4V Starmet	PREP
EOS (< 60 µm)	EOS Ti-6Al-4V	Inert Gas Atomized (argon)
	EOS Al-10Si-Mg	Gas Atomized
	EOS 316L SS	Gas Atomized (nitrogen)
	EOS MS1 maraging steel	Gas Atomized
	EOS Inconel 718	Inter Gas Atomized (argon)

6.2.2 Powder Morphology Analysis

Powder size and morphology characterization were performed via SEM image analysis in collaboration with the laboratory of Dr. Tony Rollet by PhD Student Ross Cunningham. A few grams of powder were provided in the form of sealed containers, which were vigorously agitated prior to sampling to prevent settling. A small amount of powder was then dispersed on carbon tape attached to an stub for scanning electron microscopy (SEM). The back-scattered electron (BSE) imaging mode was used to minimize topographic artifacts that may interfere with thresholding. Images were taken at various magnifications, with lower magnification images used for size distribution and morphology analysis in order to maximize particle counts.

Image analysis was performed with the open-source software developed by the National Institute of Health. Images were first thresholded into a binary image, and a watershed algorithm was used to separate touching particles. The watershed process had the effect of separating some satellite particles, thus slightly increasing the presence of small particles in the measured distribution. A built-in particle analysis feature was used to determine size and morphology distributions. For size distribution analysis, a minimum particle size of approximately 1.5 µm,

and 4 µm diameter was determined as the resolution limit for the smaller (EOS) and larger (ARCAM) powders, respectively, based on the difference in magnification used to acquire the images. Chemical analysis was performed on a random sampling of particles near the resolution limit by energy dispersive X-ray spectroscopy (EDS) to determine that they were in fact from the powder of interest and not contamination. For morphology characterization, larger minimum particle diameters of 10 µm and 20 µm respectively were used, because of the rapid increase in error in the shape descriptor calculations at low pixel counts.

6.2.3 Powder Rheometry

Tests were conducted using the stability and variable flow rate procedure of an FT4 powder rheometer, such that a confined compressive stress state, and an unconfined gravimetric stress state could be monitored for each powder. It is the belief of the authors that the confined compressive stress state, will be very similar to the flow state experienced by the powders during spreading. This is because powder particle sizes are often larger than the layer thickness chosen for a build, which leads to compressive stresses as the powder is entrained into the gap and packed into each layer. The unconfined stress state is still important as it will be representative of any hopper flow, as well as flow of the powder in front of the spreader before entrainment. This is because these flows are either totally unconfined by geometric constraints, or driven only by the force of gravity on each particle. Detailed information on the test procedure can be found in previous works utilizing the machine [59, 62, 68].

For each powder, a given run consists of three steps. Step one involves a conditioning step in which "as-poured" powder is mixed by the machine and allowed to pack gravimetrically. This ensures a reliable starting point for each run. Step two involves a downward and rotational motion of the impeller blade through the powder, which applies the confined compressive stress while monitoring torque and force response. Step three involves pulling back up, rotating in the other direction, through the powder as it is allowed to fall freely over the impeller blade. The total energy or resistance to flow is monitored in both step two and three. The average of the energy from the compressive step (step 2) is taken over 7 runs and recorded as the Bulk Flow Energy (BFE) in mJ. The same process is done for the energy in the free flowing step (step 3). The energy in this step is normalized by the sample weight, and recorded as the Specific Energy (SE) in mJ/g. The normalization by weight allows for a more direct comparison of each of the

powders resistance to flow in this state, since gravity plays more of a roll than it does in the confined compressive stress state, simply due to the motions involved. Each of these tests was conducted 5 times for each powder and so the final values for each powder material represent an average of 35 runs.

6.3 Results and Discussion

6.3.1 Powder Size Distributions

Powders from atomization processes generally follow a log-normal size distribution [2]. Figure 45 shows the powder size distributions plotted on a cumulative probability plot, where log-normal behavior appears linear. It was observed that all the samples follow log-normal behavior for at least a portion of their distribution. In most cases, a kink is observed, where the distribution changes dramatically. This is most notably observed in the Arcam, Ametek, and Starmet Ti-6Al-4v powders. For these samples, it is known that their lower sieve dimensions were 45 µm for Ametek and Arcam, and 125 µm for Starmet. These sieve sizes correspond directly with the location of the kinks in these distributions. The kink is less pronounced in the EOS powders, with a change in slope occurring in the 10–20 µm range for the 316L, maraging steel, and Inconel 718. For the EOS Al-10Si-Mg, the distribution appears to be log-normal throughout the entire distribution, suggesting no lower sieve. This would possibly explain the observation of a drastically higher presence of small (<10 µm) particles or "fines" observed in the SEM images. These types of particles cause increased particle-particle cohesion and agglomeration.

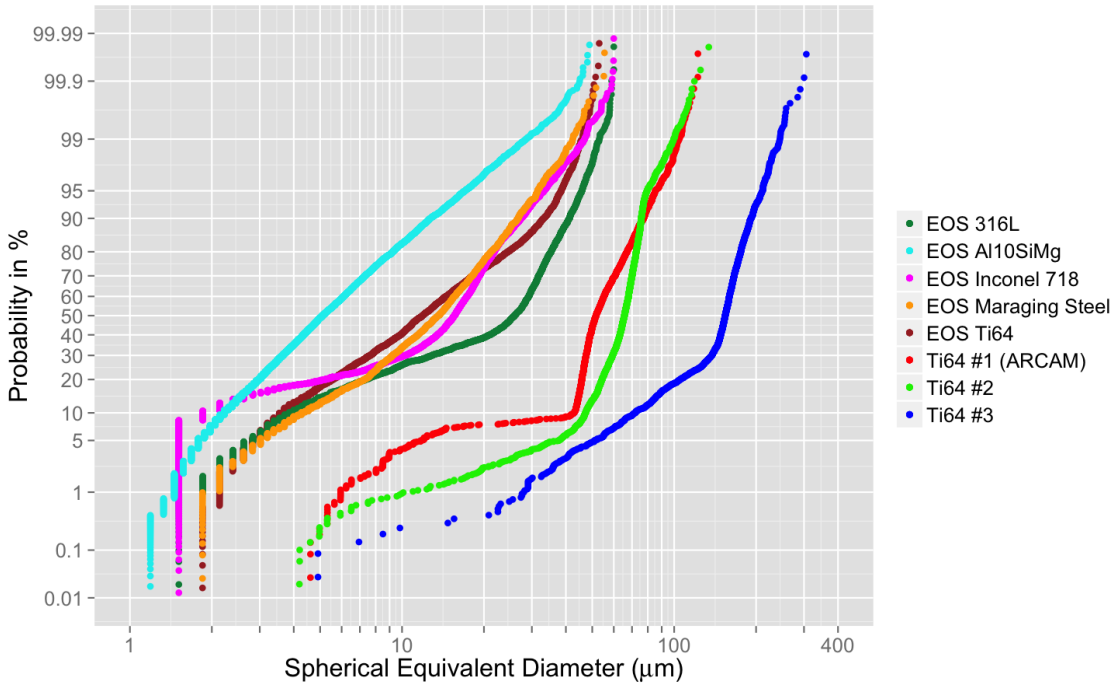

Figure 45: Cumulative probability plots of powder size distribution with axes adjusted so log-normal distribution appears linear. All distributions appear to be log-normal for at least part of their distribution. In most cases, a kink occurs, which corresponds to the lower sieve size in the powders. The aluminum appears to be log-normal through its entire distribution, except near the upper and lower tails.

6.3.2.1 Powder Morphology and Circularity

Powder morphology was measured two different metrics, namely *circularity* and *aspect ratio*. A plot of each particle's circularity is given in Fig. 46. The equation for *circularity* is given in equation 6.1, with a value of 1 corresponding to a perfect circle, and decreases as particles become more elongated and irregular. For aspect ratio, an ellipse fit is applied to the detected particle. The ratio of the major to minor axis is the *aspect ratio*.

$$C = 4\pi * \frac{(area)}{(perimeter)^2} \quad (6.1)$$

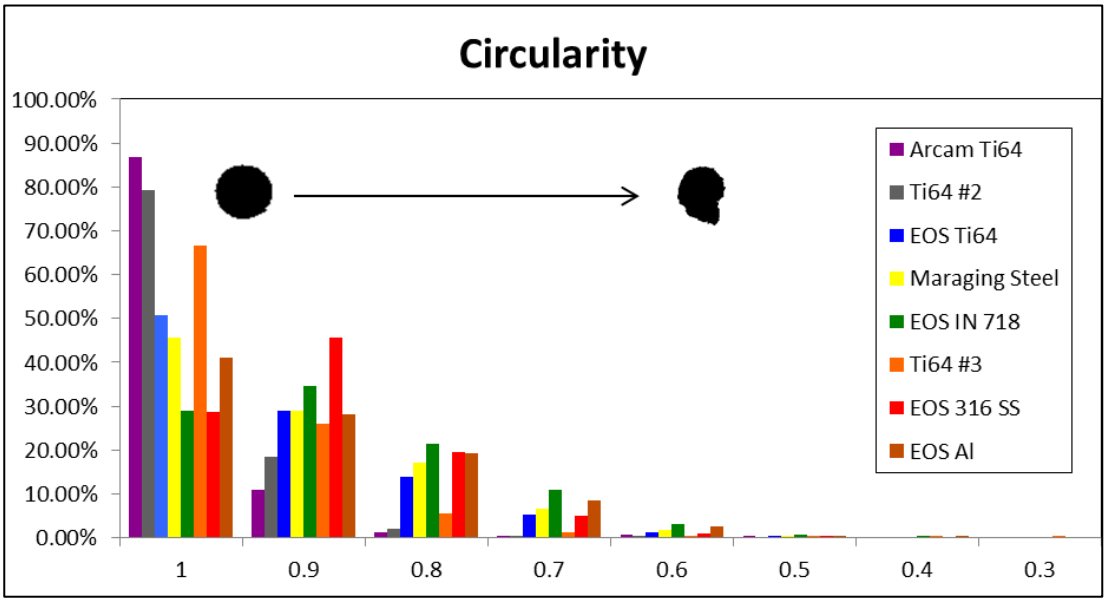

Figure 46: Circularity of Powder Samples

6.3.2.2 Morphology of EOS Powders

As seen in Fig. 47, the EOS Inconel 718, 316 Stainless Steel, and Maraging Steel; the samples were found to have very similar particle morphologies. They were found to be primarily irregular with a large amount of satellite particles. This is due to the manufacturing process described above and the fact that satellite frequency will increase as particle size decreases [64]. In terms of quantitative analysis, the powders were each found to possess a low degree of circularity, as seen in Fig. 46, as well as almost identical particle size distributions as seen in Fig. 45. The aluminum particles were found to be the only exception to this trend, in which they had a moderate degree of circularity, but were found to have very different size distributions. As seen in Fig. 45, a significantly larger proportion of fine particles were found in the Aluminum alloy indicated by the profound shift to the left and linear nature of the distribution curve. This type of morphology was found to have drastic rheological implications due to increased particle-particle cohesion that will be discussed in the section on rheological testing.

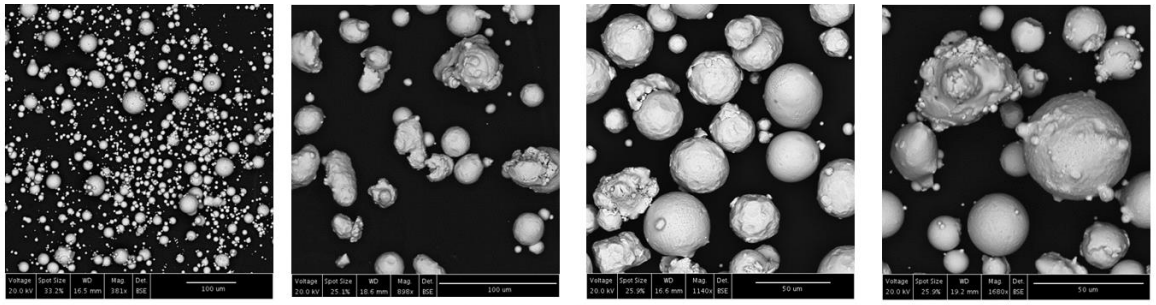

Figure 47: Average particle size and morphology of different powders for use in additive manufacturing from EOS

6.2.2 Morphology of Ti-6Al-4v Powders

As seen in Fig. 48, the Ti64 powders have similar qualitative morphologies, featuring highly spherical particles, with the exception of the EOS Ti64 which continued the morphological trend described in the previous section. These results are also reiterated by the circularity plot on in Fig. 46. In terms of size distribution, a size increase was observed in Fig. 45 between each Ti64 powder. The average particle size for each powder including the EOS powders is presented in Figure 48. These distributions allow us to study the effect of changing morphology, as well as changing size among powders that are the same material.

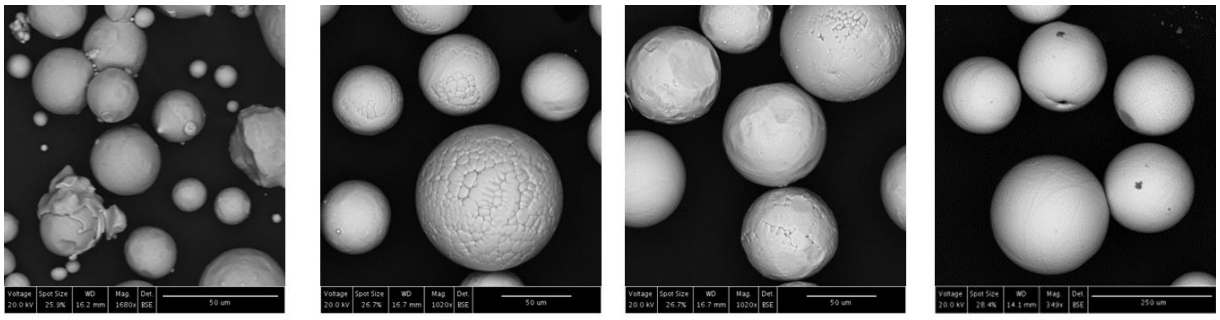

Figure: 48 Average particle size and morphology of Ti-6Al-4V powders for use in additive manufacturing from different manufacturers

6.3.3 Powder Rheometry Results

Figure 49 Showcases the results for rheological behavior of each powder under both a confined compressive stress and an unconfined gravimetric stress. Recall the confined compressive stress is best representative of the entrainment zone underneath the spreading

mechanism. This is due to the fact that during a spread, the build layer is generally chosen to be smaller than the average particle size of a given powder. As the powder is deposited through entrainment, the particles will experience a confined compressive stress when they are packed into the layer. Powders with a higher resistance to flow in this state may be more inclined to stay in front of the spreader similar to a "plug flow," rather than be entrained into the layer. Recall as well that the unconfined stress state is best representative of any gravimetric feeding mechanism such as a hopper, as well as the areas in front of the spreader. In this section of the AM process, the powder is allowed to freely flow under its own weight and often without any geometric constraint. Powders with a high resistance to flow in this state can cause problems involving agglomeration and are generally highly cohesive. Interestingly enough, powders with too low a resistance to flow in this state, can interfere with delivery of the powder from the hopper, causing a spill scenario into the build area. The parameters to represent the resistance of these powders to each flow are the bulk flow energy (BFE) under compressive flow, and the specific energy (SE) under unconfined flow.

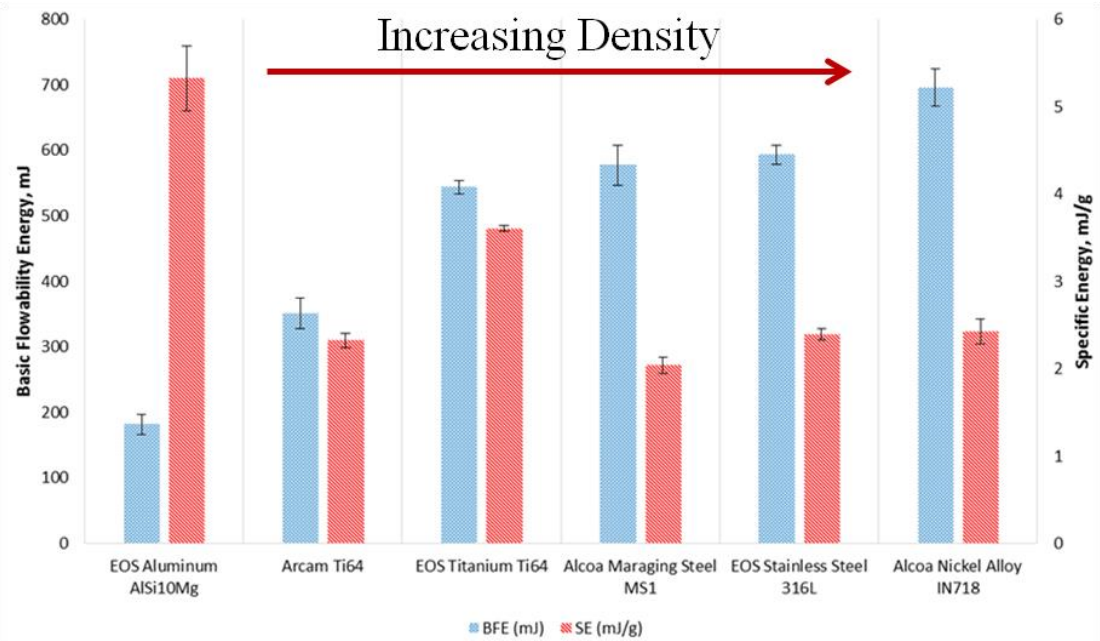

Figure 49: Bulk Flow Energy (BFE) and Specific Energy (SE) for powder flow in the spreader-like and hopper-like stress states respectively for EOS powders and Arcam Ti-6Al-4V (for comparison)

6.3.3.1 Rheology of Different Powder Materials from EOS for Direct Laser Sintering

The different powder materials have been displayed on the x axis in order of increasing consolidated bulk density (CBD), with the BFE being plotted on the left in blue, and the SE on the right in red. CBD is simply the density of the powder bulk after the conditioning step, and is a measure of how well the powder will pack on its own. It can be seen firstly that there are drastic differences between the rheology of each powder material, in which different materials require different energy's to maintain flow. In addition to this broad observation, the BFE was found to increase monotonically with increasing CBD. This makes sense as the BFE is a measure of the energy required for the impeller blade to traverse downward through the powder bulk while applying a compressive stress. A high CBD indicates that the powder has arranged itself into a very ordered state with few voids, corresponding to a high packing fraction or solid fraction. This is particularly relevant for AM because it can be counterintuitive when considering flow parameters to use when building with a new powder. If the bulk has a very high solid fraction, even if the powder appears to be free flowing, it is difficult for the powder to flow under compressive stress because it will be arranged into such a dense block. Simply put there will be a lack of space for it to flow and so powder's that pack too efficiently without yet applying any stress may resist entrainment under the spreader. On the contrary, powder with a low CBD due to higher particle-particle friction may not pack well initially due to agglomeration. But under compressive stress, the agglomerates are easily broken and the voids provide an easy avenue for the powder to flow and then become entrained into the build layer.

This type of example was highlighted well by the differences in rheological performance of the EOS powders. From Fig. 49 it can be seen that the Maraging Steel, 316 Stainless, and the Inconel alloy all displayed similarly high BFE and low SE despite being made of different material. On the other hand, the aluminum alloy Al10SiMg displayed the highest SE and the lowest BFE. These fact that the other three EOS powders displayed opposite behavior can all be explained by the effects of the aluminum alloys morphology on CBD and powder flow. Unlike the other EOS powders, the Al10SiMg powder was found to have a small average particle size, high circularity, and a much higher number of "fines". All of these morphological phenomena suggest a high degree of cohesion between particles. On the other hand, Each of the other EOS powders were found to have a lack of fines, low circularity, and a larger particle size, all of which would lead to a powder with low cohesivity. In conjunction with the low weight of the aluminum powder, the high cohesivity resulted in large a very large SE and a low CBD,

indicative of agglomeration and large voids in the powder bulk. However, Due to the lack of cohesive morphology led to low SE values and a high CBD. In other words, the aluminum powder was found to have high resistance to flow in the hopper-like stress state due to its morphology, while the other EOS powders were all found to have similar low resistance to flow in the hopper-like stress state.

It was found that these morphologies perform exactly the opposite under the spreader-like state. While the Al10SiMg powder did not flow well under its own weight due to cohesivity, the high circularity will also act to promote rolling between particles whereas the extreme irregularity of the other EOS powders will not. Under the compressive stress state similar to the spreader, the agglomerates of the Al10SiMg were easy to break apart, and a low BFE was recorded. The originally low CBD can actually be beneficial here as the voids provide room for the powder to rearranged and entrained under the spreader. On the other hand, the other EOS powders were already well packed into a coherent bulk. They also possessed a lack of circularity and a high degree of satellites which act to increase particle-particle friction during rolling. When forcing a well packed, irregular powder to flow in a confined scenario, these factors can lead to a "plug flow" scenario in which the powder is very difficult to entrain under the spreader. This was reflected in the high BFE values recorded for each of the other EOS powders. The key takeaway from these results is that powder morphology can control flow in contrasting ways in different parts of the AM process, even among powders of different materials. This type of result stresses the need for powder rheometry in contrast to simpler tests in which different flow states are not investigated. Through the use of powder rheometry, "trouble spots" for a new powder can be identified before implementation. Furthermore, by linking these rheological behaviors to a given morphology, a change in the powder processing could be used to improve flow in a given section of the AM process.

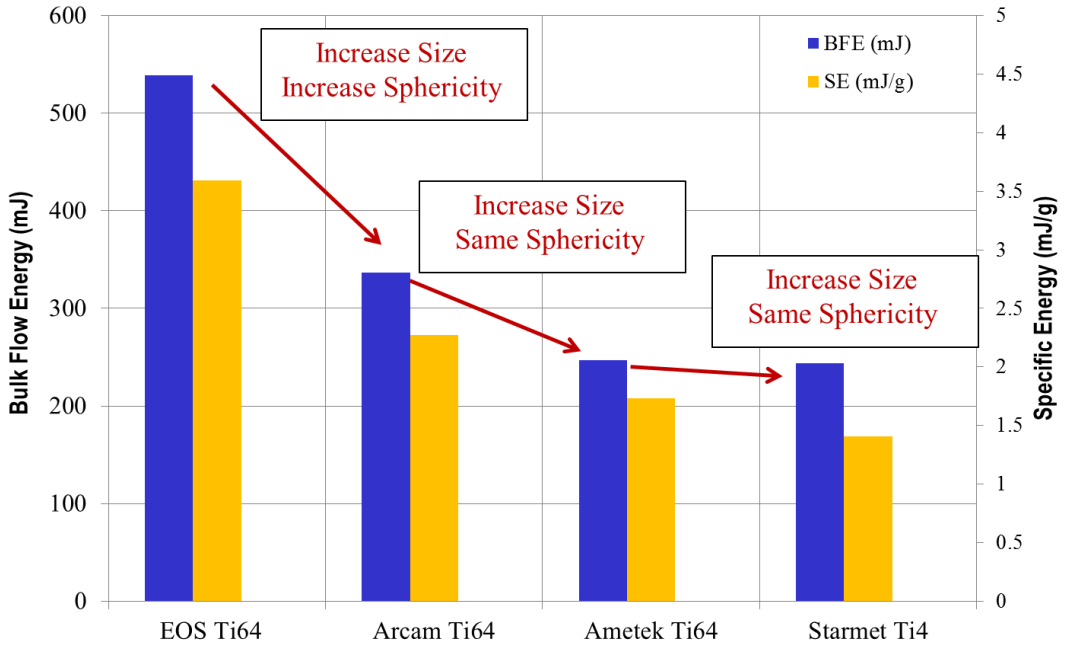

Figure 50: Bulk Flow Energy (BFE) and Specific Energy (SE) for powder flow in the spreader-like and hopper-like stress states respectively for varying Ti-6Al-4V Powders

6.3.3.2 Rheology of Ti-6Al-4v Powder from Different Manufacturers

Morphology differences can also be useful for pre-emptively explaining rheological behaviors of the same powder material, but from different manufacturers as displayed in fig. 50. This was observed directly for the four types of Ti64 powders, whose morphological characteristics are displayed in in Fig. 48. As with the other EOS powders, EOS Ti64 was found to have the smallest average particle size as well as more fines than any of the other Ti64 powders. In addition, its particle morphology was much more aspherical, irregular, and possessed a large degree of "satellites." Once again, this type of particle morphology resulted in increased BFE and SE when compared to the other Ti64 powders. The smaller particle size most likely led to higher cohesive forces between particles, while the irregular shape and large degree of satellites prevent a smooth rolling mechanism between particles. In this case, the morphology is poor for *both* stress states when compared to the other Ti64 powders. For the Arcam Ti64, which featured a larger particle size, less fines, and a large increase in circularity, the BFE and SE were drastically reduced. It is important to note that in these two features will work in tandem to increase flowability both in the stress state akin to the spreader and the hopper. The increase in size will decrease cohesion, while the circularity will decrease rolling friction between particles.

Further evidence for how both the size *and* shape affect flowability can be seen when examining the Ametek and Starmet powders. In this case the shape remained almost identical but the size was incrementally and then drastically increased. The BFE and SE were seen to decrease for the Ametek powder but by a much smaller amount than from the EOS to Arcam. In the case of the Starmet powder, the size was increased by over 100% but there was a negligible effect on the BFE. As discussed for the EOS powders, the BFE is largely dependent on the powders resistance to rolling friction, due to the fact that particles are being forced to roll over one another. Cohesion in this stress state, can actually be beneficial to low BFE as was shown with the more cohesive aluminum powder. Therefore it follows that increasing size will be somewhat less important in decreasing resistance under this stress state despite decreasing particle-particle cohesion. For The SE values in the hopper-like state, a greater dependence on cohesion was seen, as evidenced by the continuing decrease in SE as we increased particle size. This makes sense as the particles are allowed to fall freely over one another without constraint and so the dominant force will be particle-particle cohesion rather than rolling friction as particles are pressed together. It should be noted that the decrease in SE as particle size increased between Ti64 manufacturers was found to diminish. For powder flow it is known that there exists a threshold for particle flow in which increasing the particle size will have less effect on decreasing cohesion. This is due to the reliance of cohesion to surface energy which decreases drastically as the surface area to volume ratio drops (Citation). It should be noted from the data it appears that this value has not been fully reached, due to the fact the SE, which is dominated primarily by particle-particle cohesion, was still seen to decrease. These results stress the fact that particle morphology must be considered as powders are evaluated from different manufacturers even when using the same material. Large decreases can be achieved in resistance to flow by increasing circularity and particle size. Flow under the spreader appears to be dominated by resistance to rolling friction, as justified by the diminishing effect of increased particle size which primarily governs particle-particle cohesion. Flow in the hopper seems to be much more dominated by cohesion and influenced by factors like particle size. Smaller powders may perform well under the spreader, but may present problems in the hopper like scenario.

As a final note on the complexity these morphological effects can present to powder flow in the AM process, too little resistance to flow can also cause problems. For instance, while using the Ametek powder, builds were successful on an Arcam EBM machine without altering

any hopper parameters. However when switching to the Starmet powders, the flowability was so drastic that a complete redesign was required such that powder would not spill over the build plate and flow sensors which govern redundant spreads. This could be prevented through screening with powder rheometry. Testing showed that increasing the particle size from the Ametek (70 μm) to the Starmet (160 μm) powder did not affect the flow under the spreader like state, but led to decreased resistance to flow in the hopper-like state. This is an excellent example in which rheological characterization can provide pre-emptive evidence that a given powder morphology may not work without re-design of the machine. A threshold value for SE could be established as a standard for ensuring acceptable powder flow in a given hopper to which manufacturers could adhere.

6.4 Summary & Conclusions

Additive Manufacturing is considered to represent a monumental advance in the capability of human machining, due to its potential to create parts which are both cheap and featuring previously impossible geometries. Despite the impressive promise, the current state-of-the-art is marred by three key drawbacks, each of which has some reliance powder spreading process. First, finished parts can have low tolerances in the form of either sub-optimal strength due to internal porosity, or rough surface finishes. These defects can arise from non-uniform spreads in which the particles are not perfectly arranged and therefore cannot be sintered continuously. Second, machine time can be extremely costly when considering large scale manufacturing. In this case reducing spreading time is a crucial element particularly when it must be done repetitively to ensure adequate coverage of the build layer. This means that spreading as fast as possible, as uniformly as possible, will be necessary to ensuring AM can be used in large scale manufacturing. Third, AM suffers from a very particular material set. Any efforts to utilize new powders will require an understanding of how the powder will flow before it is put into the machine to avoid difficulties in uniform spreading and hopper flow.

These aspects of the AM process which rely on powder flow, stress the need for a larger understanding and control over a given powder's rheological behavior. In this work powder rheometry was used to characterize the rheology of a wide range of additive manufacturing powders from EOS, as well as four different Ti64 powders from different manufacturers. From the study of different EOS powders, it was found that different AM materials with similar

morphology can have almost identical behavior under stress states akin to both the hopper and spreader. However, changes in morphology and size can cause a powder to display the exact opposite behavior under each stress state. In terms of a stress state similar to the hopper, materials with low circularity and low number of fines were found to have the least resistance to flow most likely due to decreased cohesion. In contrast, materials with high sphericity and fines such as the EOS Al10SiMg were found to form large agglomerates which would stick together and prevent flow. In terms of a stress state similar to the spreader, materials which were highly circular with large particle sizes were found to provide the least resistance to flow. In this state, parameters like circularity and decreased sattelites were found to have the greatest impact in reducing flow resistance, most likely due to enhanced rolling. A monotonic trend was also seen in which a powder that packs more efficiently on its own, represented by a high CBD, would display increased resistance to flow under the spreader-like state. These types of rheological similarities and differences, amongst powders from the same manufacturer, as well as those of the same material from different manufacturers, help to stress how morphology can be used to explain why powders may behave differently in different areas of the AM process flow. Depending on the material, this work suggests that powder morphologies may be tailored to provide enhanced performance based on which part of the AM process is in need of flow optimization.

Section 4 Experiments in Single Cutter Interactions for Deep Well Rock Drilling

The following section contains three Chapters (7-9), which detail experimentation dedicated to elucidating the friction and rate of penetration behaviors of PDC cutters against deep-well rock substrates. A combination of *in situ* data collection and *ex situ* analysis was used to provide insight into interfacial mechanics for a given rock, as well as lubrication medium.

Chapter 7: Bit Cutter-on-Rock Tribometry: Analyzing Friction and Rate-of-Penetration for Deep Well Drilling Substrates

This chapter contains a study in which dry rock cutting was investigated for Carthage marble using hardened tool steel drill buttons. A similar version of this paper was published in *Tribology International.* [Dougherty, P., Pudjoprawoto R., Higgs III, C.F. "Bit Cutter-on-Rock Tribometry: Analyzing Friction and Rate-of-Penetration for Deep Well Drilling Substrates." *Tribology International,* 2015]

7.1 Introduction

While the search for renewable energy technologies continues, the harvesting of resources such as fossil fuels and geothermal heat, through drilling, will continue as the major source of power around the globe. In addition, as diminishing fossil resources push drills deeper into the earth, operation costs in the resulting extreme environments represent a serious obstacle for effective implementation, especially in conjunction with delays and breakdown due to drilling failure. In particular, 70% of the US deep-sea oil and renewable geothermal resources come from rock wells deeper than 1524 m (5000 ft). And in these deep wells, drilling costs are found to be an average of 50% of total project costs [74].

The breakdown and wear of these drill-bits, which are exacerbated by the high temperatures and pressures experienced in the deep well interface, play large roles in the impact of the drilling process on the total cost of a project. Firstly, the bits themselves are difficult and costly to manufacture due to both the complexity of optimal bit shapes and the employment of ultra-hard, state-of-the-art materials like diamond and WC/Co [79, 137]. Secondly, the high pressure and low temperature conditions require advanced procedures for any maintenance or replacement of bits in the field. Subsequently, any breakdowns due to bit-wear or failure can cause long shut-down periods in project operation [74, 79, 137].

In the deep drilling process there are generally two types of bits. The first referred to as the Roller Cone bit, which features three Rollers coated with teeth or cutters. The entire bit is spun around its vertical axis, and the rollers are allowed to rotate independently of the integral drill motion. The PDC bit, named for its frequent use of polycrystalline diamond compact

cutters, is somewhat less complex dynamically, yet has grown to be the industry standard. It employs many different shapes in terms of cutter face, orientation, and placement, in order to facilitate optimal drilling. During the rotary drilling process, the stationary PDC cutters facilitate a combination of scraping, gouging, and crushing mechanisms, in order to continuously wear into the rock surface. Scraping is the removal of smaller surface level asperities, whereas crushing encompasses the destruction of larger rock features comprised of multiple asperities. In general, softer rocks will wear primarily through a scraping and gouging process like the abrasive mechanisms found in sliding metals. However the crushing mechanism is more prevalent for harder and rougher rocks where larger, brittle features are ground down all at once [84, 86, 96, 138]. Both of the bits are coated with cutters comprised of hard tool steel, ceramic carbides, or machine grade diamond [84, 96, 138]. While often difficult to find due to the industry specific nature of rock drilling science, these mechanics of the drilling process are often elucidated when a combination of patent information and journal articles are reviewed.

As a result of the high importance of the drilling process, there are a number of experimental works which have attempted to catalogue the industry level drilling science in terms of field or industrial scale performance. For instance, Black et al. helped to categorize the relationships of parameters such as weight-on-bit (WOB), torque, and rpm, on rate-of-penetration (ROP) for PDC bits in a variety of deep-well rocks[78]. These works were augmented in 1999 by Fear who examined a variety of operational parameters and a number of different drilling techniques with the hopes of optimizing ROP for PDC bits [81]. While many of these works represents significant attention towards the system level parameters which govern rock drilling or cutting, it has been proposed that cutter-rock interfacial parameters, such as friction and wear, will greatly affect the efficiency of drilling [83, 91, 139]. It would follow that a tribological framework with more precise, laboratory scale equipment would be well suited to study wear in the energy drilling sector, but so far little has been done. This is largely due to the unpredictably brittle and anisotropic nature of the rock substrate, as well as the difficulty in realistically simulating such a complex process.

For example, most of the single cutter laboratory studies are dominated by the vertical turret lathe (VTL), in which a cutter is held at one given penetration depth while a cylindrical rock is rotated beneath it. Although able to study the reactionary frictional forces and reactionary normal forces, the lack of a descending cutter prevents the user from examining relationships between *in*

situ ROP data and actual cutting forces [82, 92]. In 2008, the Ultra Deep Single-Cutter Drilling Simulator (UDS) was built by the National Energy Technology Laboratory (NETL) to study single cutter interactions in a manner more representative of the true drilling process. Lyons showed in 2008 how this rig might be used to acquire ROP and Borehole Pressure as functions of WOB and RPM [74]. However, data from its operation has yet to be published. Even for the UDS, which is may be able to capture the inclusion of drilling fluid, contact level parameters like friction and *in situ* wear are very difficult to ascertain. In addition, its complexity, size, and cost make it detrimental to permitting study in the academic laboratory setting.

As a result, a need exists for extensive analysis both in terms of experiments and modeling in order to understand the drilling process both from a tribological perspective as well as a more accessible laboratory scale framework. This work will present a smaller scale framework, as well as feasibility measurements in which the cutter is allowed to freely penetrate the rock while examining friction and wear at the cutter-rock interface referred to as bit cutter-on-rock tribometry (B-CORT).

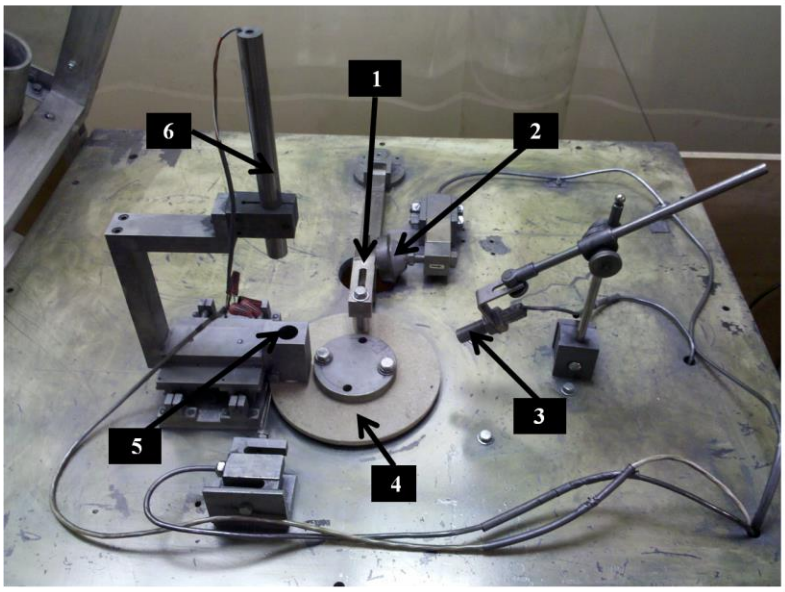

Figure: 51 Experimental Setup for the BCORT System when cutting with O1 Tool Steel

7.2 Experimental Set-up

An existing pin-on disk tribometer, developed in-house [19], has been modified to conduct B-CORT experiments, as shown in Fig. 51. System responses during testing such as frictional cutting force, linear disk speed, and depth of cut (DOC) can be measured *in situ* to elucidate the impact of these tribological parameters during a simulated drilling process.

The slider arm and cutter assembly features a slot for adjustable radial position, allowing for multiple wear tracks to be established on one disk. This is a key feature as BCORT tests are destructive to the often difficult to machine rock substrates. Given this testing constraint, the ability to conduct multiple runs on one rock disk is paramount to broad data collection. A myriad of different cutter materials, such as polycrystalline diamond compact, and cutter shapes may be easily interchanged. The first set of testing was carried out with an O1 tool steel cutter with a hemispherical tip. This cutter is loaded with a dead weight (not shown here), and allowed to *freely* penetrate into the rock as the disk rotates at a given RPM. During this process, frictional forces drag the arm into a compression *load cell from Massload Co. with a resolution of* , providing purely frictional force measurements from the cutter-rock interface. As the disk spins, its angular and linear velocities are tracked using a tachometer from *with resolution of* .

In order to ensure that DOC measurements could be obtained *in situ and* separate from the influence of bit-wear, a system was developed to measure the DOC downstream from the cutter interface. A "trench tracer" made from ultra-high molecular weight polyethylene (UHMWPE) and designed to have the same hemispherical dimensions as the cutter, was mounted with a Linear Voltage Differential Transducer (LVDT) with a resolution of 2.5 um. This tracer was allowed to descend freely into the track as the DOC progressed. The choice of the ultra-low friction, low wear UHMWPE ensures that the tracer will not introduce excess friction into the system while also experiencing negligible wear during multiple operations [140].

During a test, LabView data acquisition software was used in order to compile results for coefficient of friction (COF), tangential cutting force, linear disk speed, and DOC. A Zygo NewView 7300 optical interferometer (OI) was employed in order to analyze surface topographies and also to verify the accuracy of our *in situ* DOC. The rock specimens for BCORT testing represent samples found typically in deep wells and also used in performance modeling of drill bits. These include Carthage marble, sandstone, and shale [90]. Samples from these rocks were quite difficult to obtain, both in terms of obtaining the correct type found in deep wells, and due to the inherent challenges in machining rock samples to precise specifications. However, the

samples were successfully fabricated as 0.6223 cm thick disks, using water-jet cutting and provided by the National Energy Technology Laboratory (NETL). The sandstone and Carthage marble samples are presented in Fig. 52 along with Interferometer Scans to display their respective topographies. For preliminary testing cutter and rock materials were O1 tool steel and Carthage marble respectively.

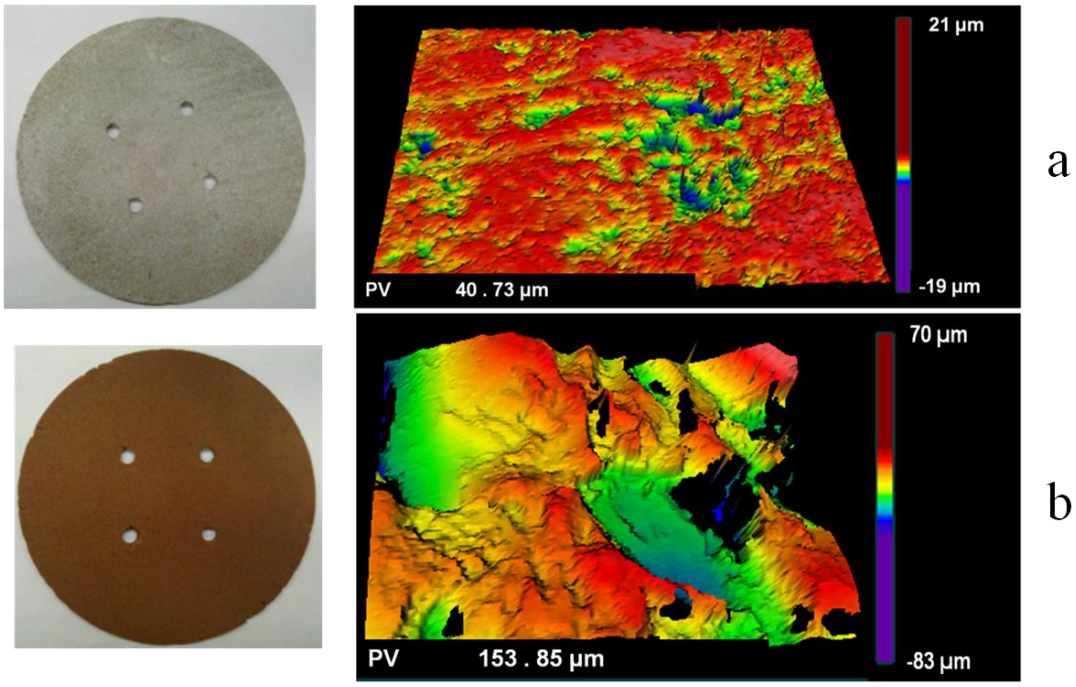

Figure 52: Initial Topographies for (a) Carthage Marble and (b) Nugget Sandstone Rocks

7.3 Experimental Procedure

7.3.1 Initial Cut Testing (IC): These tests consisted of allowing a fresh cut to develop on its own, on an otherwise untouched rock disk, and were most relevant for gaining an understanding of transient behavior which would occur during any start-up, shut down, or dynamic event, such as the creation of a cut, during the drilling operation. In addition, they also provide interesting insight into the relationship between the friction, cutting mechanism, and ROP which will be discussed later. Substrate speeds were set to 1.4 m/s or 195 rpm, to approach the somewhat lower sliding speeds utilized in previous deep drilling simulations and industry field data [74, 78, 81, 92]. Cutter loads were employed at 13.34N (3 lbs) corresponding to a mean Hertzian contact pressure of 0.23 GPa.

7.3.2 Resume Cut Testing (RC): After the conclusion of an initial cut test, the rock and cutter were allowed to cool to room temperature in order to dissipate any residual heating. At the

onset, the slider arm was adjusted such that the cutter rested in the center of the already present wear track. These tests were conducted in order to explore the steady behavior of continued rock cutting in an established cut. Cutter loads were varied between 13.43-53.38 N (3-12 lbs), along with disk speeds of 1.4 - 4m/s or 195-500 rpm.

7.3.3 Ejection Testing: Due to the presence of interesting transient and steady-state behavior, a series of tests were run in order to explore the presence and effect of interfacial wear debris, or "third bodies", in the cutting interface. During these tests, a compressed air gun was utilized as a substitute for drilling fluid which would usually act to remove rock cuttings from the interface. Periodically throughout an Ejection Cut test, the gun would be switched on in order to facilitate this removal, and the ejection of third bodies was subsequently observed using a high speed video camera. The resulting frictional behavior was monitored and analyzed after the conclusion of a test.

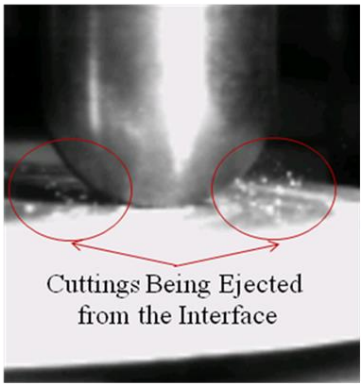

Figure 53: High-speed Camera Images of Cutting Ejection in the BCORT Interface

7.4 Results & Discussion

7.4.1 Validation Studies:

In order to understand the evolutionary cutting process, a high-speed camera was used to capture video images of rock cuttings as they form and are removed from the interface. A screenshot from these videos is presented in Fig. 53. It is important to note that a large amount of the cuttings can be seen exiting to either side, but that a number will also remain in the interface as will be discussed later.

During the cutting process shown in Fig. 53, results for both COF at the cutter and the DOC are captured *in situ* and presented in Fig. 54a. These particular results are for an IC test, as can be seen from the initially low friction coefficient which corresponds to the development of a cut. In order to validate the accuracy of the DOC capturing set-up, the trenches developed during initial cut tests were examined e*x situ* using the optical interferometer. This image is presented in Fig. 54b. The total depth of the cut, shown as the PV (peak to valley) value in Fig. 54b, was then compared to the difference between the maximum and minimum DOC values registered by the LVDT for the *in situ* data in Fig. 54a. The total depth of the *in situ* DOC data was 105.5 um,

while the interferometer reported a DOC of 102.6 um. It is believed that this small discrepancy between the two measurements may represent the small amount of wear experienced by the UHMWPE tracer used to track DOC. In essence, the measured wear using the B-CORT rig would be a combination of the UHMWPE wear, plus the DOC into the rock at any given time. This stresses the need for a very low wear material to be employed as the tracer. However, this small difference of only 2.8% provided validation for the system. Additionally, this small error in using the system is far outweighed by the ability to capture and analyze *in situ* data, namely the evolution of the DOC and the coefficient of friction simultaneously with time.

7.4.2 Transient Studies:

In the development of a cut, during the initial cut (IC) testing, there are a few regimes present which should be mentioned as they will be shown to provide insight into relevant rock cutting mechanics. Results from an IC test, which show three behavioral regimes, are presented in Fig. 55. The COF generally began as low as 0.2 as the cut was developed corresponding to Regime 1. This gradual development of the cut pervaded in most tests, lasting between 30 to 65 seconds, and always at a COF ~ 0.2. This delayed process of Regime 1 was thought to be a result of the relatively low hardness of O1 tool steel compared to that of standard industry cutters and the need for a buildup of crack propagation to incite a cut in addition to standard run-in behaviors. Around 65 seconds, the COF rose quickly to a maximum value of 1.1 as the cut widened considerably into a discernible white stripe. The maximum COF of Regime 2 pervaded until 200s where a steady, slow decrease in COF was observed and found to characterize Regime 3. In later tests, this decrease was found to continue until a limiting value was reached, which will be discussed in later sections.

It should be noted that the ROP, displayed by the slope of the DOC graph in Fig. 55b, follows a similar trend in each regime. In all tests conducted, ROP shows a directly proportional relationship with friction. Initially in Regime 1, indicated in blue, the ROP and COF are both quite low. In Regime 2 COF rises, and ROP also increases to a maximum value indicated by the steeper slope and shown in red. Then in Regime 3, denoted in green, this value decreases to a steady-state lower than the interim, Regime 2 values.

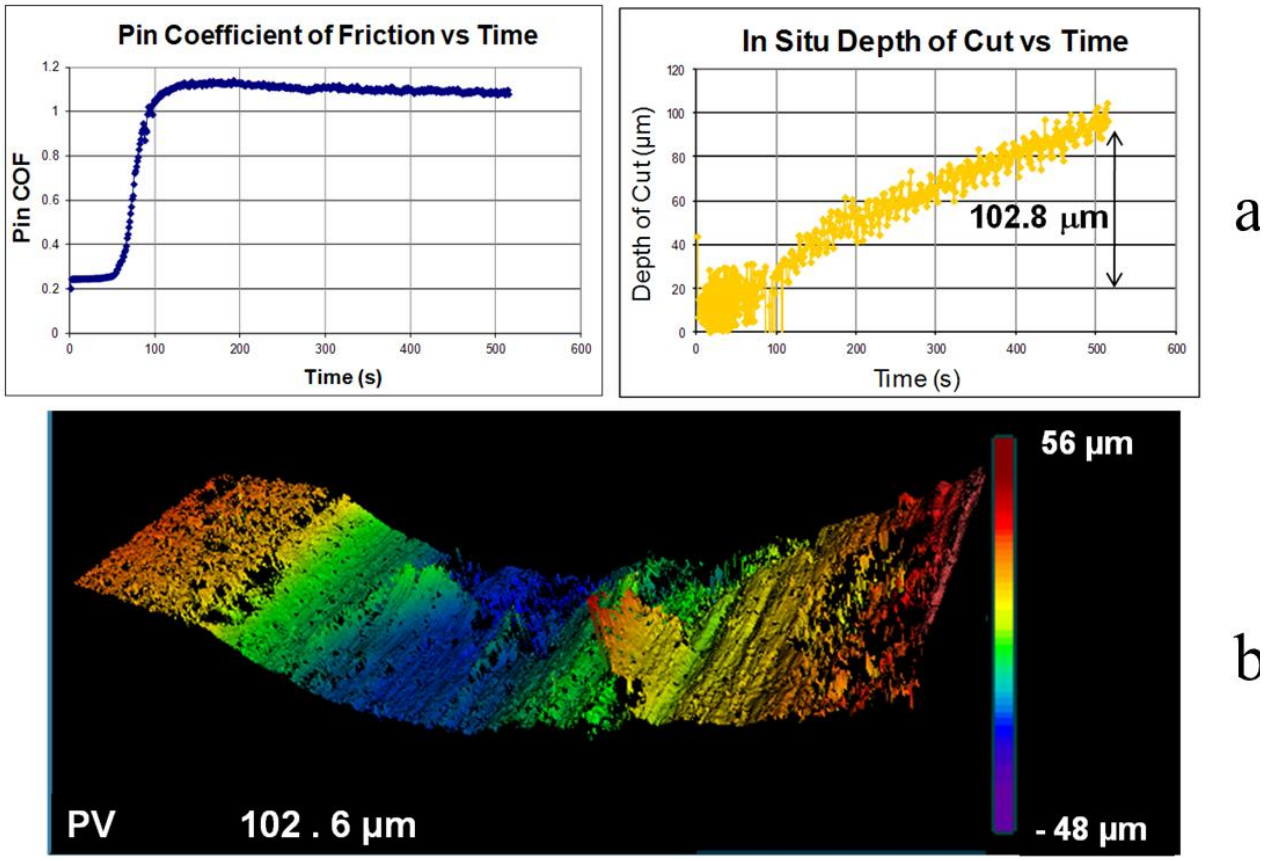

Figure 54: Results for initial cut testing of O1 tool steel on Carthage Marble detailing (a) Friction and Rate of Penetration and (b) *ex situ* surface metrology of the cut

Initially, three effects were studied to ascertain the cause for the transient behavior of both COF and ROP, which were presented in Fig. 55 to highlight Regime 1 (pre-cut), Regime 2 (interim), and Regime 3 (steady-state, post-cut). The first was to explore transient interfacial temperature rises as the primary cause for drastic changes in COF and ROP, through the use of *Resume Cut (RC) testing*. Despite allowing for this drop in temperature, friction coefficient and ROP would still resume at high values between 0.9-1.1, exactly where it left off on the previous run. A full example of these results is shown in Fig. 56. It is important to note that the COF of Resume Cut testing seemed to stay steady at about 0.9, as opposed to a steady decrease as seen in Regime 3 for Fig. 55, which will be discussed in more detail in the following sections.

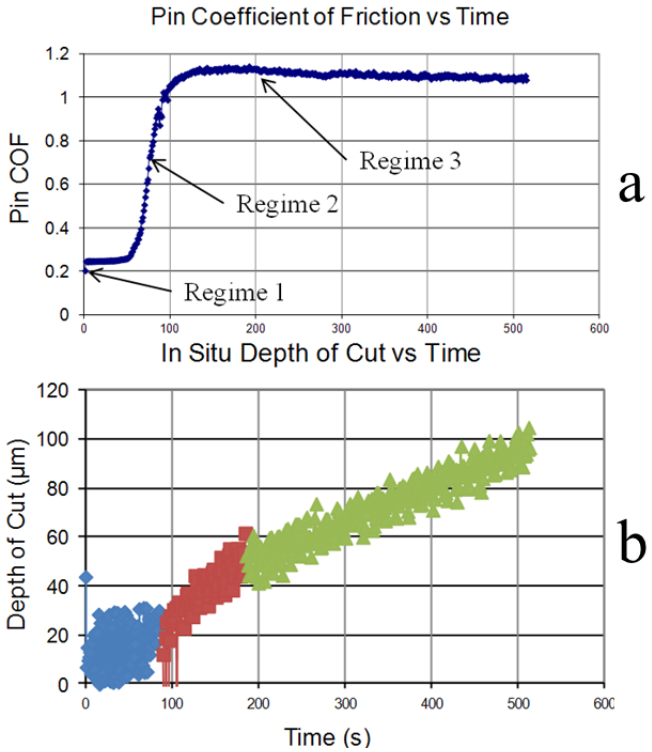

Figure 55: Results for initial cut testing of O1 tool steel on Carthage Marble detailing 3 regimes of cutting for (a) friction and (b) depth-of-cut

Secondly, the effect of "third body" accumulation in the interface was studied as a potential cause for transient increases in COF. The term "third body" concerns the presence of accumulated wear debris generated during the cutting process which, in this case, would be in the form of hard rock particles. Originally proposed by Godet in 1984, the third body concept is a phenomenon in which wear particles may drastically alter the interfacial sliding conditions [141]. As outlined in Godet's paper, third bodies have the potential to be trapped between the two first bodies, leading to an increase in friction and wear. However, in some cases they have may actually act to accommodate velocity through rolling, shearing, or colliding, subsequently improving friction and wear properties in the contact. In order to examine the effects of third bodies during B-CORT runs, ejection tests were performed to analyze friction as the rock cuttings are removed from the interface.

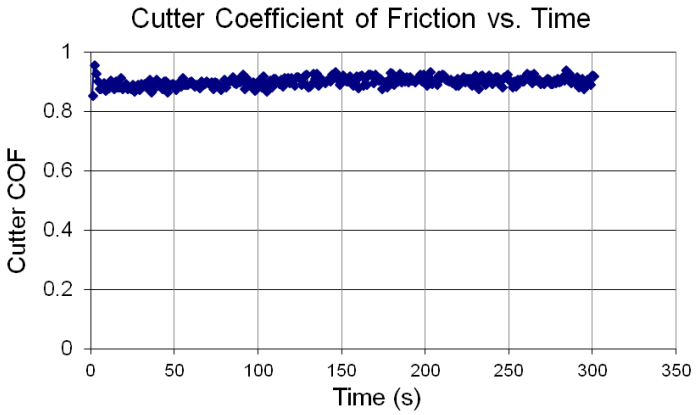

Figure 56: Friction results in resume-cut testing of O1 tool steel on Carthage Marble

Fig. 57a presents the *in situ* COF data of this test as a compressed air jet was used to remove excess cuttings from the bit-rock interface, while Fig. 57b shows the data for COF once the jet was removed. Interestingly, the COF displayed a marked increase, as third bodies were ejected, up to a value of about 1. Once the compressed air jet was removed however, the COF began to decline as cuttings were allowed to accumulate in the interface. In other words, the rock cuttings were acting to provide a lubricating effect which was described above and coined by Tichy et al. as "Granular Collision Lubrication" [142]. This influence of third bodies would increase as a test continued but would often level out around 0.9 for a cutter load of 3lbs and cutting speed of 195 RPM. This can be seen both in Fig. 56 as well as Fig. 57b. This suggests that interfacial flooding may result in a limit for the effect of debris in reducing COF in the cutter-rock interface.

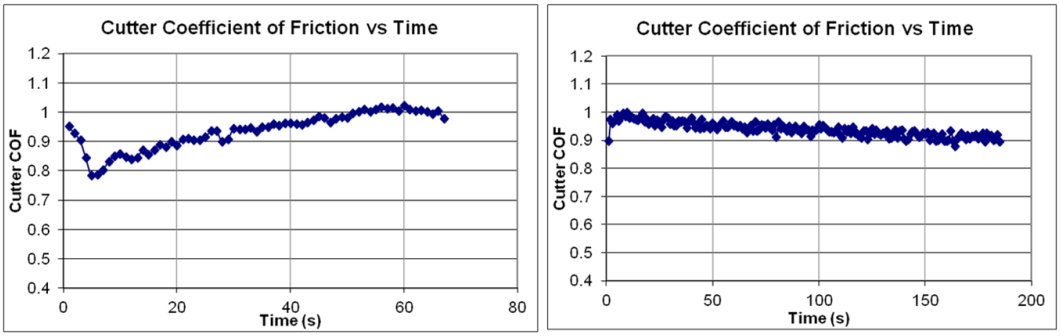

a b

Figure 57: Friction results for ejection testing of O1 tool steel on Carthage Marble: (a) with compressed air and (b) without compressed air showcasing a granular lubrication effect.

While this does not answer the question of why Regime 1 and Regime 3 drastically differ in terms of their absolute COF value, it does explain the steady drop in COF over Regime 3 as the interface is flooded with debris. At first glance it may seem that some optimal level of debris may be beneficial to extending bit life by reducing friction on the cutter. While this may be partially true, it should be noted that this does not mean it would be universally beneficial to the drilling process. For instance, while Regime 2 facilitates the highest friction, it also corresponds to the highest ROP, which would lead to faster well creation. In addition, the effect of debris in reducing friction in the field may be similarly limited to only a small reduction before a limit is reached, and therefore would be much less effective than conventional drilling fluids that remove cuttings. Although it was successful in reducing friction, the presence of third bodies in a cutter-rock interface may be desirable or undesirable based on your success criterion which is generally a maximum ROP.

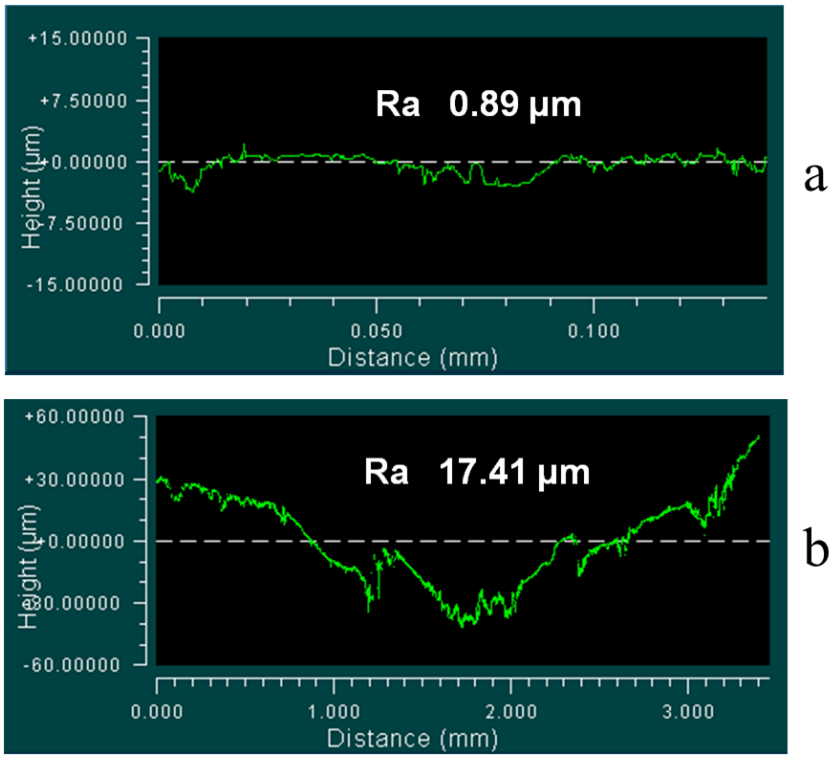

Figure 58: Before and after test line scans taken by an optical interferometer inside the cut for Carthage Marble

Though the third body effect helped to explain Regime 3 friction behavior, it was not able to account for the rise in friction over Regime 2. However, this may be explained by a simpler tribological phenomenon coupled with examination of the surface of the rock, both before and

after a cut developed. Figure 58a shows the Pre-cut surface topography dominant in Regime 1, as seen by an optical interferometer. It was found to be relatively smooth with an average roughness of only 0.89 μm. It should be remembered that the cut begins to develop and widen during Regime 2, until finally in Regime 3 it appears only to deepen.

Alternative to the original Pre-Cut surface topography, Fig. 58b displays the surface topography in the cut after Regime 3 has been established. What can now be seen, are very rough features up to 30 μm being exposed through the cutting process within the rock structure. Due to the very brittle nature of Carthage Marble, it would follow that this rise in friction may be due primarily to the interaction of these rough features in opposing the motion of the cutter with very little plastic deformation. This type of hindrance due to rough asperities being forced to climb, deform, or crush one another is generally referred to as abrasive friction [28]. In addition to their effect on friction, these features have been shown to promote crushing type cutting of rocks in the field, which would also explain the higher rates of penetration in Regimes 2 and 3 [84, 86, 96, 138].

With these hypothesis analyzed in detail, it is possible to construct a timeline of transient events during an Initial Cut test, with the quantitative values varying depending on the loading conditions explored during the next section. This is best expressed in terms of both the COF and ROP data accumulated during the cutting process:

1. Regime 1 begins with the cutter itself acting in a scraping fashion, interacting only with the relatively smooth rock surface. The chips formed are small and very little can be noticed on the surface in terms of a developing cut. COF and ROP values are low around 0.2 and $1.02*10^{-5}$cm/s ($4*10^{-6}$ in/s), respectively.
2. Regime 2 coincides with a noticeable development of the wear track even to the naked eye. During this time period the cut widens and deepens, uncovering the larger and rougher features in the sub-surface of the rock. The cutting process begins to move into a crushing mechanism. Little accumulation of wear debris in the contact interface has occurred as of yet, leading to a high, steady COF around 1-1.2, and the highest ROP of about $2.54*10^{-5}$cm/s ($1*10^{-5}$ in/s).

   Regime 3 corresponds to the period where COF exhibits a decreasing behavior due to a granular collision lubrication effect. As third bodies flood the interface, this eventually

leads to a steady, lower ROP of about $1.52*10^{-5}$cm/s ($6*10^{-6}$ in /s.) and a minimum COF of about 0.9.

8.4.3 Parametric Studies:

In addition to studying the interesting transient behavior of Initial Cut tests, parametric studies were run to explore the relationship of both cutter load and substrate speed on COF and ROP for O1 Tool Steel on Carthage Marble. Figure 59 presents the relationship of load to both COF and ROP. COF was taken as the steady-state value at the end of a Resume-Cut test, varied less than 0.02 once the initial decrease due to the granular collision lubrication effect was less pronounced. ROP was taken to be the slope of a linear regression line through the DOC data to provide a value in in/s. As can be seen from Fig. 59a COF variance with load was very small and did not display any marked trends.

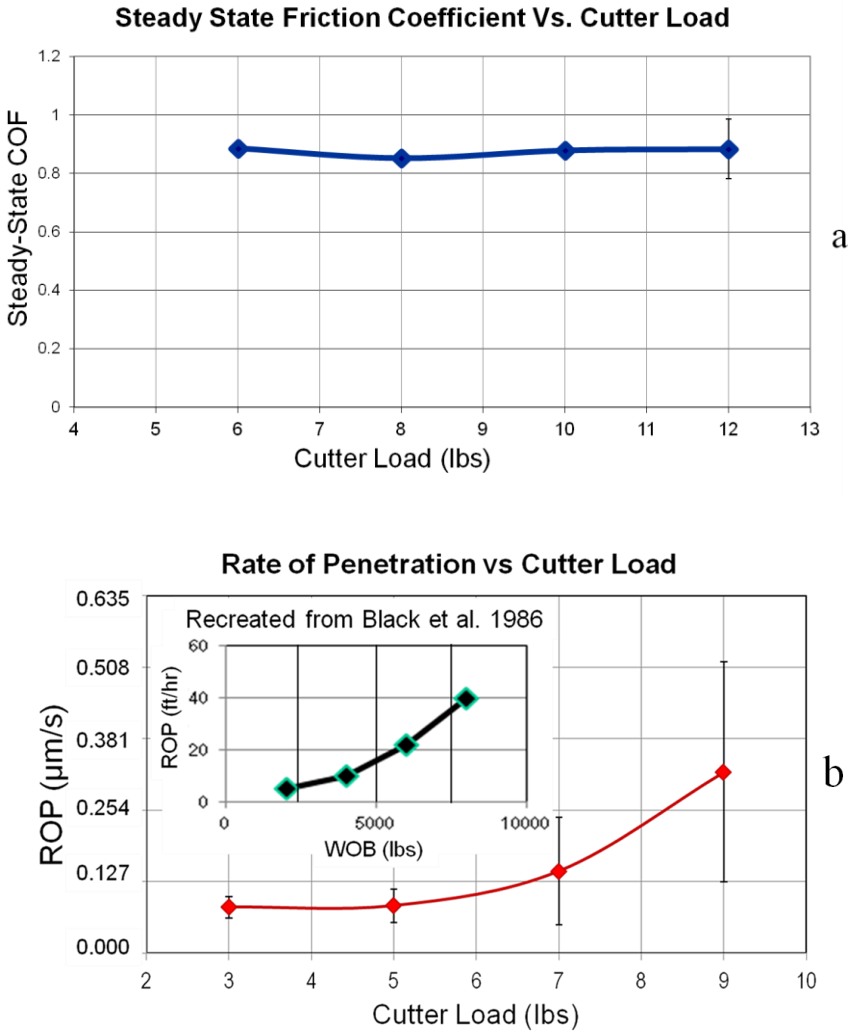

Figure 59: The Effect of load on (a) friction and (b) depth of cut for O1 Tool Steel on Carthage Marble featuring an inset from Black et al. [78].

The data for ROP presented in Fig 59b, and was far more sensitive to load. Initially a change in load led to only a small increase in ROP. However, as the load was increased further, the greater contact pressures were shown to lead to a greater and greater increase. When compared to a data-set with similar sliding speeds of 200 RPM, recreated from Black et al., we see a similar curve [78]. Although the loading conditions were much higher, it is important to note that their conditions correspond to a full drilling rig rather than a single cutter. In addition it was noted that this trend continued for all of their low load testing. The nonlinear trend can be justified if one considers that at low loads, a rise in contact pressure may not only result in more surface asperity contacts, but also in a greater amount of those being brought past their failure criterion. It should

be noted here that at higher loads, the data acquisition for ROP became more and more noisy, leading to larger error bars. However the trend remains intact qualitatively and provides validation while pinpointing an area for optimization in future iterations of the rig.

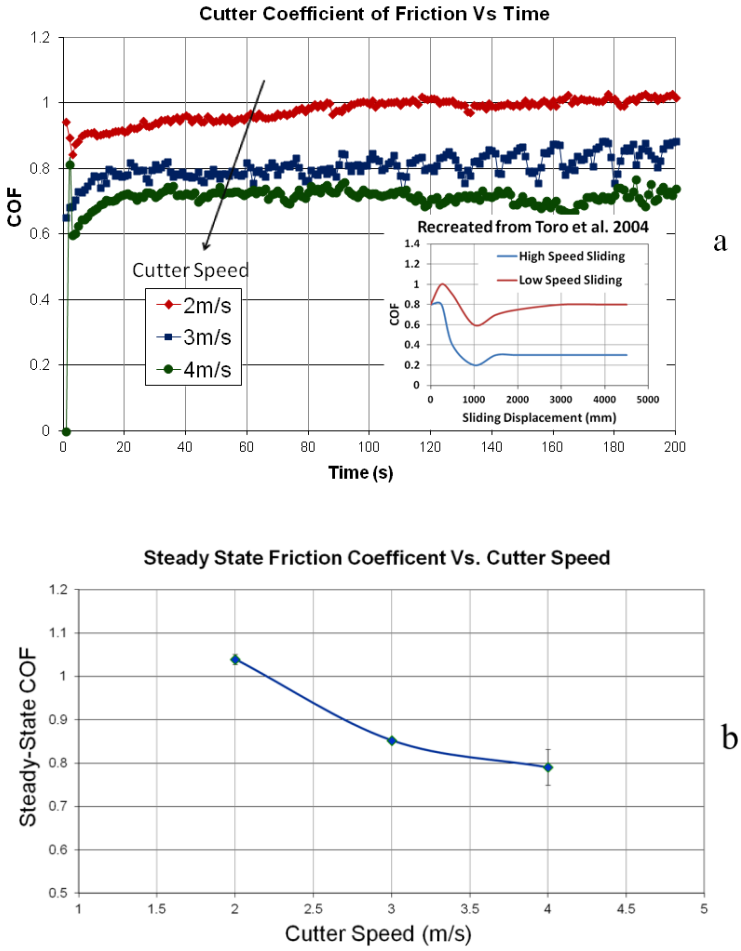

Figure 60: The Effect of speed on friction for O1 Tool Steel on Carthage Marble featuring an inset from Toro et al [143].

In addition to the relationship between load and COF/ROP, the effect of speed on cutter COF is presented in Fig. 60 and requires a bit more analysis. Though somewhat counterintuitive at first glance, the trend for COF with increasing speed portrayed an inverse relationship. This can be explained through the interplay of two different phenomena. The first was explained above in regards to the third body effect, which has been shown to be more effective in reducing COF at higher speeds [142]. As the speeds are increased, the collisions between third body particles become more energetic allowing for less interaction between the two first body surfaces and therefore reducing friction. In each case, the limit in which the collision effect would cease

to reduce friction was lower with increasing speed. The second phenomenon concerns interfacial plasticity effects during sliding. Although somewhat counterintuitive as well given the brittle nature of rocks, studies by both Toro et al. and Kilgore et al. confirmed that dry friction between sliding rocks would actually decrease with increased speed [143, 144]. At higher speeds, interfacial stresses and temperatures would lead to a slight increase in plasticity which is able to accommodate the velocity at asperity contacts and lower friction. One of These trend is represented as an inset in Fig. 60a for qualitative comparison.

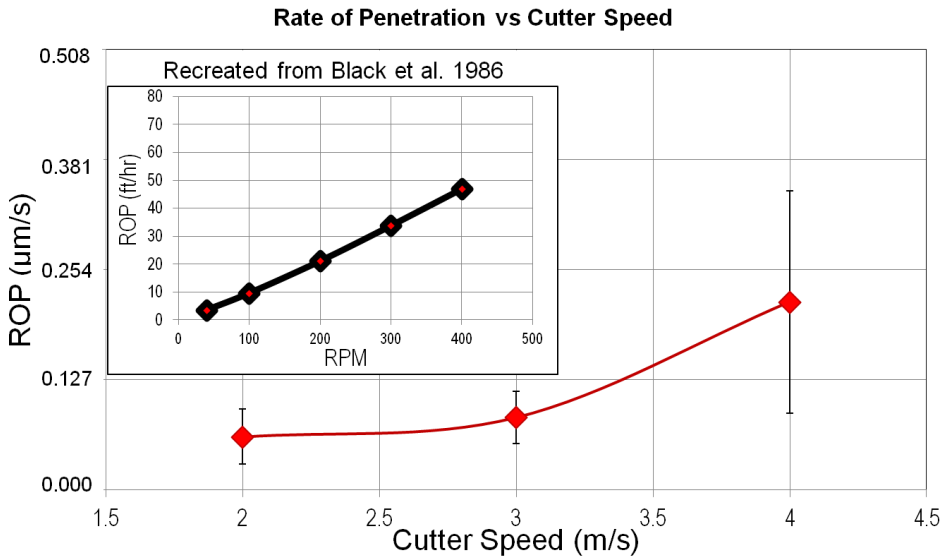

Figure 61: The Effect of speed on (a) friction and for O1 Tool Steel on Carthage Marble featuring an inset from Black et al [78].

Figure 61 presents the data for ROP with variable substrate velocity as compared with data once again recreated from Black et al for ROP of PDC bits at varying rpm. It can be seen from Fig. 61 that BCORT data corresponds well with the existing data, displaying an increasing trend which grows at an increased rate with higher speeds. Though this is difficult in the graph from Black et al., a fitted third order polynomial was used which was shown to exhibit smaller slopes out at lower speeds. The data for Black et al. was shown to level off with increasing velocity, although this was at higher speeds than tested in the current BCORT experimental procedure [78].

7.5 Summary and Conclusions

Given the macroscopic, complex, and field oriented nature of current rock drilling, it was the goal of this paper to present a simple form of experimentation for the analysis of tribological effects in deep well drilling. Throughout the paper a number of conclusions were reached which may be summarized as follows: a redesign of an in-house tribometer was conducted in order to facilitate a simplified, low-cost simulation of the dry drilling process. Using this test rig, it was possible to acquire relationships between COF and ROP, *in situ*, which are difficult to capture using the industry-standard VTL drilling simulator test rig in which depth of cut is kept constant during each run and reactionary forces are monitored. By studying these relationships during the development of individual cuts, three regimes were found to exist during the descent of the cutter which corresponded to Pre-cut, Interim, and Post-cut behavior. The drastic rise in friction between the first and second regimes was shown to be a result of the excavation of large surface features and a subsequent increase in roughness. ROP was shown to follow a similar trend where it would rise given the onset of these large features and the facilitation of a crushing versus scraping mechanism. Both COF and ROP rises were mitigated in Regime 3 before reaching steady-state through a granular lubrication effect in the form of third body rock cuttings. A qualitative agreement between loading parameters and these steady-state values for COF and ROP results found in the literature provided initial validation of the rig.

Although the current study of deep drilling contains an extensive and thorough analysis of macro-scale phenomenon in both experiments and modeling, the examination of *in situ* interfacial phenomenon is not readily available in the tribological community. While the results of such a study must eventually be integrated with actual drilling data from the field, a comprehensive look into the tribological factors, such as friction, cutting, and wear, simultaneously as a cutter descends, represent a new approach for using interfacial information to predicting the overall behavior of the drilling process. Throughout this preliminary work, a new method for rock drilling analysis, bit-cutter-on-rock tribometry, was established in order to assess the tribological behavior of a single cutter on a rock disk *in situ*. It is the hope of the authors, that with this type of simultaneous analysis, insights can be drawn which will aid in the optimized design of rock drilling machinery with a focus on tribological performance.

Chapter 8: Elucidating PDC Rock Cutting Behavior in Dry and Aqueous Conditions using Tribometry

This chapter contains a study in which friction and rate of penetration was detailed for dry and lubricated rock cutting of 3 different rock substrates using polycrystalline diamond compact cutters. A similar version of this paper was published in the Journal of Petroleum Science and Engineering. [Dougherty, P., Mpagazehe, J., Shelton, J., Higgs III, C.F. "Elucidating PDC Rock Cutting Behavior in Dry and Aqueous Conditions using Tribometry," *Journal of Petroleum Science and Engineering,* 2015]

8.1 Introduction and Motivation

Given the world's diminishing fossil fuel reserves, drilling expeditions are forced each year to delve deeper to uncover natural resources [74]. In fact, the creation process for wells further down than 1.5 km, often below the ocean floor, has been specified as "deep well drilling." Due to the fact that the cost of a well increases exponentially with depth [75], the drilling process can represent up to 50% of the total project costs [74]. This is a result of a number of effects. The first of which occurs during the surveying stage where smaller bore holes are carefully drilled to assess the potential for an economically viable project and the precise location of the final well. The setting up and threading of the drill string during this exploratory stage can be costly, as well as dangerous at these extreme depths, especially given the unknown conditions and formations [74-77]. The largest costs incurred from drilling the final well are not only due to the energy spent drilling, but also from the replacement of worn bits, referred to as "bit trips", when the rate-of-penetration (ROP) becomes insufficient [74, 77-85]. After a bit failure of this kind, a project shut down must occur, and maintenance must be conducted that involves removal, disassembly, assembly, and rethreading of the drill string at the ocean floor. The bits themselves are also difficult and costly to manufacture due to their complex shapes and materials such as carbide or polycrystalline diamond compact (PDC) [76, 79, 86].

With these factors in mind, it becomes apparent that understanding the drilling process in terms of reducing bit failure while maximizing ROP, is paramount to minimizing the cost and dangers associated with such deep wells. Specifically, this knowledge requires better understanding of the bit-rock interface in terms of how the bit is able to penetrate the rock *as*

well as how the rock damages the bit. During the deep drilling process, there are often two types of bits used. The first is called the roller cone bit, in which three cone-shaped rollers are covered in cutters and allowed to freely rotate and crush the rock [84, 87-89]. While still used often in rotary-percussive drilling, this bit has largely been replaced in standard rotary drilling with the PDC bit, so named for its implementation of PDC cutters [77, 78, 81, 82, 85, 87, 90, 91]. Since it features no moving parts, a large part of PDC bit design has been focused on the individual cutters, inspiring a greater drive to understand single-cutter rock interactions [82, 145]. PDC bits feature a plethora of cutter configurations in terms of orientation, rake angle, cutting face material, and cutting edge bevel, each of which can be initially evaluated using a single-cutter study. These investigations attempt to simplify the drilling interface to a single PDC cutter against the rock.

While drilling with PDC cutters, there are generally considered to be two mechanisms for material removal: scraping and cutting [78, 82, 87, 90-92, 138]. Scraping is quite similar to traditional sliding wear, and takes place on any cutter faces which are not penetrating the rock, including the undersides of the cutter and any developed wear flats. In addition to being a cause of energy dissipation, these are areas in which the contacting edge is actually flattened through excessive wear. After the loss in cutting edge, a much lower contact stress than that required for penetration and a subsequent reduction in ROP follows as a result [77, 78, 81, 82, 85, 87, 90-92]. The scraping mechanism features low ROP and a frictional response of an abrasive or adhesive nature between surfaces. During the cutting mechanism, the PDC uses its inclined face edge to penetrate the rock, develop a cutting face, and plough forward, removing large chips of the rock similar to a classical metal machining process [90, 91]. The primary difference between rock cutting and metal machining is that the rock will be brittle and far less predictable due to its porous and non-uniform bulk which introduces complex solid and fluid effects. When cutting *and* scraping occur, the ROP is high and the frictional response will be a combination of the scraping force from the undersides and the cutting force on the cutting face [91]. This second component is often referred to as drag rather than friction in the drilling community.

Conventionally, the breadth of single cutter studies have been carried out on lathe type machines such as the vertical turret lathe (VTL) [24, 82, 94, 95, 145]. In these machines, cutting is facilitated by the interference of a cutter against the top face of a massive cylindrical rock substrate as it rotates at high speeds. The cutter is given a constant penetration depth, usually by

machining a pre-cut such that the cutter will already be overlapping with the rock surface at start up. A key feature here is that the cutter is fixed at this height and *not able to descend*. As the rock rotates, the cutter creates a chip at its fixed height until the rotation is finished.

While able to capture very high loads and speeds, this VTL has some inherent drawbacks. Firstly, the forces are purely reactionary, which prohibits the parametric study of imposed loading. This is best depicted by Fig. 5a, in which the imposed loading conditions can be seen for a lathe type machine. Secondly, since the cut is kept at one constant depth, the data is generally far more uniform and dynamically simplified than cutters experience in the field [92]. This is due to the fact that the penetration into a rock surface during actual drilling will not remain constant, but will react to complex changes in the rock, normal load, or dynamics of the drill string [77, 78, 81, 85, 92]. This in turn has led to VTL studies being carried out primarily on extremely hard rocks such as white granite, to accelerate wear and make it more akin to that found in the field even on softer rocks. It has also been proposed that ROP and cutter wear are highly dependent on the initial creation of a uniform chip at the onset of cutting [92]. During this initial creation phase, in which the contact area is primarily on the cutters edge, stresses, temperature generation, and subsequently cutter wear will be at their most severe. These events can occur throughout the drilling process, during start and stop, as well as any dynamic events in which steady cutting is interrupted and a new cut is developed. Since the cutter in a typical VTL is not allowed to descend, it must be set at an initial depth of cut and cannot be used to study the forces and reactions present during the creation of the cut itself.

In addition, lathe-type testing makes it very difficult to study other effects which are dependent on the ability of the cutter to descend. These effects include variable penetration depths, interaction at the boundary of different types of rocks or individual grains, transitions between cutting and scraping, the hydrodynamic lift from lubrication, and dynamics such as bit-bouncing. One last difficulty with turret lathes is the technique utilized to capture extended periods of cutting. After one revolution, there will be nothing left of the rock substrate in front of the cutter. To combat this effect, most machines feature a mechanism which will allow the cutter to be moved during a test, tangentially to the cutter direction. While succeeding in being able to cut until the edge of the disk is reached, this process also results in the creation of a horizontal cutting force resisting this “feed” motion [92]. Consequently, wear profiles and forces on the cutter are further removed from the realistic drilling process.

In the field of Tribology, the phenomena of friction, lubrication, and wear (material removal) are generally analyzed together due to their interdependence. Often this is conducted through pin-on-disk tribometer testing (tribometry), which attempts to study the interfacial mechanics of relatively sliding surfaces *in situ*, such as friction and wear, while simplifying the complex sliding geometry [19, 28]. This is such that insights can be drawn about specific wear mechanisms in regard to their frictional response and lubrication regime. Then they can be optimized in an organized fashion [19, 28, 92, 96]. A key aspect of this process is that the pin is allowed to penetrate into the disk as the test progresses. This facilitates the unconstrained study of parameter relationships during the deformation, cutting, or wear of one material, as well as any hydrodynamic lift which occurs due to lubrication. The loading conditions are summarized in Fig. 5b. This suggests that tribometry would be a particularly useful way to study single-cutter drilling processes. For instance, using tribometry would permit the study of depth-based phenomena such as cut creation, dynamic changes in depth of cut and contact area, or even the encounter of different rock lithologies as a function of depth. In addition, it allows for the study of lubrication effects such as the creation of a hydrodynamic film and subsequent lift which reduces contact and friction in the cutter-rock interface. As a supplement to the *in situ* data, characterization of the two substrates is generally conducted *ex situ*; either with chemical, mechanical, or surface metrology tools, such that a full picture can be drawn of the interfacial interactions [79, 146].While this type of approach seems well-suited to the validation of single-cutter designs in both ambient and deep well scenarios, with its ability to study forces outside of a purely constant DOC, very few studies exist in which tribometry was used. This is most likely due to the difficulty in applying accurate loading conditions and relevant materials on precision tribometer rigs. However there have been works such as that by Beste et al. in which carbide buttons, rather than edged PDC cutters, were characterized for friction and wear on a number of different rock substrates [79, 80]. The authors also conducted previous research in which "Bit-Cutter on Rock tribometry" (B-CORT), was used to investigate the relationship between friction and ROP for hardened tool steel on deep well rock samples [25, 147]. Similar to the results discussed below, it was found that ROP increased for dry Nugget Sandstone given an increased

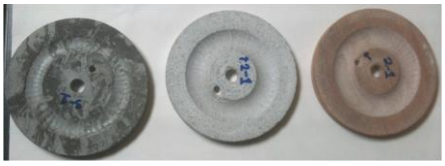

Figure 62: Rock Samples which have been cut during B-CORT testing: Mancos Shale, Carthage Marble, and Nugget Sandstone

load, despite a constant COF. In addition, despite a large increase in COF after the inception of a cut, it was found that cuttings in the interface would actually decrease COF over time. However, in both of these bodies of work, the loads were kept much lower than those typically found in the field, and the cutting materials were not fully relevant to the deep-well drilling process.

It should be noted that in the field of deep well drilling, hydrostatic borehole pressure will contribute significantly in increasing the strength and drilling force response of most rock types [74, 93, 148]. Despite its presence in the field, there are far less studies in the literature which utilize confining pressure in cutting at the laboratory scale [93, 148], and these usually provide only *ex situ* investigations of rock or PDC material strength rather than *in situ* friction and wear characterization. Standard single cutter studies, on turret lathe or tribometer rigs, are usually still conducted under ambient conditions due to the difficulty in incorporating large hydrostatic pressures in laboratory rigs [24, 78, 92, 94, 95]. While a water, air, or mud immersion or jet can be used to simulate the removal of frictional heat and rock debris, the rock often remains at ambient pressure. It is also worth noting that ambient studies such as those conducted on VTL or tribometer rigs, are also applicable to the study of ambient mining for excavation or resources such as coal and precious metals [23, 149, 150]. In particular, these rocks are generally softer, requiring lower loads to achieve cutting. As a result, despite similar mechanisms of cutting, cutters are usually made of tungsten carbide rather than PDC to reduce costs [23, 149, 150]. However, wear and replacement of drill bits remains a significant problem requiring the study of forces and responses which have been shown, similar to deep-well drilling, to vary drastically throughout the creation of a chip [23]. This focus on variable forces during dynamic events in ambient cutting, continues to stress the need for dynamically varying DOC studies to supplement those carried out by a traditional VTL.

It is the goal of this study to incorporate industrially-relevant drilling materials into the existing B-CORT framework, previously discussed by the authors, while also improving upon the loading conditions to more accurately simulate the single cutter interactions present in deep well drilling. While the tests will be conducted under ambient pressures, lubrication, cutting removal, and cooling will be included as well using water immersion. During testing, the focus will be to elucidate the tribological interactions present in the cutter/rock interface by a combination of friction and wear analysis with surface characterization of the rock substrates.

8.2 Experimental

The tribometer used in this study, different from the authors' previous works [19, 25, 146, 147], was a Bruker UMT-3. Rock samples were machined by Kocurek Industries into the disks shown in Fig. 62. The three samples include Mancos Shale, Carthage Marble, and Nugget Sandstone, all of which are different types of rock encountered during drilling for oil and gas. The cutter assemblies, displayed in Fig. 63, were designed by the authors and machined in-house, in order to mount PDC cutters at different rake angles. It should be noted however that only data from the rake angle of 20 degrees was included in this study. The industrial PDC cutters were purchased from DiDco Inc. The cutter assembly and water lubricated sliding interface are presented in Fig. 64.

Figure 63: Cutter assemblies for Rake angles of 10°, 20°, 30°, and 40°

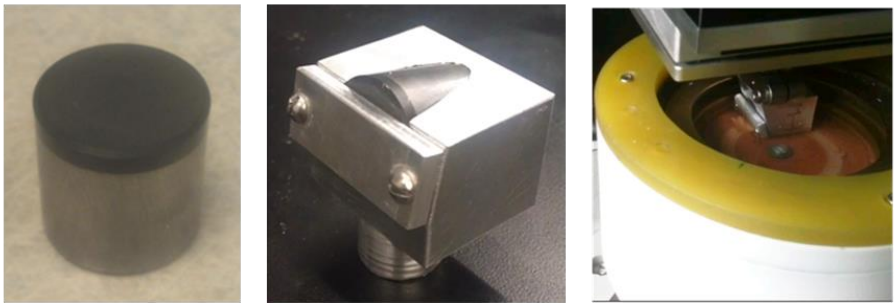

(a) (b) (c)

Figure 64: Images of (a) the PDC cutter, (b) the PDC Cutting Edge and (c) the B-CORT Cutting Interface

Dry Testing: Dry rock samples were mounted on the tribometer and the cutter was loaded against a fresh side of the rock disk for 10 seconds to ensure equilibrium. The disk was then rotated at a set speed while friction and the penetration of the cutter into the rock surface were measured *in situ*. The gross penetration of the cutter over time, which allows for the calculation of ROP, should not be confused with the depth of cut (DOC). This parameter represents the interference of the cutting edge with the current rock surface at a given time, which actually facilitates the cutting part of the cutter-rock interaction. On the other hand, the undersides of the cutter will also interact with the rock surface and facilitate the scraping mechanism in the cutter-rock interaction. During a test, rock cuttings were found to pile up on the outside of the trench, which would affect the cutters ability to descend by interfering with the cutter assembly. In order

to remove this obstacle, a vacuum pump was used to remove excess cuttings *outside* of the interface. After the test, the surfaces of the rock were cleaned with water and examined under a Zygo 7300 series optical interferometer when applicable.

Wet Testing: In the lubricated study, rock samples were first soaked for 10 minutes to approximate the effects of hydrolytic weakening on submerged rock [151, 152], such as those found in the ocean floor or in those that have been exposed to drilling fluid for extended periods of time. The wet rock was then mounted to the rig and immersed in water. The cutter was loaded for 10 seconds on an uncut side of the rock disk, before rotating at a set speed while monitoring friction and penetration of the cutter into the rock surface *in situ*. The gross penetration of the cutter over time, which allows for the calculation of ROP, should not be confused with the DOC This parameter represents the interference of the cutting edge with the current rock surface at a given time, which actually facilitates the cutting part of the cutter-rock interaction. On the other hand, the undersides of the cutter will also interact with the rock surface and facilitate the scraping mechanism in the cutter-rock interaction. During the motion of the rock substrate, lubricant is entrained into the cutting interface to simulate both the natural lubrication of the cutter and removal of rock debris or cuttings. While the majority of the drilling in the field will use drilling muds, water is commonly used in many single cutter studies, as well as the early stages of well location and creation of the first bore holes [92]. More complex drilling muds, which are generally water or oil-based slurry, may be examined in future iterations. After the test, the surfaces of the rock were cleaned with water and examined, if applicable, under an optical interferometer. The experimental parameters for testing (dry and wet) are presented in Table 8.1.

A short note should be made about the coefficient of friction or COF, as it is slightly different than that which is generally reported from tribometer experiments. As seen in Fig. 5, the cutter was allowed to descend freely into the rock, which resulted in a resistive force as it cut. Similar to the VTL setup also pictured in Fig. 5, this force was made up of 2 elements. These elements were frictional forces on the underside of the cutter known as scraping friction, and shear forces on the angled face of the cutter as a chip was sheared out of the rock bulk. This second element is known as drag friction, and is quite similar to the force experienced by a manufacturing tool during machine cutting. The reported COF was a combination of these two forces divided by the applied normal load.

Table 8.1: Experimental Test Parameters

Test Type	Loads (N)	Speeds (RPM)	Cutter Type	Rock Types
Wet, Dry	100,200,300,400	200 (0.46m/s)	PDC at 20° Rake	Carthage Marble, Nugget Sandstone, Mancos Shale

8.3 Results and Discussion

Due to the vast amount of data collected and the information which can be gleaned from examining the creation of cuts, the data has been plotted in a number of different ways for comparison purposes. First, a parametric load study will be presented with each figure containing just one rock type under both wet and dry conditions. This allows for separate analysis of wet and dry COF and ROP with respect to load. Secondly, representative results at a lighter and a heavier load will be presented for all rock types, with wet and dry conditions on the same plot. This allows for elucidation, specifically of the effect of the lubricant for each rock type. Lastly the results will be presented at one load, but with all of the rock types in separate wet and dry graphs. This final analysis emphasizes the qualitative differences between rock types under wet and dry cutting.

8.3.1 Parametric Studies with Respect to Load

The results for the first parametric study are presented in Figs. 65, 67, 68, 70, and 71 for Carthage Marble, Nugget Sandstone, and Mancos Shale. For each plot, a parametric study was conducted for loads of 100, 200, 300, and 400N, where the coefficient of friction (COF) is plotted on the left axis as a solid line and the penetration is plotted on the right as a dashed line. The ROP may be referred to as the slope of the penetration (the dashed line) in each of these plots. In conventional drilling, the rate of change of cutting depth, by the full bit, with time is considered to be the ROP.

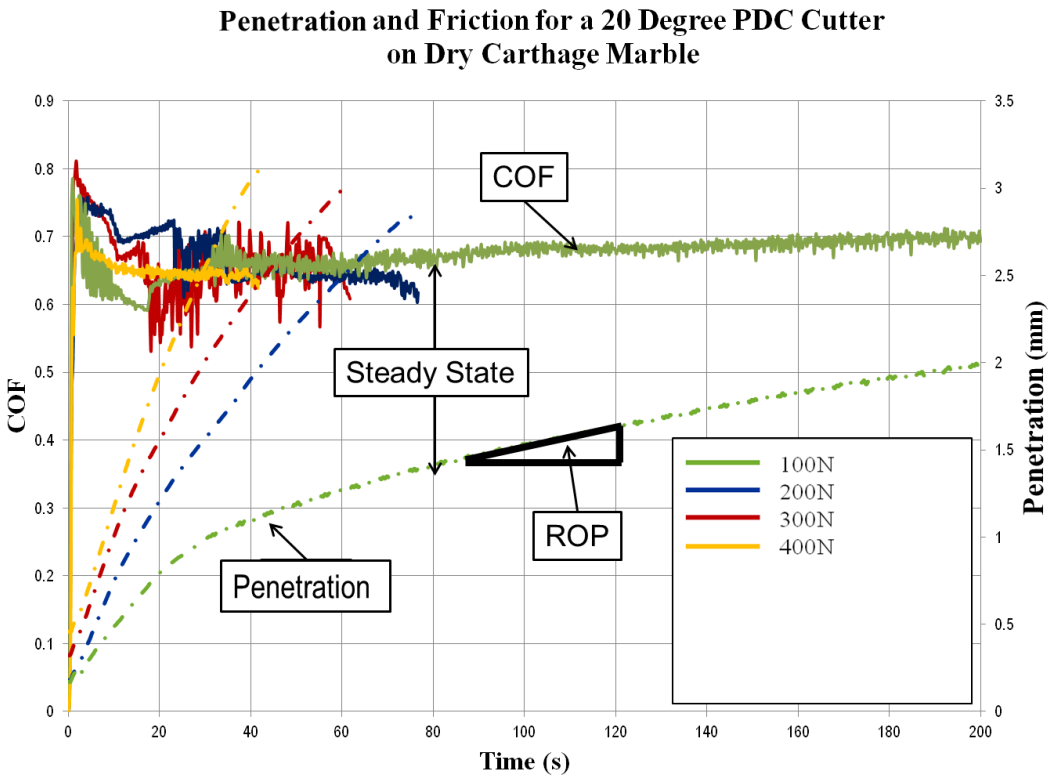

Figure 65: Parametric study for friction and penetration with respect to load for dry Carthage Marble including representative annotations for coefficient of friction, penetration, rate-of-penetration, and steady-state at 100N

8.3.1.1 PDC Cutting of Dry Carthage Marble with Respect to Load

The results for dry Carthage Marble, presented in Fig. 65, display very clear trends for ROP. It was found that ROP increased with increasing load, which is intuitive as the higher contact stresses would allow for greater penetration into the rock. For the load of 100N, it was interesting to note that a clear difference can be seen between the initially high ROP up to about 40 seconds, after which a lower ROP was found to dominate. This is most likely the result of the low load being more sensitive to changes in the area of contact. As the cutter penetrates, more of the rock will contact behind and on the sides of the cutter, thus increasing the contact area from a line contact on the cutting edge to a more conformal contact, which in turn will decrease the contact stress. After 40 seconds, a steady-state ROP is found in which this lower contact stress can no longer penetrate as deeply into the rock, resulting in less penetration area in front of the cutter. For the higher loads, 200N, 300N and 400N, there appears to be a very slight curve to each ROP, which is most likely evidence of this same effect, but far less pronounced. The selective

reduction in ROP suggests that 100N is approaching a transitional load, in which the contact stress at steady-state can no longer penetrate the rock sufficiently. Below this transitional load, a purely scraping mechanism would be expected. This effect was observed for each of the rock samples, as will be shown below.

The COF results were observed to be far less dependent on load, with a steady-state COF around 0.65 occurring around 40 seconds into the test. This was found to persist regardless of the imposed load. There was also a specific shape seen to manifest, in which the friction would begin at a high initial value and quickly decrease to a slightly lower steady-state. This trend is seen for many engineering systems, especially for machine components, and is often described as "run-in." In more ductile systems, the observed phenomenon has been found to correspond with a decrease in surface roughness until the largest asperities, that can cause high friction, are worn away. Although this has not been proposed for rock surfaces before, it is possible that a similar effect may occur which would reduce the frictional contribution of the cutter that is generated by sliding or scraping against rock asperities. As discussed previously, this force would act on the undersides of the cutter as well as any wear flats which have developed. During the remainder of the test the frictional force acting on the cutting (frontal) face will remain high, due to the resistance of the rock to its ploughing motion. But once the larger rock features in the trench are worn away, the frictional contribution from the sliding or scraping friction will be greatly reduced and would explain the slight decrease in COF.

Evidence for this effect was enhanced by examining the topography before and after a cut using a white light interferometer. Figure 66 displays these results in which the fresh topography of Carthage Marble was found to be rougher than the topography in the trench after a cut. As the cutter descends, the rough features were worn away until a more polished surface prevailed. In turn this would reduce the friction experienced by the scraping undersides of the cutter and the total frictional force would be dominated by the contribution of the cutting face. This type of effect may be important to field drilling because it emphasizes how the sudden encounter of fresh or rough rock topography may yield higher friction and therefore higher stress on the cutters than expected. This is especially the case if any wear flats exist on the scraping face, which are likely to experience the most severe effects from high scraping forces.

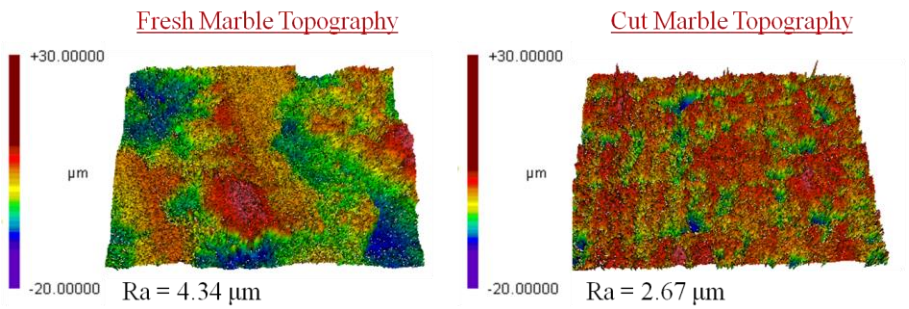

Figure 66: Topography Comparison for Fresh Carthage Marble and Dry, Cut Carthage Marble at 300N

This polishing of the rock surface may also act as a contributing factor to the distinct difference in ROP for the 100N load, in which a change in the ROP to a lower value was seen to correspond with the arrival of steady COF. Originally it was hypothesized that the low load was more sensitive to changes in the area of contact as the cutter descends, which would effectively reduce the contact stress, penetration, and therefore ROP. This sensitivity may also be due in part to roughness effects. While higher loads may overwhelm the surface roughness due to large penetrations, a lower load would cause the cutter to penetrate less into the rock. If the cutter is *initially* not penetrating beyond the surface roughness, the ROP for 100N Carthage Marble would be enhanced due to the high stresses present at asperity contacts. Eventually we see that the topography becomes smoother, which would yield lower contact stresses and a higher contact area, and steadier DOC as large asperity peaks will no longer be present to disrupt the contact. The fact that the transition into a second, lower ROP for 100N, coincides with the transition to steady COF, provides further justification for this theory. The destruction of these larger asperities would show up as a very high penetration rate *and* scraping force as the cutter tears through the exposed peaks, while the subsequent reduction in their effects would show up as a decrease in ROP *and* COF as the contact becomes smoother. It should be noted that the penetration in Fig. 65 quickly surpasses the roughness. However the DOC, which describes the interference at the point of contact, will still be dependent on the surface roughness within the cut. It can be seen from Fig. 66 that a rough surface still exists within the cut at the conclusion of the 100N test. The process from the rougher to smoother topography, will most likely be a gradual polishing, coinciding with smooth transition in both COF and ROP. This coordination is

very similar to the standard running-in effect for the initial contact of machine components in relative motion.

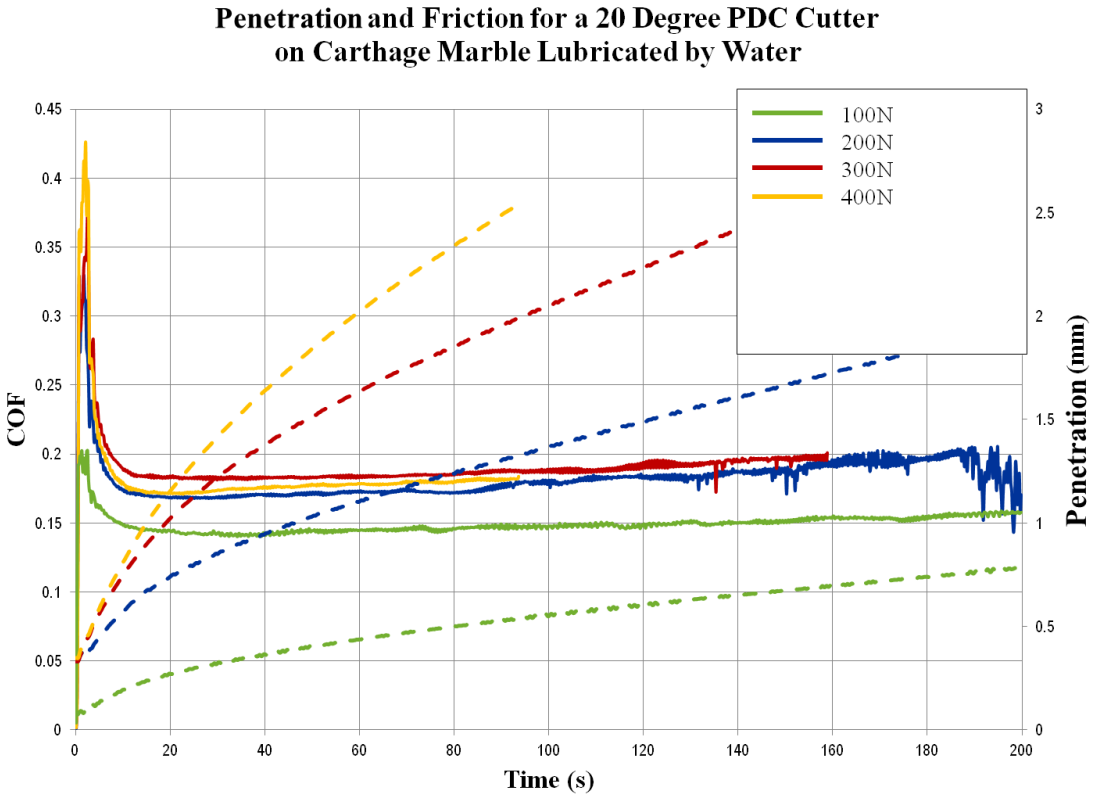

Figure 67: Parametric study for friction and penetration with respect to load for Water Lubricated Carthage Marble

8.3.1.2 PDC Cutting of Lubricated Carthage Marble with Respect to Load

The results for the lubricated cutting of Carthage Marble are presented in Fig. 67 and were quite similar. For instance, it was found again that an increase in load would lead to larger ROP. It was also observed that the COF remained more or less unaffected by the load, with the exception again of the low load 100N case. This may be elucidated by considering two effects. Firstly the 100N case may still have been low enough to be affected more readily by the increase in contact area described above. This may lead to considerably less penetration, lower ROP, and subsequently a lower contribution of the cutting face to the overall friction. Secondly, since this is a lubricated case, the 100N load may be small enough that the lubricant was more effective in separating the two surfaces through hydrodynamic lift. The potential of the 100N load to be the transition point for actual penetration into the rock was also observed for the other rock samples.

For the higher loads, an increase in the normal load produced minimal change in COF and an increase in ROP for dry *and* lubricated Carthage Marble.

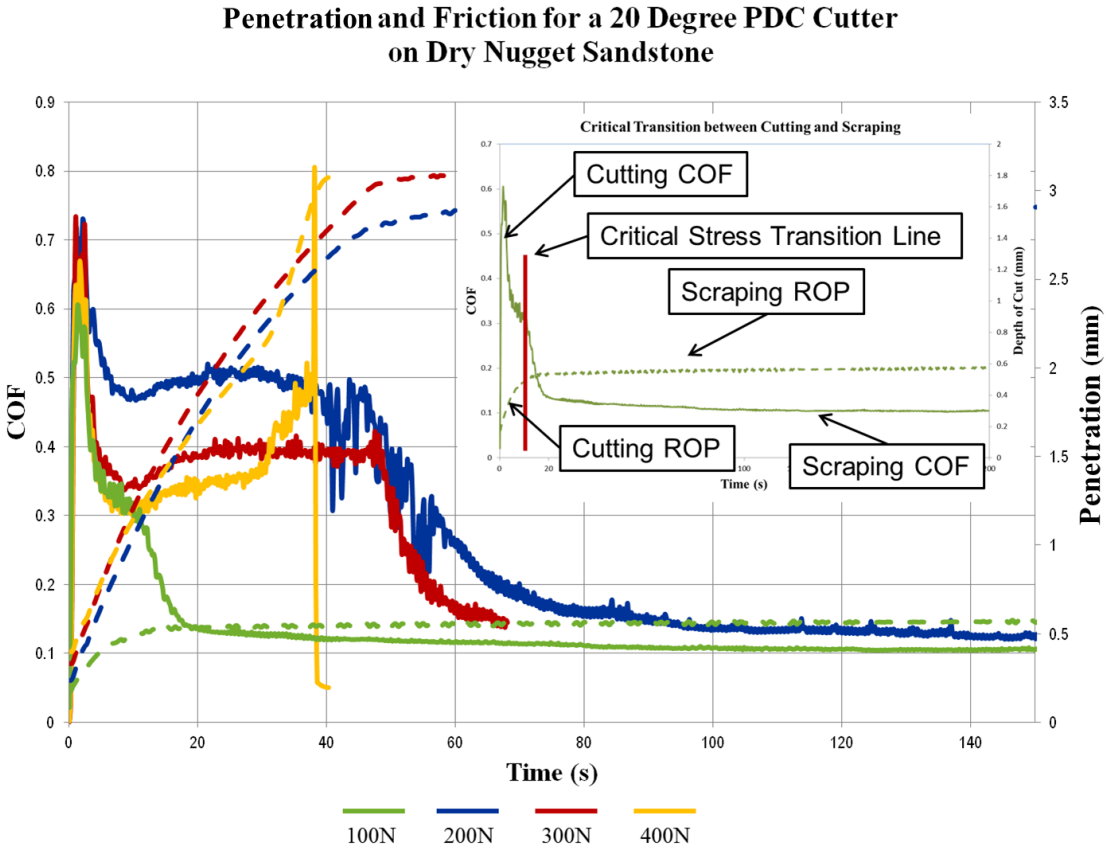

Figure 68: Parametric study for friction and penetration with respect to load for dry and water lubricated Nugget Sandstone including an inset detailing the coordinated transition between cutting and scraping mechanisms for ROP and COF in the 100N case

8.3.1.3 PDC Cutting of Dry Nugget Sandstone with Respect to Load

In Fig. 68, the results for dry Nugget Sandstone display the opposite set of relationships from Carthage Marble. No appreciable trend was observed between ROP and load, while COF actually decreased with increasing load. For a load of 200N, the steady-state COF seemed to level off around 0.5, while for 300 N and 400N this decreased to about 0.4 and 0.35 respectively. It should be noted that at the end of the 400N test around 40s, the disk actually fractured, and the slightly erratic ends to the COF and ROP curves were thought to reflect the onset of this event. These different frictional responses between rock types can be important to the drilling community because under these conditions, an increase in load on Nugget Sandstone *does not* result in a significant increase in ROP. However, it *does* result in larger frictional forces, even

though the friction coefficient is lower. These may cause increases in both cutter wear and the required torque, which can increase the costs of field drilling in terms of required energy and delays. Therefore, while an increase in normal load may be beneficial for cutting Carthage Marble because it gives higher ROP without added COF, it may not be as worthwhile for Nugget Sandstone under the tested conditions.

For the 100N case, presented for clarity in the inset of Fig. 68, the relationship to load was once again different, both in terms of COF and ROP. It should be noted that for this load, a full transition between cutting and scraping was witnessed, which one would be unable to observe in a rig like the traditional lathe. This is due to the phenomenon's dependence on the cutters ability to move up and down as contact stress decreases. Until about 15s, cutting was promoted in which the COF began high and decreased to a value below 0.4 which was still comparable to the cutting COF at higher loads. During this period, the ROP was also similar to other instances of cutting, as exhibited by the steep slope of the penetration curve. Then the COF dropped drastically alongside the ROP, which went essentially to 0 as indicated by the straight line of penetration for the inset in Fig. 68. The reason for this can be explained similar to the contact area arguments used for the 100N dry case with Carthage Marble. After a given depth, a critical stress must have been reached in which the contact stress was no longer high enough to penetrate the rock and develop a cutting face. As opposed to Carthage Marble, which experienced reduced COF and ROP indicative of a reduction in cutting, the 100N test for Nugget Sandstone fully transitioned into scraping only, which is a different mechanism of material removal altogether. By allowing the cutter to descend freely, this test provides interesting insight into just how different the COF responses of cutting or scraping can be. Specifically, this suggests that when cutting and scraping occur together, the "drag" force on the frontal cutting face must be the much greater than the scraping force. This can be observed clearly in how low the COF is when only scraping persists in the inset of Fig. 68.

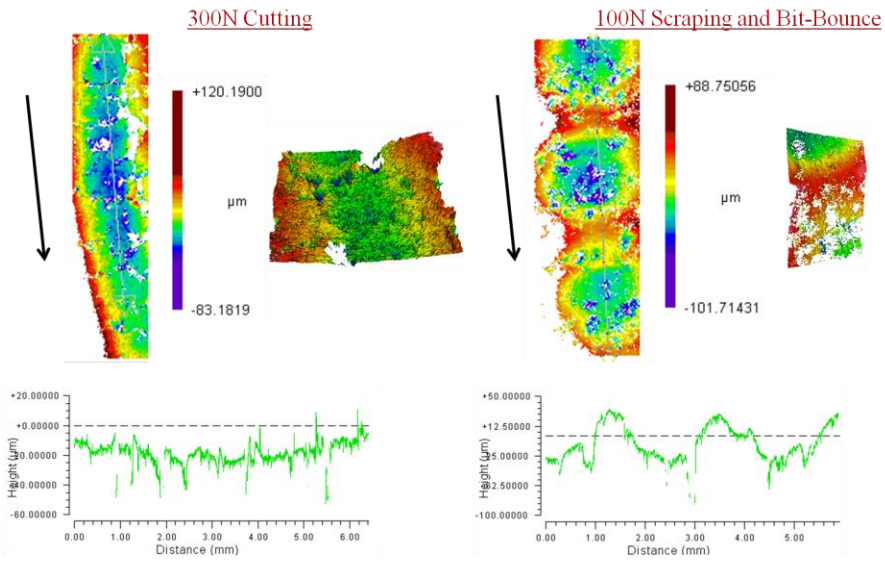

Fig. 69: Comparison of the surface topography for cutting and scraping mechanisms on Nugget Sandstone

The effects of cutting versus scraping were investigated further using optical interferometry. Figure 69 displays the results for scans from the trench for 300N, where clear cutting was observed, and for 100N where the test concluded with a scraping mechanism only. For the cutting case, the trench was found to be smooth, particularly when compared to the scraping. This can be seen from the 3D topography maps in Fig. 69, as well as the line scan which is taken *parallel* to sliding down the middle of the trench in Fig. 69. For the scraping case, the topography was comprised of periodic "scalloped" features which were far rougher on the order of almost 70 µm. Because the stress was no longer great enough to penetrate the rock and develop a continuous chip, the cutter began to scrape and "chatter" on the surface, leading to periodic moments of contact. Interestingly enough, this is quite similar to the phenomenon of "Bit-bounce," though scaled down to a single cutter phenomenon. "Bit-bounce" occurs when vibrations in the interface, often induced by stick-slip friction or lack of penetration, cause the entire bit assembly to chatter on the surface [153]. This is a large problem for the drilling community because it can damage not only the brittle cutter materials, but also the drill string due to the complicated dynamics and vibrations. However, fixed displacement methods, such as single cutter tests on the VTL, are unable to capture these events since they do not allow for the motion of the cutter up and down.

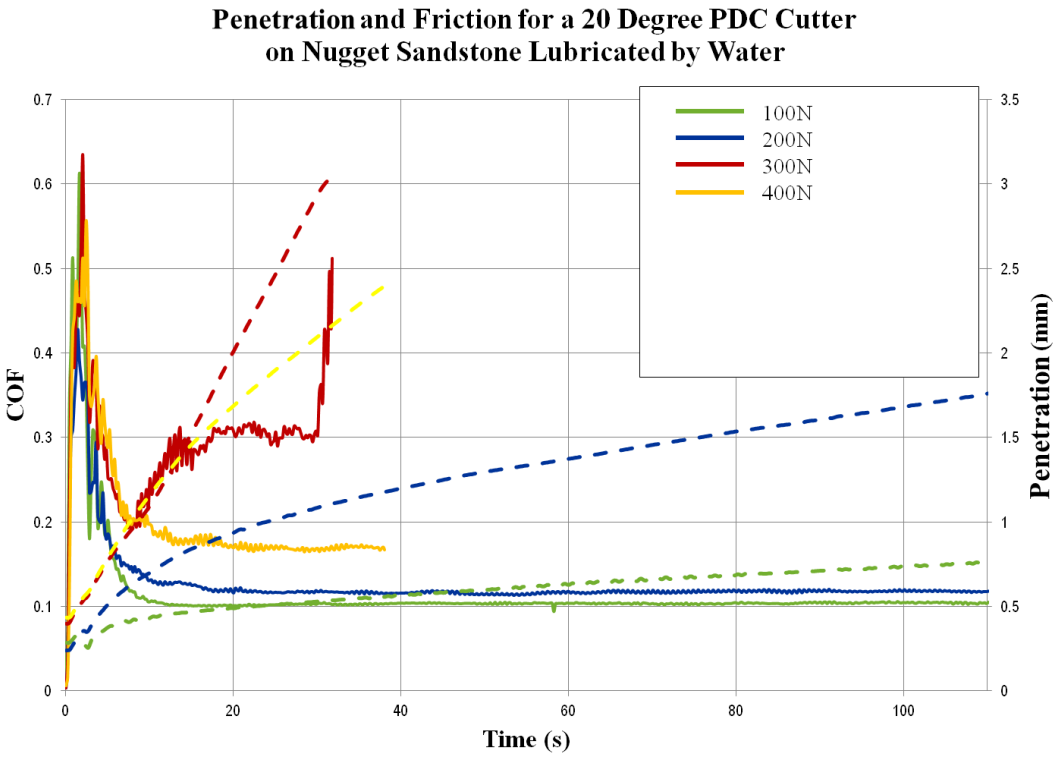

Figure 70: Parametric study for friction and penetration with respect to load for water lubricated Nugget Sandstone

8.3.1.4 PDC Cutting of Lubricated Nugget Sandstone with Respect to Load

The results for lubricated Nugget Sandstone were found to be different than those for Carthage Marble, as well as dry Nugget Sandstone, and are presented in Fig. 70. For example, it was noticed that an increase in normal load would lead to an increase in COF rather than a decrease. This is with the exception of the 300N test in which the COF began to drop as expected, but a fracturing of the rock began around 15s and was responsible for the sudden increase in both COF and ROP. For the other loads, the increase in COF of wet Nugget Sandstone can be explained due to an increase in the amount of cutting face area, due to larger penetration at higher loads. This is reinforced by the trend of increasing ROP with increasing normal load which would also stem from larger penetrations.

It is interesting to compare these lubricated trends to *dry* Nugget Sandstone. For lubricated Nugget Sandstone, increased load led to higher ROP and higher COF. This can be explained by an increase in the size of the cutting face penetrating into the rock, which would provide larger drag and remove more material. However, for dry Nugget Sandstone, added load *reduced* COF

while ROP remained unaffected. The unchanging ROP implies that the penetration and subsequent frontal cutting area did not increase with load as expected. If the cutting face was not being enlarged, it follows that the cutter would experience the same drag force as the cutter moves through the rock, thus potentially explaining why COF did not increase. The cause for the decreasing COF may be that the increased load on the cutter was actually acting to soften the rock and decrease its resistance to further shearing. In the literature there have been other examples of an increase in interfacial energy, such as increased velocity, leading to similar trends of decreasing COF. The mechanisms of these trends are hypothesized to be an increase in plasticity, the formation of lubricious tribo-layers in the interface, or drastic temperature increases leading to a pseudo-melt [143, 144]. Each of these phenomena depend on increased energy into the sliding contact, and it follows that increased load might be able to cause a similar effect. If this was occurring during the Nugget Sandstone tests, it would explain not only the decrease in COF with increased load, but could also explain how the ROP remains the same. As the rocks plasticity increases, the more ductile rock would be more likely to plastically deform rather than fracture. One similarity between all of the tests for Nugget Sandstone and Carthage Marble, was that the friction behaviors were found to fall to a steady-state value and that a decrease in surface roughness was found to exist inside the cut. As a result it is believed that both are experiencing a similar effect, in which the largest features are being worn away to reduce the scraping components of friction from the total frictional force until it is dominated by the cutting component.

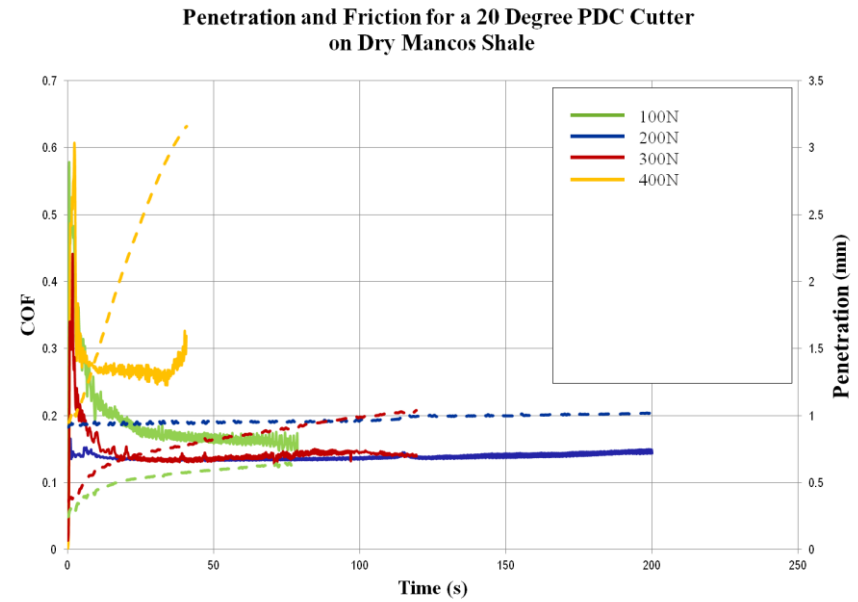

(a)

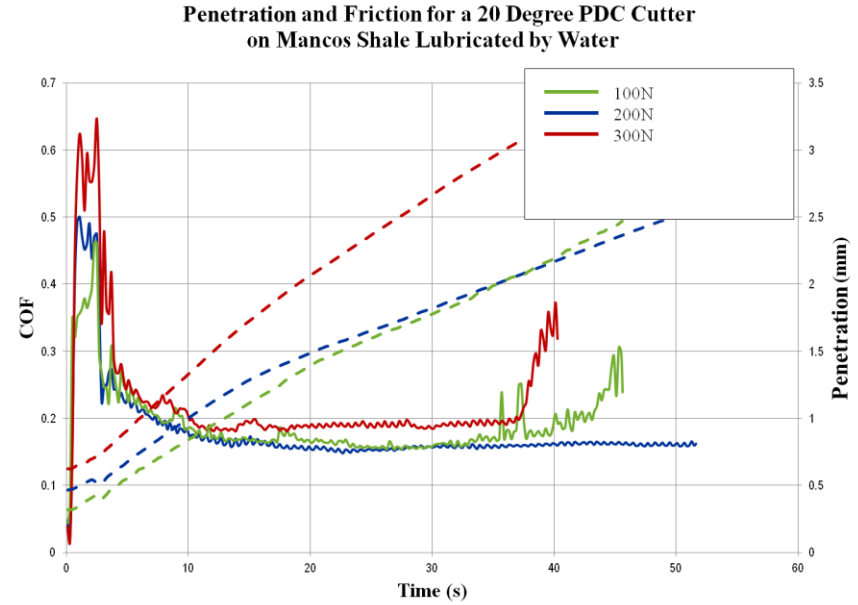

(b)

Figure 71: Parametric study for friction and penetration with respect to load for (a) dry and (b) water lubricated Mancos Shale

8.3.1.5 PDC Cutting of Dry Mancos Shale with Respect to Load

The results for dry cutting on Mancos Shale are displayed in Fig. 71a, and portray very different trends than both of the previous rock samples. Firstly it should be noted that only in the case of 400N, did dry cutting of Mancos Shale occur on the same scale as Nugget Sandstone or Carthage Marble, in terms of COF and ROP. For all of the other loads, the low ROP and COF values were

more akin to the trends of pure scraping observed in 100N on dry Nugget Sandstone. It is interesting to note that the scraping COF for 100, 200, and 300 N Mancos Shale, and 100N Nugget Sandstone, all seem to approach a similar steady-state friction value which was low and stable around 0.13. This would suggest that frictional responses for scraping are quite similar, even on different rocks or at different loads. For the 400N case, the COF of Mancos Shale was closer to 0.26, the increase of which can be attributed to the development of an actual cutting face and its subsequent "drag" friction force.

The ROP behaviors of Mancos Shale were very similar for the cases of 100 and 200N, in that almost no penetration occurred and the sliding mechanism was thought to be scraping only. In the case of 300N, similar behavior to the 100N cases of Carthage Marble and Nugget Sandstone was witnessed in which a noticeable decrease in ROP occurred during the test. This occurred right on the boundary between cutting (400N) and scraping (200,100N), suggesting that 300N may be very close to the transition point between cutting and pure scraping. This transition load, which marks the onset of cutting, was previously found to be 100N for Nugget Sandstone, and hypothesized to exist just below 100N for Carthage Marble. Only at the load of 400N was the load high enough to induce cutting and an ROP for Mancos Shale comparable to the other rock samples. These results are particularly important because the unconfined compressive strength (UCS) of Mancos Shale, shown in Table 8.2, is the lowest of the three rock samples. However, this rock required the highest load to begin cutting. This result reinforces the importance for this type of tribological testing, in order to augment the information regarding a rock's cutting behavior beyond that of standard material properties. In this case, the use of a standard material property such as the UCS would provide an insufficient measure of which rocks will be easiest to cut.

8.3.1.6 PDC Cutting of Lubricated Mancos Shale with Respect to Load

For lubricated Mancos shale, the trends in Fig. 71b were more complex and displayed clear evidence of cutting even at the lowest load of 100N. Friction began at high values between 0.4 and 0.6. During this time period leading up to about 8s, the ROP would also experience an increase over time, indicated by upward inflection in the penetration curves. Then a period followed where ROP and COF would begin to decrease, before reaching more steady values. As was consistent with the other rock types, the arrival of steady-state for COF and ROP generally occurred together, around 20s for Mancos Shale. This was most likely due to the observed

decrease in surface roughness from the original shale topography, which was described previously for the other rocks. It should be noted that both the 300 and 100N cases displayed sudden increases in COF towards the end of the test which occurred simultaneously with the beginning of an observed disk fracture.

The non-linear results for lubricated Mancos Shale make it very difficult to pinpoint specific relationships between normal load, ROP, and COF. COF seemed to remain largely unaffected by normal load, similar to dry and lubricated Carthage Marble. ROP seemed to display an increase with increased load. The ROP however, was far from uniform, often displaying sudden inflection points where large reductions or increases in ROP would occur such as at 5 and 15s. This effect is mostly likely due to the lamellar nature of shale rock. It was observed during testing that the shale was more susceptible to a weakening effect by the water, in which large layers of shale would be removed all at once. These weakening effects arise from the ability of water to more easily penetrate shale's lamellar nature, [154] which can also induce swelling as the water is adsorbed by the clays in the rock matrix. The inflection points found in the ROP study are most likely due the removal of a layer which has been drastically weakened. After this type of event, the ROP dropped while the cutter attempted to penetrate a new layer. These effects may easily be missed on lathe type machines, where the lack of penetration over time may prohibit the encounter of different layers.

8.3.2 Comparisons between Lubricated and Dry Rock Cutting

In addition to investigating the relationships between normal load, ROP and COF, it is useful to examine the effect of lubricated versus dry cutting. By examining these plots for each type of rock, it is possible to more prominently elucidate the effects of a lubricated cutting interface like those found in the field. The results for this comparison are presented in Figure 72. Each rock type, at loads of 300 and 100N, has been plotted so that a representative effect of the lubricant could be seen during instances of both cutting and scraping.

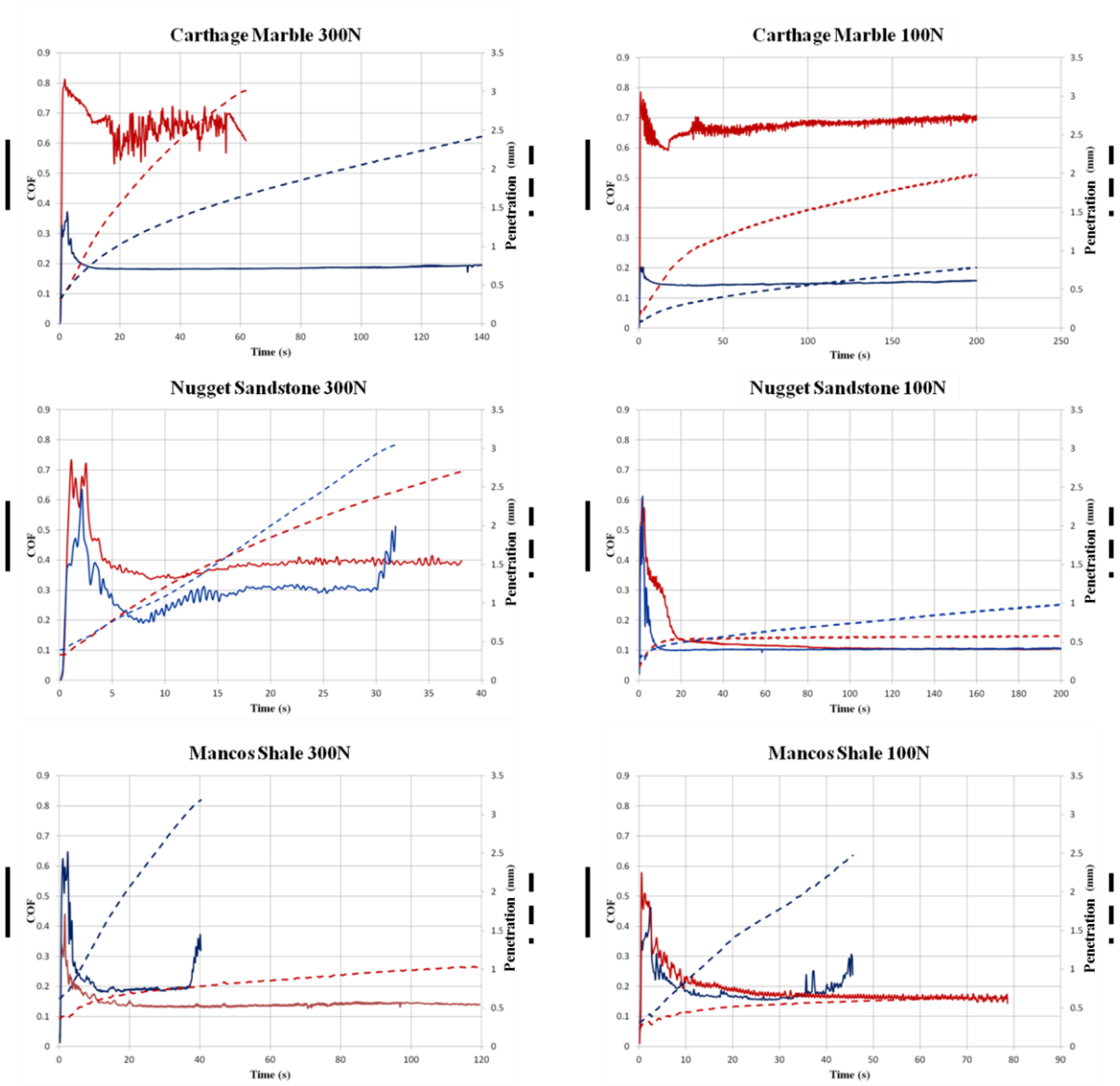

Figure 72: A Comparison of Lubricated (Blue) and Dry (Red) Cutting for Carthage Marble. COF is displayed as a solid line while penetration is displayed as a dashed line.

By starting with the lubricated and dry cutting of Carthage marble, two very important trends can be gathered for how the addition of a fluid affects the interface with the PDC cutter. First it was observed that there was a drastic reduction in COF, due to the lubricating effects of the water. Each COF for the lubricated cases began around 0.4, and decreased quickly to a steady-state of about 0.2. These low values suggest that the lubricant is most likely developing a hydrodynamic pressure capable of carrying some of the load. It is important to note that the study of these lubrication effects depend on the cutter's ability to move up and down, and

therefore would be difficult to study on the current VTL machine beyond lubricant cooling. After the generation of the lubricant (water) film, the COF remained very stable throughout the test, compared to the dry COF which remained high and noisy above 0.6. Interestingly enough, the ROP in these lubricated tests did not experience as drastic a reduction despite the presence of this lubricant film. These differences between the lubricated ROP and the dry ROP were approximated by comparing the maximum penetration at the conclusion of the dry run to the lubricated penetration at the same time. For 300N the dry case concluded at a penetration of 3mm, while the lubricated case had only reached 2.6 mm despite a reduction in COF from 0.7 to 0.2. It could be reasonably assumed that the development of lubrication would result in proportionally less penetration into the rock, and therefore an equally large reduction in ROP due to a smaller cutting face. However, it was clear from Fig. 72 that the ROP was not nearly as reduced. This may be explained by a secondary effect, which acts to counteract the lubricating effects and maintain or even increase ROP. It was theorized that this effect is the fluid's ability to weaken the other porous rock, in addition to shale, both during the initial soak time and the immersion while testing. This ability of water to weaken porous rocks through both physical and chemical changes has been documented before [151, 152, 154]. This weakening effect is descried in two ways, one is a lower interfacial temperature regime in which the failure and deformation mechanism transitions from micro cracking to dislocation glide and climb. This method would be particularly effective for the lamellar shale rock. The second weakening effect comes from the waters penetration into pores, increasing pore pressure and decreasing cohesive effects between grains even for unconfined strength tests [152, 155, 156]. Although the lubricating effects of the fluid succeed in lowering friction and reducing penetration, the weakening effects of the fluid weaken the rock, making it easier to cut. These trade-offs can be important when considering the types of drilling fluid to be employed, because fluids which lubricate more effectively reduce bit wear through low friction and cooling, but they may also reduce ROP.

For Nugget Sandstone, the reduction in COF through lubrication was less drastic than that of Carthage Marble and a similar weakening effect was observed in the ROP. This can be observed in Fig. 72 for the case of 300N cutting, in which the COF was reduced from 0.35 to 0.2, but the ROP stayed almost identical. Despite a reduction in the COF and therefore the cutting force, the same amount of rock is being removed. This implies that the rock must be easier to

cut and therefore weaker. Interestingly, the ROP for the lubricated case was actually greater in the later parts of the test. This can be explained again by the coordination between ROP and COF in a transition point witnessed around 20s. The lubricating effects were attenuated at this point, leading to an increase in COF and therefore cutting force. While the COF was still lower than the dry case, the weakening effects allowed for ROP to actually exceed that of dry cutting. The weakening effect was even more prominently displayed in the case of 100N testing on Nugget Sandstone. Although the dry case reached a transition point after which cutting was prohibited, the lubricated test was found to exhibit clear cutting throughout the test. The weakening effects of the lubricant in this case were able to facilitate cutting on Nugget Sandstone, where cutting had been previously prohibited for this load.

The weakening effects were found to be the most prominent for the comparison between dry and lubricated Mancos Shale. For 300N only a small amount of cutting was witnessed on Mancos shale, similar to the behavior of the other rocks when the load is low and near a transition point for cutting and scraping. For the 100N case the dry test was found to exhibit pure scraping. However, in the presence of the lubricant, a drastic increase in ROP was found, which was indicative of full cutting for both loads. Interestingly, different than all the other rock samples, the lubricated tests exhibited higher or similar friction than the dry tests. While seemingly counterintuitive, this can be explained by the physical difference between cutting and scraping. For the dry cases, even at 300N, the PDC cutter could not sufficiently penetrate Mancos Shale in order to develop a large cutting face and an ROP comparable to the other rock samples. This implies that a scraping effect was dominating the interface, which was found to exhibit low COF for the other rock types. In the case of Mancos shale, the lubricant reduced some of the frictional force, but also allowed for penetration into the rock that was not occurring during dry testing. As a result of this penetration, the addition of the cutting component of friction increased the total COF over that of the dry case.

8.3.3 Comparisons of Cutting across Rock Type

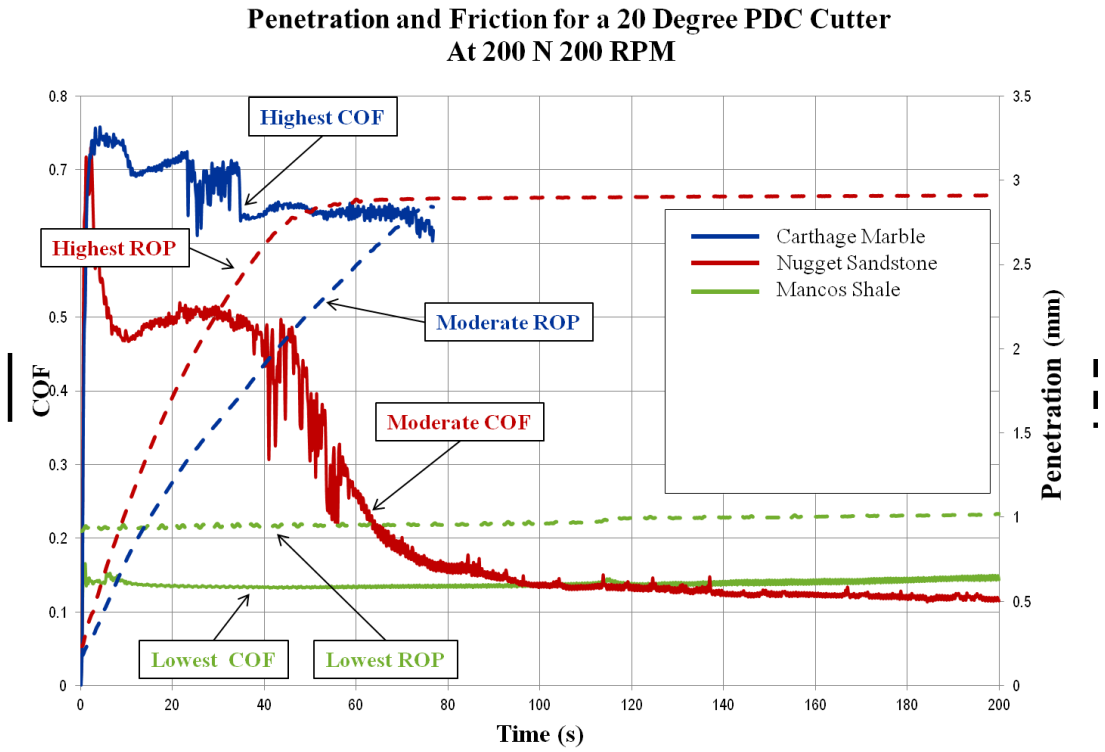

Figure 73: A Comparison of Penetration and Friction for Three Different Rock Types at 200N and under *Dry* Conditions

As a last comparison, Figs. 73 and 74 present the data for COF and ROP at the same load, but for each rock substrate in dry and lubricated configurations respectively. While it is typical to present steady-state values for these types of rock comparisons [78, 80, 81], the transient data, as presented in Figs. 73 and 74, allows for more insight into how different the friction and ROP can be as steady-state is approached. As a result, more information can be gained regarding the changes during dynamic events like the creation of a cut.

Table 8.2: Typical Unconfined Compressive Strengths of Tested Rock Samples [157-159]

Carthage Marble	Nugget Sandstone	Mancos Shale
82.7 MPa 12000 psi	124 MPa 18000 psi	62.1 MPa 9000 psi

For instance, dry Carthage Marble, presented in Fig. 73, displays very high friction before leveling out to a steadier value that is always much higher than the other rocks types.

Despite the severity of its friction and therefore cutting force, the Carthage Marble ROP is less than that of Nugget Sandstone which exhibits lower friction and cutting force. This is especially interesting because, in terms of unconfined compressive strength (UCS), Carthage Marble is slightly weaker than sandstone and by accepted standards should be easier to cut. The UCS value for each of these rock types is given both in pounds per square inch, as well as MPa, in Table 8.2. The COF for Nugget Sandstone displays a smoother descent, in which the friction quickly levels out to its steady-state value of around 0.5, after a brief period of high friction similar to marble. At the onset of the cut their friction behaviors are similar, but afterward the force required to cut sandstone is much lower. In terms of ROP, Nugget Sandstone consistently displayed the highest penetration rates, despite a higher UCS and lower cutting forces as compared to the Carthage Marble. At 200N and 200RPM, the PDC was unable to penetrate and display cutting behavior for Mancos Shale, which resulted in extremely low friction around 0.15. This was especially interesting because it was the weakest of the three rock types. It should be noted that even when cutting was found, at 300N for Mancos shale, it still exhibited lower friction and lower ROP than any of the other rocks. This type of result is important because it reinforces the fact that UCS, while a measure of rock strength, may not be the best indicator of how a rock will cut, most likely due to the different stresses experienced during cutting versus compression testing. From UCS, the bonds between rock particles in something like Nugget Sandstone may be more resistant to a failure in compression than Carthage Marble. However, from the current data, it would follow that they are less resistant to shear created by the cutter. To qualitatively summarize the dry testing: Carthage Marble had the highest COF and moderate ROP, Nugget Sandstone had moderate COF but the highest ROP, and Shale had the lowest COF and ROP. In terms of transition from scraping to cutting, Carthage Marble cut at each load although a transition point may have been close at 100N. Nugget Sandstone cut at loads higher than 100N, and Mancos Shale only cut at 400N, with the appearance of very weak cutting at 300N.

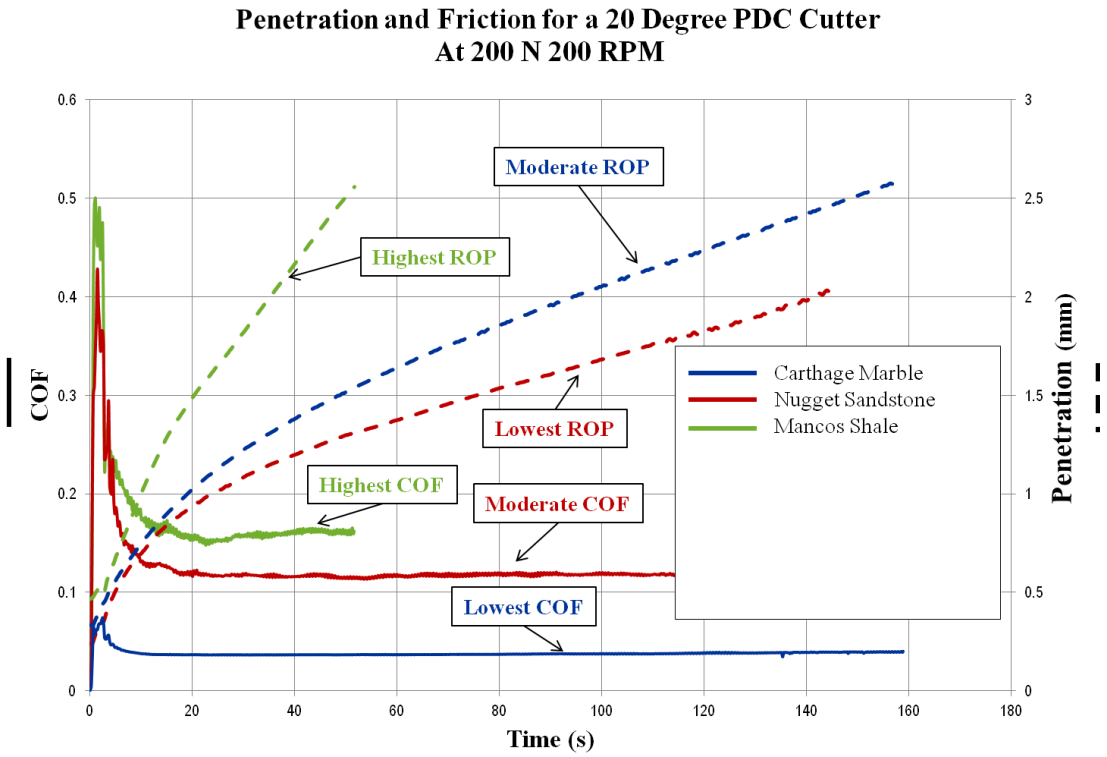

Figure 74: A Comparison of Penetration and Friction for Three Different Rock Types at 300N and under *Lubricated* Conditions

The qualitative behaviors of different rock types under water-lubricated conditions, presented in Fig. 74, were drastically different than those under dry conditions. Each rock type had less variation in its COF and the COF trends were similar in that they started high before decreasing to low and extremely steady values. Carthage Marble, which displayed the highest COF for dry cutting, displayed the lowest, and most stable, COF during lubricated cutting. Despite this drastic reduction in COF, Carthage Marble continued to display moderate ROP. Under these conditions, Carthage Marble seemed to experience the largest lubricating effect of the water, but the weakening effects were sufficient to maintain high ROP. In contrast, Nugget Sandstone continued to exhibit a moderate COF, but it displayed the lowest lubricated ROP. This suggests that the weakening effects of the water on Nugget sandstone were not quite as drastic as they were on the other two rocks. It was interesting to note that the parameters which were unaffected by load, such as COF for dry marble, and ROP for dry sandstone, were most susceptible to the effects of the water. Carthage Marble showed little dependence of COF on Load, but the lubricating effects reduced COF the most. The ROP for Nugget Sandstone was found to have little dependence on load, but under lubricated conditions it was the hardest to cut.

Shale, which previously had the lowest COF and ROP, displayed the highest ROP and COF when lubricated by water; reinforcing fact that shale is known to be extremely susceptible to weakening by the lubricant. These very different trends under lubricated conditions can be crucial in the field as they alter the relationships of ROP and the forces experienced by the cutter, to the imposed load. This is especially important since imposed load is one of the parameters which an operator might vary.

8.4 Conclusions

From the comparisons of rock types and cutting conditions discussed in this manuscript, the authors have drawn several conclusions which may be important to the drilling industry as a whole. Firstly, it was shown that a bench-top tribometer could conduct experiments to explore scraping and cutting mechanisms, *both* of which are found during drilling with PDC cutters. Secondly, it was found that smoothening effects occurred in the rocks during cutting which can explain the transient decrease in cutting forces during the creation of a cut. This behavior reinforces the need to understand chip formation, because of its higher cutting forces and their potential detrimental effects on cutter wear. Thirdly, it was found that transition points between cutting and scraping could be witnessed by adjusting the load such that an increase in contact area would decrease contact stress beyond a critical threshold for cutting. This allowed for insights into the difference between cutting and scraping mechanisms. These are valuable for analyzing the stresses on the underside of the cutter and the development of wear flats, versus the stresses solely on the cutting face. Fourthly, two effects of the lubricant were found to exist. One effect would lubricate the interface and reduce friction and ROP. The other would weaken the rock and allow for greater ROP, and when applicable, a lower load transition into full cutting from scraping. These are important because the first effect helps to protect the cutter, while the second helps to aid in maximizing ROP. Information regarding these competing effects must be considered when choosing a drilling fluid such that ROP and cutter life are both optimized to suit the project based on rock type. Lastly, a comparison of different rock types at the same load showed that each rock behaves differently under dry and lubricated conditions – sometimes in manners different than what the relative magnitude of their unconfined compressive strength would suggest. This is especially crucial because it emphasizes the need for a precise description method for the resistance of rock types to PDC cutting. This study as a whole presented justification for tribological test methods as a supplement to the current standards in drilling

research, through their ability to elucidate phenomena generally prohibited by rigs like the VTL. It is the hope of the authors that the methods described in this manuscript will be carried out at higher loads, speeds, and eventually hydrostatic pressure, such that they may bring similar insights even at the most relevant down-hole conditions.

Chapter 9: Evaluating Industrial Drilling Muds for Single Cutter Rate of Penetration and Lubrication Performance

This chapter contains a study in which friction and rate of penetration was detailed for 3 different rock substrates using polycrystalline diamond compact cutters and industrial drilling muds. It includes a first order figure of merit for ranking a drilling mud for a given rock type.

9.1 Introduction

This work aims to further the studies done in Chapter 8 by including an evaluation of industry grade drilling fluids, as well as a proposed figure of merit for ranking the efficiency of a drilling fluid in minimizing wear while maximizing ROP for a given rock type. As described previously in Chapter 8, the primary goal of optimization studies for single cutter drilling work is to minimize the time of well creation. This is due to the fact that the primary cost during a full project is the rental of oceanic drilling equipment. This means not only drilling as fast as possible through the rock, but through minimizing "Bit-trips," in which a full scale shut down must be activated in order to replace worn cutters. One of the chief methods for meeting this goal is in the careful selection of drilling fluids or "muds," due to the fact that they have been shown to protect PDC cutters through lubrication, by removing abrasive rock fragments and reducing thermal wear due to frictional heating. Interestingly, as described at length in Chapter 8, they also act to make the surface of the rock more drillable through both hydrolytic weakening and filter cake formation. Due to the proprietary nature of the rock drilling industry, very few published studies exist in which drilling fluids have been examined for their lubricating properties [160]. This is compounded by the fact that, the industry standard rig is not equipped to investigate the efficiency of a lubricant beyond a cooling effect, and only as it influences the time to catastrophic failure. The state of the literature currently centers around studies which look primarily at a fluids material properties with little or no discussion as to how it will perform in terms of lubrication on a given rock [78, 82, 160, 161]. PDC Cutter studies that have been conducted using fluids, generally use either a water or basic mineral oil [78, 145, 148], and do not feature any ability capture in situ friction data capable of discussing the lubricating efficiency of a given mud from a purely frictional perspective [74, 147, 148]. It should be noted that there have been recent studies which very carefully, explore the effects of drilling fluid under highly

pressurized conditions similar to those found down-hole [162, 163]. While this work does an excellent job to explore drilling fluid effects on ROP for different cutters, it does not include an exploration into the effect of lubrication which the cutters can provide in terms of friction reduction. As described in Chapter 8, friction will play a key role in minimizing bit wear, and therefore is crucial to representing not only the ROP element of optimization, but also the minimizing shut downs for "bit-trips". It is the goal of this chapter to combine the performance enhancing aspects of different drilling fluids from both perspectives, into a coherent, first-order figure of merit, able to rank drilling fluids for different rock types.

9.2 Experimental

The tribometer used in this study, will be identical to the authors' previous work described in Chapter 8, with the exception that 3 industrial drilling muds will be utilized from Chevron Co., and Newpark Co. In all cases, the drilling muds represented in kind contributions and as such much of the information regarding there make was proprietary . There disclosed properties are described in Table 9.1. It should be noted that despite the limited knowledge of their make-up, this does not prevent the ability to assess their performance based on ROP and COF. Therefore the discussion of drilling muds will focus on ranking their performance rather than optimizing their particular chemical compositions. Each mud was mixed using a paddle drill for 30 Minutes prior to testing as advised by the manufacturer to ensure that the particles were fully in suspension. This process as well as images of the cutting chamber and a post-test cutter, can be seen in Fig 75. The drilling procedures for dry and wet testing were kept identical to those in Chapter 8.

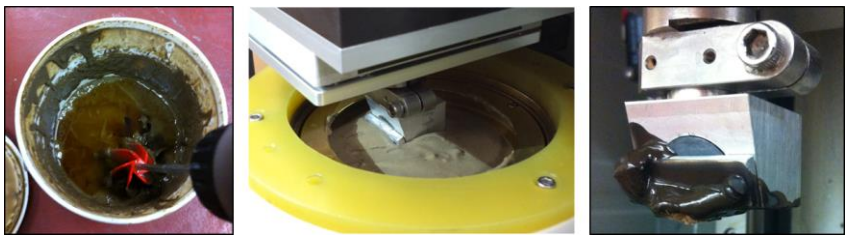

(a) (b) (c)

Figure 75: Images capturing the experimental set up for simulated rock cutting with Newpark 2 Synthetic Drilling Mud: (a) Mud mixing, (b) the cutting interface, (c) post-test cutter experiencing minor "bit-balling"

Table 9.1: Experimental Test Parameters

Mud Type	Newpark 1	Newpark 2	Chevron 2
Base and General Notes	Water-based	Synthetic Shale-inhibiting	Oil-based

9.3 Results and Discussion

9.3.1 Drilling Mud Studies for Carthage Marble

The results for the first parametric study are presented in Fig. 76. For each plot, the coefficient of friction (COF) is plotted on the left, while the depth of cut (DOC) is plotted on the right. The rate of penetration (ROP) may then be discussed as the slope of the dashed line. In Fig. 76, the results for COF and ROP for each drilling mud are presented for Carthage Marble, as well as the results of a dry test. It should be noted that each drilling fluid was able to reduce the COF of the PDC cutter. However it was also found that the dry scenario still featured an increased ROP.

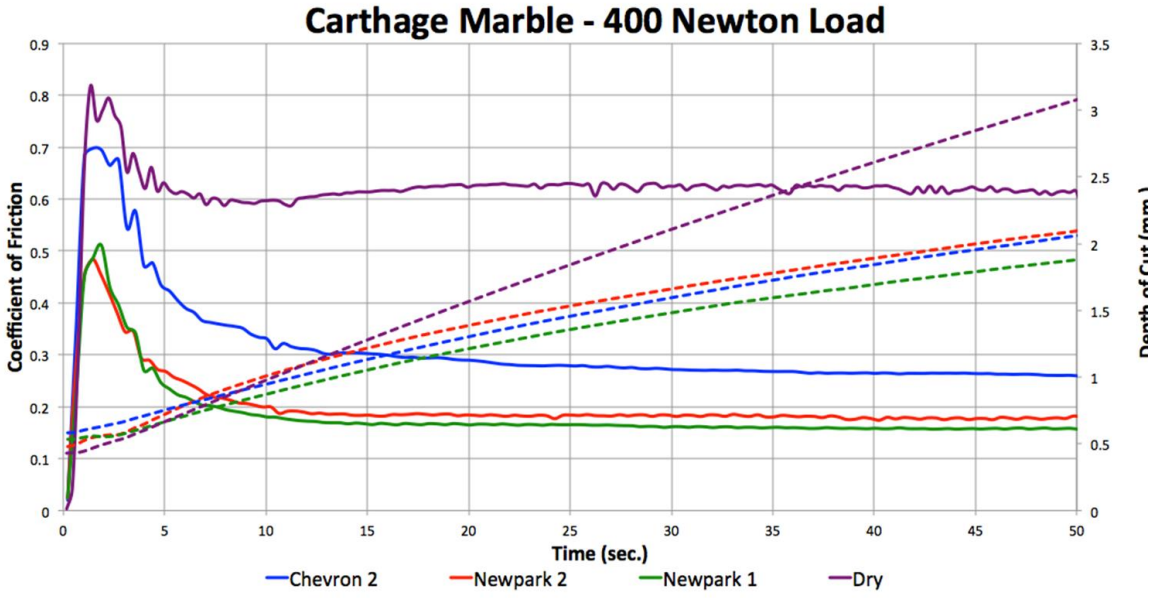

Figure 76: Parametric study for the effect of drilling mud on rate of penetration and coefficient of Friction for Carthage marble

Due to the majority of the cutting force stemming from the penetration of the cutting edge into the rock, one might assume that ROP will be directly proportional to COF. However

From Fig 76, it can be seen that the relationship between COF and ROP is representative of this simple monotonic relationship. This was discussed at length in chapter 8, and is reflective of a fluids unique ability to make the rock more drillable, while also providing a lubrication effect to the cutter. For Carthage Marble, it was found that the oil based mud Chevron 2, provided the least amount of lubrication effect, indicated by a higher COF, with a ROP somewhere in the middle. The muds from New Park provided improved reductions in COF, with the water based New Park 1 being just slightly lower. However, in terms of ROP the synthetic based New Park 2 was found to provide the greatest penetration depth.

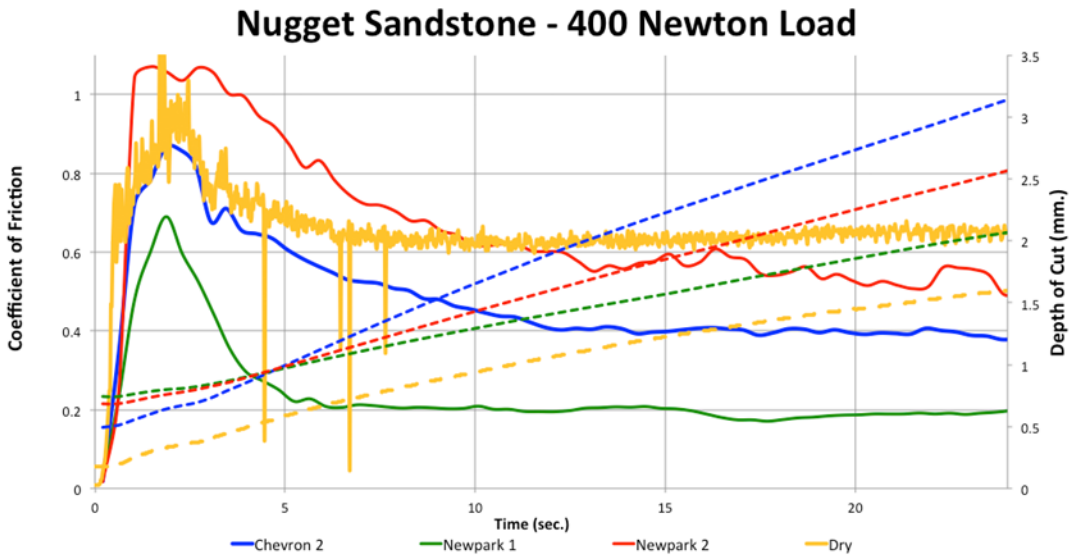

Figure 77: Parametric study for the effect of drilling mud on rate of penetration and coefficient of friction for Nugget Sandstone

9.3.2 Drilling Mud Studies for Nugget Sandstone

The results for COF and ROP for each drilling mud on Nugget Sandstone are presented in Figure 77. Once again, a much more complicated relationship is observed for friction and wear foe each drilling mud. A unique aspect of Nugget sandstone compared to Carthage marble was observed in which each mud improved upon the ROP of the dry case, showcasing the fluids ability to weaken the rock. However this was not the case for COF. The synthetic New Park 2 mud was actually shown to provide negligible reductions in COF compared to dry cutting, even providing an increase in friction during the development of the cut. This is most likely due to the enhanced penetration depths provided by the weakening of the rock and reflected in the increased ROP. While the lubricating effect will significantly decrease the scraping friction present on the undersides of the cutter, the increase in ROP over the dry will be reflected as an

increase in cutting force. This effect is reinforced by the results for water based Newpark 1, which was able to drastically reduce COF but with a reduction in ROP improvement. The most interesting result was observed for the oil based Chevron 2 mud, in which the COF was significantly reduced *and* the highest ROP was recorded. This is the type of performance result which is very difficult to consider from a holistic perspective when trying to choose the best mud, and will be discussed later in the Figure of Merit section. The mechanics behind this reduction in friction despite an increase in ROP over the Newpark 2 mud, is most likely a result of two factors. First, the Newpark 2 mud was much more viscous, which can cause large drag forces under the cutter during hydrodynamic lubrication. This effect is most likely less important, as the lubrication regime should be mixed at these high loads and moderate speeds. The mixed regime would feature loads borne by both the asperities of the rock surface, and the lubricating fluid, and so viscous shear will not be as pronounced as a fully hydrodynamic regime. Second, while weakening the rock can lead to COF due to higher penetration depths, the oil based Chevron 2 may also be more efficient in weakening the rock. This means that that it requires less energy to cut the rock at a given penetration depth. It is most likely that this is the dominant mechanism for improved ROP performance alongside reduction in COF.

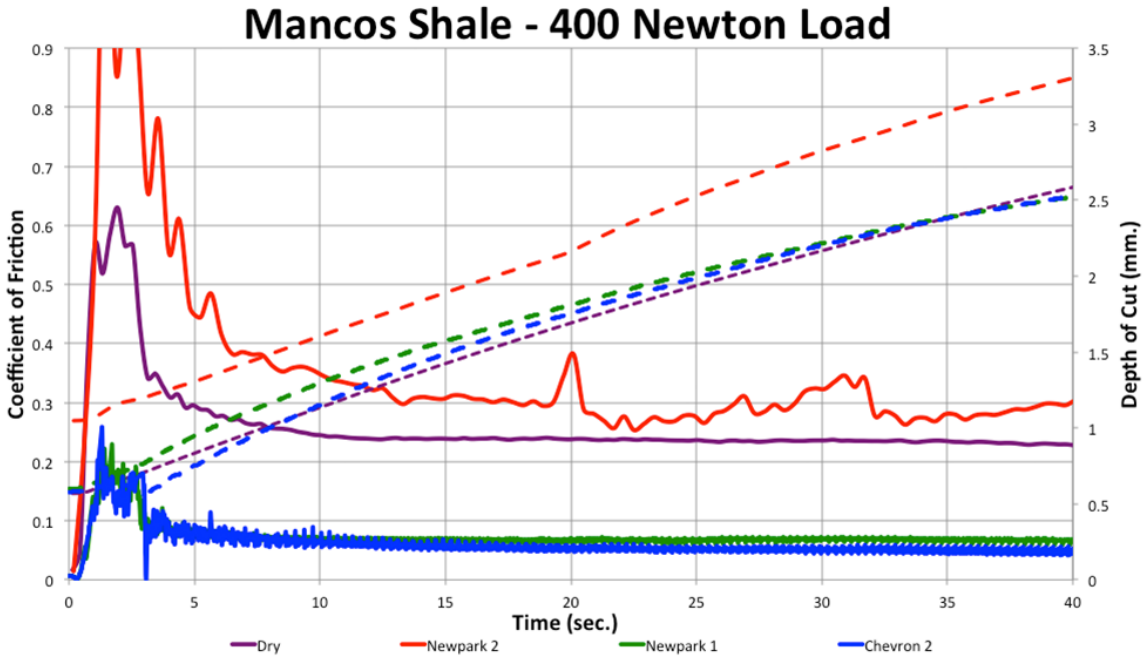

Figure 78: Parametric study for the effect of drilling mud on rate of penetration and coefficient of for Mancos Shale

9.3.3 Drilling Mud Studies for Mancos Shale

In Fig. 78, the results are presented for COF and ROP of Mancos shale with respect to each drilling fluid. Interestingly enough, very little effect was found for the muds in terms of increasing ROP over the dry case. It should be noted that this in agreement to the results presented in Chapter 8. While the lubricating fluid was found to lower the transition load for facilitating cutting, water lubricated cutting was fairly similar in terms of ROP. On the other hand, it was found that the lubricant had drastic effects in lowering the COF. These reductions continued for both the oil based Chevron 2 and the water based Newpark 1. COF values were very low when lubricated with these muds, around 0.08, despite similar ROP to that of the dry case. Once again this is most likely due to a combination of lubrication under the cutter in the scraping regime, as well as significant weakening of the rock surface to which shale is particularly prone. It must be noted that similar to the results for Nugget Sandstone, the viscous, synthetic Newpark 2 was actually found to display a COF that was s higher than that of the Dry case. Once again this is most likely due to a decreased ability to weaken the rock in addition to viscous drag affects in the lubricating interface.

9.3.4 Derivation of the first order Figure of Merit

As a result of the two fold nature of reducing the time required for well creation, it is necessary to consider both the speed at which one can destroy the rock, as well as the lifetime of the cutter. As discussed in Chapter 8, one of the most important failure modes for cutters arises due to frictional heating at the interface which reduces the integrity of the PDC. A first order simplification for dry frictional heating, when considering the rock surface to be adiabatic is presented in equation (9.1). This is not a poor assumption as the rock surface will be much less conductive, and suits the purposes herein in that it demonstrates that reducing friction coefficient is directly proportional to reducing the heat generation in the interface.

$$\dot{Q}_{COF} = \frac{(F_{n,cutter})(COF_{ss})(V_{cutter})}{A} \qquad (9.1)$$

Q_{cof} is the rate of energy input into the cutter through frictional heating, F_n is the normal force on the cutter, COF_{ss} is the steady state friction coefficient taken from the test, V_{cutter} is the sliding velocity, and A is the contact area. This is not a poor assumption as the rock surface will be

much less conductive, and suits the purposes herein in that it demonstrates that reducing friction coefficient is directly proportional to reducing the heat generation in the interface. While there will also be heat removal by the fluid, this equation succeeds in stressing the importance of reducing COF in minimizing thermal wear and maximizing cutter life.

With this in mind it is possible to use the tribometry testing described above to provide a unique Figure of Merit (FOM) for the use of selecting a particular drilling mud for a particular rock type. In order to capture the maximization of speed at which one destroy's the rock it is important for the FOM to be directly proportional to the steady state ROP. In order to capture the minimization of friction heating and potential for thermal induced wear, it is important for the FOM to be inversely proportional to steady state COF. Therefore, the FOM can first be expressed by equation (9.2)

$$FOM \sim \frac{ROP_{ss}}{COF_{ss}} \tag{9.2}$$

While this provides a way to gauge the improvement of both ROP and COF, it does not provide a way to normalize the two values. Normalization in this case is extremely important because a figure of merit from one lab should be able to be compared to one found in another, as well as provide a measure of improvement to some type of datum. Without the latter, it cannot take into account how small changes in COF or large changes in ROP may represent the same boost in performance. To combat this challenge, a normalization scheme in which each value is normalized by the dry performance was proposed. Utilizing this approach allows for FOM above 1 to represent improvement over the dry case, while less than 1 represents a performance decline. In this way, the first order figure of merit can be expressed by equation (9.3), and this value can provide a direct comparison for each mud in terms of the combined performance goals of minimized COF and maximized ROP.

$$FOM = \frac{ROP_{ss}/ROP_{Dry}}{COF_{ss}/COF_{Dry}} \tag{9.3}$$

9.3.5 Drilling Mud Evaluation using the FOM

The results for the FOM for each drilling mud on each rock are presented in Fig. 79, in which each rock type has its own sub-plot. As can be seen from initial inspection, the behaviors of a given drilling mud were different for each rock type. For Carthage marble, the synthetic

Newpark was actually the strongest drilling fluid increasing performance by 80 percent, whereas for the other two rock types it was actually the weakest. This is a result of two interesting features, the first being that for Carthage Marble, very little effect was found for fluid on ROP, implying that the marble is resistant to weakening and actually cuts fastest when dry. This made reduction in COF a much more prominent factor in the FOM. The second effect is that for Carthage Marble, synthetic Newpark displayed drastically different frictional behavior. For the other 2 rock types synthetic Newpark displayed high COF, while for Carthage Marble the COF was quite low. Water based New park proved to be the second best for Carthage Marble, while oil based chevron proved to be third best though still an improvement over the dry.

For Nugget Sandstone, the oil based Chevron was actually the most successful in optimizing both COF and ROP by a factor of 250 percent, with the water based Newpark performing second best at an increase of about 200 percent. Unlike Carthage marble, drilling fluids were able to offer performance increases in both ROP and COF. The oil based chevron performed the best due to its ability to drastically weaken the rock and increase ROP, despite only reducing COF half as much as the water based Newpark. This latter fluid was able to provide COF as low as 0.2, but this was most likely due to a decrease in penetration depth as evidenced by its decreased ROP. This is a perfect example of how the FOM will allow for ranking between two competing performance enhancements. The synthetic Newpark was still better than dry cutting, though the improvement was very slight.

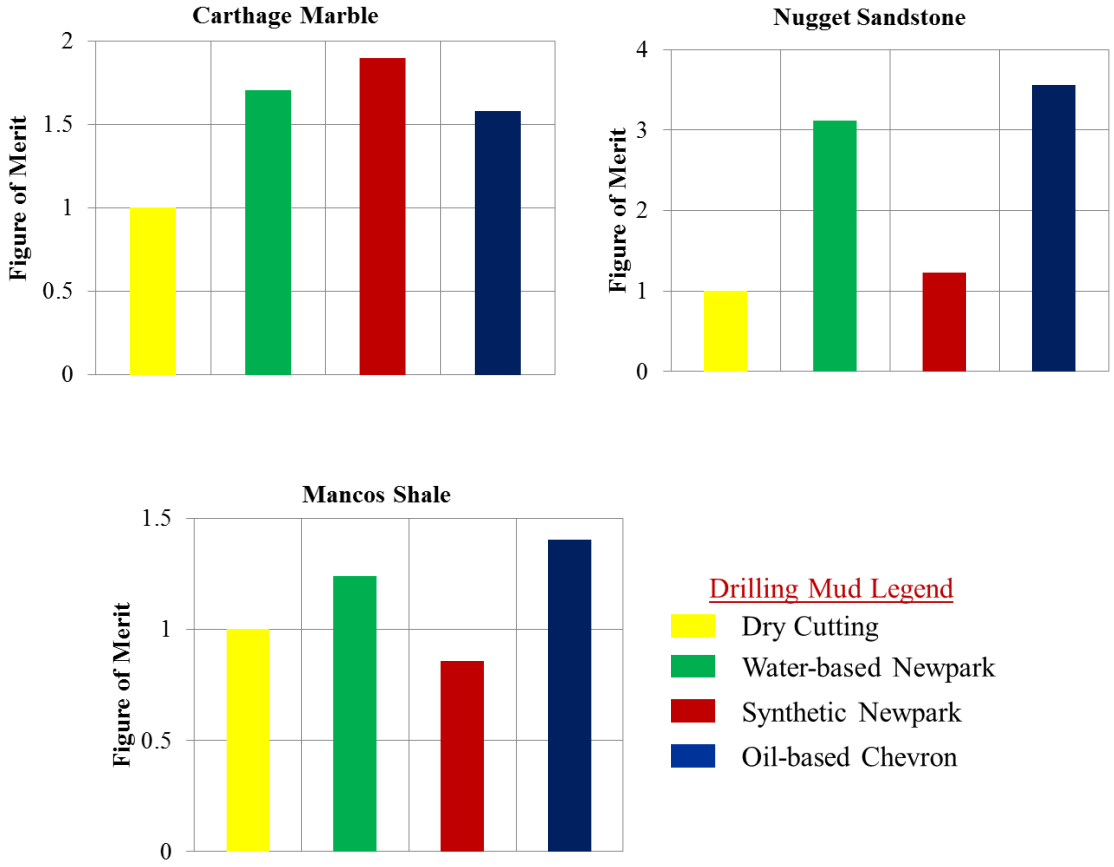

Figure 79: Figure of Merit(FOM) results for each rock type and each drilling mud

For Mancos Shale, the oil and water based muds provided an increase in performance, while the synthetic actually provided a decrease in performance. This unique FOM plot is due to the fact that Mancos shale actually saw very little increase in ROP between dry and lubricated cases. As a result, COF was the primary element in determining the magnitude of the FOM. For a rock like shale in which the lubricating fluid can reduce COF to as low as 0.08 as shown in Fig. 78, a fluid which actually increases the COF like synthetic Newpark will display a very poor FOM.

9.4 Conclusions

Drilling for natural resources will always be driven by a desire to accomplish the extraction process as cheaply as possible. As a result of the cost in well creation, the primary driver for bringing down costs is to destroy the rock as fast as possible (maximum rate of penetration) while minimizing friction which can result in thermal heating and failure. Despite the large breadth of work in single-cutter rock interaction for PDC cutters, very little has been done to

examine the effect of industrial drilling fluids on these two performance metrics in these interfaces. In this work, friction and rate of penetration were analyzed in tandem using tribometry for three different drilling muds, on three different rock substrates. A load of 400N and 200 RPM were chosen for comparison purposes, because they were sufficient to induce both cutting and scraping mechanisms during dry cutting during the previous study described in Chapter 8. Industrial drilling muds were found to improve performance in all cases but the case of a synthetic mud from Newpark on Mancos shale. In many cases, a given mud would provide different levels of performance enhancement which were difficult to compare. As such, a figure of merit (FOM), was proposed in order to concisely rank drilling mud performance. This FOM was normalized by dry conditions in a way that would take into account the importance of for maximizing ROP *and* minimizing bit wear. The FOM proved useful in discerning between competing increases in performance from mud to mud, and also from rock type to rock type. Through the use of detailed tribometry, the FOM found that the synthetic mud from Newpark would provide the best combination of minimal COF and maximum ROP on Carthage Marble. However, it was found that this mud performed the worst on Nugget Sandstone and Mancos Shale. It was found that the oil based Chevron 2 performed the best on both Nugget Sandstone and Mancos shale.

Chapter 10: Conclusions and Future Work

10.1 Conclusions

This work has detailed the execution of a research plan containing four objectives, each of which pertain to a specific industrial application. For each application, a crucial aspect of performance optimization existed in understanding events at the contact between two surfaces. Furthermore each application suffered from a lack of understanding in this interface, generally due to the difficulty in observing events at such a small and cramped scale. In order to investigate these interfacial mechanics a technique was proposed using surface metrology before-and-after testing (*ex situ)*, combined with friction and wear data captured during testing (*in situ)*. For each objective, these previously unknown interfacial mechanics were elucidated using a synthesis of *in situ* tribological data and *ex situ* surface metrology.

The first application was an investigation of the protective aspects for solid lubricant transfer films. This solid lubricant industry has had a great deal of success as an auxiliary mechanism to liquid lubrication, but has sought to become more reliable in order to meet the ever increasing severity of industrial contacts. Despite promising potential, the mechanics of how transfer films and hard tribological coatings operate are still largely unknown especially in terms of predictive capabilities. This is due to the complexity inherent in powder flows governed by discrete wear events. The difficulty in probing their performance is exacerbated further as a result of their location in the contact interface. These qualities made it a perfect area to study using the combined *in situ* and *ex situ analysis.*

Transfer film experiments were carried out in Chapter 2, which was able to describe the dynamics of a single component, self-replenishing, solid lubricant transfer film. The primary wear mechanism was determined to be abrasive wear rather than adhesive wear, and the transfer film was found to form as a collection of clumps rather than a uniform coating. The wear mechanism were justified through the observation of abrasive frictional behaviors in the *in situ* data, as well as abrasive wear profiles found through detailed *ex situ* interferometry. Both of these conclusions were different than what was previously assumed for film formation which had direct implications for modeling presented in Chapter 5. Lastly, it was found that the lubricated contact could act as a spreading mechanism, essentially smoothing out the transfer film such that it could provide better coverage and therefore protection. Each of these conclusions regarding

the transfer film was justified through isolating individual aspects of the transfer film during *in situ* testing, and performing *ex situ* metrology. These findings were shown to have important implications for the optimization of film deposition, as well as providing the foundation for a predictive model in Chapter 5.

These experiments were continued in Chapter 3 for a multi-component system. Transfer films were formed using a combination of a known solid lubricant and an inherently conductive material for the purpose of lubricating electrical sliding contacts. It was shown through *in situ* data that these composite solid lubricants suffered from inexplicable deterioration of frictional performance. Interestingly enough, this occurred despite confirmation through the *ex situ* analysis that films are still intact. Despite the fact that transfer films are considered to be governed by quasi-static phenomena, particle size segregation was proposed as an explanation for performance deterioration by the author due to the frictional signatures in the *in situ* data. This was justified through the matching of particle sizes and the subsequent shift to stable, low friction transfer film performance. The mechanism for friction performance and segregation in transfer films, was then explained through a quasi-hydrodynamic theory of lubrication. These findings proved to be extremely relevant to the solid lubricant industry, as a retrospective search through the transfer film literature that displayed numerous examples of papers with the same performance issues. Despite being previously unexplained, each of these examples was shown to possess the potential for particle size segregation.

Hard Tribological coatings were also examined as another form of solid lubrication for their ability to mitigate impact damage in Chapter 4. Rather than using a tribometer, single element drop tests were conducted on a Drop Test Rig to simulate impacts on coated surfaces in rolling element bearings. *In situ* data was captured in the form of coefficient of restitution, while *ex situ* data included optical interferometry of impact sites, as well as fixed ion beam cross sectioning for sub-surface damage. It was shown through a synthesis of *in situ* and *ex situ* data that ultra-hard coatings were found to work best for soft substrates, while elastic coatings were found to work best for harder substrates. The synthesis of both *ex situ and in situ* data was able to highlight the potential for drop testing to act as a cheap screening method for bearing materials. This was justified due to the correlation of increase in coefficient of restitution with a reduction in impact damage during the more expensive *ex situ* analysis. These findings were

crucial to the industry because they were able to highlight performance differences where traditional testing in the form of only *ex situ* material property characterization would fall short.

The final aspect of the solid lubricant research was conducted numerically in Chapter 5, as a simulation of the powder compacts used to create transfer films in Chapters 2 and 3. Due to the *in situ* and *ex situ* conclusions, the appropriate friction and wear mechanisms were isolated, and a numerical model was developed using contact mechanics equations from previous studies in the literature. By modeling each asperity contact as a sphere on flat with dimensions taken from an optical interferometer, and by calculating the stresses and subsequent wear at each contact point, the soft surface was modeled to evolve over time deterministically. As a result of this treatment, quantitative predictions were possible for friction of the wearing surface which displayed excellent agreement to experiments at steady state. In addition, the model was also able to predict worn topographies from *ex situ* analysis conducted in Chapter 2. This model is relevant because of its ability to predict the transient and evolutionary behavior of a surface. Generally, this type of prediction is impossible due to the statistic nature of modeling surface phenomena. The predictions are extremely useful as they can help to provide predictions of defect creation as well as increases or decreases in frictional severity as a surface evolves through wear.

The third research objective, was concerned with employing *ex situ* particle characterization, and *in situ* powder rheometry, in order to explain flow behaviors for additive manufacturing (AM) powders. In this industry, powder flow issues at the spreader or hopper interfaces can be tied to large scale challenges such as poor part quality, limited material selection, and costly build times. Despite these correlations, very little work exists thus far in characterizing the powders, and even less exists for intuitively relating their rheological behaviors to areas in the AM process. The author proposed that *ex situ* characterization and *in situ* rheometry could be used to precisely characterize differences in AM powders before they touch the actual machine. In this fashion, the author proposed that the technique could be used as a way to pinpoint optimal morphologies for a given AM machine.

Powders were characterized in Chapter 6 for particle aspects such as size, circularity, degree of fines, and satellites. Rheometry was conducted using an FT4 Freeman powder rheometer, under stress states akin to powder spreading and hopper flow in the AM process. It was shown that morphology changes from the same manufacturer could govern rheological

behavior even amongst powders of different materials. It was also shown how tailoring particle morphology could provide different flow behaviors for the same powder material. These behaviors were related to flow states in the AM process, in a way that displayed how rheometry could identify trouble spots of candidate powders before they are implemented on a machine. These results were crucial because they offer the ability to tailor given powders through processing, based on which aspects of a given machine might experience flow issues.

The final research objective, involved utilizing *in situ* tribometry with *ex situ* interferometry to explore the mechanics of single cutter PDC rock drilling interactions for oil, natural gas, and geothermal heat. For this industry, minimizing the time spent replacing worn cutters while maximizing the speed at which one destroys rock is the primary means of reducing project cost. In addition, the current literature is dominated by machines which are not only too costly to implement in an academic setting, but which prevent investigations concerning *in situ* data capture for friction, lubrication phenomena, and cut creation. Because of these factors and the difficulty in monitoring cutting during operation, a combination of *in situ* tribometry and *ex situ* interferometry was proposed.

Single cutter studies were performed in Chapters 7 and 8 using both hardened tool steel and polycrystalline diamond compact on a variety of rocks found during the drilling process. Friction results displayed large fluctuations present during the creation of a cut compared to steady values, which agreed well with speculations in the literature that ignoring cut creation on the current test rigs might provide data which is too steady. *Ex situ* characterization displayed that much of the transient fluctuation comes from the evolution of the rock topography, and the potential for rough features to arise when the cutter is not fixed in place. Lubricated studies with water showed the potential to study detailed lubrication phenomena including its ability to reduced friction by mitigating scraping friction, as well as by weakening the rock type to promote enhanced rate of penetration and lower drag friction. This type of testing was also able to showcase the machines ability to pinpoint transitions in cutting mechanism at different loads. In this way one could more precisely examine the type of forces present at the underside of the cutter or at the cutting face. This is particularly important to the drilling industry as it is currently very difficult to find out how the forces combine in the generation of thermal heating and cutter failure. A comparison of different rock types was also conducted, for both scraping and cutting mechanisms. Depending on the type of lubrication, testing showed that use of the ultimate

compressive strength will not always provide enough information to gauge which loads are necessary to cut the rock. Chapter 9 expanded upon the lubricated testing to include the evaluation of industrial drilling muds. Cutting tests were performed using an oil based, water based, and synthetic mud on three different rock samples. It was proposed by the author that an evaluation of the muds performance could be made which would contain information about maximizing penetration *and* minimizing the build-up of frictional heat. This would essentially provide a way to rank drilling muds based on the goals involved in minimizing project cost. A figure of merit and normalization scheme was derived based on improvements over dry cutting. Using this figure of merit, competing behaviors were condensed and each rock type was found to have unique preferences for the type of mud. This type of result is important because it allows for benchtop characterization of drilling muds otherwise precluded by the current industry standard of testing, and a simple way to provide first order screening of new muds on a given rock.

Overall, the four research objectives presented a challenge in that each industrial application suffered from a lack of clarity in its primary contact interface. Through a use of *in situ* and *ex situ* analysis, the author was able to recreate events such that performance information could be catalogued and optimization could be undertaken based on the given applications performance goals. It is the hope of the author that this technique can be expanded further to include an even broader collection of industrial applications, and a greater understanding of interfacial science.

10.2 Future Work

There are several ways in which this technique, as well as its application to each industrial objective described herein, could be furthered and improved. In terms of the solid lubrication studies, it would be beneficial to expand the material set both in the single component and multi-component transfer film systems. Design studies could be also performed in which the surface to be lubricated could be optimized for spreading of the transfer film. This would allow for a broader understanding other solid lubricants similar to that provided in Chapter 2 and 3, as well as further optimization of transfer films in general. For the study on impact damage of coatings, a more in depth study of the effect of coating thickness would be of great use and was currently precluded due to the project cost. This would help to provide further design

optimization for industrial contacts beyond the current discoveries involving material properties. The friction and wear modeling could also be improved through expanding on the material set to include constitutive relations for the wear of harder surfaces, as well as the effect of transfer film build up on the hard surface. Both of these steps could be successful in improving the qualitative agreement of wear such that it performed as successfully as the predictive friction and surface topography capabilities.

In terms of additive manufacturing, it would be extremely useful to perform experiments with the tested powders on an actual machine with variable spreading parameters. If *ex situ* analysis could be performed on built parts, a given powder's performance at varying spreading parameters could be tied to the rheological and morphological changes found on the FT4. This would fully close the loop such that technicians could utilize the results presented in this thesis to pre-screen new powders and tabulate operational AM parameters before a powder is every used. For instance, there are a few examples of projects not yet finished which would greatly aid the rheological understanding of AM powders. First, the effect of recycling the powders is a key element to the promise of AM in conserving manufacturing cost through reducing wasted material. The current state of this understanding in the literature, to the author's knowledge, is limited in both the type of powder used as well as the number of recycling steps. Particularly for electron beam based machines, recycling the powder means blasting apart a nearly sintered block in which serious morphological changes will occur to the powder. An experiment must be conducted in which numerous recycling steps are conducted with the exact same powder, while rheological and morphological changes are monitored in between. This project would greatly help the ability of manufacturers to alter process parameters as a powder is recycled over its lifetime. In addition, the author has two provisional patents involving *in situ* data capture, which require future work in the area of AM research. For both of these projects, it is imperative to expand upon the *in situ* monitoring capabilities inside an AM rig with the goal of directly observing the spreading process. It was proposed by the author that an understanding of the *in situ* friction, or of the optical state of the powder after a spread, could be used to detail if a spread was sufficient. It is quite difficult to instrument these machines, but any progress in tailoring the rheological understanding such that it can make direct design recommendations is dependent on improving this monitoring capabilities. In a preliminary work, the author conducted experiments in which current draw from the spreader's motor was tracked *in situ* for the spreading of Starmet

Ti-64 powders. It was hypothesized that the current was proportional to the frictional resistance experienced by the motor. However it was not clear if the resolution of the machine was fine enough to observe changes in the powder spreading versus the impetus required to drive the spreader itself. Further investigation of other powder materials and the creation of a calibration curve for spreads with no powder would aid in evaluating this resolution.

Another key element to the AM process which was as yet identified is an evaluation technique to assess whether a layer is uniform after a spread. It was proposed to use optical techniques utilizing roughness as a measure of layer uniformity, but the diffuse nature of each layer (poor reflectivity) and the difficulty in using something like optical interferometry inside a machine was highly prohibitive to quality measurements. The author was unable to find any advice as to the qualification of uniform layers of discrete particles in the literature and a robust methodology for describing a uniform layer, coupled with a way to do it inside a machine, would be invaluable to the AM community.

A final project which would be a great start for a student continuing this AM work, would be to compare alternative powders of a given material with different rheological performance on the FT4, to a manufacturers powder like the ARCAM Ti-64 that has established spreading parameters on a given machine. An experiment could be conducted in which deviations in rheological performance could be tied to required changes in spreading parameters. This would most likely have to be evaluated through microstructural changes of finished samples, or through evaluation of spread layers if possible.

For the work conducted in deep well rock drilling, a wider range of loads and speeds with the aim at observing precise frictional signatures leading up to failure would be extremely valuable. This would involve an upgrade in the motor capabilities of the current rig, and was currently beyond the budgetary scope of this work. This would be invaluable to industry both as a way to better explain and prevent cutter wear, as well as a way to monitor for potential failures while drilling.

Appendix A: Enhancements in the Lubrication Regime for Artificial Hip Joints

This appendix contains a study conducted in order to improve the lubrication regime present in artificial hip joints through surface texturing. The goal of this paper was to reduce surface contact by shifting to a more hydrodynamic regime of lubrication, rather than the primary mixed mode present at hip joint loads and speeds. A similar version of this work was published in *Tribology Transactions*. [Dougherty, P., Srivastava, G., Osler, R., Ozdoganlar, O.B., and Higgs III, C. F., "Lubrication Enhancement for UHMWPE Sliding Contacts through Surface Texturing", *Tribology Transactions*, 2015.]

1. Introduction

Total hip replacement has been referred to as "the operation of the century," after its wide acceptance in the 1960's provided for the ability to drastically increase the agility and comfort of both elderly patients and also of younger, more active patients with early onset hip problems [164]. The distinctive features of the joint are the acetabular cup, often a metal or polymer, and the femoral head which is often a harder ceramic or metal alloy. The joint itself is lubricated by synovial fluid with shear-thinning viscosities between 0.0025 and 0.0009 Pa-s, which are relatively low compared to common industrial lubricants but similar to water [165, 166]. While walking, the hip joint interface experiences a combination of normal loading and surface tractions often approximated as locally sliding contact between surfaces [3]. The actual loading conditions were estimated by Dowson, who reported average loads of 1346 N and average sliding speeds of 1.5 rad/s for the normal gait cycle [165]. Alternatively, in the work of Hodge et al., contact pressures were captured *in vivo* and found to vary between 1-10 MPa, also during the gait cycle [167].

Many authors have presented different mechanisms for the ongoing tribological interactions in the artificial hip joint. Because of the relatively high load, low speed, and low viscosity sliding contact, the lubrication exists primarily in the boundary and mixed lubrication regimes where the load is borne by a mixture of fluid-surface and surface-surface asperity contact. As a result, only occasionally are speeds and pressures developed which are sufficient for full film separation of the surfaces [165]. In addition, with progressive use, the lubricant can become filled with

particulate debris, thereby putting the interface into what the authors refer to as a "particle augmented mixed lubrication" regime [168]. In this special case, it has been shown that the presence of particles in the interface significantly alters the lubricating performance, most commonly by accelerating the abrasive wear process. Given the added complexity of these problems, numerical modeling approaches are generally used to capture the interplay between the fluids, particles, and surfaces [169-171].

In the presence of these more severe lubrication regimes, total hip replacement has been plagued with unacceptable clinical lifespans due to premature failures that have reduced average joint life from an expected 50 to just 12 years [164, 167, 172]. The primary cause of these failures was found to be a number of harmful effects, incited by excessive wear and debris generation at surface-surface contacts [164-166, 173, 174]. The generation of this debris is thought to occur due to a number of important wear mechanisms including two body and three body abrasion, delamination, fatigue, and oxidation effects that tend to exacerbate abrasion through the creation of added roughness [175-178].

Though the surface degradation of the cup can become a serious problem, it is generally the more biological debris effects which cause joint failure [164-166, 173, 174].These effects include granulomatosis lesions and osteolysis, which lead to bone resorption, pain, and aseptic loosening of the prosthesis. Osteolysis itself is the description of an auto-immune reaction attempting to attack the wear debris, but actually succeeding due to its tenacity in deteriorating the natural bone and inflaming the surrounding tissue [172-174]. Early attempts to mitigate these problems involved choosing material combinations which would reduce debris generation through material properties alone. Despite a recent increase of metal-on-metal combinations, the most prevalently used material combination for artificial hip joints is an ultra-high molecular weight polyethylene (UHMWPE) cup with a ceramic or metal femoral head, most often constructed from alumina, zirconia, or cobalt-chromium alloys [164, 166, 172, 174].

In addition to biomedical applications, a number of other sliding configurations have validated the use of UHMWPE for its lubricious and wear resistant nature. Particularly, these include face seals and a number of different sliding bearings, in which contacts with lower mechanical stresses allow for the use of lighter wear resistant UHMWPE. Although they promise reductions in friction and wear rate, these materials still suffer from debris generation in periods of solid-solid contact [179-181]. In terms of the orthopedics, the same debris generation issues

are especially plaguing. While combinations using UHMWPE have generally been found to produce the least amount of wear, their estimated wear rates of 1×10^{10} particles per year still make it susceptible to osteolysis and reduced joint life [172, 173]. Although other issues such as bio-compatibility must be taken into account, this problem has led to an exploration for techniques which might enhance the UHMWPE surfaces in a way that makes them even more abrasion resistant.

For instance, in non-biomedical applications, surface texturing has been shown to promote low-wear, low-friction sliding contacts [182-189]. In these works, the textures are typically fabricated through a process known as laser surface texturing (LST), in which dimples are created by a concentrated laser pulse. While proving to reduce friction in dry and lubricated contacts, this technique has thus far been implemented primarily with seals and automotive piston rings [182, 183, 185-187]. The advantages of surface textures are considered to be: (i) micro-traps for collecting unwanted wear debris from the sliding contact [177, 187], (ii) lubricant reservoirs that enhance hydrodynamic pressure and facilitate the onset of full-film hydrodynamic lubrication [182-186], and (iii) solid lubricant reservoirs for *in situ* replenishment, which is less relevant, as of yet, to the current work [188, 189]. Although debris generation in current artificial hip joints prevents long-lasting, single-surgery replacement, this work proposes that surface texturing may provide a solution through its ability to control friction and wear.

In terms of hip joint materials, work already exists in which artificial roughness, created through a water jet erosive wear process, was shown to trap UHMWPE wear debris [177]. In addition, shallower dimples created through an indentation process were also tested with the goal of trapping UHMWPE debris using a more controlled texturing process. However their results were actually shown to increase wear [171], which may have been due to insufficient dimple depth during the indentation process. Deeper, cylindrical dimples, created through electric discharge etching, were shown to have more favorable effects on hip joint simulators due to the assumed trapping of debris [169]. While these approaches may be useful to mitigate the problems of existing wear debris, including its self-exacerbating effects, a more complete approach would involve ensuring that one utilizes the pressure enhancing effects of textures as well. Although trapping can limit the adverse effects of wear debris already in the interface, the hydrodynamic pressure enhancing effects of controlled spherical dimples may help to attenuate the source of debris generation.

At low speeds, under the high loads present in the human hip, it is very difficult to generate sufficient hydrodynamic pressure to fully separate sliding surfaces. As such, the sliding contact exists likely in the regimes of boundary and mixed lubrication, both of which traditionally exhibit higher wear rates. However, in the presence of a textured surface, flow phenomena in the textures can lead to an increase in the average fluid pressure, and thus, result in an enhancement of the hydrodynamic load carrying capacity [183, 184, 190]. This is thought to occur due to the combination of four different effects, which were first proposed regarding how surface asperities or irregularities could effectively lead to load carrying capacity, without a nominally converging gap [191, 192]. The *first* is micro-cavitation in the diverging section, or inlet of the texture, which leads to the generation of a sub-ambient pressure region. In the proceeding converging section, the decreasing film thickness leads to a larger increase in fluid pressure, resulting in a net positive load carrying capacity [182, 185, 190, 192]. The *second* is due to piezo-viscous effects [190], in which fluid viscosity in the converging sections will drastically increase due to higher fluids pressures leading to an even greater load carrying capacity. This particular advantage may be less important to the hip joint, due to the shear thinning nature of synovial fluid, as well as the relatively low speeds. The *third* is due to micro-squeeze, occurring where fluid is trapped in the dimples during solid-solid contact, and pressurized without a place to escape [190]. This effect is tied to the ability of the texture to act as a micro-reservoir and may be particularly useful in the hip joint where periods of boundary lubrication would normally persist. And the *fourth* is convective inertia, where eddy formation and recirculation occurs in the texture which leads to a subsequent pressure build up [190, 193, 194].

In the case of an artificial hip joint, where relative velocities and viscosities are quite low, these effects could greatly enhance the fluid's load carrying capacity, thereby reducing detrimental surface/surface contact. The goal of this type of texturing for the hip joint is best summarized by Figure 1, which makes use of the classic Stribeck Curve to show how friction varies as a contact traverses the different lubrication regimes. With the use of texturing, the desire is to essentially shift the Stribeck curve to the left, such that the minimum friction effects at the onset of full-film lubrication are experienced at lower sliding speeds. It should be noted here for simplicity, that we have not considered the Elasto-hydrodynamic Lubrication regime (EHL). In Summary, this work will seek to take a more deterministic approach for creating precisely controlled, spherical surface textures on hip joint materials. The goal is to explore the

merits of pressure enhancing texture effects, which may optimize the lubrication regime under realistic loading conditions that typify human walking.

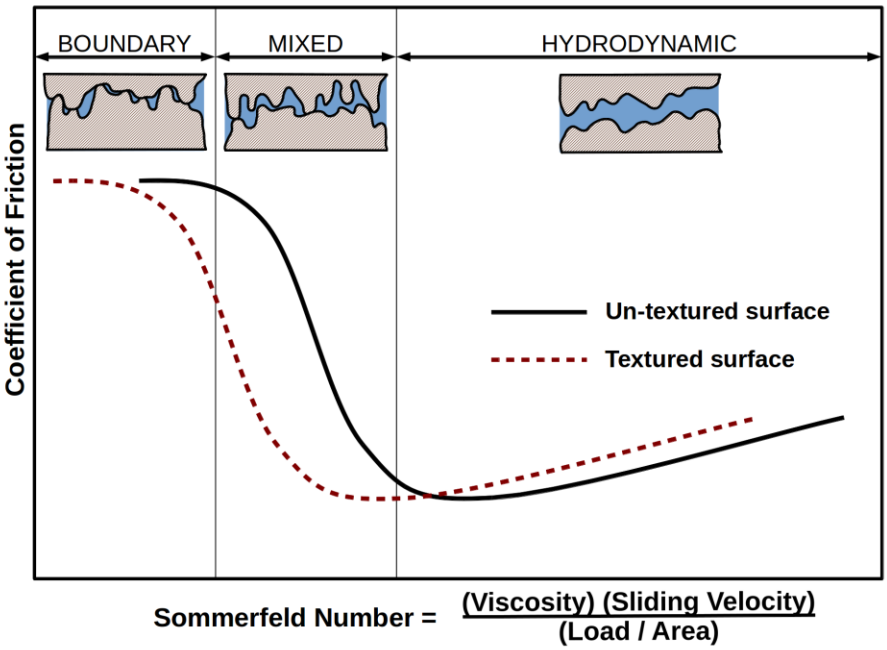

Figure 1: The Stribeck curve detailing different lubrication regimes

2. Experimental

As opposed to traditional LST or water-jet erosion, the surface textures for this study were created through a technique known as micro-machining, using a high precision five-axis micro-machining tool [195, 196]. This technique was chosen not only for its low-cost, but also for its precision and control over the dimensions and shapes of the textures, without the need for extensive calibration to the given material or the risk of heat affected zones associated with LST [192, 193, 195-199]. For this work, recessed hemispherical textures were created using different size ball-end micro-endmills at varying penetration depths to arrive at desired aspect ratios (dimple depth/dimple width). As a first approach, the aspect ratios were maintained on average at 0.1, which was found to exist in an optimal range in prior texturing for pistons and seals [184, 185]. As a result, each dimple will be quite shallow compared to its width. The texture dimensions of each tested sample are listed in Table 1, while scanning electron microscope (SEM) images may be found in Fig. 2. A constant texture per area value was maintained at 4 textures per mm^2 which corresponds to a distance between texture centers of 0.5mm.

Table 1: Textured and un-textured UHMWPE samples for testing

Sample	Approximate Texture Depth (µm)	Approximate Texture Width (µm)	Percentage of Total Area Textured
Un-Textured	N/A	N/A	N/A
Textured: Sample 1	10	100	3.1
Textured: Sample 2	20	200	12.6
Textured: Sample 3	40	400	50.2

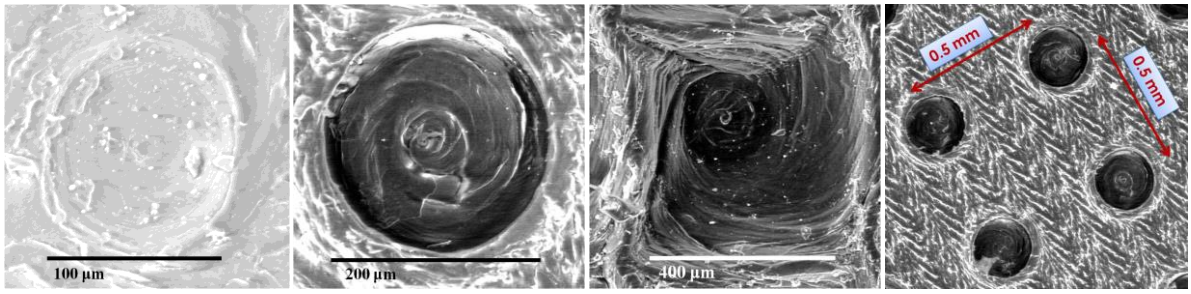

(a) (b) (c) (d)

Figure 2: Scanning electron microscopy results for analyzing the width of each texture: (a) Sample 1, (b) Sample 2, (c) Sample 3, and (d) general texture arrangement.

A Bruker UMT-3 tribometer was used to assess the tribological performance of each sample. It should be noted that using pin-on-disk tribometer configurations to investigate orthopedically relevant friction reducing techniques such as coatings and materials is not new. In fact, tribometer studies have been shown to be useful in validating the performance of new techniques which may be cost prohibitive on full scale simulators [170, 172, 200, 201], while also providing an avenue for studying phenomena such as wear rate, friction coefficient, and lubrication mechanism that may be difficult to capture on full-scale simulators [140, 166, 178, 202, 203].

The tested materials included disk specimens, which were made out of textured and un-textured UHMWPE, and pin specimens made of stainless steel. It is worth mentioning that in the future, texturing of the femoral head component, which is the harder material in the tribosystem,

would be more advantageous. This would be for two reasons: the femoral component is much less likely to deform or wear, resulting in texture shapes which may be assumed to remain unaltered for much longer during joint life. And secondly, it would be advantageous because wear trapping would be more likely to occur on the surface which is oriented to the ground more frequently while walking. In this case, the UHMWPE disk was chosen as the texturing surface solely for low-cost production. The stainless steel pins were spherical with a diameter of 3.172 mm (0.125 in), and a roughness on average of 0.135 um as measured by an optical interferometer. The hardness of the pins was rated by McMasterCarr to be the order of 3 GPa.

In order to best capture the ability of textures to enhance the lubrication regime, tests were conducted in which the speed was ramped up at discrete intervals. These speeds were varied between 5-70 mm/s to simulate typical conditions in the artificial hip [165, 167, 177], while the loads were kept constant for a given test. Each interval was held for 1.5 minutes and an average friction coefficient was calculated for the current speed, so that a Stribeck curve could be plotted for each test.

The lubricant for all tests was water, which is known to have similar viscosity to the natural synovial fluid present in human joints [164, 165, 167, 174, 196]. It should be noted that the naturally occurring lubricants, though shear thinning, may exhibit higher viscosities at the low speeds and loads in which texturing would be most beneficial. This would only improve the lubricating effects which are known improve with more viscous lubricants [184]. The other potential difference in the behavior of organic lubricants would be the effect of proteins, potentially altering texturing effects in the contact. However it has been proposed that under hip joint loading conditions, much of the shear thinning behavior of synovial fluid may actually arise from proteins being *prohibited* from entering the contact zone [202]. As a result, the potential for proteins to hinder texturing performance would be drastically reduced. While future study of the effects of organic lubricants on surface texturing must be conducted, this provided added justification for the use of water in this validation study. The interface was kept flooded through the use of the UMT's lubricant recirculation system to ensure sufficient lubricant supply. This should not be confused with a case in which the contact does not experience boundary lubrication, which will occur when speeds are not sufficient to generate load carrying capacity and the lubricant is forced out of the contact region. During these types of contact conditions, local starvation similar to those experienced in the human hip can still occur.

The loads were kept constant during a test, but were varied between 4 and 10N between tests in a separate parametric study. From a Hertzian contact analysis for steel on UHMWPE, the contact stress was found to be 44.36 MPa and 60.1 MPa for 4 and 10N respectively. In other words, the contact stress will be slightly higher than those measured in the hip [167]. This means that in terms of load alone, any lubrication enhancement witnessed in this study, should actually be more effective at the lower stresses experienced in the actual hip joint. It is important to note that the motions in the actual hip joint will be reciprocating rather than unidirectional, which will be important to take into account in later studies. However, to examine the potential effectiveness of textures in terms of rapid transitions from boundary to mixed lubrication, unidirectional motion at relevant loading conditions was utilized as a first approach. This allows for more qualitative analysis and characterization of lubrication regimes in terms of Stribeck behavior.

3. Results & Discussion

Figure 2 displays SEM images of the textures for each sample. It should be noted that there are interesting, swirled features around the edge of the dimple, which were generated due to the high speeds of the cutting tool leading to plastic flow in the soft, low melting point UHMWPE. These effects were most pronounced for the deepest textures seen in sample 3. These features could be removed through post-machining processes, although in this study, they did not appear to adversely affect the results.

Varying texture dimensions. To compare the different texture dimensions, and their effect versus an un-textured substrate, a parametric study was conducted at 10N normal load with water as the lubricating fluid. The average coefficient of friction (COF) at each speed interval, for each substrate, is plotted in order to examine the Stribeck behavior of each texture. In Fig. 3, these results are shown with regard to Sommerfeld Number for one textured case, in which the area used was the Hertzian contact area of the spherical pin against a flat UHMWPE surface. For discussion purposes, however, it can be more useful to plot these with respect to velocity, which was the varied parameter during the current set of tests. This plot allows for the more intuitive discussion of lubrication transition points, and is presented in Fig. 4.

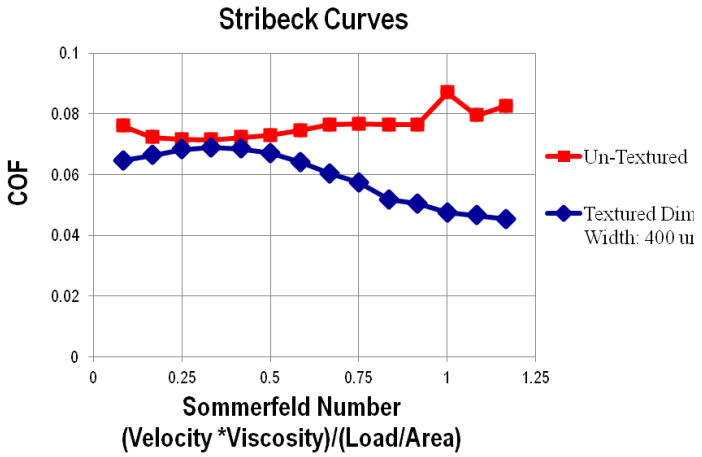

Figure 3: Stribeck curves for un-textured and textured UHMWPE

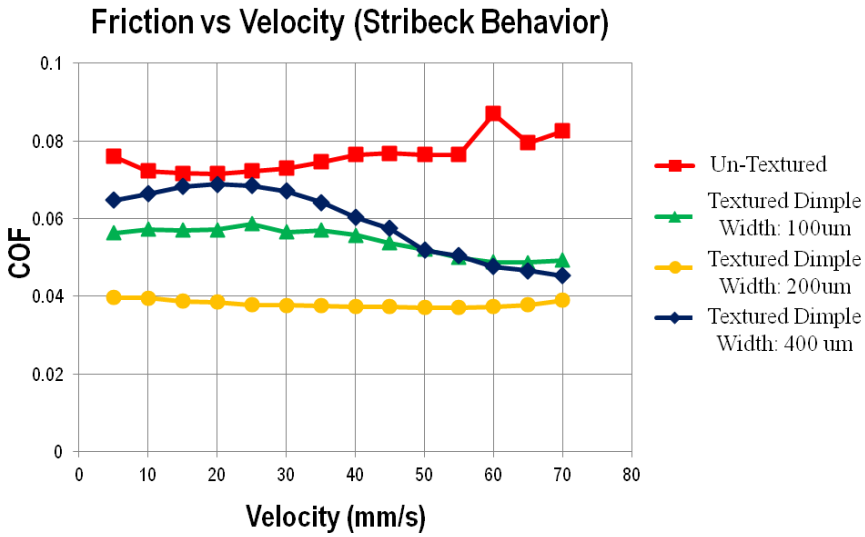

Figure 4: Parametric study for different textures dimple widths compared to an un-textured substrate at 10N load.

As Fig. 4 shows, the textured UHWMPE outperformed the un-textured sample at all speeds. However, it is the shape of the curves which allows for some interesting analysis. For the un-textured case, it is assumed that the contact exists only in the boundary lubrication regime even at the highest speeds, indicated by higher COF and a lack of any decrease with increasing speed. Although the trend is slightly increasing with increasing speed, it can be assumed from the low starting speed of 5 mm/s that the contact was not experiencing the lubricant shearing effects characteristic of the full-film lubrication regime. It has also been shown that for a roughness

larger than 0.1 μm, much smoother than the tested surface, the COF will display a small increase with increasing speed for dry UHMWPE on stainless steel [204]. While some surface films will exist in the current boundary regime, it is plausible that a similar effect is occurring since the load is borne exclusively by solid-solid contact. It would follow that this slightly increasing trend would occur until a lubricant film was able to reduce the effects of solid-solid contact, transitioning the operational mode into the mixed lubrication regime.

For example, this phenomena can be witnessed in the textured cases. For the widest dimple of 400 μm, one can observe that the friction begins with a similar increasing trend, almost touching the un-textured curve at a speed of 20 mm/s and a COF of about 0.076. In the case of primarily solid-solid contact, where the interface has yet to utilize the lubrication enhancing effects of the texture, it makes sense that the COF would be quite similar to un-textured UHMWPE on stainless steel. However, a clear transition to mixed lubrication was discovered at 20 m/s, eventually decreasing to a final COF just above 0.04. This marked decrease, which begins to level out at higher speeds, suggests that the texture effectively transitions the interface's operational mode from the boundary lubrication regime to the mixed lubrication regime *at a lower speed*. For the smallest dimple width of 100 μm, one can observe the transition around 20 mm/s once again, down towards a similar minimum COF value near 0.04. However this trend is appreciably more level, which suggests a secondary effect occurring in the boundary lubrication regime that will be discussed below. From Fig. 4, it was found that a dimple width of 200 μm, which is in the middle of the first two, provided the lowest and most level COF. For this dimple width, the COF begins and remains almost constant at the low value of 0.04, even at the low speeds of 5mm/s. This trend was almost completely level.

To discuss these effects, it is interesting to note that for all the tests at 10N, the different samples would provide COF values between 0.08 and 0.04. This suggests that an increasing COF between 0.075 and 0.08 may indicate boundary lubrication. And that a stable COF below 0.04, may represent minimum COF behavior such as the onset of hydrodynamic lubrication shown in Fig. 1. A decreasing COF between these values should then indicate the mixed lubrication regime. At first, the effect of the textures can be summarized quite simply in that it would allow the contact to achieve more beneficial lubrication regimes at lower velocities. This is due to the mechanisms such as convective inertia and micro-cavitation discussed previously which reduce the solid-solid contact due to added pressure build up. The largest texture of 400 μm exhibits the

most classic Stribeck behavior and evidence of this first effect, where the full transition from a boundary COF of 0.08, to almost the minimum value of 0.04, can be witnessed within the range of analyzed velocities.

However there is also a second effect present for the 100 and 200 μm textures, of leveling out the COF behavior and potentially extending the low-friction regimes. In other words, the range of operational velocities in the low-friction regimes appears to be dependent on the texturing dimensions, with optimal dimensions providing lower friction even where other textures are still existing in the boundary lubrication regime. The 100 μm texture still declines at a similar velocity, but the curve is much more level. One could visualize this as a case where the Stribeck curve was stretched or leveled out, and the 100 μm texture may still experience slightly increasing COF (boundary regime) further to the left if even lower velocities were tested. However in Fig. 4, what is observed for the 100 μm texture is a transition through mixed lubrication that is extended and less affected by a small change in velocity.

For the 200 μm texture this effect is even more exaggerated, suggesting that a change in velocity is having very little effect on the lubrication regime for this speed range. It should be noted that there does appear to be short declivity around 20 mm/s, and brief acclivity around 60 mm/s. What may be happening in this case, is that the curve is traversing the minimum friction zone on the Stribeck curve associated with the transition between mixed and hydrodynamic lubrication behavior. Initially, a slight decrease can be observed where a small amount of solid-solid contact (mixed lubrication) may be present between 5 and 30 mm/s. Then a stable and low COF is witnessed until 60 mm/s, where a very slight increase indicative of the true onset for full-film lubrication is displayed. Thus, it appears that the onset of the hydrodynamic lubrication regime, often experienced as a quick transition, has been extended. It would follow that at much lower speeds, the typical Stribeck behavior would still prevail and a rise to the boundary COF between 0.075 and 0.08, while at higher speeds more of the lubricant shearing effects would be experienced. Although not described in this qualitative manner, this leveling effect for textured surfaces has been witnessed before, in which a textured surface may result in lubrication phenomenon with a greatly diminished velocity dependence [184, 187].

Despite these studies, the reasoning for this effect was not discussed beyond the fact that the dimples allowed for enhanced lubrication regimes at lower sliding velocities. While the question of a mechanism for this leveling effect remains, it provides the texturing designer with an

interesting insight. Fig. 4 suggests that with *less* optimal textures, a more classic Stribeck behavior will prevail in which both low velocities and high velocities may lead to the adverse lubrication effects present in boundary and full-film lubrication. However as you approach the optimal texturing dimension, a more level Stribeck Curve will form, in which beneficial lubrication regimes are promoted for the largest range of speeds. This allows for a target behavior when designing surface textures, as well as a way to test their performance.

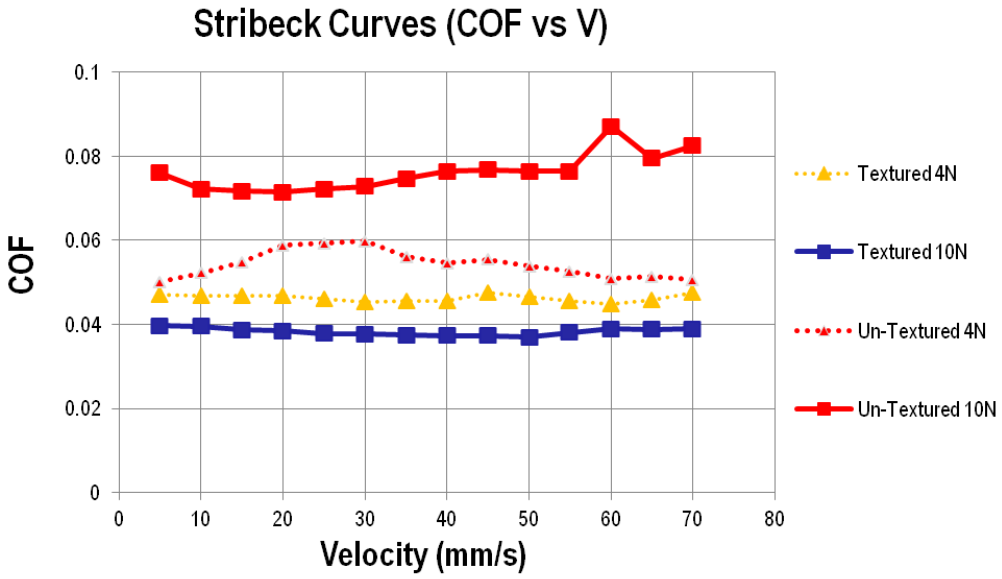

Figure 5: Comparison between the 200 µm textured vs. un-textured samples at 10N and 4N

Varying loads. To further investigate these leveling effects, a lower load of 4N was also tested for the current optimum texture and the un-textured case. These results are presented in Fig. 5 for a texture of 200 µm width compared to un-textured disk at 4 and 10N. The textured sample continued to outperform the un-textured sample while promoting a leveled Stribeck curve. However at low loads the early transition effect was not as pronounced. This is quite intuitive because at lower loads, and therefore lower Sommerfeld number, the un-textured case may already be moving into the mixed lubrication regime and therefore exhibiting lower COF behavior. This is clearly demonstrated in the 4N un-textured curve, in which COF begins with the same slightly increasing boundary lubrication behavior, followed by a decrease in COF with increasing speed indicating the transition into mixed lubrication. For the textured case, the curve still appears to exhibit the optimal leveling effect, in which it exists at a minimum COF value for the entire speed range but the overall reduction in friction was less drastic.

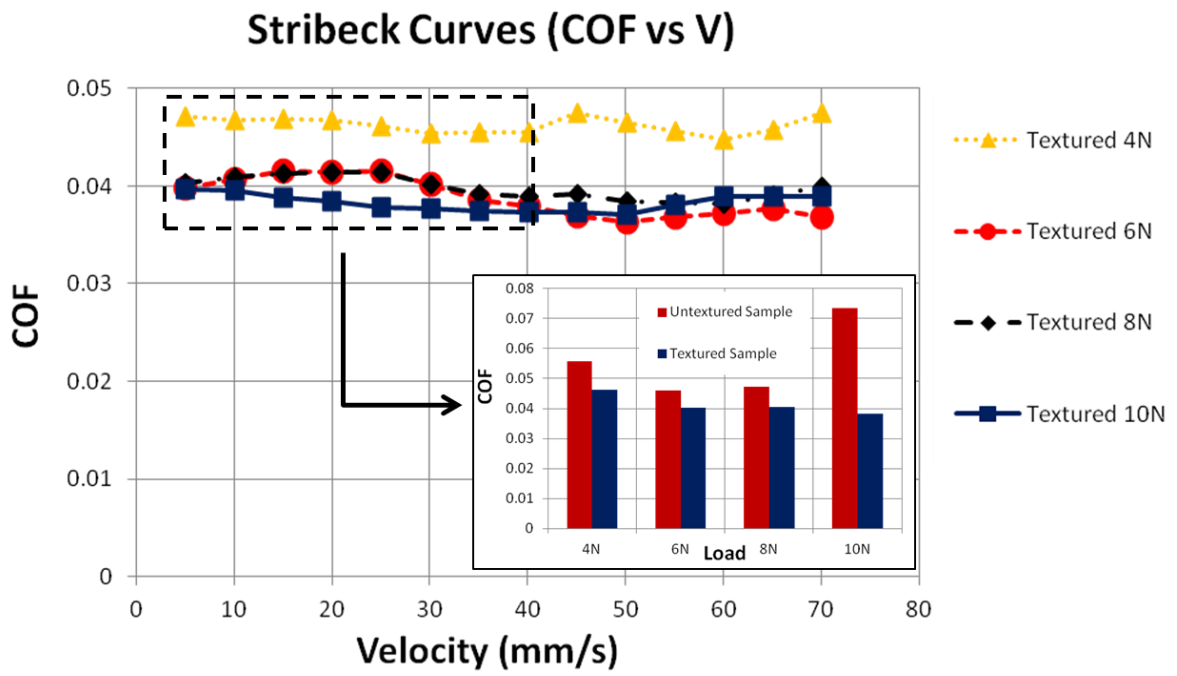

Figure 6: Parametric study for increasing load on 200 µm textured sample performance

A parametric study was also conducted, in which loads of 4, 6, 8, and 10 N were tested to further examine the effect of load on the performance of the 200µm texture. This was previously found to exhibit a level Stribeck curve indicative of a possible optimal texturing dimension for these loading conditions. Figure 6 displays these results and it was observed that each load continued to yield a more level curve. In addition, an inset to the figure was added where the average COF for the lower speed range of 5-40 mm/s is displayed for both the 200 µm dimple and the un-textured sample. At these lower speeds, it was found that the higher loads actually exhibited a lower friction coefficient. This speed range can be especially important since it represents a large portion of the low sliding speeds present in the hip joint. In addition to outperforming the textured case, it can be observed that an increase in load led to lower COF.

By considering this load relationship with regard to the third mechanism for textured pressure enhancement, micro-squeeze; one can potentially elucidate the mechanism for the leveling effect. During micro-squeeze, lubricant can be trapped and pressurized in the dimples through deformation of the contact, leading to squeeze film lubrication and low COF. These effects would be most prominent when solid-solid contact provides the greatest chance to trap lubricant in the dimple, and it would follow that this would be most probable during the

boundary lubrication regimes present for low speed sliding. Therefore the low speed behaviors for the 200 μm texture, may suggest that micro-squeeze is promoting low COF where micro-cavitation and convective inertia are still insufficient to promote mixed lubrication.

Furthermore, one would expect this effect to be even more pronounced as one increases the load. This is because at the higher loads, there would be greater deformation in the contact zone, which would allow for the lubricant to be trapped and pressurized inside the dimples more effectively. This may explain why the low speed texturing effects in Fig. 6, produce lower friction at higher loads for the same 200 μm texture.

While the more hydrodynamic effects of textures, such as micro-cavitation and convective inertia, help to shift the regime to mixed lubrication at lower speed ranges, these arguments for micro-squeeze phenomena may explain the leveling of Stribeck behavior in the boundary regime. This leveling effect is important because it allows for a way to discern between a given texturing dimension, and one that is more optimal. For instance, this effect is most pronounced at an intermediate dimension of 200 μm, between the 100 μm and 400 μm textures. Each textured sample experienced a similar transition to mixed lubrication around 20 m/s, but it was the 200 μm texture which exhibited the greatest leveling effect. Perhaps, this is due to the fact that the 400 μm textures may be too wide to capture the lubricant inside the dimples at these loads and subsequent contact deformations, leading to a more classic Stribeck shape. However, the 100 μm textures may be too small and shallow to trap sufficient lubricant for optimal squeeze film formation, leading to a slightly level shape. But the 200 μm texture appears to be just right, leading to an almost completely level shape.

4. Conclusion

UHMPWE is a tough, low-friction, self-lubricating polymer that is often abrasion-resistant. Since it is biocompatible, it is most commonly known for serving as softer of the two articulating surfaces in artificial hip and knee joints. In the artificial hip joint, surface wear and its resultant debris generation have led to a drastic reduction in clinical joint life. In order to combat this adverse effect, a micro-machined surface texturing technique was proposed, in which micro-dimples would be created on the UHMWPE surface to enhance lubricant pressure. If successful, this strategy would lower the friction and wear by effectively moving the lubrication regime away from the boundary regime towards the mixed and hydrodynamic lubrication regimes. Therefore, the tribological performance of textured UHMPWE disk samples was analyzed under

orthopedically relevant speeds and contact pressures, on a rotating tribometer. It should be noted that texturing the harder femoral component would be more effective in artificial joints, since there would be greater resistance against deformation and wear as the textures are preserved by conducting Stribeck tests on different textured samples, it was found that this technique was effective in reducing COF by altering the lubrication regime. Texture widths of 400 and 100 μm were shown to exhibit a decline in COF with increasing speed, indicative of the onset from boundary to mixed lubrication at lower speeds than the un-textured sample. As a result, a decrease in COF of about 50% was observed. A potential optimum texturing dimension was found between these two, at 200 μm, in which the interface seemed to exist almost exclusively in the low-friction onset of the hydrodynamic lubrication regime. With this dimension the COF persisted around the minimum value of about 0.04 for all of the tested speeds. It was proposed that the leveling effect, , in which the low friction lubrication regimes may be extended to larger speed ranges, was shown to increase with the current proximity to an optimal texturing dimension. It was also shown that the effectiveness of COF reduction for the optimal texture improved with increasing load, and proposed that these effects may be due to increased micro-squeeze. While further research remains to be conducted, this study provides justification for surface texturing to reduce friction, solid-solid contact, and potentially the generation of abrasive wear debris, under speeds and loads present in the artificial hip joint.

References

1. **Wornyoh, E.Y.A., V.K. Jasti, and C. Fred Higgs, *A Review of Dry Particulate Lubrication: Powder and Granular Materials.* Journal of Tribology, 2007. 129(2): p. 438.**
2. **Bares, J.A., et al., *In situ graphite lubrication of metallic sliding electrical contacts*. Wear, 2009. 267(9-10): p. 1462-1469.**
3. **Donnet, C., *Advanced solid lubricant coatings for high vacuum environments.* Surface and Coatings Technology, 1996. 80: p. 151-156.**
4. **Dougherty, P.S.M., C. Sunday, M., and C.F. Higgs III, *Adaptive solid lubricant transfer films for conductivity and oxidation control*, in *ASME/STLE 2012 International Joint Tribology Conference*. 2012, Conference Proceedings: Denver, CO.**
5. **Gamulya, G.D., et al., *Effect of low temperatures on the wear mechanism of solid lubricant coatings in vacuum.* Wear, 1993. 160: p. 351-359.**
6. **Lund, C.J., C. Persad, and Z. Eliezer, *Solid lubricant coatings using electromagmetic railgun acceleration.* Wear, 1987. 119: p. 251-255.**
7. **Voevvodin, A.A. and J.S. Zabinski, *Laser surface texturing for adaptive solid lubrication.* Wear, 2006. 261: p. 1285-1292.**
8. **Winer, W.O., *Molybdenum disulfide as a lubricant: a review of the fundamental knowledge.* Wear, 1967. 10: p. 422-452.**

9. Holinski, R. and J. Gansheimer, *A study of the lubricating mechanism of molybdenum disulfide.* Wear, 1971. 19: p. 329-342.
10. Pudjoprawoto, R., P.S.M. Dougherty, and C.F. Higgs III, *A Volumetric Fractional Coverage Model to Predict the Fricitonal Behavior for in situ Transfer Film Lubrication.* Wear, 2013. 304(1): p. 173-182.
11. Lancaster, J.K., *Lubrication by Transferred Films of Solid Lubrication.* ASLE Transaction, 1965. 8: p. 146-155.
12. Lancaster, J.K., *Anisotropy in the Mechanical Properties of Lamellar Solids and its Effect on Wear and Transfer.* Wear, 1966. 9: p. 169-188.
13. Haltner, A.J., *An Evalution of the role of Vapor Lubrication Mechanisms in MoS2.* Wear, 1964. 7: p. 102-117.
14. Mivoshi, K., *Solid Lubricants and Coatings for Extreme Environments: State-of-the-Art Survey.* NASA/TM 2007. 214668.
15. Hilton, M.R. and P.D. Fleischauer, *Applications of solid lubricant films in spacecraft.* Surface and Coatings Technology, 1992. 54/55: p. 435-441.
16. DellaCorte, C., et al., *The effect of composition on the surface finish of PS400: a new high temperature solid lubricant coating.* NASA TM, 2010. TM-2010-216774.
17. Persad, C., *Railgun tribology - chemical reactions between contacts.* IEEE Transactions on Magnetics, 2007. 43(1): p. 391-395.
18. Dougherty, P.S.M., R. Pudjoprawoto, and C.F. Higgs, *An investigation of the wear mechanism leading to self-replenishing transfer films.* Wear, 2011. 272(1): p. 122-132.
19. Higgs III, C.F. and E.Y.A. Wornyoh, *An In Situ Mechanism for Seld-Replenishing Powder Transfer Films: Experiments and Modeling.* Wear, 2008. 264(1): p. 131-138.
20. Dougherty, P.S.M., et al., *Shear-induced Particle Size Segregation in Composite Powder Transfer Films.* Powder Technology, 2014. 264: p. 133-139.
21. Bahadur, S., D. Gong, and J.W. Anderegg, *The role of copper compounds as fillers in transfer film formation and wear of nylon.* Wear, 1992. 154: p. 207-223.
22. Prasad, S.V., N.T. McDevitt, and J.S. Zabinski, *Tribology of tungsten disulfide-nanocrystalline zinc oxide adaptive lubricant films from ambient to 500 C* Wear, 2000. 237: p. 186-196.
23. Fowell, R.J., *The Mechanics of Rock Cutting.* Comprehensive Rock Engineering, 2013. 4: p. 155-176.
24. Durrand, C.J., et al., *Super-hard, thick, shaped PDC Cutters for Hard Rock Drilling: Development and Test Results*, in *Thirty-Fifth Workshop on Geothermal Reservoir Engineering*. 2010: Standfor University, Standford, California.
25. Dougherty, P.S.M., R. Pudjoprawoto, and C.F. Higgs III, *On the Role of Bit Cutter-on-Rock Tribometry to Aid the Drilling Process for New Energy Resources.* Proceedings of: ASME/STLE International Joint Tribology Conference 2011, 2011.
26. Trezona, R.I. and D.N. Allsopp, *Transitions between two-body and three-body Abrasive Wear: Influence of Test Conditions in the Microscale Abrasive Wear Test.* Wear, 1999. 229(1): p. 205-214.
27. Lasa, I. and J.M. Rodriguez-Ibabe, *Effect of Composition and Processing Route on the Wear Behaviour of Al-Si Alloys.* Scripta Materialia, 2002. 46(6): p. 477-481.
28. Rabinowicz, E., *Friction and Wear of Materials.* 1965.
29. Jones, M.H. and D. Scott, *Industrial Tribology*. 1983, Amsterdam: Elseivier Scientific Publishing Co.
30. Dougherty, P.S.M., D. Stonestrom, and C.F. Higgs III, *Modeling of Preferential Patterns found during the Abrasive Wear of Random Surfaces.* Proceedings of: STLE Annual Meeting an Exhibition. St. Louis, MO, May 2012, 2012.

31. Archard, J.F., *The Wear of Metals under Unlubricated Conditions.* Proceedings of the Royal Society of London: Biological Sciences 1956(397).
32. Challen, J.M. and P.L.B. Oxley, *An Explanation of the Different Regimes of Friction and Wear Using Asperity Deformation Models.* Wear, 1979. 53: p. 229-243.
33. Hokkirigawa, K. and K. Kato, *An Experimental and Theoretical Investigation of Ploughing, Cutting, and Wedge Formation during Abrasive Wear.* Tribology International, 1988.
34. Marinack Jr., M.C., P.S.M. Dougherty, and C.F. Higgs III, *Experimental Investigations on the Coefficient of Friction and Wear of Single Granules.* Tribology and Lubrication Technology, 2012. 68(10): p. 28.
35. Dearnaley, G., *Adhesive and Abrasive Wear Mechanism in Ion Implanted Metals.* Nuclear Inst. and Method in Physics Research, 1985: p. 158-165.
36. Quintanilla, M.A.S. and D.T. Goddard, *Lateral Force Microscopy with Micrometer-Sized Particles: Effect of Wear on Adhesion and Friction.* Wear, 2010. 268: p. 277-286.
37. Kayaba, T., K. Hokkirigawa, and K. Kato, *Analysis of Abrasive Wear Mechanisms by Successive Observations of Wear Processes in a Scanning Electron Microscope.* Wear, 1986. 110: p. 419-430.
38. Terrell, E.J. and C.F. Higgs III, *A Particle Agumented Mixed Lubrication Modeling Approach to Predicting Chemical Mechanical Polishing.* Journal of Tribology, 2009. 131(1).
39. Srivastava, G. and C.F. Higgs III, *A Full Wafer-Scale PAML Modeling Approach for Predicting CMP.* Tribology Letters, 2015. 59(2): p. 1-11.
40. Mpagazehe, J. and C.F. Higgs III, *A Comparison of Active Particle Models for Chemical Mechanical Polishing.* ECS Journal of Solid State Science and Technology, 2013. 2(3): p. 87-96.
41. Zhao, Y., D.M. Maietta, and L. Chang, *An Asperity Microcontact Model Incorporating the Transition from Elastic Deformation to Fully Plastic Flow.* Journal of Tribology 2000. 122.
42. Masen, M.A. and M.B. Rooij, *Abrasive Wear Between Rough Surfaces in Deep Drawing.* Wear, 2004.
43. Masen, M.A., M.B. Rooij, and D.J. Shipper, *Micro-Contact Based Modeling of Abrasive Wear.* Wear, 2005. 2005: p. 339-348.
44. Dickrell, D. and W.G. Sawyer, *The Electrical Contact Resistance of two Rough Surfaces with Varying Phase Conductivity.* Proceedings of Electrical Contacts 2008, 2008.
45. Dickrell, D., et al., *Direct Contact-Area Computation for MEMS using Real Topographic Surface Data.* Journal of Microelectromechanical Systems 2007. 16(5): p. 1263-1268.
46. Frazier, W.E., *Metal Additive Manufacturing: A Review.* Journal of Materials Engineering and Performance, 2014. 23(6): p. 1917-1928.
47. Bertrand, P., et al., *Ceramic Components Manufacturing by Selective Laser Sintering.* Applied Surface Science, 2007. 254(4): p. 989-992.
48. Gu, D.D., et al., *Laser Additive Manufacturing of Metallic Components: Materials, Processes, and Mechanisms.* Intrernational Materials Reviews, 2012. 57(3): p. 133-164.
49. Gibson, I., D.W. Rosen, and B. Stucker, *Additive Manufacturing Technologies*. 2010, New York: Springer.
50. Lee, S.J., E. Sachs, and M. Cima, *Layer Position Accuracy in Powder-Based Rapid Prototyping. .* Rapid Prototyping Journal, 1995. 1(4): p. 24-37.
51. Van der Schueren, B. and J.P. Kruth, *Powder Deposition in Selective Metal Powder Sintering.* Rapid Prototyping Journal, 1995. 1(3): p. 23-31.
52. Tang, H.P., et al., *Effect of Powder Reuse Times on Additive Manufacturing of Ti-6Al-4V by Selective Electron Beam Melting.* JOM, 2015. 67(3): p. 555-563.
53. Khosropour, R., et al., *Convection and Size Segregation in a Couette Flow of Granular Material.* Physical Review E, 1997. 56(4): p. 4467-4473.

54. Feinstein, D. and M. Van Hecke, *Wide Shear Zones in Granular Bulk Flow.* Nature, 2003. 424: p. 256.
55. Hui, K., et al., *Boundary Conditions for High Shear Grain Flows.* Journal of Fluid Mechanics, 1984. 145: p. 223-233.
56. Marinack Jr., M.C., et al., *Couette grain flow experiments: The effects of the coefficient of restitution, global solid fraction, and materials.* Powder Technology, 2011. 211(1): p. 144-155.
57. Dougherty, P.S., R. Pudjoprawoto, and C.F. Higgs III, *An Investigation of the Wear Mechanisms Leading to Self-replenishing Transfer Films.* Wear, 2011. 272(1): p. 122-132.
58. Dougherty, P.S., et al., *Shear-Induced Particle Size Segregation in Composite Powder Transfer Films.* Powder Technology, 2014. 264: p. 133-139.
59. Freeman, T., R. Freeman, and B. Armstrong, *The Characterisation of Powders and Bulk Materials – a Multivariate Approach Using Dynamic, Shear and Bulk Property Measurements*, in *BulkSolids India*. 2011: India.
60. Rietema, K., *The Dynamics of Fine Powders*. 1991: Elsevier Science Publisher. 5.
61. Qian, M. and F.H. Froes, *Titanium Powder Mettalurgy: Science, Technology, and Applications*. . 2015: Butterworth-Henemann.
62. Fu, X., et al., *Effect of Particle Shape and Size on Flow Properties of Lactose Powders.* Particuology, 2012. 10(2): p. 203-208.
63. Lanzetta, M. and E. Sachs, *Improved Surface Finish in 3D Printing using Bimodal Powder Distribution.* Rapid Prototyping Journal, 2003. 9(3): p. 157-166.
64. Neikov, O.D., et al., *Handbook of Non-Ferrous Metal Powders: Technologies and Applications*. 2009: Elsevier.
65. Entezarian, M., et al., *Plasma Atomization: A New Process for the Production of Fine, Spherical Powders.* JOM, 1996. 48(6): p. 53-55.
66. McCarthy, J., et al., *Quantitative validation of the discrete element method using an annular shear cell.* Powder Technology, 2010. 203(1): p. 70-77.
67. Tardos, G., S. Mcnamara, and I. Talu, *Slow and Intermediate Flow of a Frictional Bulk Powder in the Couette Geometry.* Powder Technology, 2003. 131(1): p. 23-39.
68. Freeman, R., *Measuring the Flow Properties of Consolidated, Conditioned, and Aerated Powders: A Comparitive Study using a Powder Rheometer and a Rotational Shear Cell.* Powder Technology, 2007. 174(1): p. 25-33.
69. Gildenhaar, R., et al., *Calcium Alkaline Phosphate Scaffolds for Bone Regeneration.* Key Engineering Materials, 2012. 493: p. 849-854.
70. Cooke, A. and J. Slotwinski, *Properties of Metal Powders for Additive Manufacturing: A Review of the State of the Art of Metal Powder Property Testing*. 2012: US Department of Commerce, National Institute of Standards and Technology.
71. Dawes, J., R. Bowerman, and R. Trepleton, *Introduction to the Additive Manufacturing Powder Mettalurgy Supply Chain.* Johnson Matthey Technology Review, 2015. 59(3): p. 243-256.
72. Strondl, A., et al., *Characterization and Control of Powder Properties for Additive Manufacturing.* JOM, 2015. 67(3): p. 549-554.
73. Clayton, J., *Optimising Metal Powders for Additive Manufacturing.* Metal Powder Report, 2014. 69(5): p. 14-17.
74. Lyons, K., S. Honeygan, and T. Mroz, *NETL Extreme Drilling Laboratory Studies.* Journal of Energy Resources Technology, 2008. 130.
75. Augustine, C., et al., *A Comparison of Geothermal with Oil and Gas Well Drilling Costs.* Thirty-First Workshop on Geothermal Reservoir Engineering, 2006.
76. Nicholl, D., et al., *New Hybrid Bit Exceeds Expectations in Challenging Application in Tarim Field, China.* Proceedings of the International Petroleum Technology Conference, 2013.

77. Hameed, A. and A. Al-Rushaid, *Deep Wells Bit Optimization.* Proceedings of SPE/IADC Middle East Drilling Technology Conference, 1997.
78. Black, A.D., et al., *PDC Bit Performance for Rotary, Mud Motor, and Turbine Drilling Applications.* SPE Drilling Engineering, 1986.
79. Beste, U. and S. Jacobson, *A New View of Deterioration and Wear of WC/Co Cemented Carbide Rock Drill Buttons.* Wear, 2007.
80. Beste, U. and S. Jacobson, *Friction Between a Cemented Carbide Rock Drill Button and Different Rock Types.* Wear, 2002. 253.
81. Fear, M.J., *How to Imrpove Rate of Penetration in Feild Operations.* SPE Drilling and Completion, 1999.
82. Freeman, M.A., S. Shen, and Y. Zhang, *Single PDC Cutter Studies of Fluid Heat Transfer and Cutter Thermal Mortality in Drilling Fluid*, in *AADE National Technical Conference and Exhibition*. 2012: Houston, TX.
83. Mpagazehe, J.N., A.F. Queiruga, and C.F. Higgs III, *Towards an Understanding of the Drilling Process for Fossil Fuel Energy: a Continuum-discrete Appraoch.* Tribology International, 2012. 2012.
84. Scott., D.E., *Development of Roller Cone Bits with Active Shear Cutting Elements Improves Gage-holding Ability.* SPE Drilling and Completion, 1996.
85. Fear, M.J., N.C. Meany, and J.M. Evans, *An expert System for Drill Bit Selevtion.* Proceedings of SPE/IADC Drilling Conference 1994, 1994.
86. Gupta, A., S. Chattopadhyaya, and S. Hloch, *Critical Investigations of Wear Behavior of WC Drill Bit Buttons.* Rock Mechanics, 2011. 46: p. 169-177.
87. Pessier, R. and M. Damschen, *Hybrid Bits Offer Distinct Advantages in Selected Roller-Cone and PDC-Bit Applications.* SPE Drillig &Completion, 2011. 26(1): p. 96-103.
88. Chen, S.L., K. Blackwood, and E. Lamine, *Field Investigations of Stick-Slip Lateral and Whirl Vibrations on Roller-Cone Bit Performance.* SPE Drillig &Completion, 2002. 17(01): p. 15-20
89. Warren, T.M., *Factors Affecting Torque for a Roller Cone Bit.* Petroleum Technology, 1984. 36(09): p. 1-500.
90. Warren, T.M. and A. Sinor, *Drag-bit Performance Modeling.* SPE Drilling Engineering, 1989. 2-4.
91. Detournay, E., T. Richard, and M. Shepherd, *Drilling Response of Drag Bits: Theory and Experiment.* International Journal of Rock Mechanics and Mining Sciences, 2008. 45.
92. Appl, F.C., C. Wilson, and I. Lakshman, *Measurement of Forces, Temperatures, and Wear of PDC Cutters in Rock Cutting.* Wear, 1993.
93. Garner, N.E., *Cutting Action of a Single Diamond under Simulated Borehole Conditions.* Journal of Petroleum Technology, 1967. 19(7): p. 937-942.
94. Bertagnolli, K. and R. Vale, *Understanding and Controlling Residual Stresses in Thick Polycrystalline Diamond Cutters for Enhanced Durability.* Finer Points (USA), 2000. 12(1): p. 20.
95. Azar, M., et al., *Pointing Towards Improved PDC Bit Performance: Innovative Conical Shaped Polycrystalline Diamond Element Achieves Higher ROP and Total Footage.* American Association of Drilling Engineers 13-FTCE-06, 2013.
96. Burgess, T.M., *Measuring the Wear of Milled Tooth Bits Using MWD Torque and Weight-on-Bit*, in *Proceedings of SPE/IADC Drilling Conference, Society of Petroleum Engineers*. 1985.
97. Heshmat, H., *Rheology and Hydrodynamics of Dry Powder Lubrication.* Tribology Transactions, 1991. 34(3): p. 433-439.

98. Heshmat, H. and W. Shapiro, *High-temperature, Unbalanced, Dry Contact Face Seal, Intergacial Phenomenon, and Design Considerations.* Lubrication Engineering, 1989. 45(4): p. 235-242.
99. Godet, M., *The Third-body Approach: A Mechanical View of Wear.* Wear, 1984. 100(1): p. 437-452.
100. Heshmat, H., *Tribology of Interface Layers*. 2010: CRC Press.
101. Higgs III, C.F., C.A. Heshmat, and H. Heshmat, *Comparative Evaluation of MoS_2 and WS_2 as Powder Lubricants in High Speed, Multi-Pad Journal Bearings.* Journal of Tribology, 1999. 121(3): p. 625-630.
102. Higgs III, C.F. and E.Y.A. Wornyoh, *An In Situ Mechanism for Self-replenishing Powder Lubrication: Experiments and Modeling.* Wear, 2008. 264(1-2): p. 131.
103. Heshmat, H., *The Quasi-Hydrodynamic Mechanism of Powder Lubrication. Part II: Lubricant Film Pressure Profile.* Lubrication Engineering, 1992. 48(5): p. 373-383.
104. Heshmat, H., *The Quasi-Hydrodynamic Mechanism of Powder Lubrication. I. Lubricant Flow Visualization.* Lubrication Engineering, 1992. 48(2): p. 96-104.
105. Sharf, T.W., P.G. Kotula, and S.V. Prasad, *Friction and Wear Mechanisms in MoS2/Sb2O3/Au Nanocomposite Coatings.* Acta Materialia, 2010. 58(12): p. 4100-4109.
106. Zabinski, J.S., M.S. Donley, and N.T. McDevitt, *Mechanistic Study of the Synergism between Sb203 and MoS2 Lubricant Systems using Raman Spectroscopy.* Wear, 1992. 165: p. 103-108.
107. He, D.H. and R. Manory, *A Novel Electrical Contact Material with Improved Self-Lubrication for Railway Current Collectors.* Wear, 2001. 249(626-636).
108. Ottino, J.M. and D.V. Khakhar, *Mixing and Segregation of Granular Materials.* Annual Review of Fluid Mechanics, 2000. 32: p. 55-91.
109. Gray, J.M.N.T. and C. Ancey, *Segregation, recirculation and deposition of coarse particles near two-dimensional avalanche fronts.* Journal of Fluid Mechanics, 2009. 629: p. 387.
110. Arteaga, P. and U. Tuzun, *Flow of Binary Mixtures of Equal-Density Granules in Hoppers - Size Segregation, Flowing Density and Discharge Rates.* Chemical Engineering Science, 1990. 45(1): p. 205-223.
111. Ketterhagen, W., et al., *Granular segregation in discharging cylindrical hoppers: A discrete element and experimental study.* Chemical Engineering Science, 2007. 62(22): p. 6423-6439.
112. Samadani, A. and A. Kudrolli, *Angle of repose and segregation in cohesive granular matter.* Physical Review E, 2001. 64(5): p. 051301.
113. Samadani, A., A. Pradhan, and A. Kudrolli, *Size segregation of granular matter in silo discharges.* Physical Review E, 1999. 60(6): p. 7203-7209.
114. Conway, S.L., et al., *Granular flow and segregation in a four-bladed mixer.* Chemical Engineering Science, 2005. 60(24): p. 7091-7107.
115. Fan, Y. and K.M. Hill, *Phase Transitions in Shear-Induced Segregation of Granular Materials.* Physical Review Letters, 2011. 106(21): p. 218301.
116. Golick, L. and K. Daniels, *Mixing and segregation rates in sheared granular materials.* Physical Review E, 2009. 80(4): p. 042301.
117. May, L.B.H., et al., *Shear-driven size segregation of granular materials: Modeling and experiment.* Physical Review E, 2010. 81(5): p. 051301.
118. May, L.B.H., M. Shearer, and K.E. Daniels, *Scalar Conservation Laws with Nonconstant Coefficients with Application to Particle Size Segregation in Granular Flow.* Journal of Nonlinear Science, 2010. 20(6): p. 689-707.
119. Zabinski, J.S., et al., *Lubricious zinc oxide films: synthesis, characterization and tribological behavior.* Journal of Material Science, 1997. 32: p. 5313-5319.

120. Evans, R.D., *Wear of Bearings*, in *Encyclopedia of Tribology*, Q.J. Wang and Y.W. Chung, Editors. 2013, Springer Science and Business Media New York. p. 4061-4068.
121. DellaCorte, C., *The Effect of Indenter Ball Radius on the Static Load Capacity of the Superelastic 60NiTi for Rolling Element Bearings.* NASA TM, 2014. 216627.
122. Tandon, N. and A. Choudhury, *A Review of Vibration and Acoustic Measurement Methods for the Detection of Defects in Rolling Element Bearings.* Tribology International, 1999. 32(8): p. 469-480.
123. DellaCorte, C., *The Effect of Pre-Stressing on the Static Indentation Load Capacity of the Superelastic 60NiTi.* NASA TM, 2013. 216479.
124. McFadden, P.D. and J.D. Smith, *Vibration Monitoring of Rolling Element Bearings By the High-Frequency Resonance Technique-a Review.* Tribology International, 1984. 17(1): p. 3-10.
125. Nikolaou, N.G. and I.A. Antoniadis, *Demodulation of Vibration Signals Generated by Defects in Rolling Element Bearings Using Complex Shifted Morlet Wavelets.* Mechanical Systems and Signal Processing 2002. 16(4): p. 677-694.
126. Leveille, A.R. and J.J. Murphy, *Determination of the Influence of Static Loads on the Output Torque of Instrument Ball Bearings*, in *Proceedings of the Charles Stark Draper Lab. International Ball Bearings Symposium*. 973. p. 1-24.
127. Park, W., et al., *Microstructure, Fatigue Life, and Load Capacity of PM Tool Steel REX20 for Bearing Applications.* Lubrication Engineering, 1999. 55(6): p. 20-30.
128. Evans, R.D., et al., *Prevention of Smearing Damage in Cylindrical Rolling Element Bearings.* Tribology Transactions, 2013. 56: p. 703-716.
129. Oberle, T., *Hardness, Elastic Modulus, Wear of Metals.* SAE Technical Paper 520251, 1952.
130. Marinack Jr., M.C., R.E. Musgrave, and C.F. Higgs III, *Experimental Investigations on the Coefficient of Restitution of Single Particles.* Tribology Transactions, 2012. Accepted for Publication.
131. Nosonovsky, M., *Self-Organization at the Frictional Interface for Green Tribology.* Philosophical Transactions of the Royal Society, 2010.
132. Marinack Jr., M.C., et al., *Couette Grain Flow Experiments: The Effects of the Coefficient of Restitution, Global Solid Fraction, and Materials.* Powder Technology, 2011. 211(1): p. 144-155.
133. Higgs III, C.F., et al., *Tribology for Scientists and Engineers: Particle Tribology: Granular, Slurry, and Powder Tribosystems*. 2013, New York: Springer
134. Wang, L., et al., *Experimental Determination of the Parameter Effects on the Coefficient of Restitution of Differently Shaped Maize in Three Dimensions.* Powder Technology, 2015. 284: p. 187-194.
135. Tsui, T.Y. and G.M. Pharr, *Substrate Effects on Nano-indentation Mechanical Property Measurements of Soft Films on Hard Substrates.* Journal of Materials Research, 1999. 14(01): p. 292-301.
136. Johnson, K.L., *Contact Mechanics*. 1987: Cambridge University Press.
137. Lloyd, G., *Rock Bit with Diamond Reamer to Maintain Gage*. 1979: US Patent 4140189.
138. Scott., D.E. and M.R. Pessier, *Earth-Boring Bit Having Shear-cutting Heel Elements*. 1997: US Patent 5592995.
139. Menezes, P.L., M.R. Lovell, and J.S. Lin, *Finite Element Modeling of Discontinuous Chip Formation During Rock Cutting*. Proceedings of STLE/ASME International Joint Tribology Conference, 2009.
140. Fisher, J., et al., *The Effect of Sliding Velocity on The Friction and Wear of UHMWPE for use in Total Artificial Hip Joints.* Wear, 2003.
141. Godet, M., *The Third Body Approach: A Mechanical View of Wear.* Wear, 1984. 100.

142. Yu, C.M., K. Craig, and J. Tichy, *Granular Collision Lubrication.* Journal of Rheology, 1994. 38.
143. Toro, G.D., D.L. Goldsby, and T.E. Tullis, *Friction Falls Toward Zero in Quartz Rock as Slip Velocity Approaches Seismic Rates.* Nature, 2004. 427.
144. Kilgore, B.D., M.L. Blanpied, and J.H. Dieterich, *Velocity Dependent Friction of Granite over a Wide Range of Conditions.* Geophysical Research Letters, 1993. 20.
145. Appl, F.C., C. Wilson, and I. Lakshman, *Measurement of Forces, Temperature, and Wear of PDC Cutters in Rock Cutting.* Wear, 1993. 169(1): p. 9-24.
146. Dougherty, P.S.M., R. Pudjoprawoto, and C.F. Higgs III, *An Investigation of the Wear Mechanisms Leading to Self-repleishing Transfer Films.* Wear, 2011. 272(1): p. 122-132.
147. Dougherty, P.S.M., R. Pudjoprawoto, and C.F. Higgs III, *Bit Cutter-on-Rock Tribometry: Analyzing Friction and Rate-of-Penetration for Deep Well Drilling Substrates.* Tribology International, 2014. 77: p. 178-185.
148. Rafatian, N., et al., *Experimental Study of MSE of a Single PDC Cutter under Simulated Pressurized Conditions*, in *SPE/IADC Drilling Conference and Exhibition*. 2009: Amsterdam, The Netherlands.
149. Ren, X., H. Miao, and Z. Peng, *A Review of Cemented Carbides for Rock Drilling: An Old but still Tough Challenge in Geo-engineering.* International Journal of Refractory Metals and Hard Materials, 2013. 39(Special Issue): p. 61-77.
150. Hood, M. and H. Alehossein, *A Development in Rock Cutting Technology.* International Journal of Rock Mechanics and Mining Sciences, 2000. 37(1-2): p. 297-305.
151. Masuda, K., *Effects of Water on Rock Strength in a Brittle Regime.* Journal of Structural Geology, 2001. 23(11): p. 1653-1657.
152. Tullis, J. and R.A. Yund, *Hydrolytic Weakening of Experimentally deformed Westerly Granite and Hale Albite Rock.* Journal of Structural Geology, 1980. 2(4): p. 439-451.
153. Yigit, A.S. and A.P. Christoforou, *Stick-slip and Bit-Bounce Interaction in Oil-Well Drillstrings.* Journal of Energy Resources Technology, 2006. 128(4): p. 268-274.
154. Simpson, J.P., H.L. Dearing, and D.P. Salisbury, *Downhole Simulation Cell Shows Unexpected Effects of Shale Hydration on Borehole Wall.* SPE Drilling Engineering, 1989. 4(1): p. 24-30.
155. Griggs, D., *Hydrolytic Weakening of Quartz and other Silicates.* Geophysical Journal International, 1967. 14(1-4).
156. Baud, P., W. Zhu, and T.F. Wong, *Failure Mode and Weakening Effect of Water on Sandstone.* Journal of Geophysical Research: Solid Earth, 2000. 105: p. 16371-16389.
157. Dressen, D.S. and J.H. Cohen, *Investigation of the Feasibility of Deep Microborehole Drilling.* Proceedings of Energy Week Conference Houston, TX 1997, 1997.
158. Hoover, E.R. and J.N. Middleton, *Laboratory Evaluation of PDC Drill Bits under High-speed and High-wear Conditions.* Petroleum Technology, 1981. 33(12): p. 2-316.
159. Clark, D.A., *Comparison of Laboratory and Field Data for a PDC Bit.* Proceedings of SPE/IADC Drilling Conference 1985, 1985.
160. Caenn, R. and G.V. Chillingar, *Drilling Fluids: State of the Art.* Journal of Petroleum Science and Engineering, 1996. 14(3): p. 221-230.
161. Adari, R., et al., *Selecting Drilling Fluid Properties and Flow Rates for Effective Hole Cleaning in High-Angle and Horizontal Wells.* SPE Annual Technical Conference and Exhibition, 2000.
162. Judzis, A., et al., *2006.* IADC/DPE Drilling Conference, Investigation of Smaller Footprint Drilling System: Ultra-High Rotary Speed Diamond Drilling has Potential for Reduced Energy Requirements.
163. Judzis, A., et al., *Optimization of Deep-Drilling Performance-- Benchmark Testing Drives ROP Improvements for Bits and Drilling Fluids.* SPE Drillig &Completion, 2009. 24(1): p. 25-39.

164. Learmonth, I.D., C. Young, and C. Rorabeck, *The Operation of the Century: Total Hip Replacement.* The Lancet, 2007. 370.
165. Dowson, D. and Z.M. Jin, *Metal-on-Metal Hip Joint Tribology.* The Journal of Engineering in Medicine, 2006. 220.
166. Mattei, L., et al., *Lubrication and Wear Modelling of Artificial Hip Joints: A Review.* Tribology International, 2011. 44: p. 532-549.
167. Hodge, W.A., et al., *Contact Pressures in the Human Hip Joint Measured in vivo* Proc. Natl. Acad. of Sci. USA, 1986. 83: p. 2879-2883.
168. Terrell, E.J. and C.F. Higgs III, *A Particle-Augmented Mixed Lubrication Modeling Approach to Predicting Chemical Mechanical Polishing.* Journal of Tribology, 2008. 131(1).
169. H., I., et al., *Reduction of Polyethylene Wear by Concave Dimples on the Frictional Surface in Artificial Hip Joints.* Journal of Arthroplasty, 2000. 15(3): p. 332-338.
170. Sheeja, D., et al., *Mechanical and Tribological Characterization of Diamond-like Carbon Coatings on Orthopedic Materials.* Diamond and Related Materials 2001. 10(3): p. 1043-1048.
171. Zhou, X., et al., *The Influence of Concave Dimples on the Mettalic Counterface on the Wear of Ultra-High Molecular Weight Polyethylene.* Journal of Engineering Tribology, 2012. 226(6): p. 455-462.
172. Dearnaley, G. and H. James, *Biomedical Applications of Diamond-like Carbon (DLC) Coatings: A Review.* Surface Coatings and Technology, 2005. 200(7): p. 2518-2524.
173. Harris, W.H., *The Problem is Osteolysis.* Clinical Orthopedics and Related Research, 1995. 311: p. 46-53.
174. Willert, H.G., H. Bertram, and G.H. Buchhorn, *Osteolysis in Alloarthroplasty of the Hip: the Role of Ultra High Molecular Weight Polyethylene Wear Particles.* Clinical Orthopedics and Related Research, 1990. 258: p. 95-107.
175. Buford, A. and T. Goswami, *Review of Wear Mechanisms in Hip Implants: Paper I- General.* Materials & Design, 2004. 25: p. 385-393.
176. Gispert, M.P., et al., *Friction and Wear Mechanisms in Hip Prosthesis: Comparison of Joint Materials Behavior in Several Lubricants.* Wear, 2006. 260: p. 149-158.
177. Sawano, H., S. Warisawa, and S. Ishihara, *Study on Long Life of Artificial Joints by Investigating Optimal Sliding Surface Geometry for Improvement in Wear Resistance.* Precision Engineering, 2009. 33(4): p. 492-498.
178. Fisher, J. and D. Dowson, *Tribology of Total Artificial Hip Joints.* Journal of Engineering in Medicine, 1991. 205(2): p. 73-79.
179. Lloyd, A.I.G. and R.E.J. Noel, *The Effect of Counterface Surface Roughness on the Wear of UHMWPE in Water and Oil-in-Water Emulsions.* Tribology International, 1988. 21(2): p. 83-88.
180. Okularczyk, W., *Experimental Investigations of Guide Rings Made of UHMWPE and PTFE Composites in Water Hydraulic Systems.* Archives of Civil and Mechanical Engineering, 2007. 7(4): p. 167-176.
181. Zoo, Y.S., et al., *Effect of Carbon Nanotube Addition on the Tribological Behavior of UHMWPE.* Tribology Letters, 2004. 16(4): p. 305-309.
182. Etsion, I., *State of the Art in Laser Surface Texturing.* Journal of Tribology, 2005. 127(1).
183. Etsion, I., Y. Kligerman, and G. Halperin, *Analytical and Experimental Investigations of Laser-Textured Mechanical Seal Faces.* Tribology Transactions, 1999. 42(3): p. 511-516.
184. Kovalchenko, A., et al., *The Effect of Laser Surface Texturing on Transitions in Lubrication Regimes during Unidirectional Sliding Contact.* Tribology International, 2005. 38(3): p. 219-225.
185. Ronen, A., I. Etsion, and Y. Kligerman, *Friction-Reducing Surface Texturing in Reciprocating Automotive Components.* Tribology Transactions, 2001. 44(3): p. 359-366.

186. Ryk, G., Y. Kligerman, and I. Etsion, *Experimental Investigation of Laser Surface Texturing for Reciprocating and Automotive Components.* Tribology Transactions, 2002. 45(4): p. 444-449.
187. Borghi, A., et al., *Tribological Effects of Surface Texturing on Nitriding Steel for High-Performance Engine Applications.* Wear, 2008. 265(7): p. 1046-1051.
188. Voevodin, A.A., et al., *Nanocomposite Tribological Coatings with Chameleon Surface Adaptation.* Journal of Vacuum Science & Technology A, 2002. 20(4): p. 1434-1444.
189. Voevodin, A.A. and J.S. Zabinski, *Laser Surface Texturing for Adaptive Solid Lubrication.* Wear, 2006. 261(11): p. 1285-1292.
190. De Kraker, A., et al., *A Multiscale Method for Modeling Surface Texture Effects.* Journal of Tribology, 2007. 129(2): p. 221-230.
191. Salama, M.E., *The Effect of Macro-Roughness on the Performance of Parallel Thrust Bearings.* Proc. Institution of Mech. Engineers, 1950. 163(1): p. 149-161.
192. Hamilton, D.B., J.A. Walowit, and C.M. Allen, *A Theory of Lubrication through Micro-Irregularities.* Journal of Fluids Engineering, 1966.
193. Sahlin, F., et al., *Two-Dimensional CFD-Analysis of Micro-Patterned Surfaces in Hyrdodynamic Lubrication.* Journal of Tribology, 2005. 127: p. 96-102.
194. Arghir, M., et al., *Theoretical Analysis of the Incompressible Laminar Flow in a Macro-Roughness Cell.* Journal of Tribology, 2003. 125: p. 309-318.
195. Filiz, S., et al., *Micromilling of Microbarbs for Medical Implants.* International Journal of Machine Tools and Manufacture, 2008. 48(3): p. 459-472.
196. Wilson, M.E., et al., *Fabrication of Circular Microfluidic Channels by Combining Mechanical Micromilling and Soft Lithography.* Lab on a Chip, 2011. 11(8): p. 1550-1555.
197. Li, X., J. Wang, and W. Li, *Current State and Prospect of Micro-Machining.* Automation and Logistics, 2007 IEEE International Conference, 2007: p. 1414-1419.
198. Masuzawa, T., *State of the art of Micromachining.* CIRP Annals-Manufacturing Technology, 2000. 49(2): p. 473-488.
199. Stokes, C. and P.J. Palmer, *3D Micro-Fabrication Processes: a Review.* MEMS Sensors and Actuators, Instit. Engineering Technology Seminar 2006, 2006.
200. Sheeja, D., B.K. Tay, and L. Nung, *Tribological Characterization of Surface Modified UHMWPE against DLC-coated Co-Cr-Mo.* Surface Coatings and Technology, 2005. 190(2): p. 231-237.
201. Yan, Y., *Corrosion and Tribo-corrosion Behavior of Metallic Orthopedic Implant Materials*. 2006, University of Leeds.
202. Myant, C.W. and P. Cann, *In Contact Observations of Model Synovial Fluid Lubricating Mechanisms.* Tribology International, 2013. 63: p. 97-104.
203. Affatato, S., et al., *Tribology and Total Hip Joint Replacement: Current Concepts in Mechanical Simulation.* Medical Engineering & Physics, 2008. 30(10): p. 1305-1317.
204. Barret, T.S., G.W. Stachowiak, and A.W. Batchelor, *Effect of Roughness and Sliding Speed on the Wear and Friction of Ultra-High Molecular Weight Polyethylene.* Wear, 1992. 153: p. 331-350.